



# **Technological Advances in the Diagnosis and Management of Pigmented Fundus Tumours**

Lamis AlHarbi

Student Number: [REDACTED]

Postgraduate (MPhil/PhD) Student

UCL Institute of Ophthalmology

Department of Ocular Oncology and Naevus Service

Moorfields Eye Hospital, London, UK

Thesis submitted in fulfilment of the requirements for the degree of  
Doctor of Philosophy

August 2022

**Principal Supervisor:**

**Professor Mandeep S. Sagoo**

Professor of Ophthalmology and Ocular Oncology, UCL Institute of Ophthalmology;  
Consultant Ophthalmic Surgeon, Moorfields Eye Hospital & Barts Health NHS Trust, London, UK

**Secondary Supervisor:**

**Professor Pearse Keane**

Professor of Artificial Medical intelligence, UCL Institute of Ophthalmology;  
Consultant Ophthalmic Surgeon, Moorfields Eye Hospital, London, UK

**Collaborators:**

**Professor Bertil Damato**

Consultant Ophthalmic Surgeon, Moorfields Eye Hospital, London, UK

**Mr Konstantinos Balaskas**

Consultant Ophthalmic Surgeon, Moorfields Eye Hospital, London, UK

## DECLARATION

I, LAMIS ALHARBI, CONFIRM THAT THE WORK PRESENTED IN THIS THESIS IS MY OWN, WHERE INFORMATION HAS BEEN DERIVED FROM OTHER SOURCES, I CONFIRM THAT THIS HAS BEEN INDICATED IN THE THESIS.

SIGNITURE:

DATE: 4<sup>th</sup> August 2022

NAME: LAMIS ALHARBI

## ACKNOWLEDGEMENT

First and foremost, I would like to express my sincere gratitude to my first supervisor Professor Mandeep Sagoo for his continuous support and guidance. He taught me to see the bigger picture, motivated and helped me develop a healthy attitude toward research. I will always be grateful for his time and the advice and knowledge he imparted to me.

I would also like to thank Professor Pearse Keane for being my second supervisor, particularly for introducing me to the world of AI in medicine and for his encouragement, together with Prof Mandeep Sagoo, to initiate the first AI project in the field of ocular oncology. I further appreciate his and Professor Omar Mahroo's support and feedback on my MPhil upgrade viva, which gave me confidence on my way forward.

My sincere gratitude goes to Professor Bertil Damato, the inventor of the MOLES scoring system, for allowing me to share the data and giving me the chance to be a part of a fantastic research team, including my colleagues, Dr Kelsey Roelofs and Mr Roderick O'Day. I look forward to putting everything he has taught me about MOLES and ocular oncology to good use in the future.

Furthermore, I thank my colleague Mr Konstantinos Balaskas for his collaboration and contribution to the research project of validating a virtual clinic pathway in the management of choroidal naevi. I am grateful to the Manchester Royal Eye Hospital and Moorfields Eye Hospital research group for starting this exciting project and for allowing me to take over to use and analyse the data and complete the publication.

It has been a pleasure to work together with Mr Gordon Hay on developing the virtual naevus clinic, and I thank him for supporting me to apply and fine-tune the design, pathways, and operating procedures at the Naevus Service at Moorfields Eye Hospital, as well as running the pilot with me and tackling the initial challenges.

I further like to thank the Collaborative Community on Ophthalmic Imaging (CCOI) ocular oncology working group for the fantastic international collaboration and for

letting me lead on producing the paper '*Artificial Intelligence in ocular oncology: Differentiating benign choroidal nevus from choroidal melanoma*' as the first author, and for giving the chance to significantly contribute to this important publication paving the way of AI into the field of ocular oncology.

My appreciation also goes to my friend, the data scientist Mr Gabriel Preda and my colleague Mr Edward Korot, who supported me with valuable advice on some of my queries on developing and evaluating machine learning algorithms.

It would have been impossible to pursue my dream without my friends and without their constant encouragement. I acknowledge my colleagues and friends Dr Ranaa Al Jamal who, as a PhD holder himself, shared his experiences and supported me with valuable scientific advice, and Angela Edgar, who kindly offered a final critical eye over my dissertation. I sincerely appreciate my special friend Constanze Meyer for her continuous support, friendship and inspiration. As a clinical informaticist, she always provided expert advice in the field of artificial intelligence and its implementation in clinical systems and pathways to drive digital transformation in healthcare.

Finally, I thank the Abu Dhabi Health Services Company - SEHA and Abu Dhabi Education Council (ADEC) for their generous funding, which allowed me to complete this PhD thesis.

It is impossible to mention everyone who has positively impacted my work; therefore, I am deeply thankful to everyone who helped me accomplish this thesis.

London August 2022

## ABSTRACT

Choroidal naevi are the most common intraocular tumour. They can be pigmented or non-pigmented and have a predilection for the posterior uvea. The majority remain undetected and cause no harm but are increasingly found on routine community optometry examinations. Rarely does a naevus demonstrate growth or the onset of suspicious features to fulfil the criteria for a malignant melanoma. Because of this very small risk, optometrists commonly refer these patients to hospital eye units for a second opinion, triggering specialist examination and investigation, causing significant anxiety to patients and stretching medical resources.

This PhD thesis introduces the MOLES acronym and scoring system that has been devised to categorise the risk of malignancy in choroidal melanocytic tumours according to Mushroom tumour shape, Orange pigment, Large tumour size, Enlarging tumour and Subretinal fluid. This is a simplified system that can be used without sophisticated imaging, and hence its main utility lies in the screening of patients with choroidal pigmented lesions in the community and general ophthalmology clinics. Under this system, lesions were categorised by a scoring system as 'common naevus', 'low-risk naevus', 'high-risk naevus' and 'probable melanoma.' According to the sum total of the scores, the MOLES system correlates well with ocular oncologists' final diagnosis.

The PhD thesis also describes a model of managing such lesions in a virtual pathway, showing that images of choroidal naevi evaluated remotely using a decision-making algorithm by masked non-medical graders or masked ophthalmologists is safe. This work prospectively validates a virtual naevus clinic model focusing on patient safety as the primary consideration. The idea of a virtual naevus clinic as a fast, one-stop, streamlined and comprehensive service is attractive for patients and healthcare systems, including an optimised patient experience with reduced delays and inconvenience from repeated visits. A safe, standardised model ensures homogeneous management of cases, appropriate and prompt return of care closer to home to community-based optometrists. This research work and strategies, such as the MOLES scoring system for triage, could

empower community-based providers to deliver management of benign choroidal naevi without referral to specialist units.

Based on the positive outcome of this prospective study and the MOLES studies, a 'Virtual Naevus Clinic' has been designed and adapted at Moorfields Eye Hospital (MEH) to prove its feasibility as a response to the COVID-19 pandemic, and with the purpose of reducing in-hospital patient journey times and increasing the capacity of the naevus clinics, while providing safe and efficient clinical care for patients. This PhD chapter describes the design, pathways, and operating procedures for the digitally enabled naevus clinics in Moorfields Eye Hospital, including what this service provides and how it will be delivered and supported. The author will share the current experience and future plan.

Finally, the PhD thesis will cover a chapter that discusses the potential role of artificial intelligence (AI) in differentiating benign choroidal naevus from choroidal melanoma. The published clinical and imaging risk factors for malignant transformation of choroidal naevus will be reviewed in the context of how AI applied to existing ophthalmic imaging systems might be able to determine features on medical images in an automated way. The thesis will include current knowledge to date and describe potential benefits, limitations and key issues that could arise with this technology in the ophthalmic field. Regulatory concerns will be addressed with possible solutions on how AI could be implemented in clinical practice and embedded into existing imaging technology with the potential to improve patient care and the diagnostic process.

The PhD will also explore the feasibility of developed automated deep learning models and investigate the performance of these models in diagnosing choroidal naevomelanocytic lesions based on medical imaging, including colour fundus and autofluorescence fundus photographs. This research aimed to determine the sensitivity and specificity of an automated deep learning algorithm used for binary classification to differentiate choroidal melanomas from choroidal naevi and prove that a differentiation concept utilising a machine learning algorithm is feasible.

## **IMPACT STATEMENT**

The research performed in this PhD thesis should help accomplish an organised approach and an optimal way to differentiate pigmented lesions of the fundus by using advanced imaging technology and new innovative techniques to diagnose and manage such lesions in different clinical settings in ocular oncology.

The MOLES scoring system described in this PhD has been developed to differentiate choroidal melanomas from naevi according to well-known risk factors of malignancy. When melanocytic choroidal tumours are assessed with the aid of multimodal imaging, the MOLES scores correlate well with the diagnosis made by ocular oncologists at a specialist clinic. Therefore, the MOLES scoring system provides a safe and efficient triaging and management tool for describing the clinical features of melanocytic choroidal tumours and objectively defining the risk of malignancy in such lesions. The scope of MOLES has been increased by the COVID-19 pandemic, encouraging practitioners to shift the care of patients with melanocytic choroidal tumours from ocular oncology centres to ophthalmic units closer to the patients' home and from these clinics to community optometrists. This trend reduces the risk of coronavirus infection to patients and healthcare providers, minimises patient travel costs, and conserves healthcare resources.

Another study presented in this PhD demonstrates that 'virtual' imaging-based pathways are a safe and efficient option for managing referrals for choroidal naevi, which are a common incidental finding and rarely have sufficient suspicious features to diagnose a small melanoma, but often prompt specialist referrals to ocular oncology. The clinical evaluation of this research project has led to the validation of a dedicated, 'one-stop' virtual clinic model for the safe management of patients with choroidal naevomelanocytic lesions while ensuring an optimal experience of care. The results show that images of choroidal naevi evaluated remotely using a decision-making process by masked non-medical graders or masked ophthalmologists are feasible and safe.



Based on this prospective validation of a virtual clinic pathway and validation of the MOLES scoring system, a model of a 'Virtual Naevus Clinic' has been designed and put into practice at Moorfields Eye Hospital and proved its feasibility as a response to the COVID-19 pandemic, and with the purpose of reducing in-hospital patient journey times and increasing the capacity of the naevus clinics, while providing safe and efficient clinical care for patients. This also has a positive impact to the need to avoid crowding in the waiting area and ensure patients are safe. For this purpose, the author developed a standard operating procedure (SOP) which comprises the design, pathways, and operating procedures for the digitally enabled naevus clinics in Moorfields Eye Hospital.

The PhD also explored the feasibility of developed automated deep learning models by investigating the performance of these models in diagnosing choroidal naevomelanocytic lesions based on medical imaging, including colour fundus and autofluorescence fundus photographs. This research proved that an automated deep learning model used for binary classification as a differentiation concept is feasible. Translating and fine-tuning the use of this model from the differentiation between melanoma and naevi to a refer vs non-refer model provides the potential that its application in the community can actively support referral decisions.

The author believes that this PhD research contributes to the knowledge within the field of ocular oncology and creates new, relevant, and meaningful insights with the prospect of being an inspiration for future research.

The author further feels that this dissertation which includes two publications and one submitted paper, adds to the body of literature on the advanced diagnosis of choroidal melanocytic lesions. Its research can be further developed and implemented in clinical practice as part of ocular oncology services and embedded into existing imaging technology in a field that has the potential to not only save the eye and vision but also save lives.

---

## Table of Contents

<b>DECLARATION.....</b>	<b>3</b>
<b>ACKNOWLEDGEMENT.....</b>	<b>4</b>
<b>ABSTRACT .....</b>	<b>6</b>
<b>IMPACT STATEMENT .....</b>	<b>8</b>
<b>Table of Contents.....</b>	<b>10</b>
<b>List of Abbreviations .....</b>	<b>15</b>
<b>List of Figures .....</b>	<b>19</b>
<b>List of Tables.....</b>	<b>22</b>
<b>1. CHAPTER ONE: Background and Literature Review .....</b>	<b>23</b>
1.1. General introduction.....	23
1.2. Benign melanocytic tumours of the uvea.....	24
1.2.1. Iris naevus .....	24
1.2.2. Ciliary body naevus .....	25
1.2.3. Melanocytosis .....	25
1.2.4. Melanocytoma .....	26
1.2.4.1. Uvea melanocytoma .....	27
1.2.4.2. Optic disc melanocytoma .....	28
1.2.5. Choroidal naevus.....	30
1.2.5.1. Clinical features of choroidal naevus .....	30
1.2.5.2. Epidemiology aspects of choroidal naevi.....	33
1.2.5.3. Suspicious choroidal naevi.....	33
1.2.5.4. Management of choroidal naevi.....	35
1.2.6. Other pigmented ocular fundus lesions .....	35
1.2.6.1. Congenital hypertrophy of the RPE (CHRPE) .....	35
1.2.6.2. Combined hamartoma of the retina and RPE .....	36
1.2.6.3. Simple hamartoma of the RPE.....	38
1.2.6.4. Adenoma and adenocarcinoma of the RPE.....	40
1.3. Uveal melanoma .....	40
1.3.1. Epidemiological aspects of uveal melanoma .....	40
1.3.2. Aetiology and predisposition of uveal melanoma .....	42

---

1.3.3. Congenital uveal melanoma .....	42
1.3.4. Iris melanoma .....	43
1.3.4.1. Clinical features of iris melanoma .....	43
1.3.5. Ciliary body melanoma .....	44
1.3.5.1. Clinical features of ciliary body melanoma.....	44
1.3.6. Choroidal melanoma .....	45
1.3.6.1. Clinical features of choroidal melanoma .....	45
1.3.7. TNM classification of uveal melanomas (UICC TNM 8) .....	48
1.4. Clinical investigations and examination techniques.....	52
1.4.1. Imaging .....	52
1.4.1.1. Fundus photography .....	52
1.4.1.2. Ultra-widefield retinal imaging .....	54
1.4.1.3. Ultrasonography (US) .....	56
1.4.1.4. Anterior segment photography.....	58
1.4.1.5. Fundus autofluorescence (FAF).....	59
1.4.1.6. Fluorescein angiography (FA).....	60
1.4.1.7. Indocyanine green angiography (ICG).....	61
1.4.1.8. Optical coherence tomography (OCT) .....	62
1.4.2. Transillumination (TI).....	63
1.4.3. Laboratory investigations.....	63
1.4.3.1. Histopathology.....	64
1.4.3.2. Immunohistochemistry .....	64
1.4.3.3. Genetic aberrations .....	65
1.4.4. Ancillary test in diagnosis of melanocytic choroidal lesions .....	65
1.5. Treatment of uveal melanoma .....	66
1.5.1. Radiotherapy .....	66
1.5.1.1. Plaque brachytherapy .....	67
1.5.1.2. Proton beam therapy (PBT) .....	68
1.5.1.3. Stereotactic radiotherapy .....	69
1.5.2. Transpupillary thermotherapy (TTT).....	70
1.5.3. Resection.....	71
1.5.3.1. Endoresection .....	71
1.5.3.2. Exoresection.....	72
1.5.4. Photodynamic therapy (PDT) .....	72
1.5.5. Cryotherapy .....	73
1.5.6. Enucleation .....	73
1.6. Prognosis .....	74
1.7. Methods of diagnostic differentiation of the choroidal naevi and choroidal melanoma .....	75
1.8. Role of artificial intelligence in ocular oncology and in the diagnosis of pigmented fundus tumours .....	77

---

<b>2. CHAPTER TWO: General Methodology .....</b>	<b>79</b>
<b>3. CHAPTER THREE: Distinguishing Choroidal Naevi from Melanomas using the MOLES Algorithm: Evaluation in an Ocular Naevus Clinic .....</b>	<b>84</b>
3.1. Introduction .....	84
3.1.1. Diagnosing melanocytic choroidal tumours .....	84
3.1.2. MOLES scoring system .....	85
3.2. Patients and methods .....	87
3.3. Results .....	90
3.4. Discussion .....	96
3.4.1. Discussion of results .....	96
3.4.2. Strengths and weaknesses .....	96
3.4.3. Discussion of methods and MOLES rationale .....	97
3.4.4. Comparison with other studies .....	101
3.4.5. Clinical implications .....	102
3.4.6. Research implications .....	103
3.5. Related study 1: The MOLES system for planning management of melanocytic choroidal tumours: is it safe? .....	105
3.5.1. Background of the study .....	105
3.5.2. Methodology .....	107
3.5.3. Results and main findings .....	108
3.5.4. Clinical implications .....	108
3.5.5. Implication of the MOLES scoring system for tele-oncology .....	109
3.5.6. Strengths and weaknesses of study .....	110
3.5.7. Implications for research .....	110
3.6. Related study 2: Detecting progression of melanocytic choroidal tumours by sequential imaging: Is ultrasonography necessary? .....	111
3.6.1. Background of the study .....	111
3.6.2. Methodology .....	112
3.6.3. Results and main findings .....	113
3.6.4. How important is monitoring tumour thickness? .....	115
3.6.5. Value of ultrasonographic evaluation in addition to measurement of tumour thickness 116	
3.6.6. Optimal method for measuring tumour thickness .....	116
3.6.7. Benefits of omitting ultrasonography from the monitoring of choroidal naevi .....	117
3.6.8. The role of internal reflectivity and internal vascularity in the monitoring of choroidal melanocytic tumours .....	118
3.6.9. Strengths and weaknesses .....	119
3.6.10. Further research .....	119

---

<b>4. CHAPTER FOUR: Prospective Validation of a Virtual Clinic Pathway in the Management of Choroidal Naevi.....</b>	<b>121</b>
4.1. Introduction .....	121
4.2. Patients and Methods .....	122
4.2.1. Study design .....	122
4.2.2. Patient pathway, clinical and imaging assessments, management decisions .....	123
4.2.3. Masked grading and definition of gold standard.....	125
4.2.4. Outcomes analysis .....	125
4.3. Results .....	128
4.3.1. Agreement of clinical management decision between gold standard versus masked ophthalmologist and masked non-medical reader.....	128
4.3.2. Agreement of diagnosis of choroidal naevi or other lesions between gold standard versus masked non-medical grader .....	133
4.3.3. Agreement between gold standard and masked non-medical grader for risk factors of growth .....	134
4.4. Discussion.....	135
4.4.1. Discussion of results.....	135
4.4.2. Limitations of this study .....	136
4.4.3. Benefits and outlook .....	137
<b>5. CHAPTER FIVE: Model of a Virtual Naevus Clinic in Practice at Moorfields Eye Hospital .....</b>	<b>139</b>
5.1. Purpose and scope .....	139
5.2. The MOLES Scoring System and its rationale .....	141
5.3. Design .....	142
5.4. Virtual Naevus Clinic: Diagnostic Hub and Virtual Assessment .....	145
5.4.1. Diagnostic Hub .....	145
5.4.2. Virtual Assessment Centre .....	148
5.4.3. Failsafe .....	149
5.4.4. Roles and responsibilities.....	149
5.5. Face-to-face (F2F) naevus clinic .....	151
5.6. Experience and future plans .....	153
<b>6. CHAPTER SIX: Artificial Intelligence in Ocular Oncology: Differentiating Benign Choroidal Naevus from Choroidal Melanoma .....</b>	<b>156</b>
6.1. Background.....	156
6.1.1. Imaging in ocular melanocytic lesions.....	160
6.1.2. AI in other medical conditions.....	161
6.1.3. Lessons from cutaneous melanoma .....	162
6.1.4. AI applications in differentiating choroidal naevi from melanoma .....	162

6.1.5. Summary of the Collaborative Community on Ophthalmic Imaging (CCOI) .....	164
6.2. Introducing automated deep learning design for differentiating benign choroidal naevus from choroidal melanoma (A proof of concept).....	167
6.2.1. Introduction .....	167
6.2.2. Methods .....	168
6.2.2.1. Datasets and study design .....	168
6.2.2.2. Dataset details.....	169
6.2.2.3. Data processing and labelling .....	171
6.2.2.4. AutoML platform selection.....	173
6.2.2.5. Model training.....	174
6.2.2.6. Model output & evaluation.....	175
6.2.2.7. Model test & use.....	177
6.2.2.8. Statistical analysis .....	178
6.2.3. Results.....	179
6.2.3.1. Evaluation of the trained models.....	179
6.2.3.2. Internal validation .....	186
6.2.4. Discussion .....	188
6.2.4.1. Summary and discussion of results .....	188
6.2.4.2. Discussion of methods .....	191
6.2.4.3. Future outlook and how to overcome limitations.....	192
6.3. General discussion of AI in ocular oncology .....	196
6.3.1. Potential benefits of AI.....	196
6.3.2. Key challenges of AI.....	197
6.3.3. Regulatory concerns in US, Europe, and Globally .....	202
6.3.3.1. The U.S. approach .....	202
6.3.3.2. The EU and UK approach .....	205
6.3.3.3. WHO guidelines for digital health (A global approach) .....	207
6.3.4. Society and patient perspective.....	207
6.3.5. How to implement AI in ocular oncology .....	209
<b>7. CHAPTER SEVEN: Summary of the Research Conclusions and Recommendations.....</b>	<b>212</b>
<b>REFERENCES .....</b>	<b>217</b>
<b>APPENDICES.....</b>	<b>247</b>
Appendix 1 – Guide for diagnostic hub technicians to collect patients history for virtual naevus clinics .....	247
Appendix 2 – AutoML screenshots of AF and CL model evaluation.....	249

## List of Abbreviations

A	Absent
ABCDE	Asymmetry, Border irregularity, Colour, Diameter >6 mm, Evolving size, shape, or colour
ACC	Accuracy
AF	Autofluorescence
AI	Artificial Intelligence
AJCC	American Joint Committee on Cancer
AMA	American Medical Association
anti-VEGF	Anti-Vascular Endothelial Growth Factors
AU-011	AU-011 (Aura Biosciences) is a highly tumour targeted treatment for ocular melanoma
AUPRC / PR AUC	Area Under the Precision-Recall Curve
AutoML	Automated Machine Learning Platform
BAP1	BAP1 gene provides instructions for making a protein called ubiquitin carboxyl-terminal hydrolase BAP1
BRCA1	BRCA1 gene
B-scan	Brightness Scan
C	Confluent
CCOI	The Collaborative Community on Ophthalmic Imaging
CDRH	Center for Devices and Radiological Health
CF	Count Fingers, when measuring visual acuity
CFDL	Code-Free Deep Learning
CHR	Combined Hamartoma of the Retina
CHRPE	Congenital Hypertrophy of the Retinal Pigment Epithelium
CI	Confidence Interval
CL	Colour Fundus, in relation to imaging
CM	Choroidal Melanoma
CME	Continuing Medical Education
CN	Choroidal Naevus
CNL	Choroidal Naevomelanocytic Lesion
CNS	Central Nervous System
CNV	Choroidal Neovascularisation
CNVM	Choroidal Neovascular Membrane
COM	Congenital Ocular Melanocytosis
COMS	Collaborative Ocular Melanoma Study
COVID-19	Coronavirus disease caused by the SARS-CoV-2 virus (severe acute respiratory syndrome coronavirus 2)
CPE	Ciliary Body Pigment Epithelium
CR	City Road
CSV	Comma-Separated Values
CT	computed tomography
DD	Disc Diameter

DIM	Diameter
DL	Deep Learning
DNA	Did Not Attend
DRCR.net	Diabetic Retinopathy Clinical Research Network
EAP	Expedited Access Pathway
EDI-OCT	Enhanced Depth Imaging - Optical Coherence Tomography
EEC	European Economic Community
EIF1AX	Eukaryotic Translation Initiation Factor 1A X-Linked (protein coding gene)
EU	European Union
EyeArt	Autonomous AI system for diabetic retinopathy screening
F	Subretinal Fluid
F2F	Face to Face
FA	Fluorescein Angiography
FAF	Fundus Autofluorescence
FAP	Familial Adenomatous Polyposis
FDA	Food & Drug Administration
FFA	Fundus Fluorescein Angiography
FN	False negative
FNAB	Fine-Needle Aspiration Biopsy
FP	False Positive
GC	Green Channel, in relation to imaging
GDPR	General Data Protection Regulation
GmbH	Gesellschaft mit beschränkter Haftung
GMLP	Good Machine Learning Practice
GPU	Graphics Processing Unit
GUI	Graphical User Interface
HIPAA	Health Insurance Portability and Accountability Act of 1996
HM	Hand Motions, when measuring visual acuity
ICG	Indocyanine Green Angiography
ICGA	Indocyanine Green Angiography
ID	Identification
IDx-DR	Diabetic Retinopathy Detection Device
IOP	Intraocular Pressure
IT	Information Technology
IV	Intravenous
IVDR	In Vitro Diagnostic Medical Device Regulation
K	Kappa Score
LBD	Largest Basal Diameter
LogMAR	Logarithm of the Minimum Angle of Resolution
LUMPO	Liverpool Uveal Melanoma Prognosticator Online
M	Margin, in relation to risk factor of growth
M	Melanoma
MDR	Medical Devices Regulation
MEDDEV	Medical Devices Directive



MEH	Moorfields Eye Hospital
MELANOMA	Melanoma visible externally, Eccentric visual phenomena, Lens abnormalities, Afferent pupillary defect, No optical correction, Ocular hypertension, Melanosis oculi, Asymmetrical episcleral
ML	Machine Learning
mm	Millimetre
MMCCB	Malignant Melanoma of the Choroid and Ciliary Body
MOLES	Mushroom shape, Orange pigment, Large size, Enlargement, and Subretinal fluid
MOST	Melanoma, Orange pigment, Subretinal fluid, Thickness
MPhil	Master of Philosophy
MR	Medical Retina
MREH	Manchester Royal Eye Hospital
MRI	Magnetic Resonance Imaging
N	None, in relation to no tumour enlargement
N	Nil, in relation to no treatment performed
NF1	Neurofibromatosis type 1
NF2	Neurofibromatosis type 2
NHS	National Health Service
NIS Directive	Cyber Security' Directive on security of network and information systems
NLP	No Light Perception
NPV	Negative Predictive Value
O	Orange Pigment
OCT	Optical Coherence Tomography
OCTA	Optical Coherence Tomography Angiography
PAS	Patient Administration System
PBT	Proton Beam Therapy
PDT	Photodynamic Therapy
PhD	Doctor of Philosophy
PHI	Protected Health Information
PII	Personally Identifiable Information
PIL	Patient Information Leaflet
POFL	Pigmented Ocular Fundus Lesions
PPV	Positive Predictive Value
PSQ	Patient Satisfaction Questionnaire
PVD	Posterior Vitreous Detachment
RC	Reading Centre based at City Road
RC	Red Channel, in relation to imaging
RCH	Retinal Capillary Haemangioma
RD	Retinal Detachment
RPB	Ruthenium Plaque Brachytherapy
RPE	Retinal Pigment Epithelium
RWP	Real-World Performance
S	Symptoms
S	Significant, in relation to evaluating risk factors of growth

SaMD	Software as a Medical Device
SD	Standard Deviation
SD-OCT	Spectral Domain Optical Coherence Tomography
SF3B1	SF3B1 gene is encoding splicing factor 3B subunit 1 protein in humans
SOP	Standard Operating Procedure
SRF	Subretinal Fluid
SS-OCT	Swept-Source Optical Coherence Tomography
T	Thickness
T	Trace, in relation to evaluate risk factors of growth
TD-OCT	Time-Domain Optical Coherence Tomography
TFSOM	To Find Small Ocular Melanoma
TFSOM-DIM	To Find Small Ocular Melanoma Doing IMaging
TFSOM-UHHD	To Find Small Ocular Melanoma Using Helpful Hints Daily
TN	True Negative
TNM	Tumor, Node, Metastasis
TNR	True Negative Rate
TP	True Positive
TPR	True Positive Rate
TTT	Transpupillary Thermotherapy
U.S.	United States of America
UBM	Ultrasound Biomicroscopy
UCL	University College London
UICC	Union for International Cancer Control
UK	United Kingdom
UM	Uveal Melanoma
US	Ultrasound
USG	Ultrasonography
UV	Ultraviolet
UWF	Ultra-Widefield
VA	Visual Acuity
VF	Visual Field
VPT	Vasoproliferative Tumours
WF	Widefield
WHO	World Health Organization

## List of Figures

- Figure 1: Slit lamp colour photograph of a left eye melanocytic iris naevus between 5 o'clock and 6 o'clock position, it extends into the angle but shows no deeper invasion posteriorly. Ultrasound B-scan measured thickness of 0.6 mm with horizontal base of 2.1 mm. (Image source: MEH) ..... 25
- Figure 2: Right eye optic disc melanocytoma, (A) colour optos ultra-widefield (UWF) photograph, (B) autofluorescence optos, ultra-widefield (UWF) photograph, (C) OCT spectralis, shows no subretinal fluid (SRF) nor intraretinal fluid (IRF). (Image source: MEH) ..... 29
- Figure 3: Right eye halo choroidal naevus, (A) colour optos ultra-widefield (UWF) photograph, on (C) OCT spectralis shows a posterior vitreous detachment (PVD). The choroidal naevus is not associated with subretinal fluid (SRF) or intra retinal fluid (IRF) and no lipofuscin on the OCT and (B) autofluorescence optos, ultra-widefield (UWF) photograph. (Image source: MEH) ..... 32
- Figure 4: Right eye suspicious melanocytic choroidal naevus, (A) colour optos ultra-widefield (UWF) photograph, with trace of subretinal fluid detected on (B) autofluorescence optos, ultra-widefield (UWF) photograph and (C) OCT spectralis image. (Image source: MEH) ..... 34
- Figure 5: Right eye congenital hypertrophy of the retinal pigment epithelium (CHRPE), (A) colour optos ultra-widefield (UWF) photograph, (B) autofluorescence optos, ultra-widefield (UWF) photograph, (C) OCT spectralis. (Image source: MEH) ..... 36
- Figure 6: Left eye combined hamartoma of the retina and retinal pigment epithelium with traction and subretinal fluids. (A) colour optos ultra-widefield (UWF) photograph, (B) autofluorescence optos, ultra-widefield (UWF) photograph, (C) OCT spectralis scan shows an epiretinal membrane with some retinal disturbance including fluid and the architecture of retina is disturbed to full thickness with some underlying retinal pigment epithelial changes. (Image source: MEH) ..... 37
- Figure 7: Right eye simple hamartomas of the RPE, (A) colour optos ultra-widefield (UWF) photograph, (B) autofluorescence optos, ultra-widefield (UWF) photograph, (C) OCT spectralis, shows no SRF nor IRF. (Image source: MEH) ..... 39
- Figure 8: Slit lamp colour photograph of a right eye iris melanoma associated with iridocorneal touch, and uveal ectropion. Ultrasound B-scan measured thickness of 3.3 mm with horizontal base of 3 mm. There was no involvement of the ciliary body, but the iris mass extends into the angle and abstract any clear view under gonioscopy, no angle seeding or pigment dispersion was present, and the intra ocular pressure is normal measuring 14mmHg. (Image source: MEH) ..... 44
- Figure 9: Right eye choroidal melanoma, (A) colour optos ultra-widefield (UWF) photograph, (B) autofluorescence optos, ultra-widefield (UWF) photograph shows significant amounts of lipofuscin, (C) OCT spectralis shows amount of subretinal fluids and lipofuscin. (Image source: MEH) ..... 47

Figure 10: Left eye colour photographs showing malignant transformation from a melanocytic choroidal naevus with marginal tumour recurrence after conservative therapy. (A) colour optos ultra-widefield (UWF) photograph from May 2019, (B) colour optos ultra-widefield (UWF) photograph from March 2021. (Image source: MEH).....	53
Figure 11: Ultrasonography of a right eye choroidal melanoma showing a large ‘mushroom’ shape lesion, Location grossly nasal extending beyond the equator. Internal echogenicity: medium to low, Thickness of 14.4mm with a transverse base of 9.2mm x longitudinal base 11.2 mm. (Image source: MEH) .....	58
Figure 12: Autofluorescence image, showing a right eye with orange lipofuscin pigment overlying small choroidal melanoma, associated with a trace of subretinal fluid. (Image source: MEH) .....	60
Figure 13: MOLES Score examples: Colour photograph, fundus autofluorescence image and optical coherence tomography of representative patients according to MOLES score. (A) MOLES = 0; (B) MOLES = 1; (C) MOLES = 2, (D) MOLES >2. ....	89
Figure 14: OCTs and fundus autofluorescence images of 6 tumours with a MOLES score >2 and diagnosed by experts as naevus.....	95
Figure 15: Progression of choroidal melanocytic tumours detected by various combinations of imaging modalities. <sup>430</sup> .....	114
Figure 16: Colour photographs, OCTs and fundus autofluorescence images of 3 cases: (A–C) Total agreement case between gold standard versus masked reader and masked ophthalmologist, with basal diameter <3 DD, no SRF and US no thickness detected. (D–F) Under-referral case, where masked graders decided to follow up because of lesion within 1 DD of optic disc and no presence of subtle peripapillary SRF graded, while the gold standard advised referral to oncology. (G–I) Over-referral case, where masked graders referred to ocular oncology due to physical findings and symptoms, but the gold standard advised to follow up in a naevus monitoring clinic. DD, disc diameter; OCT, optical coherence tomography; SRF, subretinal fluid; US, ultrasound. ....	132
Figure 17: Diagram depicting the flow of patients via diagnostic hub through the two different clinic models within the Naevus Service .....	143
Figure 18: Patient flow diagram for the diagnostic hub and virtual assessment clinic model .....	147
Figure 19: Patient flow diagram for the F2F assessment clinic model.....	152
Figure 20: Colour fundus photographs, fundus autofluorescence images, and OCTs of three cases: (A–C) with basal diameter 2mm, no subretinal fluid (SRF) and flat on ultrasonography (USG), representing choroidal naevus. (D–F) with basal diameter 5 mm, presence of SRF, and 1.1mm thickness on USG, representing indeterminate choroidal lesion. (G–I) with basal diameter >5 mm, confluent orange pigment, presence of SRF, and 1.6mm thickness on USG, representing choroidal melanoma. ....	158
Figure 21: Precision and Recall and PR curve of the AF model .....	180
Figure 22: Precision and Recall of the AF model for individual diagnostic classes .....	181
Figure 23: Examples of incorrect predictions for melanoma and naevus in AF images .....	182

Figure 24: Precision and Recall and PR curve of the CL model ..... 183

Figure 25: Precision and Recall of the CL model for individual diagnostic classes ..... 184

Figure 26: Examples of incorrect predictions for melanoma and naevus in CL images ..... 185

Figure 27: Flowchart depicting the Development of AI models for distinguishing choroidal lesions  
..... 195

## List of Tables

Table 1: TNM classification of uveal melanoma (TNM 8th edition) <sup>204, 205</sup> .....	51
Table 2: MOLES scoring system for evaluating malignancy in melanocytic choroidal tumours .....	87
Table 3: Patient demographics according to MOLES score and expert diagnosis of choroidal lesion .....	92
Table 4: Clinical findings according to MOLES score .....	93
Table 5: Clinical features of 16 tumours whose size category was determined by thickness.....	94
Table 6: Clinical features of 6 tumours with a MOLES score exceeding 2 and diagnosed by the expert as naevus .....	94
Table 7: MOLES tumour categories and suggested management .....	106
Table 8: Management algorithm .....	124
Table 9: Summary of comparisons of clinical management decisions between face-to-face (gold standard) and virtual pathways (masked non-medical graders) .....	129
Table 10: Comparison of clinical management decisions between two versions of virtual pathway (masked ophthalmologist vs masked non-medical grader) .....	130
Table 11: Comparison of clinical management decisions between face-to-face (gold standard) and virtual pathways (masked non-medical grader and masked ophthalmologist) when refer and follow up decisions are pooled .....	131
Table 12: Comparison of clinical management decisions between face-to-face (gold standard) and virtual pathways (masked non-medical grader and masked ophthalmologist) when refer and follow up decisions are pooled (sensitivity analysis) .....	131
Table 13: Comparison of choroidal naevi or ‘other’ diagnosis between face-to-face (gold standard) and virtual pathway (masked non-medical grader) .....	133
Table 14: Agreement between gold standard and masked non-medical grader for risk factors of growth.....	134
Table 15: MOLES scoring system (simplified) .....	141
Table 16: Eligibility criteria for the two specific Naevus clinics in Moorfields Eye Hospital.....	144
Table 17: Dataset splits for AF and CL deep learning models (imported and used) .....	172
Table 18: Confusion matrix for deep learning model validation .....	176
Table 19: Confusion matrix and statistical parameters with formulae.....	178
Table 20: Confusion matrix and statistical parameters of the AF model evaluation .....	180
Table 21: Confusion matrix and statistical parameters of the CL model evaluation .....	183
Table 22: Internal validation MEH confusion matrix and statistical parameters for the AF model ..	186
Table 23: Internal validation MEH confusion matrix and statistical parameters for the CL model ..	187
Table 24: Summary of results for model evaluation and internal validation for AF and CL models	189

## 1. CHAPTER ONE: Background and Literature Review

### 1.1. General introduction

Lesions that occur in the ocular fundus are encountered commonly and can portend a benign or malignant tumour. These can be pigmented or non-pigmented and have a predilection for the posterior uvea. The research presented in this PhD thesis should help to achieve an organised approach which is important to establish a differential diagnosis and an optimal way to manage these lesions with the use of modern imaging technology.

A choroidal melanocytic naevus is the most common intraocular tumour. Several forms of choroidal melanocytic lesions exist, making it challenging to distinguish between benign naevi, indeterminate lesions that may be malignant or pre-malignant and melanomas. From a healthcare point of view, it is important that this variety of choroidal lesion cases can be managed properly, and to optimise ways to distinguish serious cases that need robust management in ocular oncology from cases that can be managed in non-specialist or community clinics, either face to face or virtually.

A second aspect of this research work seeks to equip generalists and optometrists with a system to evaluate pigmented fundus lesions. Community optometrists are discovering and identifying more and more pigmented lesions. Establishing new, improved methods of diagnostic differentiation will support their work and help them decide on the seriousness of the pigmented spots.

Pigmented fundus tumours can originate in the choroid and rarely in the retinal pigment epithelium (RPE). Choroidal tumours are a central component of ocular oncology, and this chapter will introduce a broad overview of pigmented lesions of the fundus and their clinical features. Tumours of the retinal pigment epithelium (RPE) can be congenital or acquired. They may also be classified as reactive, hypertrophic, hamartomatous, and neoplastic.<sup>1</sup> Those present at birth can be associated with systemic conditions such as familial adenomatous polyposis (FAP)

or neurofibromatosis 2 (NF2). Acquired RPE tumours include benign and malignant lesions that are sometimes difficult to differentiate from choroidal neoplasms were it not for ancillary tests such as ultrasonography, optical coherence tomography, and fluorescein angiography.

## 1.2. Benign melanocytic tumours of the uvea

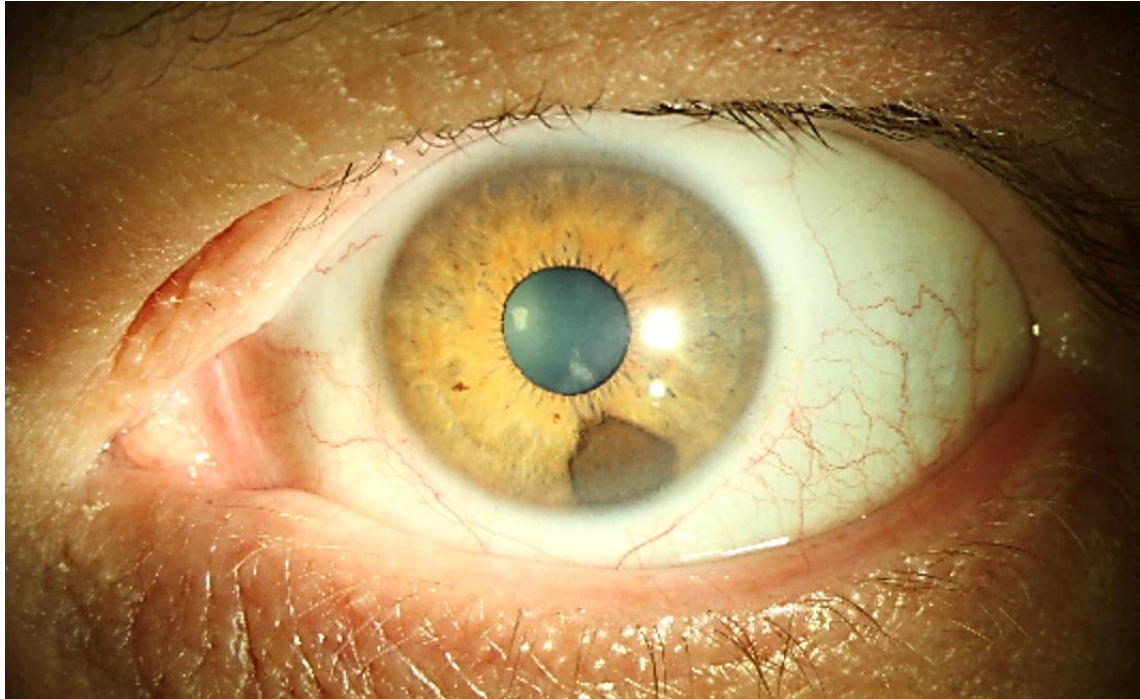
Benign melanocytic uveal tumours are generally known as naevi. Naevus is a Latin word meaning birthmark or mole and is a general term for a mark on the skin. The term naevus refers to an abnormal, hamartomatous cluster of melanocytes in ophthalmology. Uveal melanocytes are derived from neural crest cells and share this embryologic origin within cutaneous melanocytes.<sup>2</sup>

### 1.2.1. Iris naevus

Iris naevus is a stromal lesion and quite different from an iris freckle, in which melanocytes collect only superficially, without stromal involvement. (Figure 1) Iris freckles can be seen in up to 60% of the population, whereas naevi are less common (4–6%).<sup>3, 4</sup> Both iris freckles and naevi are more frequent in light-coloured irides.<sup>3, 4</sup> Patients with dysplastic naevus syndrome may have a tendency to develop iris naevi.<sup>5, 6</sup>

Although an association between iris naevi and uveal melanomas has been reported<sup>5</sup>, it is doubtful whether the two conditions are genuinely associated.<sup>3</sup> Overall, iris naevi have a good prognosis. Territo et al. showed in a series of 175 patients observed for a mean duration of 4.7 years, less than 5% of iris naevi showed clinical evidence of enlargement.<sup>7</sup>





**Figure 1:** Slit lamp colour photograph of a left eye melanocytic iris naevus between 5 o'clock and 6 o'clock position, it extends into the angle but shows no deeper invasion posteriorly. Ultrasound B-scan measured thickness of 0.6 mm with horizontal base of 2.1 mm. (Image source: MEH)

### 1.2.2. Ciliary body naevus

Although iris and choroidal naevi are well characterised, ciliary body naevi have rarely been described in the literature.<sup>8-10</sup> Moreover, because of their obscure location, their clinical features are lacking. Taban et al. reported six cases of ciliary body naevi and found that ciliary body naevi exist and may be more common than previously thought.<sup>11</sup> They are often overlooked secondary to their hidden location, but ultrasound biomicroscopy (UBM) can be a helpful diagnostic tool. Clinical characteristics of ciliary body naevi are not distinctive enough to differentiate them from melanoma with certainty.<sup>11</sup>

### 1.2.3. Melanocytosis

Oculodermal melanosis (melanosis oculi, naevus of ota) is also known as oculodermal melanocytosis, oculomucodermal melanocytosis, or congenital ocular melanocytosis (COM).<sup>12</sup> It is a benign mesodermal melanosis that involves the

distributions of the ophthalmic and maxillary trigeminal nerve with associated hyperpigmentation of the eye and its adnexa.<sup>13</sup> It is associated with a 1 in 400 risk of uveal melanoma, which tends to be relatively aggressive.<sup>14, 15</sup> There is an association between melanocytosis and bilateral Sturge-Weber syndrome.<sup>16</sup>

COM is managed in the same fashion as naevi, with an annual ocular examination with mydriasis. Ciliary body melanoma is detected by noting dilated episcleral vessels if UBM is not possible.<sup>17</sup> Multiple ocular melanomas can occur in this condition. COM can cause glaucoma, which needs to be excluded at every visit.<sup>18, 19</sup>

#### 1.2.4. Melanocytoma

Melanocytoma, or magnocellular naevus, is a rare intraocular tumour.<sup>20</sup>

It is a benign pigmented ocular tumour that predominantly involves the optic disc and uvea.<sup>21</sup> Other rare sites include the sclera<sup>22</sup> and the conjunctiva.<sup>23</sup> The term melanocytoma was proposed by Zimmerman and Garron<sup>24</sup> because they observed a resemblance between melanocytoma cells and those seen in ocular melanocytosis (melanosis oculi).

Histopathological examination of melanocytomas, different from melanoma or conventional uveal naevus,<sup>25</sup> shows that the tumour is composed by uniformly shaped polyhedral naevus cells that are pigmented and closely packed.<sup>26</sup>

Nevertheless, the morphology of the cells is usually obscured by a large amount of melanin, and special techniques to remove the melanin are typically necessary to make the correct diagnosis.<sup>27</sup>

The management of the melanocytoma is similar to the naevus, with clinical, photographic and sonographic monitoring,<sup>28</sup> and most classical cases do not require a histopathological examination to confirm the diagnosis.<sup>28</sup>

### 1.2.4.1. Uvea melanocytoma

Histologically, uveal melanocytomas are similar to optic disc melanocytomas.<sup>27</sup> Such tumours have been rarely seen in the iris, ciliary body, and choroid. Uveal melanocytomas are clinically indistinguishable from uveal naevus and melanoma, and most are probably managed as such. As with optic disc melanocytoma, uveal melanocytoma can give rise to melanoma.<sup>29</sup>

Some reports in the literature deal with primary melanocytomas of the choroid and ciliary body.<sup>20, 27, 30</sup> It is believed that most of these tumours are clinically diagnosed as naevi or melanoma, and are followed up or treated without surgical resection, respectively. Some clinical features, described further in this subchapter, can give a clue as to the correct diagnosis.<sup>20</sup>

#### 1.2.4.1.1. Clinical features of ciliary body melanocytoma

Only around 40 cases of ciliary body melanocytoma have been published.<sup>25</sup> The usual age at presentation is about 47 years,<sup>25</sup> with rare presentations in childhood.<sup>31</sup> The tumours are invariably darkly pigmented and nodular in appearance, and there is no preference for any particular quadrant.<sup>21</sup> Despite being benign, ciliary body melanocytomas tend to extend into the anterior chamber and extra-ocularly. Such extension can mimic extra scleral growth of a ciliary body melanoma.<sup>31</sup> One feature suggestive of melanocytoma is a uniform, black appearance, which is rare in ciliary body melanoma.<sup>20</sup>

#### 1.2.4.1.2. Clinical features of choroidal melanocytoma

Only around 15 cases of choroidal melanocytoma have been published,<sup>30</sup> with rare presentation in childhood.<sup>30, 32</sup> The tumours are usually darkly pigmented and dome-shaped in appearance.<sup>30</sup> A diffuse variant has also been described.<sup>33</sup> A choroidal melanocytoma can be indistinguishable from melanoma on ophthalmoscopy, ultrasonography, and angiography.<sup>29, 34</sup> In the Collaborative Ocular Melanoma Study (COMS), several cases of choroidal melanocytoma have been treated by plaque

radiotherapy, presuming a clinical diagnosis of melanoma. The correct diagnosis could be made only retrospectively once the eye was enucleated for radiation-related complications.<sup>34</sup>

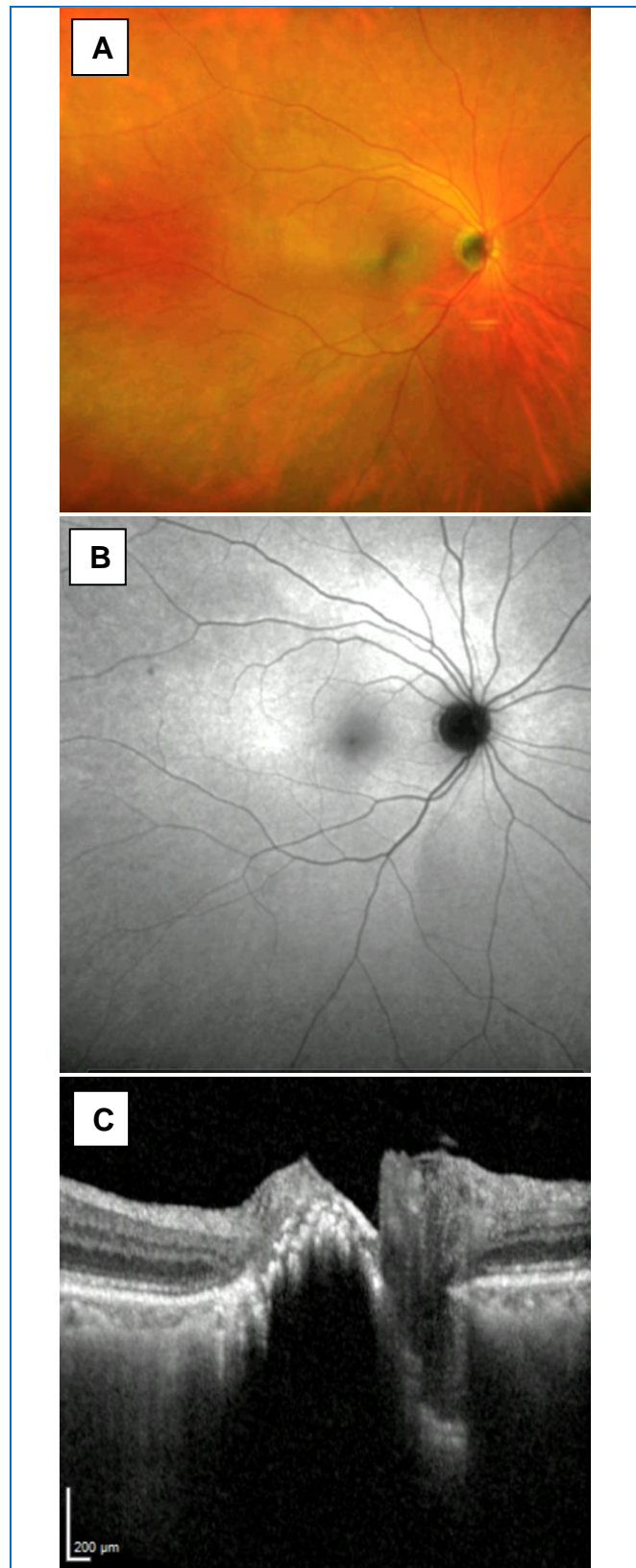
#### 1.2.4.2. Optic disc melanocytoma

Optic disc melanocytoma is a dark pigmented tumour, often extending from the optic disc to the surrounding choroid and retina.<sup>24, 35</sup> (Figure 2) Optic disc and uveal melanocytomas are considered to be congenital hamartomas,<sup>24</sup> arising from dendritic uveal melanocytes scattered throughout the uvea.<sup>27</sup>

Although optic disc melanocytoma is a congenital condition, it is rarely detected in childhood, the mean age at diagnosis being 50 years.<sup>36</sup> Optic disc melanocytoma is more commonly seen in black and darker skin than in white skin races.<sup>27</sup> Most patients are asymptomatic,<sup>36</sup> and the condition is detected on routine ophthalmoscopy.<sup>21</sup>

##### 1.2.4.2.1. Clinical features of optic disc melanocytoma

The choroid is involved in about 54% of cases, and a retinal component is present in about 30%.<sup>36</sup> The retinal involvement usually appears darker than the choroidal component and has feathery margins because of extensions into the nerve fibre layer.<sup>28, 36, 37</sup> Larger melanocytoma may completely obscure the optic disc and lead to pigment dispersion into the vitreous cavity. Prominent intrinsic vasculature, subretinal fluid, and retinal exudation are not usually present.<sup>38</sup> Unilateral optic disc melanocytoma is not associated with other ocular or systemic anomalies; however, bilateral tumours have been reported in association with optic nerve hypoplasia and central nervous system abnormalities.<sup>33, 36</sup>



**Figure 2:** Right eye optic disc melanocytoma, (A) colour optos ultra-widefield (UWF) photograph, (B) autofluorescence optos, ultra-widefield (UWF) photograph, (C) OCT spectralis, shows no subretinal fluid (SRF) nor intraretinal fluid (IRF). (Image source: MEH)

### 1.2.5. Choroidal naevus

Benign melanocytic uveal tumours are generally known as naevi.<sup>39</sup> Naevus is akin to a birthmark or mole and is a general term for a congenital mark on the skin. In ophthalmology, the term naevus originates from an abnormal, hamartomatous cluster of melanocytes. Uveal melanocytes are of neural crest origin and share embryologic source with cutaneous melanocytes.<sup>40</sup> (Figure 3)

Although a strict clinical definition of typical choroidal naevus is lacking,<sup>24</sup> the Collaborative Ocular Melanoma Study Group defined it as a choroidal melanocytic lesion that is 5 mm or smaller in largest basal dimension and not more than 1 mm in height.<sup>41</sup>

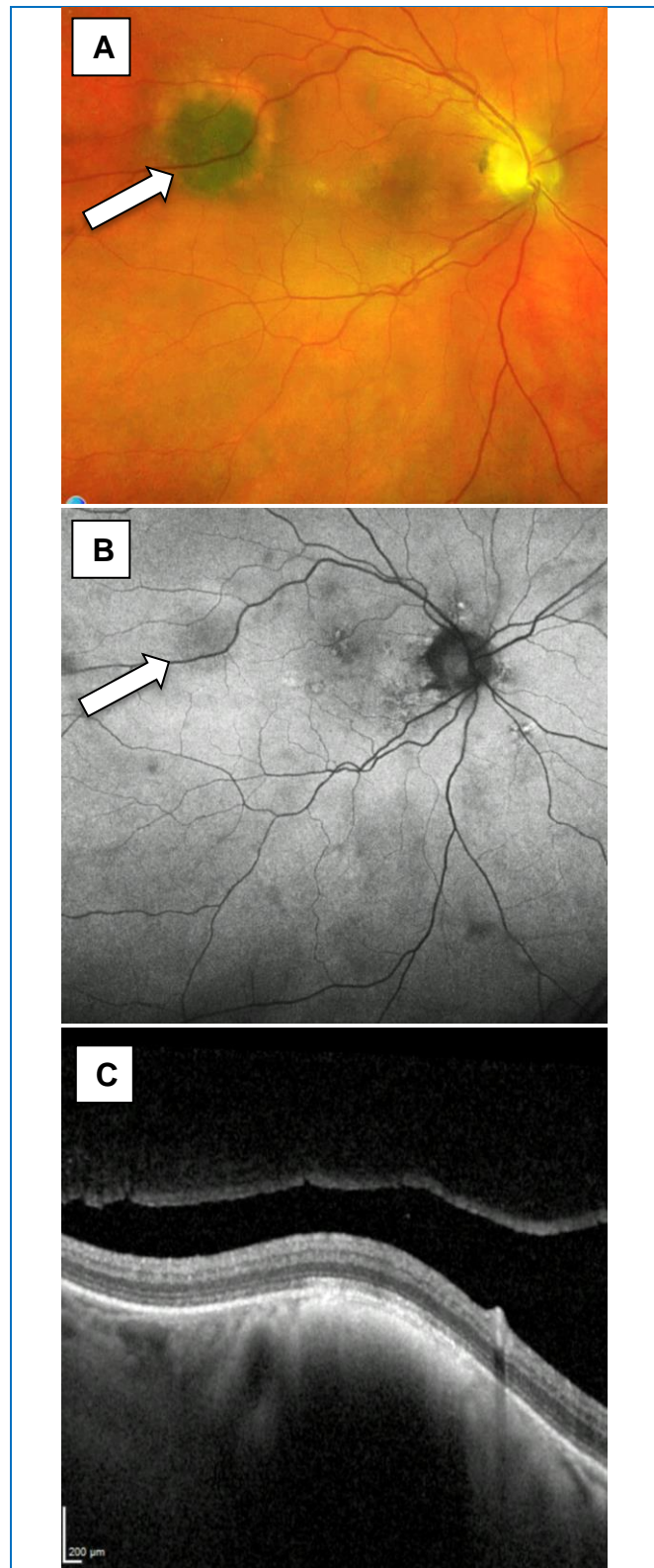
A choroidal naevus is the most common intraocular tumour,<sup>21, 22, 33, 36, 42-78</sup> occurring in approximately 5% of adults. It likely is a precursor of most choroidal melanomas. Therefore, clinicians should be aware of choroidal naevus and its variations.<sup>79</sup>

Choroidal naevi do not usually cause any symptoms,<sup>59</sup> and most are diagnosed on routine ophthalmoscopy.<sup>62</sup> (Figure 3) A macular naevus can cause visual loss from photoreceptor atrophy or occasionally from choroidal neovascularisation or associated polypoidal choroidal vasculopathy.<sup>80</sup> Subretinal fluid in association with naevus may induce symptoms of metamorphopsia or photopsia.<sup>58, 69</sup> Choroidal naevus appears as a slate-grey to brown and maybe amelanotic lesion with minimal thickness.<sup>81, 82</sup> The margins are usually ill-defined.<sup>69, 79</sup>

#### 1.2.5.1. Clinical features of choroidal naevus

Although it may be congenital,<sup>83</sup> choroidal naevus is rarely observed in young children.<sup>69, 84</sup> The precursor cells can be present at birth but do not become clinically visible until puberty, possibly due in part to acquisition of pigment of a previously non-pigmented lesion.<sup>85</sup> Choroidal naevus usually is first detected in adulthood and can be flat or minimally elevated and pigmented or amelanotic.<sup>69, 86</sup> Based on the Blue Mountain population based study, Sumicht et al.<sup>77</sup> found choroidal naevus

detected in 7% of Caucasians over the age of 49 years and was on average 1.5 mm in diameter. Based on a large clinic-based study by Shields *et al.*,<sup>69</sup> most choroidal naevi are <2mm in thickness.<sup>79</sup> Overlying drusen develop with time. Retinal Pigment Epithelium (RPE) detachment occurs in about 10% of cases<sup>57, 87</sup> and choroidal neovascularisation (CNV) overlying naevus in <1%.<sup>69, 80, 88</sup> Some choroidal naevi have a large size (>10mm diameter) but still lack risk factors for growth and they are classified as giant choroidal naevus.<sup>49</sup> Another interesting finding with naevus is the non-pigmented halo that can be seen in 5% of choroidal naevi.<sup>89</sup> Halo choroidal naevus (Figure 3) has been associated with a previous diagnosis of cutaneous melanoma and might represent an autoimmune reaction.<sup>89, 90</sup> Halo naevus is a favourable sign that implies less chance of undergoing malignant transformation.<sup>91</sup> The fervency with which a choroidal naevus grows or evolves into melanoma had been estimated in several reports.<sup>75, 79, 84</sup> Enlargement of a choroidal naevus is believed to be highly suggestive of malignant transformation into melanoma.<sup>56, 59, 61, 68, 75, 79</sup> However, some naevi can show growth over many years of approximately 1mm or less and still remain benign.<sup>45, 60</sup>



**Figure 3:** Right eye halo choroidal naevus, (A) colour optos ultra-widefield (UWF) photograph, on (C) OCT spectralis shows a posterior vitreous detachment (PVD). The choroidal naevus is not associated with subretinal fluid (SRF) or intra retinal fluid (IRF) and no lipofuscin on the OCT and (B) autofluorescence optos, ultra-widefield (UWF) photograph. (Image source: MEH)



### **1.2.5.2. Epidemiology aspects of choroidal naevi**

Uveal naevi, on the other hand, seem to have a relatively low lifetime risk of progressing to melanoma.<sup>56, 60</sup> Recently, the annual rate of malignant change of a choroidal naevus in Caucasians was estimated to be 1 in 8,845 on average, ranging from 1 in 269,565 in the youngest to 1 in 3,664 in the oldest age group.<sup>47</sup>

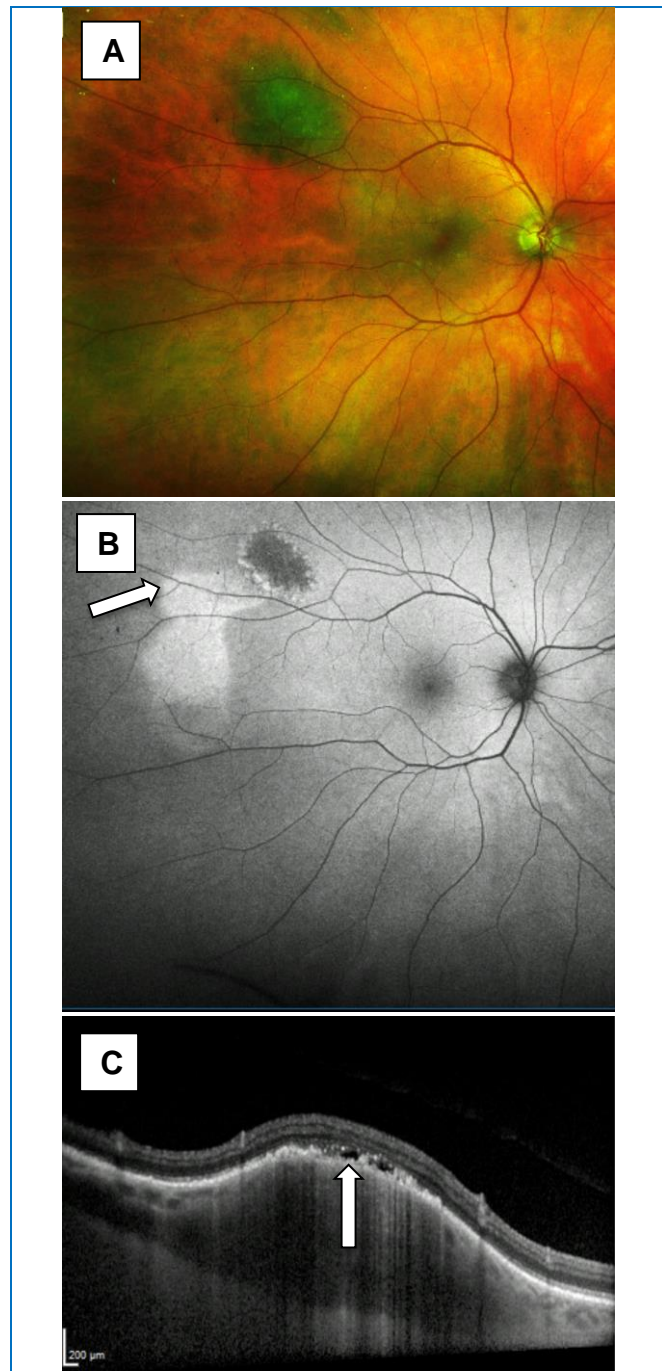
The estimated prevalence of choroidal naevi ranges widely from 3 to 20%, depending on the population and study design. The most recent estimate suggests the prevalence in Caucasians to be between 5 and 10%.<sup>75</sup> To make an efficient diagnosis, it is useful to be familiar both with the epidemiology of naevi and with signs that suggest growth and consequently malignancy.<sup>63, 92, 93</sup>

These calculations can be carried a step further, bringing the focus to the patient level. Starting from a 15-year-old individual and cumulating the risk over lifetime, the risk of a choroidal naevus undergoing malignant change can be estimated to be 0.04% by the age of 40 years, 0.28% by the age of 60 and 0.78% by the age of 80 years.<sup>48</sup> The presumption is then that all melanomas would develop from naevi, which is unlikely. As argued, about 20% of melanomas may develop from naevi, in which case the adjusted lifetime risk would be 0.06% by the age of 60 years and would eventually approach 0.2% or 1 in 500 after the age of 80 years.<sup>47, 63</sup>

### **1.2.5.3. Suspicious choroidal naevi**

In addition to typical choroidal naevi, larger choroidal lesions have been variously categorised as suspicious naevi,<sup>94</sup> intermediate lesions, indeterminate lesions, and even small melanomas.<sup>76</sup> Patients with a choroidal melanocytic tumour with at least one risk characteristic benefit from referral to an ocular oncologist.<sup>59, 79, 95</sup> (Figure 4) The rest of the patients can be made aware of their presumed naevus and that they should be observed periodically.<sup>61, 78</sup> The patients should be told to return immediately if they develop new visual symptoms.<sup>58, 70</sup>

Clinical characteristics and methods of diagnostic differentiation of the choroidal naevi and choroidal melanoma are explained in detail in chapter 1.7.



**Figure 4:** Right eye suspicious melanocytic choroidal naevus, (A) colour optos ultra-widefield (UWF) photograph, with trace of subretinal fluid detected on (B) autofluorescence optos, ultra-widefield (UWF) photograph and (C) OCT spectralis image. (Image source: MEH)

#### **1.2.5.4. Management of choroidal naevi**

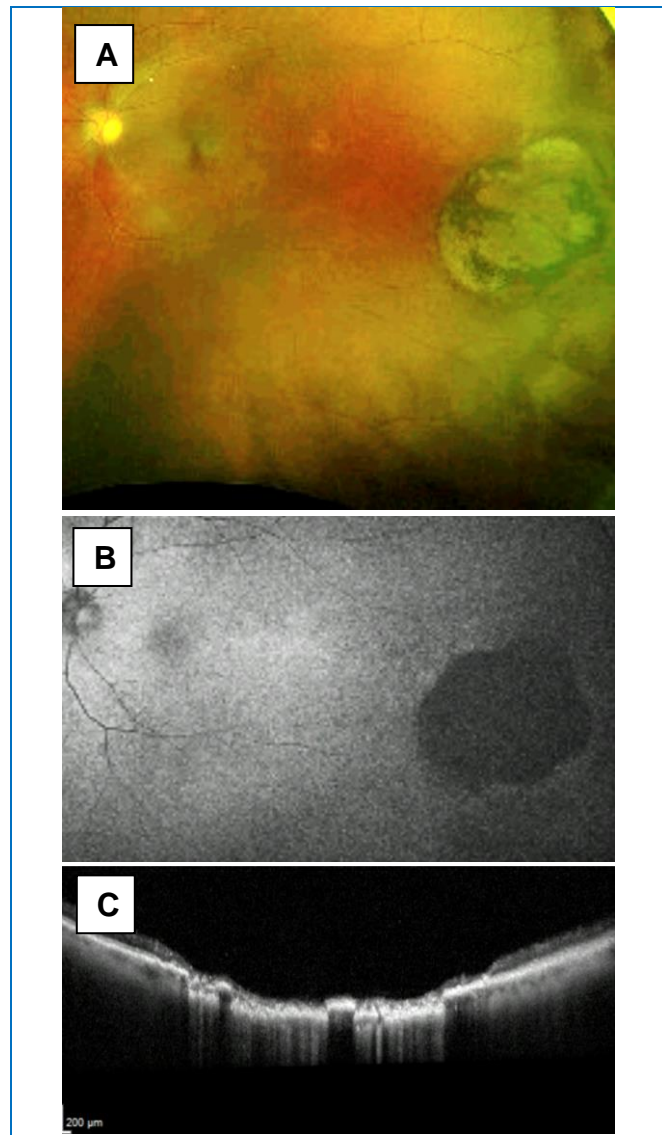
A typical choroidal naevus generally does not require any active therapy.<sup>79</sup> Baseline colour fundus photography,<sup>81, 96, 97</sup> autofluorescence photography<sup>50, 73, 98, 99</sup>, ultrasound,<sup>100-103</sup> and EDI-OCT<sup>57, 64, 104-106</sup> should be performed,<sup>94, 107</sup> and the patient should be assessed every 6 to 12 months to detect any growth of the lesion or other risk factors growth and metastasis. In cases with symptomatic secondary choroidal neovascularisation (CNV) or subretinal fluid,<sup>80</sup> specific methods of laser photocoagulation, photodynamic therapy,<sup>108-112</sup> transpupillary thermotherapy, or injection of anti-vascular endothelial growth factors (anti-VEGF) have been employed to bring about resolution of related subretinal fluid.<sup>69, 88, 110-112</sup> Lesions that show growth or have two or more risk factors for growth or metastasis should generally be considered for treatment, assuming that it could be an early melanoma.<sup>68, 74, 113</sup>

#### **1.2.6. Other pigmented ocular fundus lesions**

Pigmented ocular fundus lesions (POFL) is a descriptive term that has been used to refer to fundus lesions observed in patients with familial adenomatous polyposis (FAP). It is preferred to use the term POFLs rather than CHRPE in FAP because the variety of CHRPE described above is generally not associated with FAP.<sup>114</sup> There are distinct ophthalmoscopic features that distinguish CHRPE from lesions in FAP,<sup>115</sup> and only some of the lesions have histopathologic characteristics compatible with CHRPE.

##### **1.2.6.1. Congenital hypertrophy of the RPE (CHRPE)**

Congenital hypertrophy of the retinal pigment epithelium (CHRPE) is a dark, round, pigmented, flat lesion of the ocular fundus situated at the level of the retinal pigment epithelium.<sup>116</sup> In previous literature, CHRPE was classified as a benign melanoma of the retinal pigment epithelium.<sup>43</sup> (Figure 5)



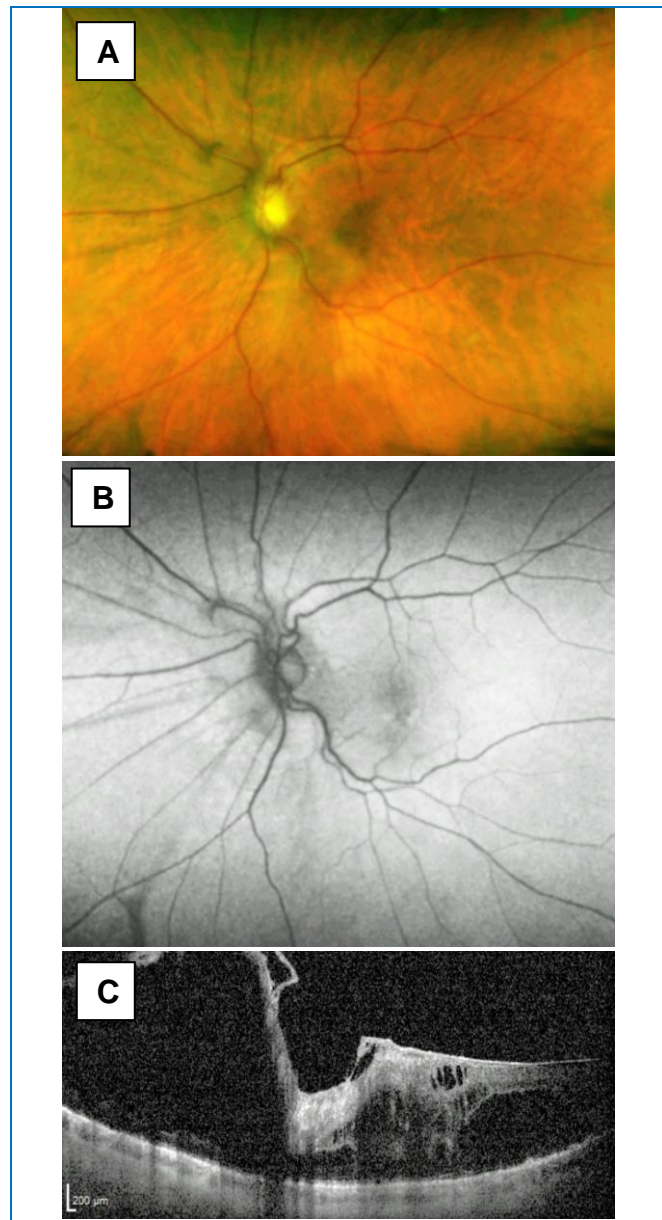
**Figure 5:** Right eye congenital hypertrophy of the retinal pigment epithelium (CHRPE), (A) colour optos ultra-widefield (UWF) photograph, (B) autofluorescence optos, ultra-widefield (UWF) photograph, (C) OCT spectralis. (Image source: MEH)

#### **1.2.6.2. Combined hamartoma of the retina and RPE**

Combined hamartoma of the retina and retinal pigment epithelium (CHR), a term first mentioned by Gass,<sup>117</sup> is a rare development disorder involving the retina and the retinal pigment epithelium. CHR is important because it is often confused with malignancies such as choroidal melanoma or retinoblastoma. Because of the suspicion of a malignant lesion, there have been patients who were enucleated.

Combined hamartoma of the retina and RPE typically appears as a unilateral grey-black coloured lesion with epiretinal membrane. (Figure 6)

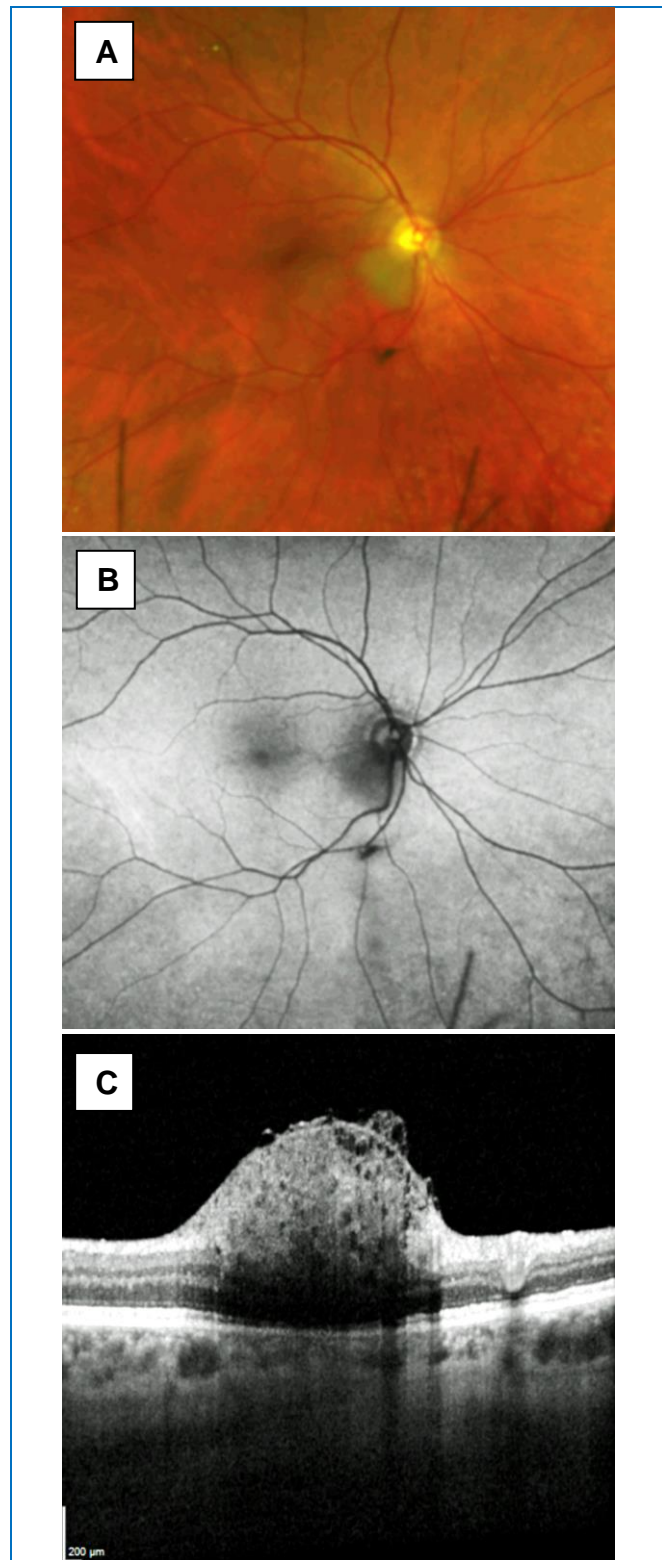
Literature has also described associations of combined hamartomas with neurofibromatosis 2 (NF2),<sup>118, 119</sup> and it is recommended that that a combined hamartoma of the retina and retinal pigment epithelium in children is screened for neurofibromatosis type 2.<sup>120, 121</sup>



**Figure 6:** Left eye combined hamartoma of the retina and retinal pigment epithelium with traction and subretinal fluids. (A) colour optos ultra-widefield (UWF) photograph, (B) autofluorescence optos, ultra-widefield (UWF) photograph, (C) OCT spectralis scan shows an epiretinal membrane with some retinal disturbance including fluid and the architecture of retina is disturbed to full thickness with some underlying retinal pigment epithelial changes. (Image source: MEH)

### **1.2.6.3. Simple hamartoma of the RPE**

The term RPE hamartoma was proposed by Gass.<sup>1</sup> Simple hamartomas of the RPE are extremely rare congenital lesions that were first described by Laqua in 1981,<sup>122</sup> who reported three architectural patterns: superficial retinal involvement, full-thickness retinal involvement and pre-retinal extension, and intrinsic vascularisation. Other clinicians have used the term congenital hamartoma of the RPE to describe these tumours.<sup>123</sup> (Figure 7)



**Figure 7:** Right eye simple hamartomas of the RPE, (A) colour optos ultra-widefield (UWF) photograph, (B) autofluorescence optos, ultra-widefield (UWF) photograph, (C) OCT spectralis, shows no SRF nor IRF. (Image source: MEH)

#### **1.2.6.4. Adenoma and adenocarcinoma of the RPE**

These are rare, acquired tumours of the RPE. The differentiation between adenoma and adenocarcinoma can only be made on the basis of histopathologic findings because of similar clinical findings in both types of tumours. Benign and malignant epithelioma (adenoma) can also originate from the ciliary body pigment epithelium (CPE).<sup>124-127</sup>

### **1.3. Uveal melanoma**

Melanoma is a rare tumour arising from melanocytes located at various anatomic locations, including skin, mucous membrane (nasal mucosa, oropharyngeal, pulmonary, gastrointestinal, vaginal, anal/rectal, urinary tract), ocular region (uvea, conjunctiva, eyelid, orbit), and rarely from unknown primary sites.<sup>128</sup>

Uveal melanoma (UM) is the most common primary intraocular tumour in adults with a mean age-adjusted incidence of 5.1 cases per million per year. In a study of 8033 patients with uveal melanoma by Shields et al., the tumour was located in the iris in 285 (4%), ciliary body in 492 (6%), and choroid in 7256 (90%) cases. The majority (95 %) of ocular melanomas are uveal in origin.<sup>14, 130</sup>

#### **1.3.1. Epidemiological aspects of uveal melanoma**

UM is the commonest intraocular malignancy in adult Caucasians,<sup>130</sup> as a study showed that the risk of developing the disease in choroid and ciliary body, the ratio of black skinned to white skinned patients is 1:98.<sup>131</sup> The increased occurrence of uveal melanoma in lighter skinned people and those with light coloured eyes may be related to less melanin in the retinal pigment epithelium and choroid, which means less protection from ultraviolet light, and increased risk of developing uveal melanoma.<sup>131, 132</sup>



The mean age at the time of diagnosis is between 50 and 60 years.<sup>130, 133-135</sup> A slight predominance of male gender is evident from large series of UM, but the reason for this male predominance is unknown.<sup>65, 69, 70</sup>

Approximately 5% of all melanomas arise in ocular and adnexal structures. Most (85%) ocular melanomas are uveal in origin, whereas primary conjunctival and orbital melanomas are very rare.<sup>128, 136</sup> Uveal melanoma is the most common primary intraocular malignant tumour in adults.<sup>137</sup> Primary uveal melanoma is rarely bilateral.<sup>138</sup> About 90% of all uveal melanomas involve the choroid, the remainder being confined to ciliary body and/or iris. Presentation peaks at around the age of 60 and is rare before adulthood.

Uveal melanomas usually occur sporadically, but there have been rare instances indicative of an inherited predisposition, such as familial uveal melanoma (UM)<sup>139</sup> in young individuals, bilateral primary uveal melanoma, and multifocal puberty<sup>140</sup>, although they can very rarely be present at birth.<sup>141</sup>

However, the genetic basis of metastasis remains unclear, although the presence of BAP1 has a role in preventing of metastasis in UM, while loss of BAP1 is associated with metastasis.<sup>142-144</sup>

Neurofibromatosis type 1 (NF1) is a common autosomal dominant hamartomatous disorder, which is considered to be a neurocristopathy. The association of NF1 and uveal melanoma is controversial. The possibility of an association between NF1 and uveal melanoma has been proposed on the basis of a common neural crest origin.<sup>145, 146</sup> Increased incidence of choroidal naevi in patients with NF1<sup>147</sup> and the supposition that melanomas arise from these naevi may also explain the possible association.<sup>145, 148</sup> Despite the theoretical possibility of an association, the frequency of patients with co-existing NF1 and uveal melanoma is rare.<sup>148</sup>

### 1.3.2. Aetiology and predisposition of uveal melanoma

The aetiology of UM remains unknown. Light blue eyes are also predisposing factors for increased risk for UM.<sup>149</sup> People with lightly pigmented skin, hair, and irises are at a slightly increased risk of developing UM.<sup>150-154</sup>

The Collaborative Ocular Melanoma Study (COMS) found the mean age at diagnosis to be 60 years.<sup>155-157</sup> No risk factors were associated with occupation, tobacco, and hormonal causes.<sup>158-161</sup>

Environmental risk factors include sunlight exposure, and several case-control studies have attempted to investigate the relation between sunlight and the risk of developing uveal melanoma.<sup>133</sup> There is no conclusive evidence that sunlight is implicated in posterior uveal melanoma formation.<sup>162</sup>

In summary, the aetiology of uveal melanoma remains obscure, although several host and environmental factors have been explored in case-control studies. Clinical, epidemiological, physiological, and genetic evidence argues against a major role of UV light in the causation of uveal melanoma.<sup>163</sup>

### 1.3.3. Congenital uveal melanoma

Uveal melanoma is rare in children under the age of 5 years.<sup>164-169</sup> Based on Shields et al. study of 8033 patients and other smaller series, the prevalence of UM in patients younger than 21 years has constituted 0.8% to 1.1%.<sup>170</sup> Accordingly, given the prevalence of fewer than 7000 worldwide cases of UM each year, about 60 cases per year should be included in the youth group.<sup>170</sup>

Other studies showed that children with different ocular melanoma have a more favourable life prognosis compared to adult's ocular melanoma published reports and the association between gender and site of melanoma is varied between age groups.<sup>171-173</sup>

### 1.3.4. Iris melanoma

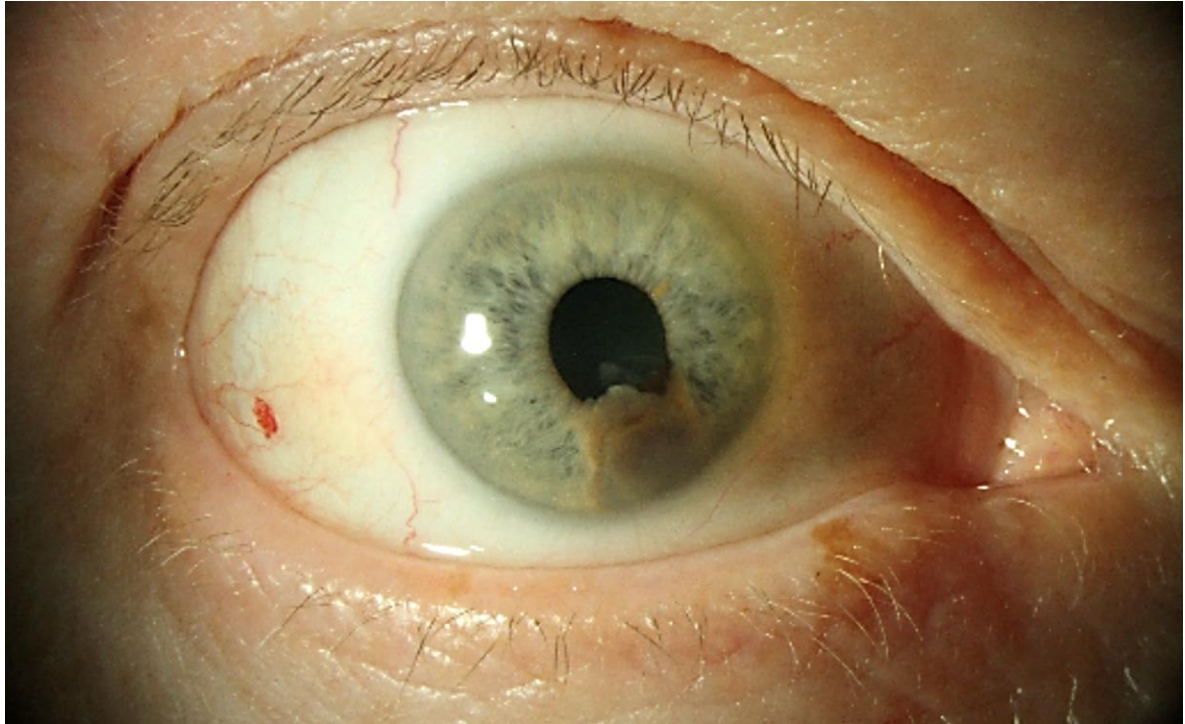
Iris melanoma is the least frequent of all uveal melanomas.<sup>4, 154, 172</sup> Due to its anterior location, iris melanoma can be diagnosed and treated when relatively small in comparison to tumours located in the choroid and ciliary body.

Iris melanoma is also inclined to be less aggressive than melanomas in other uveal locations.<sup>18</sup> The 5-year rates of metastasis rate are reported to range from 3% to 10%.<sup>149, 174</sup>

#### 1.3.4.1. Clinical features of iris melanoma

Iris melanoma may be circumscribed or diffuse. Slit lamp examination, gonioscopy, and ultrasound biomicroscopy (UBM) allow staging of the tumour to guide the most appropriate treatment.

The clinical factors predictive of metastasis include diffuse melanoma, elevated intraocular pressure, and extraocular extension.<sup>153, 174</sup> Melanoma located in the peripheral iris (Figure 8) may represent anterior extension of a ciliary body tumour. Therefore, it is crucial to examine the ciliary body in cases of iris melanoma when all iris margins of the tumours are not visualised.<sup>175, 176</sup>



**Figure 8:** Slit lamp colour photograph of a right eye iris melanoma associated with iridocorneal touch, and uveal ectropion. Ultrasound B-scan measured thickness of 3.3 mm with horizontal base of 3 mm. There was no involvement of the ciliary body, but the iris mass extends into the angle and abstract any clear view under gonioscopy, no angle seeding or pigment dispersion was present, and the intra ocular pressure is normal measuring 14mmHg. (Image source: MEH)

### 1.3.5. Ciliary body melanoma

Ciliary body melanoma is a subtype of uveal melanoma and a common primary malignant tumour of the eye.<sup>177</sup>

Ciliary body melanoma may be circumscribed or annular (ring).<sup>178</sup> Slit lamp examination, gonioscopy, transillumination, and ultrasound biomicroscopy (UBM) allow staging of the tumour to guide the most appropriate treatment.<sup>17, 19</sup>

#### 1.3.5.1. Clinical features of ciliary body melanoma

The tumour can have a dome shape or can grow circumferentially, and it can be pigmented or amelanotic.<sup>179</sup> Almost all cause dilatation of the overlying episcleral vessels ('sentinel vessels'). As with choroidal melanomas, it can also cause retinal detachment. Pressure on the lens can lead to astigmatism and cataract<sup>178</sup> and the

tumour can spread into the anterior chamber or extraocularly to appear under the conjunctiva.

### 1.3.6. Choroidal melanoma

The choroid is rich in blood vessels and can be imagined as a sponge-like membrane between the retina and the outer sclera at the back of the eye.<sup>46, 47, 180</sup> The choroid supplies nutrients to the retina.<sup>181</sup> This layer contains melanocytes which can form tumours such as naevus or melanoma.

With time, many choroidal melanomas enlarge and cause the retina to detach, potentially leading to vision loss.<sup>72, 76, 182, 183</sup> The tumours can also spread and metastasise to other parts of the body, with the liver being the most common site for metastasis, causing this cancer to be fatal.<sup>14, 46, 184-186</sup>

The diagnosis of choroidal melanoma (Figure 9) is based on clinical examination with the slit lamp, and indirect ophthalmoscope together with optical coherence tomography (OCT), autofluorescence fundus photography (AF), and ultrasonography of the eye.<sup>47, 102</sup> Choroidal melanomas can also be missed unless the fundus is meticulously examined after full pupillary dilatation. Digital photography is most useful for documenting their size and location.<sup>47, 65</sup> Newer modalities such as OCT and AF are also useful.<sup>64, 87, 187, 188</sup>

#### 1.3.6.1. Clinical features of choroidal melanoma

Uveal melanomas develop from melanocytes that reside within the stroma of the choroid, ciliary body, and iris. The basement membrane does not need to be breached when the tumour develops,<sup>189</sup> in contrast to systemic cancers. Choroidal melanoma typically presents as a sessile, dome-shaped (with brown/grey colour from multi-layering of the RPE, which can also show drusen and clumps of lipofuscin located in the retina), or mushroom-shaped mass deep to the sensory retina.<sup>162, 176</sup>

A smaller posterior choroidal melanoma may have overlying orange pigment at the level of the retinal pigment epithelium (RPE).<sup>68, 69, 74, 113, 170, 190</sup> (Figure 9)

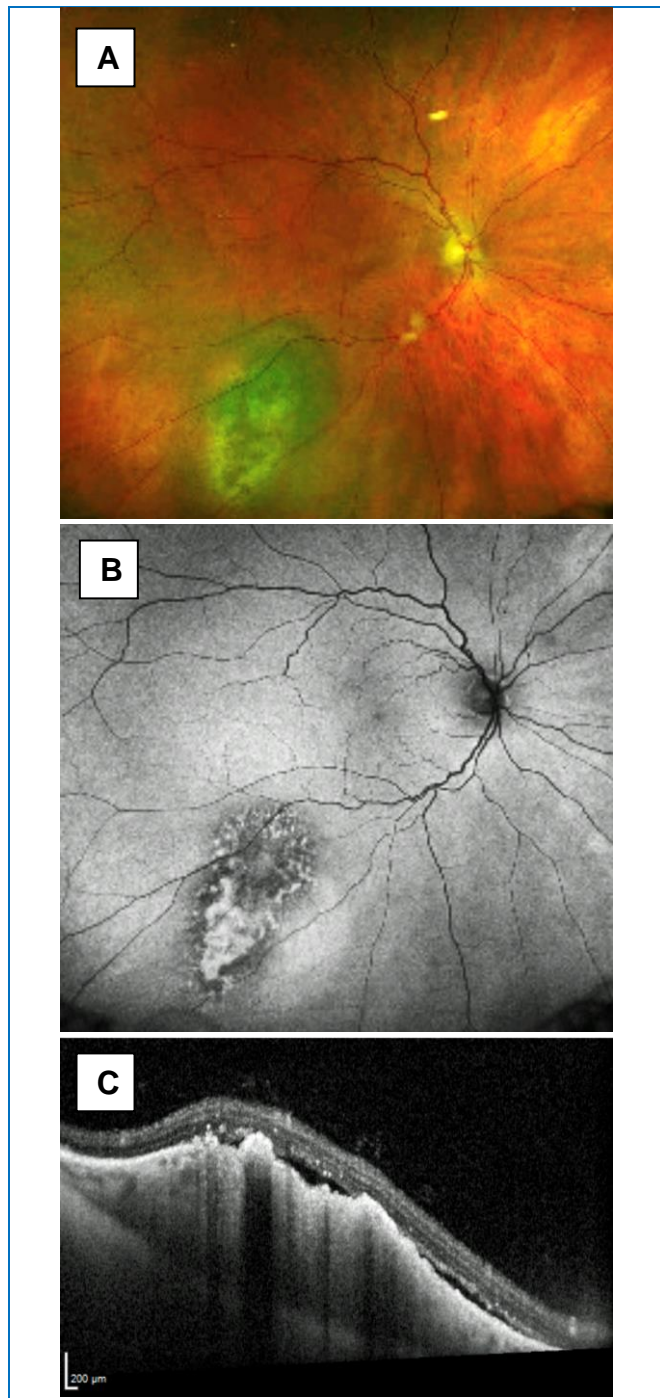
A secondary non-rhegmatogenous retinal detachment often occurs. In contrast to a rhegmatogenous detachment, in which the subretinal fluid does not shift, the fluid with a melanoma and other tumour shifts with positional changes of the patient's head. In some cases, a choroidal melanoma can be partly or entirely non-pigmented.<sup>107, 191</sup> When the tumour is amelanotic, blood vessels in the tumour are visible ophthalmoscopically.<sup>69</sup> A choroidal melanoma can rupture the Bruch's membrane and assume a mushroom shape with continued growth. (Figure 11)

When that occurs, the tumour has a tendency to bleed, and vitreal or subretinal blood can sometimes obscure a view of the underlying tumour. Choroidal melanoma can also assume a diffuse growth pattern with only minimal elevation of the tumour.<sup>46, 189, 190</sup> In this case, it can be infiltrative, often with extraocular extension by the time diagnosis is made.<sup>33, 192</sup> Exudative retinal detachment, initially only over the tumour surface, eventually becoming total.<sup>190</sup>

Retinoinvasive melanoma is rare and tends to evolve from a ring melanoma. They grow slowly, which may favour emergence of tumour clones able to migrate, adhere to, and invade into the neuroretina, analogous to the metastatic cascade.<sup>193, 194</sup> Ocular inflammation may be the first clinical sign in patients with malignant melanoma of the choroid and ciliary body (MMCCB).<sup>195-197</sup>

Tumours adjacent to the optic nerve can simulate the optic nerve.<sup>198</sup> Other manifestations can lead to choroidal neovascular membrane (CNVM) and retinal vascular occlusion, which are rare.<sup>199, 200</sup>

In some other cases, ciliary body or choroidal melanoma can cause total cataract, secondary glaucoma and extraocular extension into the orbit. Such tumours are generally larger and carry a worse prognosis.<sup>69, 190</sup>



**Figure 9:** Right eye choroidal melanoma, (A) colour optos ultra-widefield (UWF) photograph, (B) autofluorescence optos, ultra-widefield (UWF) photograph shows significant amounts of lipofuscin, (C) OCT spectralis shows amount of subretinal fluids and lipofuscin. (Image source: MEH)

### 1.3.7. TNM classification of uveal melanomas (UICC TNM 8)

The primary purpose of the TNM system is to provide an anatomic-based classification to depict cancer prognosis adequately. Accurate cancer staging is essential for treatment selection, outcome prediction, research design, and cancer control activities.<sup>201, 202</sup>

The Tumor, Node, Metastasis (TNM) System is an international classification developed in collaboration by the American Joint Committee on Cancer (AJCC) and the Union for International Cancer Control (UICC) to aid in the management, research and assessment of prognosis for different forms of cancer.<sup>203</sup> The TNM classification for UM has evolved in recent years.<sup>204, 205</sup>

TNM classification categorises tumours according to the extent of the primary tumour and the presence or absence of lymph node involvement and metastasis.<sup>206</sup> For example, choroidal melanomas are grouped according to basal tumour diameter, tumour height, and extraocular extension.<sup>207</sup> It must be emphasised that this is actually a staging system, because the different groups represent various levels of advancement of the same tumour rather than different classes.<sup>204, 208</sup> In other words, what is being classified is the stage of disease and not the disease itself. It is not simply a play on words, because when survival statistics are based on the TNM system it must be remembered that the different groups are time dependent, so that it is essential to take lead-time bias into account.<sup>209</sup>

Pathologic stage classification (pTNM) is provided by the pathologist, and is based on gross and microscopic examination, such as melanoma cell type, mitotic count, extravascular matrix patterns, chromosome 3, and chromosome 8q gain. The Liverpool Uveal Melanoma Prognosticator Online (LUMPO),<sup>210</sup> a freely available online tool, has been developed to establish the prognosis for uveal melanoma patients.<sup>211</sup> It generates an all-cause mortality curve according to age, sex, AJCC TNM size category (based on basal tumour diameter and tumour height), ciliary body involvement, melanoma cytomorphology, closed loops, mitotic count, chromosome 3 loss and presence of extraocular spread.<sup>212 213</sup>



It is the managing clinician's responsibility to define the final pTNM stage based on all relevant information.<sup>214</sup>

Clinical classification (cTNM) is typically carried out by the clinician during the initial clinical evaluation of the patient (before treatment) or when pathologic classification is not possible.

The current TNM 8th Edition provides clinical useful definitions of tumour size, location, and metastatic disease for almost all eye cancers, including UM. This classification will allow ocular oncologists to compare treatments on equivalently sized and 'staged' tumours. Introducing this staging system will improve participation in clinical trials and compliance with cancer centre status.<sup>202, 204, 205, 215, 216</sup>

Lymph node metastases arising from uveal melanomas are very rare since the eye does not bear lymphatic vessels.<sup>217</sup> Therefore, TNM/ Regional lymph node (N) application to malignant melanoma is not useful.

Table 1 provides information on staging using UICC TNM 8, which should be used for all tumours diagnosed after 1 January 2018.<sup>204, 205</sup>

TNM classification of uveal melanoma (UICC TNM 8)	
<b>Anatomical sites</b>	
C69.4	Iris
C69.4	Ciliary body
C69.3	Choroid
<b>Primary tumour (T)</b>	
TX	Primary tumour cannot be assessed
T0	No evidence of primary tumour
<b>IRIS</b>	
NB: Iris melanomas originate from, and are predominantly located in, this region of the uvea. If less than half of the tumour volume is located within the iris, the tumour may have originated in the ciliary body and consideration should be given to classifying it accordingly.	

T1		Tumour limited to the iris
	T1a	Not more than 3 clock hours in size
	T1b	More than 3 clock hours in size
	T1c	With secondary glaucoma
T2		Tumour confluent with or extending into the ciliary body, choroid, or both
	T2a	Tumour confluent with or extending into the ciliary body without secondary glaucoma
	T2b	Tumour confluent with or extending into the choroid without secondary glaucoma
	T2c	Tumour confluent with or extending into the ciliary body and/or choroid with secondary glaucoma
T3		Tumour confluent with or extending into the ciliary body, choroid, or both, with scleral extension
T4		Tumour with extrascleral extension
	T4a	Less than 5 mm in diameter
	T4b	Greater than 5 mm in diameter

### CILIARY BODY and CHOROID

Primary ciliary body and choroidal melanomas are classified according to the four tumour size categories below:

Thickness (mm)							
>15	4	4	4	4	4	4	4
12.1–15.0	3	3	3	3	3	4	4
9.1–12.0	3	3	3	3	3	3	4
6.1–9.0	2	2	2	2	3	3	4
3.1–6.0	1	1	1	2	2	3	4
≤3.0	1	1	1	1	2	2	4
	<3.0	3.1–6.0	6.1–9.0	9.1–12.0	12.1–15.0	15.1–18.0	>18
	Largest basal diameter of tumour (mm)						

T1		Tumour size category 1
	T1a	Without ciliary body involvement and extraocular extension
	T1b	With ciliary body involvement
	T1c	Without ciliary body involvement but with extraocular extension ≤5 mm in diameter
	T1d	With ciliary body involvement and extraocular extension ≤5 mm in diameter

T2	Tumour size category 2
T2a	Without ciliary body involvement and extraocular extension
T2b	With ciliary body involvement
T2c	Without ciliary body involvement but with extraocular extension $\leq 5$ mm in diameter
T2d	With ciliary body involvement and extraocular extension $\leq 5$ mm in diameter
T3	Tumour size category 3
T3a	Without ciliary body involvement and extraocular extension
T3b	With ciliary body involvement
T3c	Without ciliary body involvement but with extraocular extension $\leq 5$ mm in diameter
T3d	With ciliary body involvement and extraocular extension $\leq 5$ mm in diameter
T4	Tumour size category 4
T4a	Without ciliary body involvement and extraocular extension
T4b	With ciliary body involvement
T4c	Without ciliary body involvement but with extraocular extension $\leq 5$ mm in diameter
T4d	With ciliary body involvement and extraocular extension $\leq 5$ mm in diameter
T4e	Any tumour size category with extraocular extension $\leq 5$ mm in diameter
<b>Regional lymph nodes (N)</b>	
NX	Regional lymph nodes cannot be assessed
N0	No regional lymph node involvement
N1	Regional lymph node metastasis or discrete tumour deposits in the orbit
N1a	Metastasis in one or more regional lymph node(s)
N1b	No regional lymph nodes are positive, but there are discrete tumour deposits in the orbit that are not contiguous to the eye
<b>Distant metastasis (M)</b>	
M0	No distant metastasis by clinical classification
M1	Distant metastasis
M1a	Largest diameter of the largest metastasis 3 cm or less
M1b	Largest diameter of the largest metastasis greater than 3 cm but less than or equal to 8.0 cm
M1c	Largest diameter of the largest metastasis greater than 8 cm

**Table 1:** TNM classification of uveal melanoma (TNM 8th edition)<sup>204, 205</sup>

## 1.4. Clinical investigations and examination techniques

### 1.4.1. Imaging

Ocular cancers are unique among eye diseases, threatening both vision and life. The diagnosis can be made using a careful clinical history and specialised ocular examination in most cases.<sup>53, 94</sup> Eye cancer diagnoses rely strongly on imaging techniques such as high-frequency ultrasound, anterior and posterior segment optical coherence tomography, fluorescein angiography, magnetic resonance imaging (MRI), and computed tomography (CT).<sup>45, 50, 65, 72, 81, 97, 105, 188, 218-220</sup> Once the diagnosis is confirmed, treatment decisions depend on the tumour's location, size, local extension, patterns of growth, and secondary complications. The core of the following section is an overview of applicable imaging modalities and techniques used in ocular oncology to help diagnose ocular tumours.

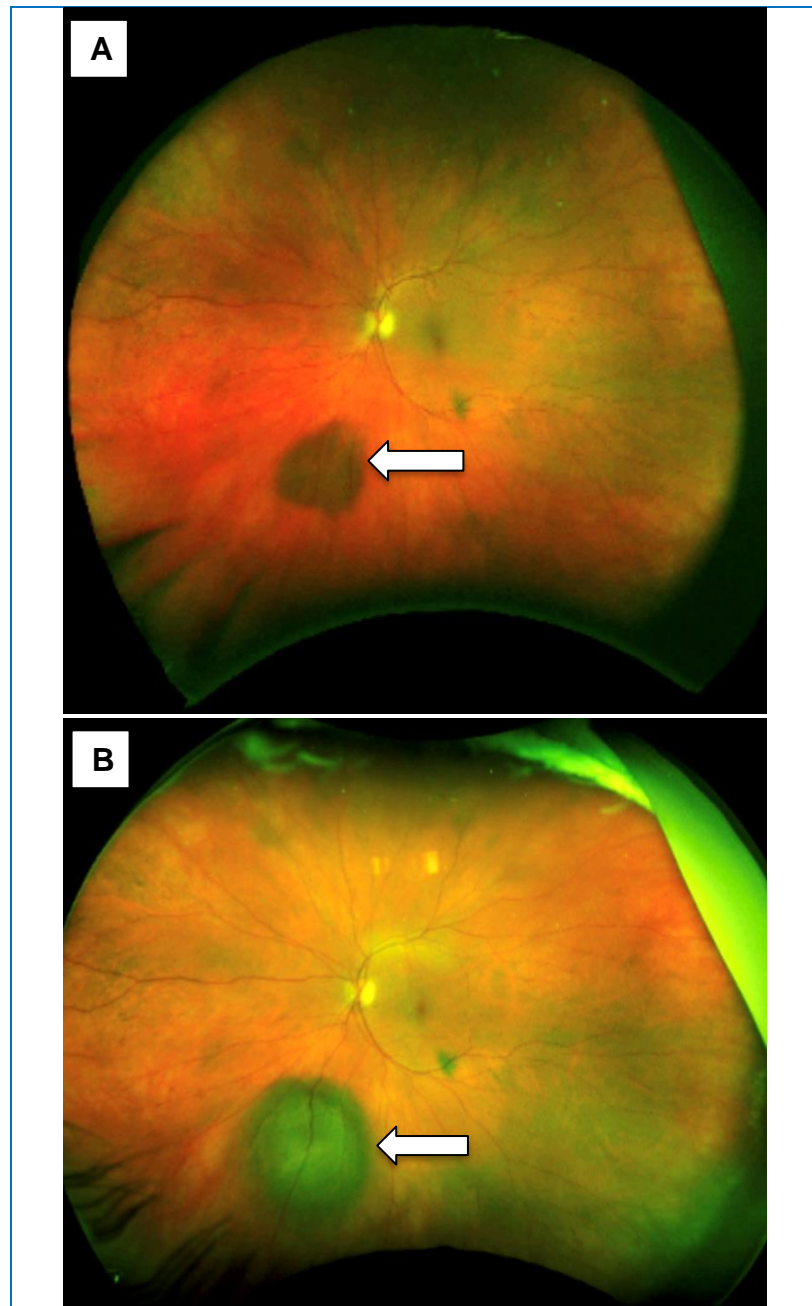
#### 1.4.1.1. Fundus photography

Fundus colour images help in viewing and baseline documentation of the abnormalities observed within the fundus on clinical examination.<sup>221</sup> They help monitor the progression or resolution of the posterior segment manifestations within the retina and choroid.<sup>65</sup>

Fundus colour images help in viewing and baseline documentation of the abnormalities observed within the fundus on clinical examination. They help monitor the progression or resolution of manifestations within the retina and choroid.<sup>50</sup>

Documenting the tumour size and its distances from optic disc and fovea (e.g., in disc diameters) is particularly useful when the tumour shows diffuse spread that is not adequately defined with ultrasonography.<sup>53, 86</sup> Capturing the circumferential location of the tumour with respect to fovea is useful when preparing a 3-D model of the eye for planning radiotherapy.

Colour photography helps determine whether the tumour is growing, for example, differentiating naevus from melanoma or detecting marginal tumour recurrence after conservative therapy.<sup>79, 94, 222</sup> (Figure 10)



**Figure 10:** Left eye colour photographs showing malignant transformation from a melanocytic choroidal naevus with marginal tumour recurrence after conservative therapy. (A) colour optos ultra-widefield (UWF) photograph from May 2019, (B) colour optos ultra-widefield (UWF) photograph from March 2021. (Image source: MEH)

#### 1.4.1.2. Ultra-widefield retinal imaging

The widefield systems include laser, optical, and lens-based systems that are contact or non-contact lens systems, each with its own benefits and drawbacks.<sup>81</sup>

Heidelberg Spectralis (Heidelberg, Engineering, Inc., Heidelberg, Germany) and Optos (Optos PLC, Dunfermline, UK) are two commonly used non-contact, laser-based systems.<sup>223</sup> Because of the green filter over the image, colour distortion is, at the time of this review, the main limitation of optos.<sup>224</sup> Optos has attained popularity in clinics because it is a clinic-based, non-mydratiac system with ultra-wide fields of view.<sup>81, 221, 225</sup> The Clarus 500 (Carl Zeiss Meditec Inc., Dublin, CA) has been recently released for commercial use and reported the widest field of view with minimal colour distortion.<sup>226</sup> Like all widefield imaging technologies, the camera attempts to capture a three-dimensional structure with a two-dimensional image, and this can result in artefacts and peripheral aberrations.<sup>188</sup> Ret Cam 3 (Clarity Medical Systems, Pleasanton, CA), a contact lens optical system, is commonly used in paediatric ophthalmology because of its FA capability and widefield of view.<sup>227-229</sup>

As imaging characteristics of fundus tumours have been better characterised, using multiple imaging modalities may enhance the diagnostic accuracy of the clinician.<sup>230</sup>

The periphery of the retina is affected by a variety of choroidal and retinal disorders. Traditional fundus cameras captured only 30-50° of the retina, and the peripheral retina remained undocumented.<sup>222</sup> Documentation is important for management, monitoring, and follow-up of retinal diseases and serves an irreplaceable part in medical teaching, counselling, and patient education.<sup>53</sup> The role of documentation in the modern medicolegal telemedicine era has become more critical.<sup>231-236</sup>

Optos (Optos Inc, Dunfermline, UK) is an ultra-widefield (UWF) imaging system that allows the capture of 200 degrees of the retina (approximately 82% of retinal surface area) in a single click.<sup>220</sup> It provides non-contact, high-resolution images of the retina quickly, even through a small pupil, using an ellipsoid mirror and virtual point technology.<sup>97</sup> Optos is based on a confocal scanning laser ophthalmoscope and

uses red (633 nm) and green (532 nm) lasers for colour images, blue laser (488 nm) for fundus fluorescein angiography (FFA), green laser for fundus autofluorescence (AF), and infrared laser (802 nm) for indocyanine green angiography (ICGA).<sup>222</sup>

In the literature, widefield and ultra-widefield imaging have been used interchangeably without clear definitions. The Diabetic Retinopathy Clinical Research Network (DRCR.net) defined UWF images to have at least a 100° view of the fundus.<sup>222</sup> Recently, a group of experts in the field introduced that the term widefield should be used for photographs showing retinal features beyond the posterior pole but posterior to vortex vein ampulla in all four quadrants. UWF should be restricted to photographs in a single capture showing retinal features anterior to vortex vein ampullae in all four quadrants.<sup>237</sup> An image which can detail ora to ora in 360 degrees is termed 'Panretinal'. Though montaging techniques with optos can produce panretinal images, currently, no device can capture such an image in a single click.<sup>237</sup>

UWF imaging plays an important role in ocular oncology and has been used extensively in the evaluation and management of choroidal tumours.<sup>46, 72, 78, 94, 107, 188, 238</sup>

In the field of oncology, UWF imaging has found a particular role for diagnosis and documentation of tumours, planning their management, following their course and monitoring complications.<sup>96, 188, 219, 239, 240</sup> Its utilisation has expanded from fundus photography initially, to include autofluorescence, optical coherence tomography and angiography.<sup>188, 240, 241</sup> UWF imaging is essential in the context of multiple choroidal metastases that are present anterior to the equator and could have potentially been missed on examination. Furthermore,<sup>242</sup> it may also aid in easier differentiation between benign naevi and choroidal melanoma by allowing meticulous measurements of the tumour size, assessment of overlying pigment changes, and evaluating change in the tumour size on follow-up.<sup>79, 94, 188</sup>

Ayres et al.<sup>239</sup> compared various radiological, conventional and UWF imaging techniques with clinical examination for measuring the choroidal tumours. UWF

imaging was considered more comparable to the clinically estimated tumour basal diameter than the findings of other imaging tools. Kernt et al.<sup>81</sup> also found UWF measurements to correlate well with ultrasound measurements for melanotic tumours. They also used two lasers of UWF imaging to differentiate between benign and malignant lesions of the choroid, both sensitivity and specificity exceeding 70%, with malignant lesions being darker with red spectrum.<sup>81</sup> Fundus images are captured with two low-powered laser wavelengths: green channel (GC) at 532 nm and red channel (RC) at 633 nm that scan the retina simultaneously. The single image can be disassembled to analyse the individual wavelength views. The GC allows a perspective from the sensory retina to the retinal pigment epithelium (RPE), and the RC scans the deeper structures from the RPE to the choroid.<sup>187</sup>

UWF-FAF is another valuable tool for differentiating melanomas from naevi. Reznicek et al.<sup>99</sup> reported mean FAF intensity to be significantly lower in malignant lesions as compared to the benign naevi.

However, UWF imaging should be used carefully when measuring the size of tumours as ultrasound may be better when tumour height exceeds 3 mm and in presence of exudative retinal detachment.<sup>239</sup> Further estimation of tumour dimensions can be tricky as peripheral most areas of the fundus appear to be stretched specifically in the horizontal axis.<sup>96</sup> UWF being primarily based on pseudo-colour images, there have also been concerns over the difficulty in differentiating between tumours on UWF, specifically between melanotic and vascular tumours.<sup>222</sup>

UWF imaging has enhanced ocular oncologists' ability to fully examine the retina in several disease states.<sup>188, 240, 241</sup> Given how UWF imaging can improve diagnosis and monitoring, modern retina practices stand to benefit by utilising this platform.<sup>96, 220, 226, 240</sup>

#### **1.4.1.3. Ultrasonography (US)**

Ultrasonography (US) is used routinely for uveal melanoma diagnosis and tumour size measurement.<sup>102, 243</sup>

The diagnosis of UM is most often based on the typical appearance of the tumour on fundus examination and B scan ultrasound.<sup>19, 100, 102, 244, 245</sup> The key clinical



features are size, shape, exudative retinal detachment and orange lipofuscin pigment.<sup>41, 74, 76, 79, 246, 247</sup>

The inner parts of the tumour give a low-reflective shadow in B-scan ultrasound.<sup>175</sup>

Ultrasonography can define the shape of the tumour (i.e., Dome, diffuse, multi-lobe or mushroom shape) and may as well detect posterior extraocular tumour extension.<sup>100, 248</sup> (Figure 11) Ultrasonography is also essential in atypical retinal detachments where the choroidal tumour may underlie detached retina, where there are smooth retinal bullae, where fluid shifts, where no break is visible, and where intraocular pressure elevates.<sup>249</sup> Ultrasound examination is significant in eyes with opaque media (cornea, aqueous, lens, vitreous) when a choroidal tumour is suspected.<sup>249</sup>

A mushroom shape is almost pathognomonic of uveal melanoma. Ultrasonography is not useful for monitoring small tumours to measure tumour dimensions because colour photography and OCT are usually more sensitive.<sup>86, 103</sup>

Colour Flow Mapping is a technique to image blood flow in colour and is available on array scanners. Most melanomas have a maximum systolic velocity of around 11 cm/s (range 5–30 cm/s). The higher velocities in this range are only seen in aggressively growing lesions. Choroidal haemangiomas appear highly vascular on colour flow mapping, and systolic velocity within most is around 20 cm/s. (range 15–50 cm/s).<sup>247</sup>

Furthermore, ultrasound demonstrates internal acoustic reflectivity, which may suggest a particular diagnosis.<sup>86</sup> It provides acoustic information in ophthalmoscopically visible masses: differentiation from choroidal or retinal detachment, cystic lesion, or subretinal haemorrhage; accurate size and height measurement with serial sectioning; and tumour type characterisation by acoustic profile.<sup>249</sup>

In conclusion, ultrasound techniques are an essential part of ocular oncology, particularly as most intraocular tumours do not undergo diagnostic biopsy. B-scan

with colour flow mapping is very useful in refining the differential diagnosis. 17, 102, 243, 249



**Figure 11:** Ultrasonography of a right eye choroidal melanoma showing a large 'mushroom' shape lesion, Location grossly nasal extending beyond the equator. Internal echogenicity: medium to low, Thickness of 14.4mm with a transverse base of 9.2mm x longitudinal base 11.2 mm. (Image source: MEH)

#### **1.4.1.4. Anterior segment photography**

Anterior segment photography is used to document the size, shape, and surface features of iris lesions such as cysts, naevi, and melanomas. Anterior segment

photography can also help capture large ciliary body melanomas<sup>250</sup> when they are visible through a widely dilated pupil.<sup>251</sup>

OCT angiography (OCTA) has been applied to visualise malignant iris melanomas compared to benign iris lesions, such as iris freckles, naevi, and pigment epithelial cysts. In one cross-sectional study, OCTA of iris melanomas demonstrated vascular tortuosity and disorganisation with increased intralesional vascular density as compared to benign iris lesions and normal controls.<sup>252</sup> These findings were previously described using FA.<sup>253, 254</sup>

Ultrasound biomicroscopy is a valuable newer technique in assessing anterior segment tumours. It provides diagnostic information, accurate localisation of lesions, and the ability to accurately measure lesions too small to be measured by any other means.<sup>101, 255</sup>

#### **1.4.1.5. Fundus autofluorescence (FAF)**

Fundus Autofluorescence (FAF) is a non-invasive, valuable diagnostic tool for assessing intraocular tumours and the related features, based primarily on the effects on the overlying RPE.<sup>98</sup> Some findings are strongly characteristic of certain tumours, particularly the bright hyperautofluorescence overlying small choroidal melanoma (Figure 12) and the dark hypoautofluorescence of congenital hypertrophy of the RPE.<sup>98</sup> (Figure 5)

The orange pigment can be clinically visualised as geographic flat, dull orange debris on the tumour surface, but often it is subtle and nearly invisible. Lipofuscin can also develop over other kinds of tumours, such as metastases and haemangiomas.<sup>73, 256</sup> Imaging with autofluorescence is ideal for the detection of orange lipofuscin pigment overlying small melanoma and has evolved into an important test for the differentiation of melanoma from naevus.<sup>129</sup> (Figure 12)



**Figure 12:** Autofluorescence image, showing a right eye with orange lipofuscin pigment overlying small choroidal melanoma, associated with a trace of subretinal fluid. (Image source: MEH)

#### **1.4.1.6. Fluorescein angiography (FA)**

In the past, fluorescein angiography (FA) has been commonly used in the diagnostic evaluation of choroidal tumours to identify the double circulation pattern typical of UM.<sup>257</sup> However, double circulation is only seen if Bruch's membrane breaks. It has been proven useful in the differential diagnosis of vascular tumours, such as choroidal haemangiomas, disciform lesions, choroidal detachments, retinal vasoproliferative tumours (VPT), retinal capillary haemangioma (RCH) and haemorrhagic lesions. Anterior segment fluorescein angiography has limited applications in rare cases of iris haemangiomatous lesions.<sup>253</sup>

At an average of 18 minutes after injection of the dye, choroidal melanomas achieve maximal fluorescence.<sup>258</sup> In general, non-pigmented choroidal melanomas show an earlier onset of fluorescence (<1 minute) than the pigmented variety (3 minutes).<sup>259</sup>

Fluorescein angiography is most useful when investigating retinal vascular tumours and ocular neovascular complications.<sup>260, 261</sup>

If late diffuse leakage is absent within the choroidal tumour goes against the diagnosis of choroidal melanoma.<sup>257</sup>

#### **1.4.1.7. Indocyanine green angiography (ICG)**

Indocyanine green angiography (ICG), a more recent diagnostic method,<sup>262, 258</sup> that has been recently introduced into clinical practice. It permits better visualisation of choroidal vasculature and has been shown to be superior to FA in imaging tumour vascularisation.<sup>263</sup>

The principles of fluorescein angiography apply to indocyanine green angiography (ICG), except that the infrared light is not absorbed by melanin and haemoglobin to the same extent as fluorescein, so that changes in the RPE and retina are less conspicuous, so that choroidal vasculature is visible. Although choroidal haemangiomas show typical features on ICG angiography, this investigation is not usually necessary because the ophthalmoscopic appearances are so characteristic.<sup>264</sup>

Indocyanine green angiography allows improved visualisation of the tumour vasculature than fluorescein angiography because of several physicochemical properties of indocyanine green (ICG).<sup>259, 265</sup> Indocyanine green absorbs and emits light in the near-infrared spectrum, with wavelengths absorbed less by the choroid and retinal pigment epithelium.<sup>266</sup> Due to its high affinity to bind with plasma proteins,<sup>267</sup> ICG has the tendency to stay within fenestrated choriocapillaris, with slow extravasation into choroidal stroma.<sup>268</sup> This allows visualisation of larger choroidal vessels.<sup>251</sup>

#### 1.4.1.8. *Optical coherence tomography (OCT)*

Optical coherence tomography (OCT) is a non-invasive, non-contact, transpupillary imaging method that can analyse the retina and choroid in cross-section with 8-10  $\mu\text{m}$  depth resolution.<sup>269</sup> Optical coherence tomography is a potentially useful technique for high depth resolution, cross-sectional examination of the fundus.<sup>269</sup> Enhanced depth imaging optical coherence tomography is an important tool for the imaging of retinal and RPE tumours in adults and children. In comparison to OCT, the resolution of ultrasound is limited by the acoustic wavelength in ocular tissue to about 150  $\mu\text{m}$ .<sup>270</sup>

OCT is also a powerful imaging modality for the posterior segment of the eye.<sup>271</sup> Initially, with time-domain OCT (TD-OCT) technology, cross-sectional imaging of the retina was possible with a resolution of approximately 10  $\mu\text{m}$ .<sup>64, 272</sup> Additional refinements with spectral domain OCT (SD-OCT) has enabled the depiction of the different layers of the neurosensory retina. Enhanced depth imaging OCT (EDI-OCT) recently has provided a better resolution of approximately 3-4  $\mu\text{m}$  with the ability to image deeper within the choroid and sclera.<sup>218</sup> Imaging with OCT has become a routine, nearly essential step of ophthalmology, particularly for diagnosis and therapy of retinal disease.<sup>79, 86</sup>

Optical coherence tomography may also provide information about the retinal structure overlying prominent tumours and the extent of adjacent retinal detachment.<sup>273</sup> In its present state of development, OCT is especially valuable in the differential diagnosis of small choroidal tumours in detecting incipient retinal detachment. Its possible benefit for the follow-up of shallow tumours needs further investigation.<sup>273</sup>

Several features make OCT attractive for imaging ocular tissue. OCT has a superior resolution to conventional clinical ultrasound that is limited by the acoustic wavelength in tissue.<sup>274</sup> Unlike ultrasound, optical coherence tomography does not require contact with the tissue examined or saline immersion of the eye.<sup>275</sup> High-resolution imaging is possible in the posterior part of the eye, where signal

attenuation limits the application of high-frequency ultrasound, and ocular optics prevent high depth resolution in scanning laser confocal imaging systems. In contrast to both scanning laser tomography and scanning laser ophthalmoscopy, the axial resolution of OCT depends only on the temporal coherence properties of the source and not on the pupil-limited numerical aperture of the eye or ocular aberrations. The micrometre scale axial resolution of OCT might be crucial for the early diagnosis and monitoring of degenerative retinal diseases.<sup>269</sup>

OCT demonstrates abnormalities such as cystoid oedema, retinal detachment, drusen, lipofuscin, and RPE detachment and atrophy. This investigation can also provide diagnostic clues (e.g., choroidal metastases and lymphomas, as well as posterior scleritis tend to have a lumpy surface not usually seen with other lesions). OCT is also useful for measuring thickness of small, posterior tumours.<sup>57, 105</sup> OCT angiography reveals radiation-vasculopathy providing information that can help predict response to anti-angiogenic agents in patients with macular oedema after radiotherapy.<sup>276-279</sup>

#### **1.4.2. Transillumination (TI)**

Transillumination may show tumour edges extending anterior to the ora serrata,<sup>280</sup> which can be helpful to detect pigmented tumours in the ciliary body.<sup>19, 281</sup> Although it is best seen with high-frequency ultrasound,<sup>175, 243</sup> TI is also useful to detect an intraocular tumour when the media are opaque, for example, in the presence of vitreous haemorrhage or cataract, but it does not substitute the use of ultrasound. TI is also useful to differentiate amelanotic melanomas.<sup>243</sup>

#### **1.4.3. Laboratory investigations**

Various clinical, cytogenetic and histopathological features of uveal melanoma can identify patients who are at high risk of developing metastasis and who probably

benefit from appropriate prophylactic/therapeutic adjuvant and adjunctive treatments.<sup>153, 282, 283</sup>

#### **1.4.3.1. Histopathology**

Histologic factors play an essential role in diagnosing and estimating prognosis in UM, and staining techniques have significantly developed in recent years.<sup>284</sup>

In contrast to most other cancers, histopathologic specimens are rarely obtained for diagnosing UM,<sup>285</sup> as this might increase the risk of local spread and vision loss. Beside the sample might not represent the entire tumour.<sup>126, 286</sup> Nevertheless, fine-needle aspiration biopsy (FNAB) is used to confirm difficult diagnoses.<sup>126, 286, 287</sup> Today, biopsies are also performed for prognostic purposes,<sup>288</sup> thereby increasing the diagnostic accuracy.<sup>289</sup>

The tumours are classified according to cell type by the modified Callender classification to; spindle cell, mixed cell, and epithelioid cell melanomas.<sup>208</sup> When the entire tumour is available for analysis, e.g., after enucleation or local resection, the number of mitoses per high-power field indicates the tumour growth rate and metastasis risk.<sup>153, 290</sup>

Spindle cell melanomas grow more slowly and have a better prognosis than other types.<sup>291</sup> Epithelioid cells are associated with an increased risk of metastatic disease.<sup>292</sup>

Tumour extravascular morphology in UM was first described by Folberg et al. in 1992.<sup>293</sup> The presence of extravascular matrix patterns in UM and their association with metastatic death are well established.<sup>293</sup>

#### **1.4.3.2. Immunohistochemistry**

Uveal melanoma has the potential to be a fatal cancer with a strong tendency to metastasise<sup>294, 295</sup> Immunohistochemistry using stains such as Melan-A confirms the



diagnosis of melanoma. Recently, nuclear BAP1 staining has been found to be a useful prognostic tool, with BAP1 loss associated with metastasis.<sup>296</sup> A strong predictor for metastasis is the loss of chromosome 3.<sup>295, 297</sup> Inactivating mutations in BAP1 encoding the BRCA1-associated protein 1 and located on chromosome 3p21.1, have been described in uveal melanoma and other cancer types.<sup>294, 295, 298</sup>

#### **1.4.3.3. Genetic aberrations**

Several studies in the past confirmed the importance of monosomy 3 as an important prognostic cytogenetic factor for metastatic disease in UM.<sup>282, 297-300, 301, 302</sup>

Posterior uveal melanomas have non-random alterations that affect chromosomes 3, 6, and 8.<sup>303</sup> Loss of chromosome 3, loss of 6q, and gain of 8q are strongly associated with poor overall survival.<sup>302, 297, 304</sup> Studies indicate that metastasised primary uveal melanomas and metastases have significantly more copy number changes than non-metastasised primary uveal melanomas. Losses of chromosome 3, 6q, and 1p, and gains of 8q are prognostically poor signs, while 6p gain is associated with a relatively good prognosis.<sup>298</sup> The loss of chromosome 3 may be associated with isochromosome formation of 1q, 6p, 8q, 16p, 20q, and 22q.<sup>302</sup>

Furthermore, BAP1 and SF3B1 mutations indicate a high risk of metastasis, whereas EIF1AX suggests a better prognosis.<sup>143, 144, 214, 294, 296</sup>

#### **1.4.4. Ancillary test in diagnosis of melanocytic choroidal lesions**

As UM grows slowly, the symptoms are usually not specific.<sup>47, 285</sup> The most typical symptoms are blurred vision (50-69%), visual field defect (9-30%) and photopsia (18-26%).<sup>305-307</sup> In 25-30% of patients, the diagnosis is made during a routine exam, while a minimum 50% of them are asymptomatic.<sup>288</sup>

The traditional view of the fundus provided by ophthalmoscopy is limited. Innovations in ophthalmic imaging have profoundly impacted the diagnosis and treatment of ocular disease. In ocular oncology, the development of OCT with enhanced depth

imaging and swept source techniques has made it possible to visualise the anatomical features of melanocytic choroidal lesions with a level of detail previously unobtainable on clinical examination alone. Subsequently, the understanding of the pathophysiology of vision loss in choroidal melanoma has improved. These modalities also aid identifying fundoscopically ‘invisible’ tumours and risk-stratify pre-malignant choroidal lesions, making a solid case for their inclusion in all screening evaluations. On the other hand, OCTA has allowed non-invasive imaging of the uveal and retinal vasculatures, offering insight into vascular changes in combination with malignant transformation and vision loss following radiation exposure. Although the impact of new imaging technologies on clinical outcomes and overall survival in ocular oncology has yet to be established, various reports offer promising results.<sup>251, 254</sup>

Historically, choroidal naevi and melanomas have been diagnosed and monitored with fundoscopic examination, fundus photography, and ocular ultrasonography.<sup>46, 107, 190</sup> Invasive methods, such as indocyanine green angiography (ICGA) and fluorescein angiography (FA), have been utilised where necessary to aid in differentiating melanoma from masquerading pathology, in order to assess for secondary neovascularisation or ischaemia, or to assist in visualising lesions obscured by media opacity.<sup>254, 262</sup> More recently, OCT and OCTA enabled to non-invasively image superficial and deep structures of the choroid and retina with a level of detail previously unobtainable by clinical exam alone.<sup>254</sup>

## 1.5. Treatment of uveal melanoma

### 1.5.1. Radiotherapy

In most centres in the UK, the first choice of treatment is brachytherapy, which is administered with a radioactive plaque.<sup>308</sup> Radiotherapy is a treatment given either through episcleral radioactive plaques (Co60, I125, Ru106, Ir192 or Pd103) or through accelerated particles such as protons or helium ions. The advantage of

these methods is to preserve some vision in the affected eye, especially in eyes with small tumours.<sup>277, 278, 309, 310</sup>

In general, UM is quite resistant to radiation, unless high doses are given, which leads to visual complications due to accompanying cataract, radiation retinopathy, and optic neuropathy.<sup>277, 278, 309-312</sup> Iodine plaques emit gamma irradiation and can successfully treat tumours up to 10 mm in thickness. However, they transfer high doses of radiation and can potentially cause collateral damage to healthy ocular structures.<sup>313</sup> To reduce secondary damage to optic disc and fovea, the plaque can be placed with its posterior edge close to the posterior tumour margin. This can be achieved by using a right-angled transilluminator and a perforated template to ensure accurate plaque insertion.<sup>313</sup>

The recurrence rate of UM post radiotherapy ranges from 5 to 10% over 5 years.<sup>314, 315</sup> Local recurrences may also increase the risks of distant metastasis up to five times.<sup>186, 316</sup>

#### **1.5.1.1. Plaque brachytherapy**

Plaque radiotherapy or brachytherapy for UM was first explored by Stallard in England in the 1940s.<sup>317</sup> The first used applicator was radioactive cobalt 60, followed by iridium 192, ruthenium 106, Iodine 125 and palladium 103.

Following the COMS trial,<sup>318</sup> plaque brachytherapy became the central component for the treatment of medium-sized UM,<sup>319</sup> whereas enucleation was generally abandoned as a primary modality for this indication. The most commonly used applicator today is iodine 125, mainly in North America, and ruthenium 106 in Europe.<sup>310, 320, 321</sup>

The treatment involves an operation to suture the plaque to the sclera over the tumour. A few days later, once the prescribed radiation dose has been delivered, a second operation is performed to remove the plaque.<sup>322</sup>

While the COMS trial data did not include juxtapapillary choroidal melanoma, Sagoo et al. reported the results of a study on treating juxtapapillary choroidal melanoma with plaque brachytherapy.<sup>321</sup> Tumour control was found in 14% and 21% after 5 and 10 years, respectively. On analysis, they also found that eyes treated with adjuvant transpupillary thermotherapy (TTT) had lower chances of recurrence.

#### **1.5.1.2. Proton beam therapy (PBT)**

Proton beam radiotherapy for UM was first described in Boston in 1980 by Gragoudas et al.<sup>323</sup> Since its introduction, it has become an important conservative therapeutic alternative for this indication, used by many centres across the world.<sup>324-326</sup>

Several studies showed that proton beam radiotherapy enables a high dose of radiation aimed precisely at a uveal melanoma irrespective of the tumour's size, shape and location.<sup>326-331</sup>

Damato et al. reported the results of 349 UM patients (all choroidal melanoma).<sup>326</sup> The 5-year actuarial rates were 3.5% for local tumour recurrence and 9.4% for enucleation. Papakostas et al. have also used this modality for large UM.<sup>276</sup>

PBT delivers a homogenous dose of radiation within the tumour volume, whereas, with brachytherapy, the tumour base receives several times the dose of the tumour apex.<sup>327</sup> PBT avoids any risk of radiation exposure to the surgeon's hands.<sup>311, 327</sup> In some centres, this therapy is selected for all UM undergoing radiotherapy treatment.<sup>327</sup> Compared to brachytherapy, it is expensive and may cause significant side effects in ocular and extra-ocular structures.<sup>326</sup> It is usually used for a particular group of patients.<sup>326</sup> It permits radiotherapy in larger tumours not suitable for brachytherapy and may be preferred for tumours located close to the optic disc or macula.<sup>326, 328</sup>

The PBT treatment comprises ultrasound measurements of tumour dimensions and distance from the optic disc, followed by the surgical insertion of tantalum markers at known distances from tumour margins, from each other, and from limbus. These steps will be followed by creating a 3-D computer model of the eye and tumour, using the ultrasound and intra-operative measurements and x-rays of the tantalum markers. The treatment further involves preparing a tight-fitting face mask and dental bite to immobilise the head during treatment, and concluded with proton beam radiotherapy, delivered once a day over four consecutive days.<sup>326, 328</sup>

Proton beam radiotherapy of large uveal melanomas often develops a 'toxic tumour syndrome' caused by secondary neovascular glaucoma, rubeosis and persistent exudative retinal detachment.<sup>327, 331</sup> This condition can be prevented by antiangiogenic therapy or treated successfully by removing the irradiated tumour with transscleral local resection or endoresection.<sup>332-336</sup>

### **1.5.1.3. Stereotactic radiotherapy**

Stereotactic radiotherapy is based on collimated beams of gamma rays or gamma knife electronic linear accelerator, which converge to an exact volume.<sup>337-341</sup> It can be used to treat small, medium sized and some large UM.<sup>342-344</sup>

With stereotactic radiotherapy, a highly collimated beam of radiation is pointed at the tumour from various directions, simultaneously or in sequence, so that a large radiation dose is delivered to the melanoma with relatively low impact on healthy tissues.<sup>338, 345</sup> This approach is an alternative to proton beam radiotherapy in centres where a cyclotron unit is unavailable.<sup>14, 339</sup>

Stereotactic radiotherapy is useful for tumours that are considered unsuitable for brachytherapy, either because of posterior location or large size. With large tumours, stereotactic radiotherapy is contraindicated if the patient does not accept the increased chances of retinal detachment and neovascular glaucoma. Similarly, patients with posterior tumour extension must accept the increased likelihood of optic neuropathy and maculopathy.<sup>346</sup> For large uveal melanoma, stereotactic

radiotherapy followed routinely by endoresection has been advocated as a means of improving local control while avoiding neovascular glaucoma.<sup>347</sup>

The scope of stereotactic radiotherapy in the treatment of iris melanoma has not yet been evaluated.<sup>346</sup>

### 1.5.2. Transpupillary thermotherapy (TTT)

Focal laser therapy for small UM was explored in the 1970s and on with variable results. Xenon-arc and argon laser were used in various centres in an attempt to reach tumour control while preserving vision.<sup>348, 349</sup>

Oosterhuis et al. subsequently introduced TTT, a diode laser that can penetrate deeper into the melanoma.<sup>350</sup> The technique was adopted by several centres as a primary treatment modality for small UM, but some have questioned its efficacy in terms of local tumour control and, specifically the risk of iatrogenic extraocular spread.<sup>351</sup>

If there is uncertainty about the adequacy of radiotherapy, TTT is generally conducted as a secondary treatment after radiotherapy. It is also performed as a treatment for exudation, either at the time of presentation or when exudation develops after treatment.<sup>352</sup>

In selected cases, primary TTT may help to preserve vision by arresting the progression of tumour growth.<sup>353</sup> The trade-off between potential loss of vision and the risk of local tumour recurrence and metastasis must be carefully discussed with each patient.<sup>354</sup> Current data indicate that TTT as primary therapy, even for small choroidal melanocytic lesions, is not as effective as radiation.<sup>264, 328, 354-357</sup> The overall effect of primary TTT on survival is not currently known, but some studies suggested that TTT may be a clinically effective method for conservative treatment of selected, non-parapapillary, small posterior choroidal melanoma.<sup>354</sup> TTT may be included in the armamentarium of conventional treatment of selected, non-parapapillary, small pigmented posterior choroidal melanomas not involving the foveal area.<sup>354</sup>

With this therapy method, a 3 mm diode laser beam administered through a contact lens will heat the tumour by a few degrees for approximately one minute. The power of the laser is calibrated so that retinal blanching does not develop for at least 40 seconds. The effects of TTT can extend to a depth of up to 4 mm.<sup>355</sup> Adjunctive brachytherapy is recommended to avoid local tumour recurrence from intrascleral tumour.<sup>352</sup>

### 1.5.3. Resection

Surgical resection of UM is an alternative eye-salvaging approach compared to the more commonly used irradiation techniques. There are two surgical resection techniques: “Endoresection” via a pars plana vitrectomy and “Exoresection” or transscleral resection via a partial lamellar sclerouvectomy.

Both endoresection and exoresection can be undertaken as a primary procedure, or after other conservative therapy as treatment for recurrent or toxic tumour.<sup>358</sup>

#### 1.5.3.1. Endoresection

Intraocular resection or endoresection is another method of treating UM.<sup>359-362</sup> The tumour is removed through a vitreoretinal surgical approach. The advantage of this method being that only limited radiation from a plaque used as a safety measure is needed. Therefore, the risk of neovascular glaucoma and optic neuropathy is lower, and the chances of preservation of vision are higher.<sup>320, 363, 364</sup>

This method also has disadvantages as it carries a higher risk of local recurrence.<sup>359, 365</sup> Studies showed that most complications had been caused by the vitrectomy and not the endoresection itself.<sup>361, 366, 367</sup>

Endoresection is relatively straightforward for experienced vitreoretinal surgeons; however, this method is limited by the choice of tumour, which has to be tall, with narrow base and peripheral location. Because of the need for hypotensive anaesthesia and other measures to control intra-operative haemorrhage, the surgery requires the patient to be young and fit.<sup>358</sup>

### 1.5.3.2. Exoresection

Exoresection or transscleral local resection applies more to anteriorly located tumours with ciliary body and/or iris involvement. The main indication for a local resection of uveal melanoma is a tumour size deemed excessive for radiotherapy<sup>368</sup> and is aimed at conserving the eye and useful vision while removing any threat of metastatic spread.

Bechrakis et al. has reported that transscleral resection could be an alternative to enucleation for the treatment of large UM,<sup>364</sup> and if combined with adjuvant radiotherapy, could be the treatment of choice in cases of large tumours.<sup>320, 363</sup>

Exoresection of small, ciliary body melanomas has been performed for many years.<sup>176, 358, 369, 370</sup> Advances in microsurgery and hypotensive anaesthesia have also made it possible to remove large tumours extending as far posteriorly as the fovea.<sup>369</sup> This operation is complex and therefore conducted only in a few centres, where it is reserved for tumours that are considered too large for radiotherapy.<sup>365, 368, 371</sup> The main complications are local tumour recurrence and rhegmatogenous retinal detachment.<sup>358, 369</sup>

### 1.5.4. Photodynamic therapy (PDT)

Studies have shown that Photodynamic therapy using Verteporfin is associated with a high failure rate.<sup>111, 112</sup> For this reason, this modality is applied for 'leaking naevi' and exudation or macular oedema after radiotherapy.<sup>110</sup> Aura biosciences has developed AU-011, which is injected into the vitreous and activated by a laser.<sup>372</sup>

Fabian et al. reported PDT with verteporfin for small pigmented posterior-pole choroidal melanoma, with encouraging results, achieving 80% tumour control rate after 15 months of follow-up, eliminating subretinal fluid and attaining significant improvement of visual acuity.<sup>112</sup> Further investigation however, on a larger cohort and for a longer period, were less encouraging, showing that this modality was useful



only in 60% of eyes, and according to Kaplan-Meier estimates, 51% of eyes after 3 years.<sup>111</sup>

### 1.5.5. Cryotherapy

Cryotherapy has not gained widespread acceptance, although this form of therapy has been reported to be effective for some choroidal melanomas.<sup>353, 373, 374</sup>

### 1.5.6. Enucleation

For many years the treatment of choroidal melanomas, once the diagnosis had been established with reasonable certainty, was relatively straight forward: the affected eye was removed, a prosthesis fitted, and the patient discharged.<sup>375</sup>

Enucleation used to be the only treatment for UM until the late 1940s when eye conserving methods were introduced.<sup>376, 377</sup> Enucleation is still an option in many developing countries, and for some patients, when the tumour has progressed to a large size and the chances of saving the eye and vision are limited.<sup>360</sup>

In 1978, Zimmerman et al. published an article suggesting that enucleation accelerated metastatic death by physically spreading tumour cells from the eye into the general circulation. This hypothesis was mainly based on the observation that the mortality rate peaks in the second postoperative year.<sup>378</sup>

Nowadays, primary enucleation for uveal melanoma is executed only when other treatments are unlikely to preserve the eye and sufficient vision. The enucleation is performed in a traditional way, using the implant depending on the surgeon's preference.<sup>379</sup>

Enucleation has some advantages. It is a straightforward procedure to perform at most ophthalmic units. It prevents local tumour recurrences if there has been no extrascleral extension prior to surgery.<sup>380</sup> Besides, it provides the ophthalmic pathologist with large samples for analysis. The disadvantage is an immediate loss

of the eye and remaining vision.<sup>316, 318</sup> No significant difference in survival has been observed between equivalent groups of patients with a primary choroidal or ciliary body melanoma treated by enucleation versus plaque radiation therapy.<sup>316</sup>

## 1.6. Prognosis

The 10-year cumulative melanoma-related survival is about 60%, and then decreases about 1% each year.<sup>177, 292, 381</sup> Death is mainly due to metastasis, which in some studies has been documented even decades after enucleation.<sup>10, 142, 382-384</sup> UM has a predilection to metastasize to the liver.<sup>74, 170, 186, 385-387</sup> In 50% of the cases, the liver is the only organ involved in metastasis.<sup>387</sup> Annual screening with liver function tests and abdominal ultrasound will identify 59% of patients while they are still asymptomatic.<sup>184</sup> Other more frequent sites involved are skin, lung, bone and the central nervous system (CNS).<sup>184, 386</sup>

The median expected survival after metastasis is about 12 months, although there have been some reports regarding slower growing metastases in patients who have survived between 36 and 48 months.<sup>185, 388-391</sup>

Treating metastatic UM is frequently disappointing.<sup>136, 214, 392</sup> Chemotherapy, chemoimmunotherapy, and chemoembolisation may have increased survival to a mean of over one year.<sup>388, 392-396</sup> This may, however, be due to lead time bias.<sup>397</sup> Patients treated with surgery for slow growing metastases have rarely survived for long periods.<sup>398-401</sup>

The course of UM is modulated by both tumour and host. Some patients with a large tumour may live longer than those with a smaller tumour. This applies to other prognostic factors as well.<sup>282, 383, 384</sup>

## 1.7. Methods of diagnostic differentiation of the choroidal naevi and choroidal melanoma

In the 1970s, Gass identified various features distinguishing choroidal naevi from melanomas.<sup>183</sup> Harbour, who trained with Gass, credited him with devising the acronym **DOCTOR GASS**, which represents: Drusen, Overlying retinal degeneration, Chronic RPE changes, Thickness >2 mm, Orange pigment, Reflectivity (low) on ultrasonography, Girth (diameter) of tumour, Angiographic hot spots, Subretinal fluid, and Symptoms.<sup>59</sup>

Several of these clinical characteristics which independently predict growth of small choroidal melanocytic tumours were confirmed and popularised by Shields et al.<sup>74</sup>, who devised a well-known mnemonic **TFSOM**, '*To Find Small Ocular Melanoma...*', which represented Thickness, Fluid, Symptoms, Orange pigment, and Margin near optic disc<sup>74, 113</sup> later adding '*...Using Helpful Hints Daily.*' to represent Ultrasound hollowness, Halo absence and Drusen absence<sup>41, 68</sup>

As recent studies showed margin near the disc, absence of drusen and absence of halo to be statistically insignificant, Shields et al. revised this mnemonic to **TFSOM-DIM**, '*To Find Small Ocular Melanoma Doing IMaging,*' with the 'M' representing 'Melanoma hollow on ultrasound' and 'DIM' representing 'diameter > 5 mm' on fundus photography.<sup>65</sup>

The mnemonic helps the ophthalmologist to remember to look for risk factors that are predictive of growth of a naevus, this being a surrogate marker of malignancy: tumour thickness more than 2 mm, subretinal fluid, visual symptoms, orange pigment and tumour margin at the optic disc when evaluating small choroidal melanocytic tumours.

The trend is toward taking a biopsy of suspicious small choroidal tumours as an alternative to documenting growth before treating them as melanomas,<sup>47</sup> but in practical terms, this is a difficult procedure. Sampling bias may lead to a false negative or false positive spurious conclusion.

In the community, optometrists may not have the experience or the facilities to use the Shields TFSOM system. For this reason, Damato has created the **MOLES** scoring system to help optometrists and ophthalmologists differentiate choroidal melanomas from naevi. The MOLES score system will be presented and validated as a separate study in this thesis.<sup>402</sup>

While other systems, such as TFSOM-DIM and DOCTOR GASS require ultrasonography and other imaging, which are not widely available in the community in the UK,<sup>65</sup> the MOLES scoring system does not require assessment of internal acoustic reflectivity by ultrasonography and can be based on ophthalmoscopy alone, based on the risk factors of malignancy as Mushroom shape, Orange pigment, Larger size, Enlargement and Subretinal fluid of choroidal naevi.<sup>86</sup>

While TFSOM ascribes an all-or-none value to each of its clinical signs, MOLES scores include an intermediate value for features that are borderline, subtle or uncertain. This additional category will be especially useful in the community, where findings are more likely to be inconclusive because of limited experience or equipment.<sup>79</sup> TFSOM-DIM estimates risk of future growth, whereas MOLES estimates risk of malignancy on presentation.

Dr Finger created the mnemonic **MOST**.<sup>403</sup> It is based on the most common characteristics of choroidal Melanoma. As a choroidal melanoma infiltrates and destroys the overlying retinal pigment epithelium, accumulations of Orange pigment (lipofuscin and melanolipofuscin) can be uncovered on the surface of the melanoma. Meanwhile, incontinent tumour blood vessels leak serum beneath the retina, exudative Subretinal fluid. Lastly, choroidal melanomas are typical >2 mm Thick. Though not all choroidal melanomas exhibit all three findings, MOST is diagnostic when all three are present.<sup>403, 404</sup>

For situations where mydriasis is performed selectively, Damato has also devised the mnemonic/ acronym, **MELANOMA**, to alert the clinician to the presence of an intraocular tumour in situations, and to help remember the symptoms and external signs that might indicate the presence of an uveal melanoma.<sup>405</sup>

Features suggestive of uveal melanoma include:

- Melanoma visible externally, as extraocular extension, an iris tumour, or iris heterochromia.
- Eccentric visual phenomena (i.e., field loss, photopsia) caused by the tumour or secondary retinal detachment.
- Lens abnormalities such as astigmatism and cataract, caused by a ciliary body tumour.
- Afferent pupillary defect, caused by tumour or retinal detachment.
- No optical correction, because of retinal damage by macular oedema, retinal detachment, or tumour.
- Ocular hypertension from rubeosis iridis or tumour cells or macrophages in angle.
- Melanosis oculi (naevus of ota).
- Asymmetrical episcleral ('sentinel') vessels, indicating a ciliary body tumour.

### 1.8. Role of artificial intelligence in ocular oncology and in the diagnosis of pigmented fundus tumours

Despite pigmented fundus tumours being common, and the large majority are not harmful, distinguishing small melanomas from benign naevi remains challenging.<sup>77, 146</sup> A major unmet need is an easy method to differentiate suspicious choroidal naevi from small choroidal melanoma. Choroidal naevus and small choroidal melanoma can show several overlapping features, and the challenge is to identify the single small malignant melanoma among the thousands of benign choroidal naevi.<sup>75, 406</sup>

Driven by the strong interest for early, objective, and repeatable diagnosis of choroidal melanoma, algorithmic image analysis techniques have garnered interest for differentiating between these lesions. In 1956 at the Dartmouth Artificial Intelligence Conference, McCarthy et al. postulated that *'every aspect of learning or any other feature of intelligence can in principle be so precisely described that a machine can be made to simulate it'*.<sup>407, 408</sup> Artificial intelligence (AI), which

developed from this concept, describes the creation of computerised systems which perform tasks requiring synthesising knowledge and intelligence. Ophthalmic screening is well-suited for the application of AI due to well-understood relationships between clinical features and disease severity and the ready availability of imaging to effectively capture these features. Screening programs have been extensively investigated for glaucoma and diabetic retinopathy.<sup>409-413</sup>

Deep learning (DL), a branch of AI, has shown robust results that have surpassed human performance in many areas of healthcare.<sup>411, 414, 415</sup> As a subset of machine learning (ML), DL is a highly specialised artificial neural network that consists of layers of 'neurons' with activation functions forming complex neural networks inspired by the ones constituting the human brain. Similar to human learning from experience, DL algorithms are trained on a task and fine-tune based on specific examples allowing for generalisation and inference on previously unseen input. These attributes make them powerful tools for segmentation, classification, and predictive modelling.<sup>414,416</sup>

To bring ocular oncology to the next technological level, AI could be harnessed to read images and identify patients at high risk. The long-standing use of clinically identified risk factors in differentiating choroidal naevus from melanoma<sup>74, 406, 417</sup> and the more recent extensive use of ophthalmic diagnostic imaging to both identify and monitor choroidal naevus and melanoma<sup>65, 72, 406, 417</sup> provide substantial data to explore applications of AI. A good approach in ocular oncology would be first to study a very common tumour like choroidal naevus. The six known multimodal imaging risk factors for transformation to melanoma can be identified by machines for computer interpretation. If all naevi can be successfully identified, and if the ML model can discriminate those at risk for malignant transformation, it might be possible to treat melanoma very early or even eradicate melanoma by treating those naevi at highest risk, as quoted by Shields CL at the 2020 Collaborative Community on Ophthalmic Imaging (CCOI) Conference: *'It's like we're planting a seed in ocular oncology, with the hopes that it will evolve into knowledge that a computer might generate through artificial intelligence, and hopefully identify 'at-risk' nevi to prevent melanoma'*.

## 2. CHAPTER TWO: General Methodology

As a starting point, a broad literature review has been conducted to provide the theoretical framework, situate the studies presented in this thesis within the body of the relevant literature, and provide context for the reader. Published online papers and articles, specialised textbooks, and collateral from the Joint Library of Ophthalmology, Moorfields Eye Hospital & UCL Institute of Ophthalmology were the main sources to congregate relevant content. Furthermore, internet search engines, e.g., Google Scholar, subject-specific public databases, e.g., PubMed, Medline, but also additionally research in unconventional media such as scientific internet forums and technical blogs, have been utilised. The purpose of the literature review is focused on the individual research questions, aiming to identify, appraise, select and synthesise all high-quality research evidence and arguments of relevance.<sup>418</sup>

A part of this research work seeks to equip community optometrists with a new system to evaluate pigmented fundus lesions. The study '*Distinguishing Choroidal Nevi from Melanomas using the MOLES Algorithm: Evaluation in an Ocular Naevus Clinic*' aims to determine the sensitivity and specificity of the MOLES scoring system in differentiating choroidal melanomas from naevi according to the five risk factors Mushroom shape, Orange pigment, Large tumour size, Enlarging tumour, and Subretinal fluid (SRF). For this retrospective study, patients were included if diagnosed with a melanocytic choroidal tumour at the Moorfields Naevus Clinic and excluded if the tumour extended anterior to ora serrata or if melanocytoma was diagnosed. Colour photographs, fundus autofluorescence, optical coherence tomography, and, in selected cases, ultrasonography of 222 melanocytic choroidal tumours were reviewed. Each MOLES feature was retrospectively scored between 0 and 2, and tumours were categorised as 'common naevus', 'low-risk naevus', 'high-risk naevus', and 'probable melanoma' according to whether the sum total of these five scores was 0, 1, 2 and >2, respectively. The MOLES scores were compared with the experts' diagnosis of melanoma.

The related study *'The MOLES system for planning management of melanocytic choroidal tumors: is it safe?'* evaluates the MOLES system for identifying malignancy in melanocytic choroidal tumours in patients treated for choroidal melanoma. Records of 615 patients undergoing treatment for uveal melanoma between 1 January 2017 and 31 December 2019 have been reviewed. Patients were excluded from the study if: (a) they had undergone previous treatment for uveal melanoma (11 patients), (b) the tumour extended anterior to ora serrata, to involve the iris and/or ciliary body (106 patients), and/or (c) imaging of the tumour was lacking or inadequate (47 patients). Demographic data and AJCC TNM Stage were collected. Optical coherence tomography (OCT), colour fundus and autofluorescence photographs (AF), and B-scan ultrasounds were prospectively analysed. MOLES scores were given according to five criteria: mushroom shape, orange pigment, large size, enlarging tumour and subretinal fluid.

The related study *'Detecting progression of melanocytic choroidal tumours by sequential imaging: Is ultrasonography necessary?'* determined if ultrasonography is necessary to detect progression of choroidal melanocytic tumours undergoing sequential multimodal imaging with colour photography, autofluorescence (AF) and optical coherence tomography (OCT). All patients with choroidal melanoma undergoing treatment at Moorfields Eye Hospital between January 2016 and March 2020 were analysed to identify those with treatment deferred by  $\geq 2$  months. Tumours that showed progression prior to treatment, defined as an increase in (a) basal dimensions, (b) thickness, (c) orange pigment and/or (d) sub-retinal fluid, were included. MOLES scores were assigned to all tumours at the earliest date and date of treatment. A total of 99 patients with a mean age of 66 years (range, 26-90) were included.

Statistical analysis for MOLES studies was completed using commercially available software (Stata Statistical Software. StataCorp LP). Conventional descriptive statistics were used, and data was presented as mean  $\pm$  standard deviation (SD). The MOLES studies were approved by the Moorfields Eye Hospital clinical audit department (No; 452) and were conducted in accordance with the declaration of Helsinki.



Choroidal naevi are a common incidental finding prompting specialist referrals to ocular oncology. Rarely do such lesions have sufficient suspicious features to diagnose a small melanoma. The study *'Prospective Validation of a Virtual Clinic Pathway in the Management of Choroidal Naevi'* aims to show that 'virtual' imaging-based pathways are a safe and efficient option to manage such referrals. A prospective cohort study at the Manchester Royal Eye Hospital and Moorfields Eye Hospital between June 2016 and July 2017 of the management decision of 400 patients was reviewed by an ophthalmologist in a face-to-face consultation (gold standard) supported by fundus photography, optical coherence tomography (OCT), autofluorescence (AF) and B-mode ultrasound. The images were also read independently by masked graders (non-medical) and masked ophthalmologists, and a management decision was made based on image review alone (virtual pathway). The two pathways were compared for safety. The study had ethical approval (16/NW/0288) and adhered to the tenets of the Declaration of Helsinki.

Based on the outcome of this prospective validation of a virtual clinic pathway and validation of the MOLES scoring system, a model of a 'Virtual Naevus Clinic' has been designed and put into practice at Moorfields Eye Hospital and proved its feasibility as a response to the COVID-19 pandemic, and with the purpose of reducing in-hospital patient journey times and increasing the capacity of the naevus clinics, while providing safe and efficient clinical care for patients.

In June 2020, a standard operating procedure (SOP) has been developed which outlines the design, pathways, staffing, roles needed, and operating procedures for the digitally enabled naevus clinics in Moorfields Eye Hospital, including what this service provides and how it will be delivered and supported. The virtual naevus clinic was piloted with an initial capacity of 8 patients per assessor per session, and monitoring allowed to increase this capacity over time.

The paper *'Artificial Intelligence in ocular oncology: Differentiating benign choroidal nevus from choroidal melanoma'* has been created to discuss in detail the potential role of AI in differentiating benign choroidal naevus from small choroidal melanoma.

The author reviewed published clinical and imaging risk factors for malignant transformation of choroidal naevus, and how AI applied to existing ophthalmic imaging systems may be able to determine features on medical images. The author explored current knowledge to date and described potential benefits, limitations and key issues that could arise with this technology in the ophthalmic field, as well as how AI could be implemented in clinical practice and be embedded into existing imaging technology with the potential to improve patient care and the diagnostic process.

Furthermore, the author explored the feasibility of developed automated deep learning models and investigated the performance of these models in diagnosing choroidal naevomelanocytic lesions (CNL) based on medical imaging, including colour fundus and autofluorescence fundus photographs. The aim of this project was to determine the sensitivity and specificity of an automated deep learning algorithm used for binary classification to differentiate choroidal melanomas from choroidal naevi and prove that a differentiation concept utilising an ML algorithm is feasible. Two de-identified ophthalmic imaging datasets for training and validating two deep learning models were utilised, one for autofluorescence fundus and one for colour fundus images, using Google's Cloud AutoML platform. The images of both datasets originated from approved Moorfields Eye Hospital MOLES studies and included autofluorescence fundus (AF) and colour fundus (CL) photography images, representing diagnoses of choroidal naevus and choroidal melanoma, defined by the MOLES algorithm.

Dataset 1 used for model training and development comprised 402 images, of which 201 autofluorescence fundus photographs (AF) with 82 melanomas and 119 naevi and 201 colour fundus photographs (CL) (Optos California [Optos plc, Dunfermline, Scotland]) with equally 82 melanomas and 119 naevi have been collected and prepared for data processing and labelling. For the supervised training of the respective AF and CL deep learning models, the 201 AF and 201 CL labelled images have been randomly split into sub-datasets for training (80%), validating (10%), and testing (10%).

Dataset 2 used for internal validation comprised 208 images, of which 104 autofluorescence fundus photographs (AF) with 54 melanomas and 50 naevi and 104 colour fundus photographs (CL) (Optos California [Optos plc, Dunfermline, Scotland]) with equally 54 melanomas and 50 naevi have been collected to further test the models on new unseen data, after successful training and model evaluation. The AutoML Cloud Vision platform provides various model metrics, including confusion matrices, precision and recall percentage values, and the area under the precision-recall curve (AUPRC) or average precision for the default confidence threshold of 0.5.

Statistical analysis was performed with Microsoft Excel. Contingency tables have been constructed, and manual calculations of sensitivity, specificity, positive and negative predictive value (PPV and NPV), the F1 score, and accuracy (ACC) have been executed using the confusion matrices provided by the AutoML platform.

### 3. CHAPTER THREE: Distinguishing Choroidal Naevi from Melanomas using the MOLES Algorithm: Evaluation in an Ocular Naevus Clinic

#### 3.1. Introduction

##### 3.1.1. Diagnosing melanocytic choroidal tumours

Early treatment of choroidal melanoma optimises any opportunities for conserving the eye and vision. There is some evidence, albeit tenuous, that treatment of small choroidal melanomas may prevent metastatic spread in some patients.<sup>382, 419</sup> It can be difficult, however, to distinguish choroidal naevi from small melanomas. As a result, patients with a benign lesion may undergo excessive surveillance, which may cause undue anxiety and unnecessary expense. Conversely, patients with malignancy may experience long delays in treatment.<sup>420</sup> Management of these patients can be burdensome to healthcare services because of the high prevalence of choroidal naevi, especially in the White population (i.e. ~6%).<sup>63</sup> This can delay the care of patients with serious conditions, including choroidal melanoma.<sup>421</sup>

Various mnemonics and acronyms have been developed to aid differentiation between choroidal naevi and melanomas.<sup>59, 65</sup> For example, Shields et al. have prepared TFSOM-UHHD (To Find Small Ocular Melanoma Using Helpful Hints Daily), which represents: Thickness of greater than 2 mm; subretinal Fluid; symptoms of reduced vision or photopsia; Orange pigment; Margin of tumour less than or equal to 3mm from the optic disc; ultrasound Hollowness; absence of depigmented Halo surrounding tumour; and absence of overlying Drusen.<sup>68</sup> This has recently been altered to TFSOM-DIM (To Find Small Ocular Melanoma Doing Imaging), which represents Thickness >2 mm measured by ultrasonography, Fluid subretinally, assessed with OCT, Symptoms, vision loss, Orange pigment, assessed with autofluorescence, Melanoma hollowness on ultrasonography, and DiaMeter >5 mm, assessed by fundus photography.<sup>65</sup>

These mnemonics are widely used but require assessment of internal acoustic reflectivity by ultrasonography, which is not widely available in the community. There is scope for aids enabling practitioners to estimate likelihood of malignancy from widely used imaging, such as colour photography, optical-coherence tomography (OCT) and fundus autofluorescence imaging (FAF) when ultrasonography is not possible, as in virtual clinics and in optometric and general ophthalmic clinics.

For these reasons, Damato has devised the mnemonic, MOLES, which represents Mushroom shape, Orange pigment (i.e., lipofuscin), Large tumour size, Enlarging tumour, and Subretinal fluid (SRF). Each of these features is given a score of 0, 1 or 2 according to whether it is absent, borderline, or present. Tumours are categorised as ‘common naevus’, ‘low-risk-naevus’, ‘high-risk naevus’ and ‘probable melanoma’ according to whether the sum total of these five scores is 0, 1, 2 or >2. (Table 2)

The aim of this study was to determine the sensitivity and specificity of the MOLES scoring system in differentiating choroidal melanomas from naevi in the setting of a clinic where naevi are evaluated routinely.

This study was published in March 2021 by Al Harby et al. in *Ocular Oncology and Pathology*.<sup>79</sup>

### 3.1.2. MOLES scoring system

**‘Mushroom shape’** is almost pathognomonic for choroidal melanoma. It occurs when the tumour extends through Bruch’s membrane and retinal pigment epithelium. When this happens, the tumour thickness increases so that the MOLES score exceeds 2. A score of 1 indicates that the tumour bulges slightly through a defect in Bruch’s membrane.

Rapidly growing tumours, such as melanomas and metastases, tend to disrupt RPE function, so that waste products accumulate in the form of lipofuscin, which on ophthalmoscopy appears orange, hence the term **‘Orange pigment’**. Light dusting

of orange pigment can occur over choroidal naevi and is given a MOLES score of 1; however, clumps of confluent orange pigment indicate more severe RPE dysfunction, which tends to occur with melanomas, hence the score of 2. Over amelanotic tumours, lipofuscin can appear brown. This pigment is bright on fundus autofluorescence imaging, which is performed routinely in specialist centres.

Choroidal melanomas tend to have a '**Larger size**' than naevi, although there is some overlap.<sup>52</sup> If possible, the thickness of small, posterior lesions should be documented by performing optical coherence tomography (OCT). Ultrasonography is useful when OCT is not possible because of large tumour size or posterior shadowing or peripheral location.<sup>274</sup> Tumours rarely become thicker without also showing an increase in diameter; colour photography should therefore be adequate when OCT and ultrasonography are not possible.<sup>82</sup>

'**Enlargement**' of choroidal naevi is rare after the age of 25 years, and when it occurs, it is minimal and slow, developing over many years. Fundus photography makes it easier to detect tumour growth. Sequential fundus photography is ideal but not essential as long as a baseline photograph is available. Tumour enlargement confirmed photographically is given a MOLES score of 2. The enlargement parameter also includes a size component, where a tumour diameter of more than 7.5 mm (5 disc diameters) and tumour thickness greater than 3.0 mm, is considered to be indicative of growth, and thus the score for the Enlargement category is given 2.<sup>422</sup> If photography is suggestive of growth but inconclusive, because of poor image quality, a score of 1 is given. A score of 0 is given if a lesion is detected when previous ophthalmoscopy indicated no such abnormality. This is because the lesion may have been missed or because the clinician did not mention the presence of the lesion to the patient.

'**Subretinal fluid (SRF)**' develops when RPE function is disturbed by an underlying choroidal tumour, as usually happens with melanomas. The retina is flat over typical naevi (i.e., MOLES score = 0) but some larger lesions may show minimal or localised detachment or cystoid intra-retinal spaces; these features are given a score of 1. Significant and extensive retinal detachment that is easily seen ophthalmoscopically

is given a MOLES score of 2. Subretinal fluid is best detected with OCT. When such imaging is not available, it is reasonable to assume that SRF is present if the patient reports metamorphopsia or other visual symptoms for which no other cause can be found. This feature should be given a MOLES score of 1.

Risk Factor	Severity	Score
<b>M</b> ushroom shape	Absent	0
	Incipient (i.e., erosion of RPE over tumour, possibly with bulging of tumour)	1
	Present (i.e., with definite overhang)	2
<b>O</b> range pigment	Absent	0
	Trace	1
	Confluent (i.e., forming clumps)	2
<b>L</b> arge Size	<b>Thickness &amp; Diameter</b>	
	Small (i.e., base <3 DD and thickness <1 mm)*	0
	Borderline (i.e., base 3–4 DD or thickness = 1–2 mm)*	1
	Large (i.e., base >4 DD or thickness >2 mm)*	2
<b>E</b> nlargement**	None (or lesion not documented or mentioned to patient previously)	0
	Uncertain	1
	Definite (i.e., with photographic proof of growth >1/3 DD per year)	2
<b>S</b> ubretinal fluid	Absent	0
	Trace (i.e., detected only with OCT)*	1
	Significant (i.e., visible by colour photography or ophthalmoscopy)	2
	<b>Total Score</b>	
DD, disc diameter (=1.5mm); OCT, optical coherence tomography; RPE, retinal pigment epithelium; SRF, subretinal fluid. *If ultrasonography is not available, tumour thickness is measured with OCT. If OCT is not possible, thickness is estimated to be <1 mm, 1-2 mm or >2 mm if the tumour ophthalmoscopically appears flat, minimally thickened or having a prominent dome or mushroom shape. Cystic intra-retinal oedema and retinal pigment epithelial abnormality with cobblestone degeneration or hyper-autofluorescence are not significant if the retina is flat. **Assume enlargement has occurred if thickness >3 mm or diameter >5 DD and give this score of 2.		

**Table 2:** MOLES scoring system for evaluating malignancy in melanocytic choroidal tumours

### 3.2. Patients and methods

Patients were included if seen for the first time at the naevus clinic of Moorfields Eye Hospital between January 2013 and December 2018. Cases were excluded if diagnosed with melanocytoma or congenital ocular melanocytosis, or if the tumour extended anterior to ora serrata.

Initial assessment was performed by an ocular oncologist and included measurement of Snellen visual acuity, binocular indirect ophthalmoscopy, fundus photography with optos (Optos, Dumfermline, UK) or Topcon (Topcon fundus camera, Topcon Corporation, Tokyo, Japan), fundus autofluorescence imaging (FAF) (Optos, Dumfermline, UK), optical coherence tomography (OCT) (Spectralis, Heidelberg Engineering GmbH, Heidelberg, Germany), and, in selected cases, B-scan ultrasonography.


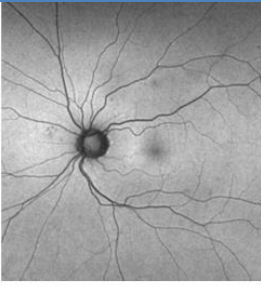
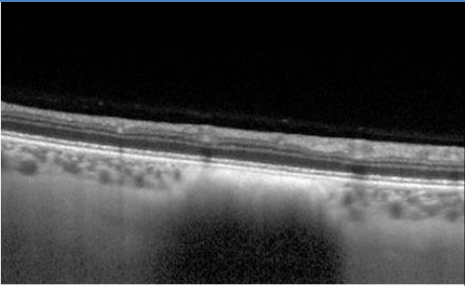
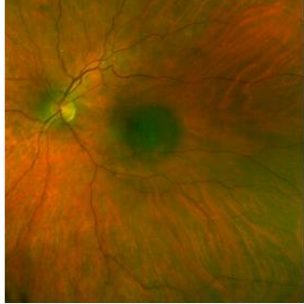
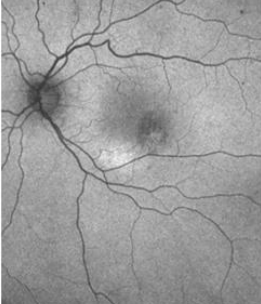
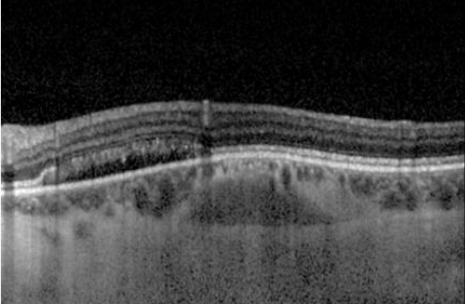
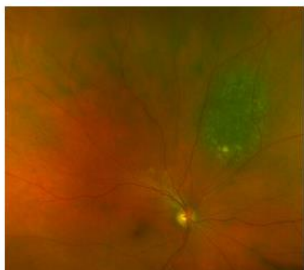

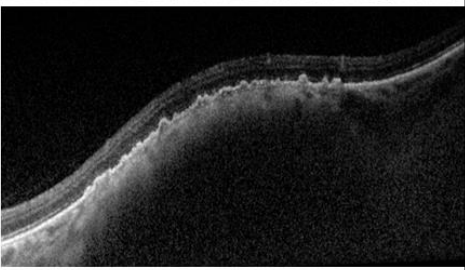


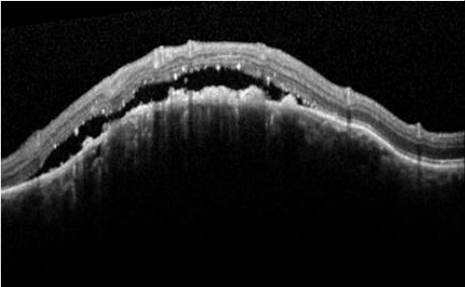
Tumours were diagnosed by the ocular oncologist as ‘typical naevus’, ‘suspicious naevus’ or ‘melanoma’ (referred to as ‘expert diagnosis’ in this text and tables). Patients were discharged, monitored at Moorfields Eye Hospital or treated with a variety of methods, which comprised photodynamic therapy, ruthenium plaque radiotherapy, proton beam radiotherapy, or enucleation.

Medical records and digital images were retrospectively scored, and tumours were categorised according to the MOLES system as ‘common naevus’, ‘low-risk naevus’, ‘high-risk naevus’ and ‘probable melanoma’. This has been done according to clinical features documented at the patient’s first visit at the hospital as described in [Table 3](#), except that enlargement was documented if tumour growth was mentioned in the charts or referral letter. The experts’ diagnosis was retrospectively categorised as melanoma if this was specified at the initial assessment or if the patient underwent radiotherapy or other treatment for this condition. ([Figure 13](#)) ([Table 3](#))

The MOLES scores were compared with the expert diagnosis to compute sensitivity and specificity in differentiating melanomas from naevi (i.e., common, low-risk, and high-risk lesions). Follow-up was measured from the first clinic date to November 2019, when this analysis was performed.

Data were analysed with Stata (StataCorp, College Station, Texas, USA). Approval from the Audit Committee of Moorfields Eye Hospital was obtained (Number: 452). Patient consent was not required. The study adhered to the Tenets of Helsinki.



	Colour Photograph	Autofluorescence	OCT
<b>Score</b> <b>=00000</b> <b>=Common</b> <b>naevus</b>			
<b>Score</b> <b>=00001</b> <b>=Low-risk</b> <b>naevus</b>			
<b>Score</b> <b>=00200</b> <b>=High-risk</b> <b>naevus</b>			
<b>Score</b> <b>=02202</b> <b>=Probable</b> <b>melanoma</b>			

**Figure 13:** MOLES Score examples: Colour photograph, fundus autofluorescence image and optical coherence tomography of representative patients according to MOLES score. (A) MOLES = 0; (B) MOLES = 1; (C) MOLES = 2, (D) MOLES >2.

### 3.3. Results

The cohort comprised 222 patients (61.7% male) with a median age of 62.5 years (range, 17.3 – 89.9). (Table 3)

No tumours had a present mushroom shape; however, one tumour had broken through retinal pigment epithelium (RPE) but had only developed an incipient mushroom shape. Confluent orange pigment and significant SRF were present in 37 (16.7%) and 61 (27.5%) eyes respectively. Growth was documented in 13 (5.9%) tumours, all with MOLES scores exceeding 4, and all have been treated subsequently. (Table 3)

According to the MOLES scoring system, the tumours were categorised as ‘common naevus’, ‘low-risk naevus’, ‘high-risk naevus’ and ‘probable melanoma’ in 71 (32%), 36 (16.2%), 28 (12.6%), and 87 (39.2%), respectively.

Table 4 itemises the tumour features according to the MOLES score. According to the MOLES scoring system, the tumours were categorised as ‘common naevus’, ‘low-risk naevus’, ‘high-risk naevus’ and ‘probable melanoma’ in 71 (32%), 36 (16%), 28 (13%) and 87 (37%) respectively. By definition, none of the ‘common naevi’ showed any risk factors for malignancy. With respect to the clinical findings at presentation (i.e., excluding history of any growth), almost all ‘low-risk naevi’ had this category because of their borderline size (92%). Similarly, most ‘high-risk naevi’ were categorised as such because of size alone (61%), the next common combination being borderline size with a trace of subretinal fluid (32%). With ‘probable melanomas’, 23% of tumours showed all three features of malignancy, with 17% having a borderline size with confluent orange pigment and significant subretinal fluid and 16% being large with significant subretinal fluid.

Table 5 lists the clinical features in 16 tumours whose size category was determined by tumour thickness, resulting in a higher risk category in 6 naevi, having a tumour thickness of  $\geq 2$  mm.

The ocular oncologists diagnosed 79 tumours as melanoma and 143 as naevus; however, 2 diagnosed as naevi subsequently received brachytherapy so that

diagnosis was revised to melanoma and naevus in 81 and 141 tumours respectively. One naevus received PDT to improve vision by reducing SRF. The melanomas were treated with PDT (n=6), brachytherapy (n=68), proton beam radiotherapy (n=5) or enucleation (n=2). (Table 3)

Three (25%) of the 12 tumours with a MOLES score of 3, and 3 out of 75 with higher MOLES scores were not treated, because the oncologists had diagnosed naevus. (Figure 14) (Table 6)

Four of these 6 tumours had basal diameters exceeding 6 mm, all with SRF and/or orange pigment, and 2 small tumours showed either significant SRF with traces of lipofuscin, or vice versa.

These results indicate that MOLES correctly identified all 81 melanomas (100% sensitivity) and 135 out of 141 choroidal naevi (95.7% specificity; 95% Confidence Interval 92.4 – 99.1).

Clinical Findings		Categories	MOLES Category								Total	
			Common Naevus		Low-risk Naevus		High-risk Naevus		Probable Melanoma			
			n	%	n	%	n	%	n	%	n	%
<b>Sex</b>	Male		49	69	24	67	17	61	47	54	137	62
	Female		22	31	12	33	11	39	40	46	85	38
<b>Eye</b>	Left		35	49	18	50	11	39	39	45	103	46
	Right		36	51	18	50	17	61	48	55	119	54
<b>Visual Acuity</b>	20/20 - 20/30		59	83	31	86	25	93	64	74	179	81
	20/40 - 20/60		11	15	4	11	2	7	16	18	33	15
	20/80 - 20/200		1	1	1	3	0	0	2	2	4	2
	CF		0	0	0	0	0	0	3	3	3	1
	HM-NLP		0	0	0	0	0	0	2	2	2	1
<b>MOLES Score</b>	<b>Mushroom shape</b>	0: Absent	71	100	36	100	28	100	86	99	222	100
		1: Incipient (i.e., erosion of RPE over tumour, possibly with bulging of tumour)	0	0	0	0	0	0	1	1	0	0
		2: Present (i.e., with definite overhang)	0	0	0	0	0	0	0	0	0	0
	<b>Orange Pigment</b>	0: Absent	71	100	35	97	27	96	24	28	158	71
		1: Trace	0	0	1	3	1	4	24	28	27	12
		2: Confluent (i.e., forming clumps)	0	0	0	0	0	0	39	45	37	17
	<b>Large Size</b>	0: Small (i.e., base <3 DD & thickness <1 mm)*	71	100	3	8	1	4	1	1	76	34
		1: Borderline (i.e., base 3-4 DD or thickness = 1-2 mm)*	0	0	33	92	10	36	29	33	72	32
		2: Large (i.e., base >4 DD or thickness > 2 mm)*	0	0	0	0	17	61	57	66	74	33
	<b>Enlargement</b>	0: None	71	100	36	100	28	100	74	85	209	94
1: Uncertain		0	0	0	0	0	0	0	0	0	0	
2: Definite (i.e., with photographic proof of growth > 1/3 DD per year)		0	0	0	0	0	0	13	15	13	6	
<b>Subretinal Fluid</b>	0: Absent	71	100	34	94	18	64	2	2	125	56	
	1: Trace (i.e., detected only with OCT)*	0	0	2	6	9	32	25	29	36	16	
	2: Significant (i.e., visible by colour photography or ophthalmoscopy)	0	0	0	0	1	4	60	69	61	27	
<b>Treatment</b>	Nil	71	100	36	100	28	100	5	6	140	63	
	Photodynamic therapy (PDT)	0	0	0	0	0	0	7	8	7	3	
	Brachytherapy	0	0	0	0	0	0	68	78	68	31	
	Proton Beam	0	0	0	0	0	0	5	6	5	2	
	Enucleation	0	0	0	0	0	0	2	2	2	1	
	<b>Total</b>		71	32	36	16	28	13	87	39	222	100

Tumours are categorised as 'common naevus', 'low-risk naevus', 'high-risk naevus' and 'probable melanoma' according to whether the sum total of the scores for the five indicators of malignancy is 0, 1, 2 or >2. CF, count fingers; DD, disc diameters; HM, hand motions; NLP, no light perception; PDT, photodynamic therapy; SRF, subretinal fluid. \*If ultrasonography is not available, tumour thickness is measured with OCT. If OCT is not possible, thickness is estimated to be <1 mm, 1-2 mm or >2 mm if the tumour ophthalmoscopically appears flat, minimally thickened or having a prominent dome or mushroom shape. Cystic intra-retinal oedema and retinal pigment epithelial abnormality with cobblestone degeneration or hyper-autofluorescence are not significant if the retina is flat.

**Table 3:** Patient demographics according to MOLES score and expert diagnosis of choroidal lesion

MOLES Score	Size Category	Orange Pigment	Subretinal Fluid (SRF), n (%)			Total, n (%)
			Absent	Trace	Significant	
0	Small	Absent	71 (100%)	0	0	71 (32%)
		Trace	0	0	0	
		Confluent	0	0	0	
1	Small	Absent	0	2(6%)	0	36 (16%)
		Trace	1 (3%)	0	0	
		Confluent	0	0	0	
	Borderline	Absent	33 (92%)	0	0	
		Trace	0	0	0	
		Confluent	0	0	0	
2	Small	Absent	0	0	1 (4%)	28 (13%)
		Trace	0	0	0	
		Confluent	0	0	0	
	Borderline	Absent	0	9 (32%)	0	
		Trace	1 (4%)	0	0	
		Confluent	0	0	0	
	Large	Absent	17 (61%)	0	0	
		Trace	0	0	0	
		Confluent	0	0	0	
3	Small	Absent	0	0	0	12 (5%)
		Trace	0	0	1 (8%)	
		Confluent	0	0	0	
	Borderline	Absent	0	0	2 (17%)	
		Trace	0	2 (17%)	0	
		Confluent	0	0	0	
	Large	Absent	0	6 (50%)	0	
		Trace	1 (8%)	0	0	
		Confluent	0	0	0	
>3	Small	Absent	0	0	0	75 (32%)
		Trace	0	0	0	
		Confluent	0	0	0	
	Borderline <sup>2</sup>	Absent	0	0	0	
		Trace	0	0	7 (9%)	
		Confluent	0	5 (7%)	13 (17%)	
	Large <sup>3</sup>	Absent	0	4 (5%) <sup>1</sup>	12 (16%)	
		Trace	0	5 (7%)	8 (11%)	
		Confluent	1 (1%)	3 (4%)	17 (23%)	
Total			125 (56%)	36 (16%)	61 (27%)	222 (100%)

<sup>1</sup> One case with incipient mushroom shape. <sup>2</sup> Two cases with documented growth. <sup>3</sup> Eleven cases with documented growth.

**Table 4:** Clinical findings according to MOLES score

Case No.	MOLES score	Size category	Mushroom shape	Orange pigment	Tumour diameter (DD)	Tumour thickness (mm)	Enlargement	Subretinal fluid	Clinical diagnosis
107	1: Low-risk naevus	1	A	A	1.5	1.1	N	A	CN
79		1	A	A	1	1.2	N	A	CN
89		1	A	A	2	1.2	N	A	CN
99		1	A	A	2.5	1.2	N	A	CN
118	2: High-risk naevus	1	A	T	2	1.1	N	A	CN
110		1	A	A	2.5	1.1	N	T	CN
148	>3: Probable melanoma	1	A	T	1.5	1.2	N	S	CN
157		1	A	C	2	1.7	N	T	CM
149		1	A	T	2	2	N	S	CM
164		2	A	A	3	2.2	N	S	CM
171		2	A	T	3	2.3	N	T	CM
161		2	A	A	4	2.7	N	S	CM
183		1	A	C	2	1.1	N	S	CM
185		1	A	C	2	1.2	N	S	CM
197		2	A	C	3	2.6	N	T	CM
204		2	A	C	4	2.3	N	S	CM

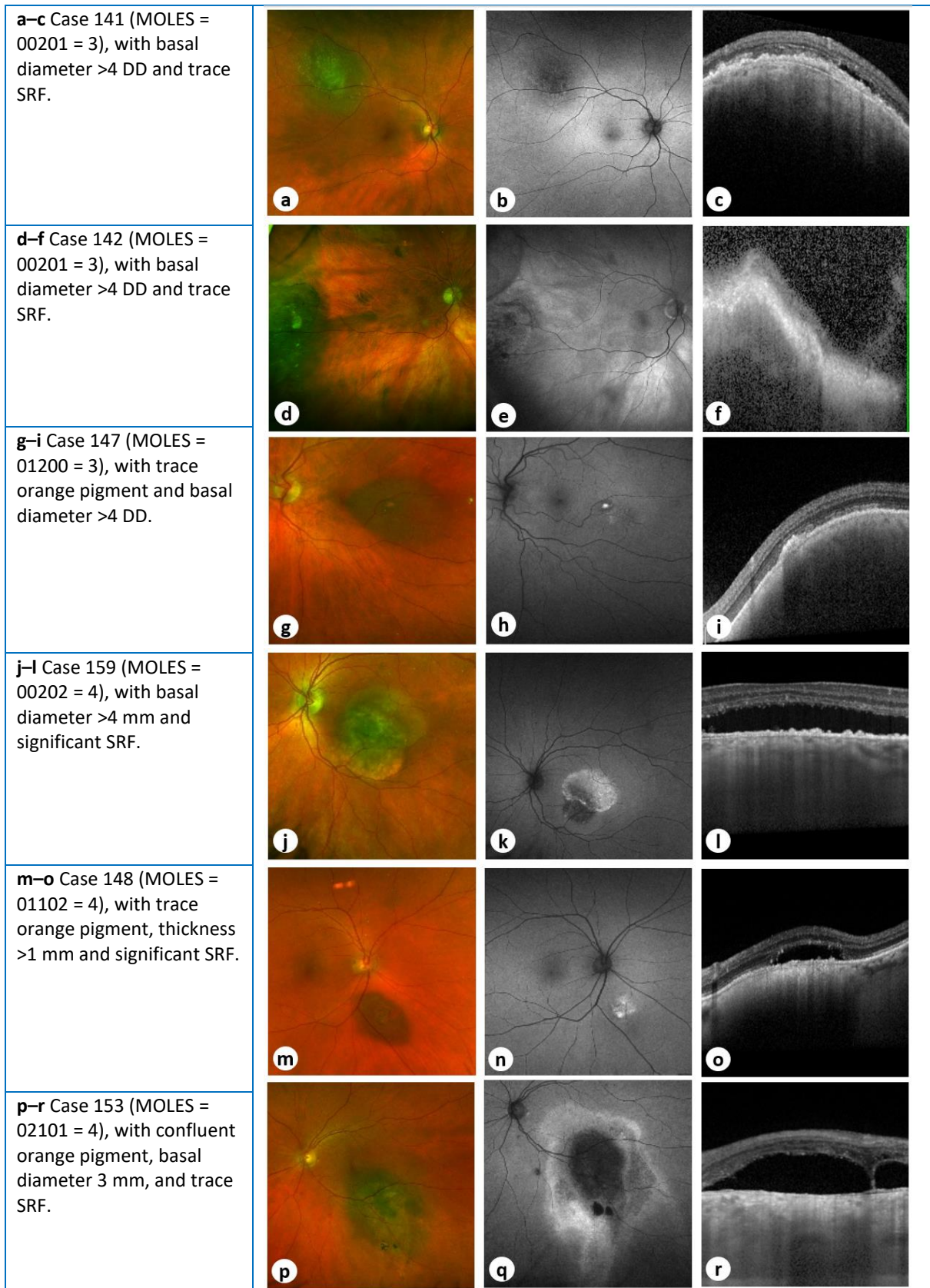
A Absent; C Confluent; CM Choroidal melanoma; CN Choroidal naevus; DD Disc diameters; mm Millimetres; N None; S Significant; T Trace

**Table 5:** Clinical features of 16 tumours whose size category was determined by thickness

Case No.	Age (years)	Sex	Eye	MOLES score	Orange pigment	Basal diameter (DD)	Thickness (mm)	Enlargement	Subretinal Fluid	Follow-up (years)	Treatment
141	74	F	R	3	A	4.5	1.4	N	T	2.9	N
142	88	M	R	3	A	8.5	1.2	N	T	2.7	N
147	70	F	L	3	T	5	1	N	A	3.1	N
148	56	F	L	4	T	1.5	1.2	N	S	2.7	PDT
153	58	M	R	4	C	3	0.5	N	T	3.1	N
159	63	M	L	4	A	6	0.9	N	S	2.5	N

A Absent, C Confluent, DD Disc diameters, F Female, L Left, M Male, mm Millimetres, N Nil, PDT Photodynamic therapy, R Right, T Trace,

**Table 6:** Clinical features of 6 tumours with a MOLES score exceeding 2 and diagnosed by the expert as naevus



**Figure 14:** OCTs and fundus autofluorescence images of 6 tumours with a MOLES score >2 and diagnosed by experts as naevus.

## 3.4. Discussion

### 3.4.1. Discussion of results

The MOLES scoring system indicated melanoma in all 81 tumours diagnosed as such by ocular oncologists, and naevus in 135 of 141 tumours given this diagnosis by these experts. Of the 6 tumours with discordant diagnoses, 4 had basal diameters exceeding 6 mm, all with SRF and/or orange pigment, and 2 small tumours showed either significant SRF with traces of orange pigment, or vice versa.

The MOLES scores correlated well with the experts' diagnoses of choroidal melanoma and naevus, with sensitivity and specificity levels of 100% and 96%, respectively. The discrepancy between the MOLES score and the experts' diagnosis in 6 tumours is not surprising, considering that there is no consensus on how patients with indeterminate lesions should be diagnosed and managed.<sup>52, 59</sup>

MOLES has a relatively low threshold for indicating malignancy; this is to reduce the risk of misdiagnosing choroidal melanomas as naevi in situations where expertise and equipment are limited and also because it is only designed to guide investigation and monitoring, not treatment.

The ultrasound measurements of tumour thickness increased the MOLES category in 6/222 (2.7%) tumours. This may have been spurious as it is known that ultrasonographic thickness measurements tend to be greater than those obtained by OCT or histology.<sup>87, 423</sup>

### 3.4.2. Strengths and weaknesses

The strengths of this study are the large number of patients (222) and the multimodality imaging. The reliability of having a team of well-known experts in the field of ocular oncology at Moorfields enabled a high-quality diagnostic standard the MOLES decisions could be validated against. There are several weaknesses. First, the



retrospective data collection from patients' charts prevented from determining the oncologists' estimate of risk of malignancy, which was not always documented. Second, it was not known how many untreated tumours would have grown with long-term monitoring. It could also not be known how many treated tumours would have remained unchanged if left alone. It would have been unethical to leave diagnosed melanomas untreated, because of the risk of metastasis. This problem is compounded by the lack of consensus amongst ocular oncologists as to which suspicious tumours should be diagnosed as melanoma. Third, MOLES scores were based on images not live examinations; this is an advantage, because it replicates the way images are assessed remotely in virtual clinics. Fourth, the oncologists' diagnosis was not confirmed histologically. It is not conventional practice to biopsy small melanocytic choroidal tumours to confirm malignancy, except in rare, selected cases. This is because with small tumours it is difficult to obtain sufficient tissue for analysis and because of the risk of complications. Finally, despite the large number of patients, no formal sample size calculation has been conducted, so further robust studies are required to confirm the validity of the research findings.

### 3.4.3. Discussion of methods and MOLES rationale

All consecutive patients irrespective of tumour size have been included in the study, because some large melanocytic choroidal tumours are benign (i.e., 'giant naevi').<sup>49</sup>

Melanocytomas and patients with congenital ocular melanocytosis have been excluded because the need for monitoring these is accepted and because the MOLES scoring system is not applicable to such lesions.

Basal tumour diameter has been measured in horizontal DD, accepting that this does not always correspond to 1.5 mm; this is because with thin and flat tumours this method is more accurate than ultrasonography. It is also a method that is easy to replicate outside of specialist centres.

The MOLES scoring system is based on clinical signs that are well accepted as features that differentiate choroidal naevi from melanomas. A study of more than 3000 cases by Shields et al. confirmed orange pigment ( $p=0.0004$ ), diameter  $>5$  mm ( $p=0.0275$ ), thickness  $>2$  mm ( $p<0.0001$ ) and SRF ( $p<0.0001$ ) to be statistically associated with tumour growth, which was taken to indicate malignancy.<sup>65</sup>

Choroidal naevi only rarely perforate RPE, and when they do, they do not develop a mushroom shape.<sup>42</sup> With such strong evidence in the published literature, further studies to show associations between the MOLES signs and malignancy in melanocytic choroidal tumours would have been redundant.

Some points regarding the MOLES scores require discussion. Mushrooming is a rare event and can be picked up only with ancillary tests. Although almost pathognomonic for melanoma, mushroom shape is given a MOLES score of only 2 to simplify scoring; this is justified because mushroom-shaped tumours inevitably have a total score exceeding 2 because of thickness. This should ensure that patients are referred for specialist opinion even in the rare event that mushroom shape is the only sign of melanoma. None of the tumours in this study had a mushroom shape present, and this is because tumours with this sign were triaged directly to the oncology clinic and not the naevus clinic. Occasionally, choroidal naevi can break through Bruch's membrane to invade the retina,<sup>42</sup> which is why this feature is given a score of only 1.

Several studies have shown orange pigment to be helpful in differentiating choroidal melanomas from naevi.<sup>41, 68, 74, 183, 424, 425</sup> Lipofuscin can accumulate over other choroidal tumours, such as metastases and hemangiomas;<sup>256, 426, 427</sup> however, MOLES is not designed to differentiate between melanocytic tumours and these lesions, which have other diagnostic clues, such as colour and shape. Confluent clumps of orange pigment, which should readily be seen with ophthalmoscopy or colour photography, are given a score of 2, with a score of 1 reserved for subtle dusting.

The size categories used by the MOLES system are mostly based on a study by Augsburger et al., who found approximately 125 choroidal naevi for every melanoma

in the thickness range of 1.5 to 2 mm, approximately 25 naevi for every melanoma in the thickness range of 2 to 2.5 mm, and approximately 5 naevi for every melanoma in the thickness range of 2.5 to 3 mm.<sup>52</sup>

It can be difficult to assess tumour thickness ophthalmoscopically. When OCT and ultrasonography are not available, it is recommended categorising thickness as 'absent', 'minimal' and 'significant' if the lesion appears flat, possibly raised, and definitely dome- or mushroom-shaped, respectively. With MOLES, tumour thickness > 2mm is given a score of 2 because it is associated with the most significant hazard ratio out of all the risk factors for growth at 5 years.<sup>65</sup>

The mean largest basal diameter LBD of choroidal naevi documented in the Blue Mountain Eye Study was only 1.25 mm.<sup>77</sup> In a histopathological study of 102 eyes, 13% of naevi were > 5.5 mm.<sup>283</sup> Augsburger et al. found 70 naevi for every choroidal melanoma in the basal diameter range of 5 to 6 mm, 10 naevi for every melanoma in the diameter range of 6 to 7 mm, and 3 naevi for every melanoma in the range 7 to 8 mm, approximately.<sup>52</sup>

Without OCT and US, it can be difficult to estimate tumour thickness; however, MOLES minimises this problem by combining thickness with diameter when categorising size, because it is rare for melanocytic tumours to grow in thickness without also increasing in diameter. Although choroidal naevi and melanomas overlap significantly with respect to size,<sup>52</sup> the discriminatory function of MOLES is enhanced by considering other indicators of malignancy.

Enlargement is included in MOLES because growth is such a strong indicator of malignancy and because, in some cases, it is the only suspicious feature. Naevi tend to enlarge during the first two or three decades of life. It is nevertheless necessary to monitor any naevi that are growing to ensure that such growth eventually ceases. This is because melanoma can develop in early life, albeit rarely. Some naevi can enlarge in adulthood, but such growth is rare and tends to be slow and subtle (i.e., <0.5 mm/year).<sup>60, 78</sup> A faster rate of growth (mean 1.0 mm/year, range 0.0 – 8.0 mm/year)<sup>65</sup> is representative of malignancy. An enlargement score of 1 is given when the change in size is minimal or when fundus photography suggests growth but is inconclusive

due to poor image quality. Growth before adulthood is not usually a sign of malignancy but nevertheless requires monitoring as choroidal melanoma can developed at a young age.<sup>428</sup>

Some patients present with what appears to be a common naevus that was not noted previously. Monitoring of such lesions usually reveals no growth, suggesting that these naevi were missed previously. For this reason, the MOLES system requires enlargement to be confirmed by sequential imaging.

There have been cases of patients presenting in later life with small, pigmented choroidal lesions with typical features of common naevus and growth over a short period, but which were definitely absent in previous photographs. Some ocular oncologists treat such tumours to remove any risk of metastasis should the lesion be malignant once the options are discussed with the patient, especially as there is evidence suggesting that some choroidal melanomas metastasise at a very early stage, when they are clinically indistinguishable from naevi.<sup>386</sup>

Subretinal fluid can develop over choroidal naevi, but it is usually minimal. In such cases, optical coherence tomography shows only a small area of retinal detachment over the tumour surface, together with an absence of retinal abnormalities such as retinal receptor disorganisation ('shaggy receptors').<sup>71</sup> Fundus autofluorescence imaging may show retinal pigment epithelial changes inferior to the tumour.<sup>429</sup> For these reasons, with the MOLES scoring system subretinal fluid is considered to be significant only if it is visible ophthalmoscopically, or if OCT shows marked subretinal fluid extending beyond the tumour margins. Some examiners with limited skills or equipment may find it difficult to see retinal detachment that should be given a score of 2 with the MOLES system. If such detachment involves the fovea, this would cause blurred vision or metamorphopsia. For this reason, the MOLES system recommends a score of 1 if the patient reports these symptoms and if no cause can be seen. Although choroidal melanomas commonly cause photopsia, these symptoms can also be caused by retinal traction and can be confused with migraine fortification spectra.

The MOLES system omits several features considered to indicate increased risk of malignancy. Statistical studies show that tumour proximity to the optic disc is not an

indicator of malignancy.<sup>65</sup> Many naevi do not show drusen on their surface and, conversely, these deposits can develop on some melanomas. Haloes around naevi are rare, so these cannot be considered to be a useful discriminator for screening.<sup>68</sup> A recent study has shown this feature to be statistically insignificant.<sup>65</sup> Assessment of internal acoustic reflectivity requires ultrasonography;<sup>65</sup> however, as mentioned, this is not widely available outside specialist units.

The TFSOM mnemonics categorise signs of malignancy in a binary fashion;<sup>65, 407</sup> however, it may not be possible to decide categorically whether a particular feature is present. The MOLES scoring system therefore includes an intermediate category for borderline and uncertain findings.

Tumours with a high MOLES score are categorised as 'probable melanomas' and not 'melanomas' because non-oncologists may not feel confident or qualified to distinguish melanomas from other tumours.

#### **3.4.4. Comparison with other studies**

There is extensive literature on clinical features predicting growth of melanocytic choroidal tumours. The largest study, performed by Shields et al., includes more than 3000 cases.<sup>65</sup> Using Kaplan-Meier analysis, it reports 5-year rates of 'malignant transformation' of choroidal naevi to melanoma in 1% to more than 50% of cases according to the number of risk factors that are detected.<sup>65</sup> The findings of the current study are consistent with those of Shields et al; however, Alharby et al. propose the MOLES mnemonic, which is more intuitive and perhaps more memorable in view of the lay term for melanocytic naevi (i.e., 'moles'). Furthermore, the MOLES system is designed for use by non-specialists, who may not have access to ultrasonography and other imaging modalities, and hence its greatest utility lies in community optometry and general ophthalmic practices, as a screening method for appropriate specialist referral.

In a further collaborative work, Roelofs et al. evaluated the MOLES system in 451 choroidal melanomas treated at Moorfields Eye Hospital and found a MOLES score

<3 in only one patient, whose tumour was located pre-equatorially.<sup>430</sup> This indicates that when used by an expert the risk of misdiagnosing choroidal melanomas as naevi is low. The present study extends the findings of that investigation, also including naevi to investigate the specificity of the MOLES scoring system.

Roelofs et al. also evaluated MOLES in a cohort of 99 patients who were treated for choroidal melanoma after a period of surveillance found that tumour progression was detected without ultrasonography in 98 cases.<sup>86</sup>

The two latter studies are further described in subsequent sections 3.5. and 3.6.

### 3.4.5. Clinical implications

The close correlation between the MOLES scores and the diagnosis at the ocular oncology clinic suggests that the MOLES scoring system should be useful as a triaging tool for describing the clinical features of melanocytic choroidal tumours and objectively defining the risk of malignancy in such lesions. This may be helpful to general ophthalmologists and optometrists who rarely encounter choroidal melanomas in their practice. The MOLES acronym should make it easier for ophthalmologists and optometrists to remember the key signs differentiating melanomas from naevi. Additionally, MOLES should be useful to a wider range of practitioners than mnemonics and acronyms that require ultrasonography to assess internal tumour reflectivity.

MOLES enables practitioners to concisely describe melanocytic choroidal tumours, encouraging more detailed documentation. For example, a MOLES score of '02201 = 5' succinctly conveys that the tumour is probably a melanoma with a basal diameter >6 mm and/or a thickness >2 mm together with confluent orange pigment and traces of SRF but no mushroom shape and no documented growth.

It is hoped that such objective categorisation of risk of malignancy will make it easier for optometrists and ophthalmologists to reassure patients with common naevi without

referring them to hospital for intensive investigation. The MOLES system may also enable ophthalmologists to discharge patients with common naevi from hospital, possibly providing such patients with a photograph of their lesion to take with them to their community optometrist at every routine 'check-up'. These measures should greatly relieve the burden on hospital resources, in view of the high prevalence of naevi, thereby shortening waiting times so that patients needing urgent care for ocular melanoma and other conditions can be seen and treated more quickly. Such personalised care should also prevent patients with minimal risk of malignancy from experiencing unnecessary anxiety, also preventing inconvenience to them and their families.

The scope of MOLES has been increased by the COVID-19 pandemic, which at least in the UK is encouraging practitioners to shift the care of patients with melanocytic choroidal tumours from ocular oncology centres to ophthalmic units closer to the patients' home and from these clinics to community optometrists.<sup>238</sup> This trend reduces the risk of coronavirus infection to patients and healthcare providers as well as minimising travelling costs for patients and conserving healthcare resources.

#### 3.4.6. Research implications

This investigation pertains only to the performance of MOLES when used by ocular oncology experts (e.g., as in virtual clinics); further studies are needed to validate this diagnostic aid when deployed by optometrists<sup>431</sup> and other ophthalmologists, who may lack the expertise and equipment needed to identify the clinical features of malignancy. Spurious MOLES scores may result if practitioners fail to recognise incipient mushroom formation or SRF, or if orange pigment is missed or mistaken for drusen, or if basal tumour diameter is not measured accurately (e.g., omitting callipers or a ruler).

The present investigation suggests that there is scope for such studies evaluating the MOLES algorithm in a wider context to determine its efficacy when deployed by optometrists and ophthalmologists in the community and in general ophthalmic clinics.

This should be done also in centres without access to any imaging other than colour photography, if possible, comparing the performance in such centres with that in clinics where optical coherence tomography, autofluorescence imaging and/or ultrasonography are readily available. These studies would provide some indication of the ability of optometrists and ophthalmologists to assess tumour dimensions and to detect orange pigment and subretinal fluid with and without special imaging.<sup>432</sup> Furthermore this would indicate which patients should be referred for specialist opinion and whether expert advice can reliably be based solely on images submitted with the referral documentation, with or without ultrasonography.

To this end, it is intended to investigate the ability of optometrists and ophthalmologists to assess tumour diameter and thickness and to detect orange pigment and SRF with and without special imaging. In keeping with the use of telemedicine during the Covid-19 pandemic, this investigation will be performed online. The planned investigation and other studies may also determine whether tumour thickness can be omitted from the MOLES scoring system as implied by the finding that this feature only rarely influences tumour categorisation.

There is a need for evidence from long-term outcomes studies on which to base categorisation of orange pigment and SRF in MOLES scoring. Albertus et al.<sup>50</sup> have developed a method of image analysis that compares autofluorescence of the tumour with that of a control region in the adjacent fundus (i.e., Index of Retinal Autofluorescence),<sup>50</sup> however, a simple system not requiring special software would be more likely to be deployed generally.

Differentiation between choroidal naevi and melanomas may be enhanced by the application of image analysis with artificial intelligence, as is already happening with other fundus disorders, and by genetic analysis of biopsy specimens, as has recently been achieved with cutaneous melanocytic tumours.<sup>409 433</sup>



The successful deployment of the MOLES system will depend on the efficiency of educational initiatives aimed at improving awareness and detection of clinical indicators of malignancy.

### 3.5. Related study 1: The MOLES system for planning management of melanocytic choroidal tumours: is it safe?

#### 3.5.1. Background of the study

This study was published in May 2020 by Roelofs et al. in *Cancers*. The author of this PhD thesis is a co-author of the study and contributed by critical review of results, writing and editing the manuscript.<sup>434</sup>

Choroidal melanomas in non-subspecialty clinics are infrequently seen, and up to one third of patients referred to an ocular oncology centre for uveal melanoma are found to have a simulating lesion. Most of them are commonly choroidal naevi,<sup>46, 435</sup> with a small risk of malignancy. Concurrently, patients with melanoma often experience long delays in diagnosis and referral, because their tumour is incorrectly classified as a 'suspicious naevus', in many cases due to the referring clinician being falsely reassured by its relatively small size. Consequently, patients potentially suffer more substantial ocular morbidity, visual loss, and perhaps metastatic disease that could have been prevented by timely referral and treatment.

The MOLES scoring system has been developed to help non-specialists improve their care of patients with melanocytic choroidal tumours. This comprises the MOLES acronym to highlight the clinical signs of choroidal melanoma; the MOLES score (Table 2) for estimating the probability of malignancy in melanocytic choroidal tumours; and the MOLES referral guidelines (Table 7) for managing patients according to the tentative diagnosis. Studies at the Ocular Oncology Service at Moorfields Eye Hospital and the Oxford Eye Hospital have revealed that a significant proportion of patients referred to these centres have common or low-risk naevi. If managed entirely in the

community, these patients could be saved the inconvenience and cost of travelling to hospital eye clinics. Transferring care to community optometrists could reduce waiting lists, lighten the burden on hospital clinics, and free up resources for patients in greater need of urgent specialist care.

The MOLES protocol advises patients with common naevi to undergo review by a community optometrist every two years, ideally with sequential colour photography. For other patients, multimodal imaging evaluated by an ophthalmologist is recommended. Referral for such care is considered non-urgent for patients with low-risk or high-risk naevi and urgent for patients with probable melanoma. (Table 7)

MOLES Score	Suggested management
<b>0 = Common naevus</b>	<b>Monitoring in community</b> with colour photography: annually.
<b>1 = Low-risk naevus</b>	<b>Non-urgent referral</b> for specialist investigation comprising widefield photography, autofluorescence imaging, optical coherence tomography and, in selected cases, ultrasonography. Subsequent surveillance to be undertaken at a specialist clinic or in the community according to risk of malignancy.
<b>2 = High-risk naevus</b>	
<b>&gt;2 = Probable melanoma</b>	<b>Urgent referral</b> to ophthalmologist with urgent onward referral to ocular oncologist if suspicion of malignancy is confirmed.

**Table 7:** MOLES tumour categories and suggested management

While various combinations of the risk factors for future growth are the basis for counselling and treatment decisions,<sup>425</sup> their role in establishing the urgency of referrals to an ocular oncologist has not been studied. There will be concerns that the MOLES scoring system will delay the treatment of some patients with choroidal melanoma, because the probability of malignancy is underestimated. To address these worries, this study has been performed to determine how many patients treated for choroidal melanoma at the oncology centre had a MOLES score indicating common or low-risk naevus at the time of treatment. In a subset of patients, who were treated after a period of monitoring, the tumours were scored according to the findings at the first assessment.

### 3.5.2. Methodology

The electronic health records of 615 patients undergoing treatment for uveal melanoma between 1 January 2017 and 31 December 2019 with laser (photodynamic therapy or trans-pupillary thermotherapy), plaque brachytherapy, proton beam radiotherapy or enucleation have been reviewed. The following data were collected: dates of birth, sex, first assessment and treatment, therapeutic modality, the affected eye, and presence and size of any extraocular tumour extension. Tumours were staged according to the 8th edition of the American Joint Cancer Committee (AJCC) TNM (tumour, node, metastasis) classification.<sup>159</sup> (Table 1) Patients were excluded from the study if: (a) they had undergone previous treatment for uveal melanoma (11 patients), (b) the tumour extended anterior to ora serrata, to involve the iris and/or ciliary body (106 patients), and/or (c) imaging of the tumour was lacking or inadequate (47 patients).

Imaging of the tumour comprised widefield, colour and autofluorescence photography (Optos California [Optos plc, Dunfermline, Scotland]), optical coherence tomography (OCT) (Heidelberg Spectralis; Heidelberg Engineering GmbH, Heidelberg, Germany), and B-scan ultrasonography (ACUSON S2000; Siemens Healthcare Limited, UK). Mushroom shape, orange pigment, large size, enlarging tumour and subretinal fluid were scored and tumours categorised as common, low-risk, high-risk naevus or probable melanoma, as described in Table 2.

Statistical analysis was completed using commercially available software (Stata Statistical Software. StataCorp LP). Conventional descriptive statistics were used, and data presented as mean  $\pm$  standard deviation (SD). This study was approved by the Moorfields Eye Hospital clinical audit department (No; 452) and was conducted in accordance with the declaration of Helsinki.

### 3.5.3. Results and main findings

A total of 451 patients (mean age,  $63.9 \pm 13.9$  years) were included. At treatment, the mean largest basal tumour diameter (LBD) and thickness were  $10.3 \pm 2.8$  mm (range, 3.0 – 23.0) and 4.3 mm (range, 1.0 – 17.0). All but one (0.2%) had MOLES scores of  $\geq 3$ . Eighty-two patients were treated after surveillance lasting a mean of 1.5 years. Initially, most (63/82; 76.8%) had a MOLES score  $\geq 3$ . Importantly, none of the 451 tumours had a score of  $< 2$ , and as such, the MOLES protocol would have indicated referral to an ocular oncologist for 100% of patients.

The study's main finding was that none of the 451 patients would have experienced a delay in referral to an ocular oncologist if their tumour had been correctly scored with MOLES and management organised following MOLES recommendations. This is because all the patients in the cohort had a MOLES score of 2 or more.

The main aim of this study was to determine whether patients with choroidal melanoma would suffer delays in referral and treatment because of a low MOLES score. The findings suggest that delays are likely to occur only in exceptional cases because none of the 451 patients in the cohort had a low score at the time of treatment, or in the 82 cases with deferred treatment, at initial assessment.

### 3.5.4. Clinical implications

Singh et al. estimated an overall annual risk of uveal melanoma arising from a pre-existing naevus to be 1 in 8845, with this risk exceeding 1 in 3000 in patients older than 70 years.<sup>75</sup> Kivelä et al. took these calculations a step further, taking into account that some uveal melanomas arise de novo, and refined the lifetime risk estimate to 1 in 500.<sup>436</sup> As mentioned, surveillance of common and low-risk melanocytic tumours in the community could reduce costs and inconvenience for patients, most of whom are elderly. Such community care could also reduce hospital waiting lists, allowing limited resources to be allocated to patients with a higher need for urgent specialist care.

Currently, a sizable proportion of melanocytic choroidal tumours are categorised as 'suspicious naevi', 'nevomas'<sup>437</sup> or 'melanocytic tumours of indeterminate malignancy'.<sup>438</sup> There is much variation in the management of patients with such lesions. It is hoped that MOLES would make the care of these patients more systematic by splitting these indeterminate tumours into 'low-risk' and 'high-risk' naevi and defining the clinical features of each of these.

There will be lesions with a low MOLES score that eventually prove to be malignant. This may happen if clinical signs of malignancy are missed or because a de novo melanoma is identified at a very early stage, when it may be identical to a common naevus. Such lesions are possibly to be small and slow growing, so that serious consequences of misdiagnosis should be avoided if all patients are reassessed every 1 - 2 years in the community.

There is a longstanding controversy about treating small choroidal melanomas or observing these until growth is documented.<sup>439</sup> Important and difficult as they are, these dilemmas are less relevant to the MOLES scoring system, which is intended as a guide to recommended investigation and monitoring, not timing and method of treatment.

### **3.5.5. Implication of the MOLES scoring system for tele-oncology**

Tele-oncology platforms for monitoring choroidal and iris naevi have been previously reported.<sup>232</sup> Considering that the MOLES scores in this study were purely based on a prospective review of patient imaging, the results are generalisable to tele-ophthalmology platforms. Since alternative healthcare delivery platforms continue to be developed, there may be a bigger scope for virtual consultation and remote triaging of patients.<sup>95</sup> Previous studies evaluating optometric referrals found that triage via tele-ophthalmology reduced office visits to retina specialists by 48%, saving patients time and cost associated with travel and improving efficiency of clinical examination and testing for those requiring treatment.<sup>440</sup> Implementing the MOLES scoring system may similarly avoid referrals for choroidal melanocytic lesions. Innovations in this field can

increase access to sub-speciality care in a cost-effective way, particularly in geographic regions where the mean number of ophthalmologists falls as low as 9 per million population.<sup>441, 442</sup>

### 3.5.6. Strengths and weaknesses of study

The main strengths of this study are the large number of patients, the multimodal imaging, and the expertise of the ocular oncologists reviewing the images and deciding on patient care. This study has several weaknesses. Some data were missing due to lacking or inadequate imaging. It was not always possible to estimate the horizontal disc diameter accurately, so that measurements of basal tumour diameter were imprecise. Optical coherence tomography was not possible in many patients, because the tumour was too thick or peripheral. These limitations reflect real-world challenges, thereby enhancing the relevance and applicability of the results.

### 3.5.7. Implications for research

Further studies are needed to evaluate the use of the MOLES scoring system in the community. The diagnostic accuracy of this system will depend on the ability of clinicians to recognise the relevant signs of malignancy, with and without the aid of optical coherence tomography, fundus autofluorescence imaging, and ultrasonography. The success of the MOLES program will also depend significantly on educational methods and campaigns that are instituted and need to be developed. There is scope for long-term follow-up studies to determine how many patients ever show growth of their tumour after discharge from specialist care for monitoring in the community. This could be done by asking patients or their optometrists to complete a brief electronic questionnaire every 1-2 years, possibly attaching a colour photograph of the lesion to the questionnaire for assessment at the specialist centre.

### 3.6. Related study 2: Detecting progression of melanocytic choroidal tumours by sequential imaging: Is ultrasonography necessary?

#### 3.6.1. Background of the study

This study was published in July 2020 by Roelofs et al. in *Cancers*. The author of this PhD thesis is a co-author of the study and contributed by critical review of results, writing and editing the manuscript.<sup>434</sup>

The past decade has seen advances in multimodal ocular imaging and in telemedicine platforms, allowing innovative delivery of care in several ophthalmic subspecialties,<sup>233-236, 443</sup> including oncology.<sup>53, 231, 232</sup> This technology enhances opportunities for virtual monitoring of melanocytic choroidal tumours of uncertain malignancy. Additionally, such remote surveillance is particularly beneficial for patients who live far from ocular oncology centres, and it provides the potential to be adopted more broadly as a result of the COVID-19 pandemic and its aftermath.<sup>238</sup>

Choroidal naevi are common, with a prevalence ranging from 0.3% to 6.5%.<sup>63, 77, 444-447</sup> It is estimated that malignant transformation occurs in less than 1 in 8000 choroidal naevi/year,<sup>75</sup> correlating to an adjusted lifetime risk estimate of 0.2%.<sup>436</sup> There is increasing evidence that some choroidal melanomas metastasise early.<sup>386, 439</sup> Therefore, monitoring choroidal naevi to identify early transformation to melanoma is widely recommended.

Several imaging modalities are used to monitor choroidal naevi, including fundus photography, autofluorescence (AF), optical coherence tomography (OCT) and ultrasonography (US). The intensity of monitoring is often classified according to the number of clinical risk factors present.<sup>41, 68, 74, 113</sup> Unlike fundus photography, OCT and AF, ultrasonography needs a highly skilled operator, which means that tele-oncology programs still require patients to travel to a central location where this imaging equipment and expertise are available.<sup>232</sup>

The developed MOLES acronym, score and management protocol enable non-subspecialty assessment of melanocytic choroidal tumours without ultrasonography and other specialised equipment.<sup>448</sup>

This study aimed to determine if ultrasonography is necessary to detect progression of choroidal melanocytic tumours undergoing sequential colour photography, AF and OCT from a population of cases that demonstrated documented growth after a period of observation.<sup>430</sup>

### 3.6.2. Methodology

As part of this study, all cases of choroidal melanoma treated at Moorfields Eye Hospital between January 2016 and March 2020 have been reviewed, to identify those with prior sequential imaging spanning a time interval  $\geq 2$  months. Patients were excluded if the entire tumour margin was not identified on widefield fundus photography (Optos California [Optos plc, Dunfermline, Scotland]). In cases with more than one melanocytic choroidal tumour, only the lesion that eventually progressed to treatment was considered.

Ocular imaging consisted of fundus photography, AF, OCT and US. Patient medical files were then reviewed for demographic data, including sex, tumour laterality, age, the reason for delaying ocular therapy, and type of treatment.

Tumours were categorised using the MOLES system (Table 2) and given MOLES scores according to earliest available imaging and the latest imaging preceding treatment. Lipofuscin was assigned a score of 1 if detected by FAF alone and a score of 2 if visible on colour images. Similarly, SRF was scored as 1 if identified only by OCT and as 2 if apparent in fundus photographs.

Longitudinal and transverse basal tumour dimensions were measured using the Optomap callipers, converting pixel number to distance in millimetres using the horizontal disc diameter as a scale, assuming this to be 1.5 mm. Tumour thickness



was assessed by B-scan ultrasonography, measuring the distance from the internal scleral surface to the thickest part of the tumour, excluding retina.

Tumour growth was assessed by reviewing sequential photographs and comparing any change in distances between tumour margins and fundus landmarks, such as optic disc and retinal blood vessels. Detection of tumour progression was categorised as being achieved by: (A) photography, if there was a visible increase in basal tumour dimensions and/or if confluent clumps of orange pigment became apparent (O=2); (B) fundus autofluorescence imaging, if hyperfluorescent dusting of lipofuscin appeared (O=1); (C) OCT, if traces of SRF were detected only with OCT imaging technique (S=1); and (D) ultrasonography, if the measured tumour thickness increased by more than 0.5 mm.

The largest basal tumour diameter was estimated from transverse and longitudinal measurements, whichever was larger. In some cases, photographic growth was captured without any increase in LBD, because such growth does not always develop in the same direction as the largest basal diameter.

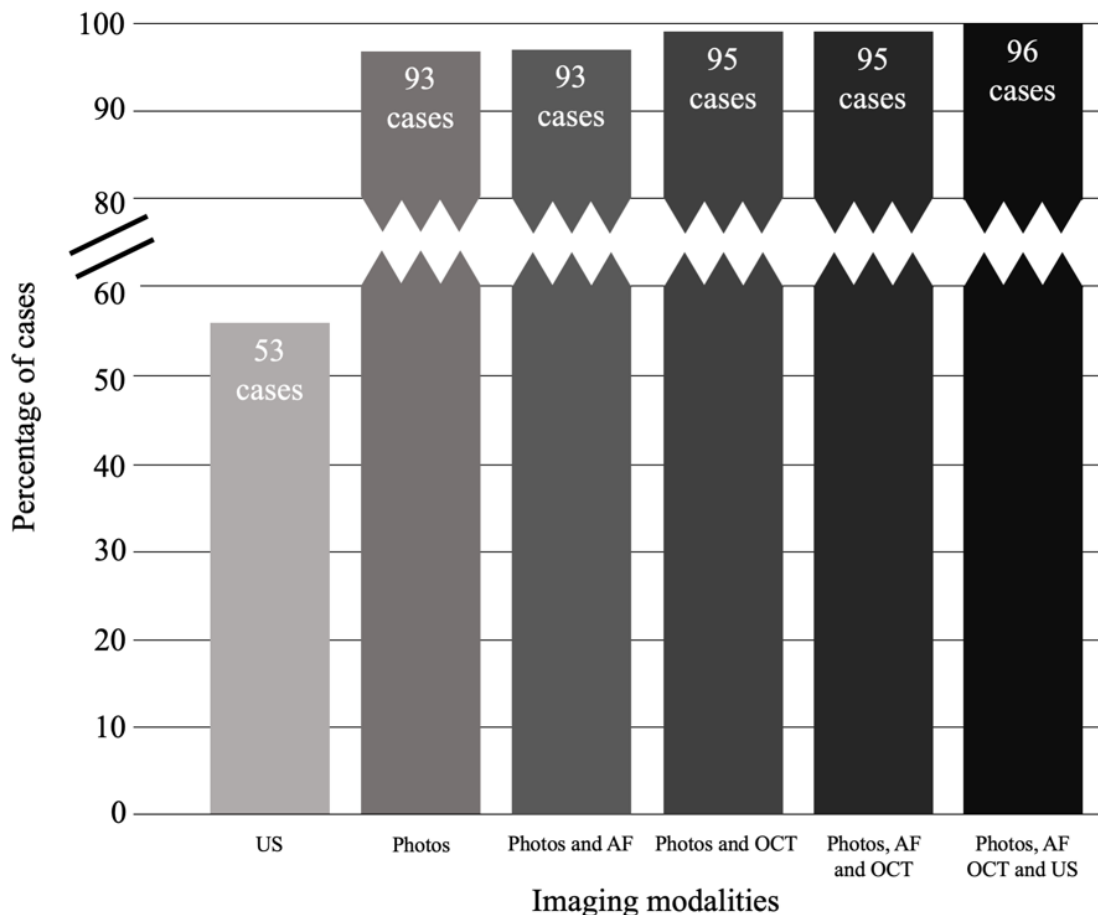
Statistical analysis was completed using commercially available software (Stata Statistical Software. StataCorp LP). This study was approved by the Moorfields Eye Hospital clinical audit department (No; 452) and was conducted in accordance with the declaration of Helsinki.

### **3.6.3. Results and main findings**

A total of 99 patients with a mean age of 66 years (range, 26-90) were included. The initial MOLES score was 1 in 2 cases, 2 in 23 cases, and  $\geq 3$  in 74 cases. Progression was detected with sequential colour photography alone in 100% of MOLES score 1 and 2 and 97% of lesions with a MOLES score of  $\geq 3$ . When findings on AF and OCT were included, sensitivity for detecting subtle change without ultrasonography improved to 100% for MOLES score 3 and 97% for MOLES score 4 and 5. Only one

patient included in this study had an isolated increase in thickness that may have been missed had sequential ultrasonography not been performed.

In this study, it was found that progression of melanocytic choroidal tumours could be detected by sequential colour photography alone in 100% of lesions with a MOLES score of 1 or 2 (i.e., low-risk and high-risk naevi, respectively) and 97% of lesions with a MOLES score of  $\geq 3$ . Failure to detect progression without ultrasonography would have occurred in only 1/99 (1%) cases; this tumour had a MOLES score of 4, so according to the MOLES protocol, the patient would be already under the care of an ocular oncologist, who would have had ready access to ultrasonography. Three cases did not show any progression. (Figure 15)



\*Criteria for detection of progression on photos includes (a) growth in basal dimensions and/or (b) development of clumps of orange pigment.

**Figure 15:** Progression of choroidal melanocytic tumours detected by various combinations of imaging modalities.<sup>430</sup>

### 3.6.4. How important is monitoring tumour thickness?

Tumour thickness is a well-documented indicator of malignancy in melanocytic choroidal tumours<sup>65</sup> and is also a predictor of metastatic death post treatment of choroidal melanoma.<sup>159</sup> Moreover, an increase in tumour thickness and/or basal diameter of a choroidal melanocytic lesion has historically been regarded as a reliable factor of malignancy.<sup>61, 449</sup> Thinner tumours (1.1 – 2.0 mm) show proportionally larger increases in basal diameter than in thickness (2.7 mm versus 1.0 mm) compared to thicker tumours (>3.0 mm), in which basal diameter and thickness increase with a ratio of 1:1 (i.e., 1.0 mm versus 0.9 mm).<sup>65</sup> The results of this study align with this finding, as they show an increase in basal dimensions occurred in 96% of MOLES 1 and 2 lesions, with a mean initial thickness of 1.6 mm. 36 cases with tumour progression did not show a corresponding increase in thickness on US, compared to only 1 case that grew on US but was missed by photography/AF/OCT.

In an effort to minimise reliance on ultrasonography, the MOLES scoring system categorises lesions by size based on a combination of thickness and/or largest basal dimension (Table 2), which poses the question: how often do choroidal melanocytic tumours exhibit isolated growth in thickness without accompanying increases in basal dimensions or other signs of progression? The study suggests that progression indicated by ultrasonography alone is rare, occurring in only about 1% of cases. As the study was conducted at a tertiary, ocular oncology centre, lesions were larger and had more signs of malignancy than would be encountered in a typical community setting. Therefore, there was a reasonably large proportion of patients with MOLES scores  $\geq 3$  for whom the MOLES protocol recommends referral to an ocular oncology centre. As tumours monitored in the community would be expected to be smaller, cases showing isolated progression detected only on ultrasonography are probably to be even less common than the 1% found in this study.

In this study, photographic presentation of growth in basal dimensions was determined by comparing the lesions' extent in relation to disc and vascular landmarks, as is usually done in clinical practice. However, calliper placement for the quantification of basal dimensions was challenging in some lesions, particularly those with indistinct

margins. This introduced an undeniable level of variability and error in the LBD measurements and the determination of change in LBD over time. Moreover, as an increase in lesion dimensions did not always occur along the meridian of the LBD, in isolation these values do not accurately represent the true degree of change in the lesion size. Therefore, it is important to emphasise that comparison of lesion margins in relationship to retinal vascular landmarks, rather than sequential measurement of LBD, should be used to identify growth on colour photography.

### **3.6.5. Value of ultrasonographic evaluation in addition to measurement of tumour thickness**

Low internal acoustic reflectivity (i.e., 'ultrasonographic hollowness') can support differentiation of choroidal naevi from melanomas<sup>68, 72, 239, 425</sup> and is helpful in a subspecialty ocular oncology practice when weighing the benefits and risks of treatment against observation. In regard to echographic changes over time, Doro et al. found that naevi <1.5 mm thick showed no change, whereas a progressive increase in hollowness on B-scan occurred in 18% of tumours with thickness >1.5 mm.<sup>450</sup>

Monitoring relatively small tumours with ultrasonography has various limitations.<sup>82</sup> First, this modality may fail to detect thin tumours.<sup>53</sup> Second, with thin tumours, it frequently overestimates lesion thickness.<sup>87</sup> Third, thickness measurements can be over-estimated by accidental inclusion of the scleral and/or retinal thickness or unintentional oblique scans. Fourth, the well-established and documented 0.5 mm inter- and intra-observer variability in tumour thickness measurement represents a large percentage change in thickness of small tumours.

### **3.6.6. Optimal method for measuring tumour thickness**

With small, posterior tumours, enhanced depth imaging OCT (EDI-OCT) may be a reasonable alternative in community practices if posterior shadowing does not limit this. EDI-OCT can detect posterior scleral bowing in 5-14% of choroidal naevi,<sup>82, 106</sup> especially those with a surrounding halo,<sup>89</sup> less/mixed pigmentation or posterior

location.<sup>106</sup> In such cases, ultrasonographic measurement may underestimate true tumour thickness, although, in most instances, ultrasound overestimates the thickness of minimally elevated choroidal tumours. OCT is superior to ultrasound for measuring thickness of small choroidal tumours (<1 mm thick). However, measurement of tumour thickness with OCT may not be possible if this imaging does not show the interface between tumour and sclera, if the tumour is thicker than 2 mm or if located in the peripheral fundus.<sup>87</sup>

### 3.6.7. Benefits of omitting ultrasonography from the monitoring of choroidal naevi

Ultrasonography requires specialised equipment and an experienced operator, and as such, it is often a limited resource in community settings. As a result, even where ocular oncology care is delivered via telemedicine platforms, patients are required to travel to centralised hubs where ultrasonography is available.<sup>231, 232</sup> Omission of ultrasonography from monitoring of choroidal naevi may help to implement tele-oncology programs and maximise benefits for patients by decreasing time and cost associated with travel. In addition, these programs would likely enhance the cost-utility of monitoring choroidal naevi.<sup>451</sup> Widefield fundus photography, AF and OCT are commonly available in the community. In this study, only one case of progression would have been missed had ultrasonography not been performed; however, the increase in thickness in this case was only 0.7 mm and may have represented measurement variability rather than true growth. As mentioned, this patient had clinical features strongly suggestive of melanoma with a MOLES score of 4 indicating 'probable melanoma' and triggering referral to an ocular oncologist.

There are scenarios in which ultrasonography is needed to assess tumour thickness, including tumours that are too peripheral or too thick to be accurately measured with OCT. Smaller lesions have the tendency to grow disproportionately in basal dimensions compared to height and thus, are improbable to increase  $\geq 0.5$  mm in thickness without also demonstrating an increase in basal dimensions. However, monitoring the tumour thickness is more important for larger tumours (LBD >6 mm),

where thickness and LBD tend to increase in an approximately 1:1 ratio. Therefore, in larger tumours, sometimes, an increase of  $\geq 0.5$  mm in thickness may be accompanied by only a small increase in basal dimensions.

### 3.6.8. The role of internal reflectivity and internal vascularity in the monitoring of choroidal melanocytic tumours

Emphasising the importance of multimodal imaging, particularly in cases where ultrasonography is not performed, the purpose of this study was not to determine the usefulness of ultrasonography, but rather to determine if the sum of findings on multimodal imaging could compensate adequately in order to detect progression of choroidal melanocytic lesions in cases where echography is not performed. In this series, 100% of lesions categorised as MOLES 1 or 2 would have had progression detected without the need for ultrasonography. Therefore, the data show that in these lesions, the sensitivity for detecting progression is not affected by eliminating echography, regardless of what additional information it may or may not contribute.

In certain circumstances, echographic findings, including intra-tumoral vascularity and internal reflectivity, can be helpful. A thorough literature review did not show any scientific evidence to support that changes in internal reflectivity and/or intra-tumoral vascularity reliably identify progression of choroidal naevi to melanoma.<sup>434</sup>

The study advocates that MOLES 1 and 2 can be safely monitored without the need for ultrasonography. In the majority of cases, lesions that are classified as MOLES 1 and 2 have a thickness of less than 2 mm, and therefore, many are too thin to accurately and reliably assess internal reflectivity and intrinsic vascularity on ultrasonography. Moreover, the thickness of these relatively small lesions is perhaps more accurately measured with OCT rather than ultrasonography.<sup>87</sup>

### 3.6.9. Strengths and weaknesses

The greatest strength of this study is the large number (96) of progressing melanocytic choroidal tumours. As the study included only tumours that were eventually treated, only three cases did not show any progression. This is not a weakness as it was not an intention to investigate how many choroidal naevi show progression. A large retrospective study of nearly 4,000 choroidal naevi showed malignant growth in only 90 cases.<sup>65</sup>

However, as Singh et al.<sup>402</sup> have demonstrated, it is rare for choroidal tumours with a MOLES score of 0 or 1 to grow, and as such, a study assessing this sub-set of patients would have to be incredibly large in order to have enough cases of progression to draw any meaningful conclusions. It is also important to note that the MOLES scoring system is not intended to be used by ocular oncologists to select patients for treatment, but rather to guide non-specialists in optimising monitoring and referral decisions.

It is possible that tumours that progressed were excluded from this study because they were not treated. Such cases are likely to be very rare because all patients were assessed by experienced ocular oncologists in a tertiary referral centre and regularly underwent assessment with serial colour photographs, AF, OCT and ultrasonography.

### 3.6.10. Further research

As all the imaging of all cases included in this study was reviewed by authors with subspecialty training in ocular oncology, further research is required to determine the ability of non-specialists to detect lateral extension and orange pigment.

Additionally, all fundus photographs were obtained using widefield fundus photography (Optos California [Optos plc, Dunfermline, Scotland]). Future studies aimed to assess the effect of various imaging platforms and quality on the observer's ability to detect progression are necessary.

Further studies could also explore in more detail whether thickness measurement is required for MOLES scoring of melanocytic choroidal tumours by examining if the patient's MOLES tumour size categories were determined by tumour thickness.

The largest basal tumour diameter and tumour thickness could be measured from optos and OCT images, respectively, to find if tumour thickness could be ignored under specific conditions, e.g., if the assessment of the largest basal diameter alone is adequate, as this parameter influences the impact of MOLES thickness score and therefore the size score.



## 4. CHAPTER FOUR: Prospective Validation of a Virtual Clinic Pathway in the Management of Choroidal Naevi

### 4.1. Introduction

Choroidal naevus describes an ocular fundus lesion akin to a mole. They are common, present in up to 7% of the general population and are increasingly identified during routine eye checks in community optometry services as an incidental finding.<sup>77, 146</sup> The majority are benign, but the potential for missing an early melanoma often prompts urgent over-referrals to ophthalmologists and even ocular oncologists.<sup>51</sup>

Choroidal naevus is a common tumour, particularly in Caucasian patients, and carries a small potential for transformation into melanoma.<sup>54, 58, 61, 70, 75, 77</sup> There are exceptions, such as giant choroidal naevi (10 mm or more in diameter), which were estimated to transform into melanoma in 18% over ten years.<sup>44, 45</sup>

In several reports, risk factors of growth have been outlined, including thickness (T) more than 2 mm, subretinal fluid (F), symptoms (S) flashes/floaters/blurred vision, orange lipofuscin pigment (O) and margin (M) less than 3 mm from optic disk.<sup>41, 55, 59</sup> This schema has been modified recently to include imaging and autofluorescence (AF) to judge orange pigment and optical coherence tomography (OCT) to ascertain the presence of fluid.<sup>72, 113</sup>

In a previous pilot-study,<sup>53</sup> a model of managing such lesions in a virtual pathway was described, comparing retrospectively the outcomes from imaging graded by a masked non-medical grader or a masked ophthalmologist versus clinical assessment of patients by an ophthalmologist, the gold standard. In 101 cases, the agreement was impressive at 96.1% between the masked non-medical grader and 100% between the masked ophthalmologist with the gold standard clinical encounter. However, the study group cautioned against the widespread adoption of this pathway until a larger cohort had been prospectively assessed. In the digital era, evolutions in imaging and communication technologies offer unprecedented opportunities for service

transformations that are particularly relevant to Ophthalmology. Although such innovative service redesigns are often piloted at small scale and demonstrate early potential, the decisions by policy makers to transition to such novel service models need to be informed by robust evidence from well-designed implementation science research. This study was designed to address all aspects of implementation science for the proposed virtual model of care, including safety, cost-effectiveness and acceptability by patients and healthcare practitioners.

The study presents the results on a large prospective cohort to validate a virtual model for managing choroidal naevi referrals in terms of its safety.

It was published in 2020 by Al Harby et al. in the *British Journal of Ophthalmology*. The author of this PhD thesis is the first author on this publication<sup>95</sup>

## 4.2. Patients and Methods

### 4.2.1. Study design

The method included prospective analysis of the clinical details and imaging of patients attending the naevus clinics at the Manchester Royal Eye Hospital (MREH) and Moorfields Eye Hospital (MEH). It was aimed to evaluate the outcomes of a one-stop, dedicated virtual clinic to image 400 eyes referred with choroidal naevi, comparing masked decisions by non-medical graders and ophthalmologists based on the review of images alone against the gold standard of full clinical evaluation by an ophthalmologist in a face-to-face consultation, including indirect fundoscopy.

The study had ethical approval (16/NW/0288) and adhered to the tenets of the Declaration of Helsinki. It was supported by a National Institute of Health Research/Research for Patient Benefit (PB-PG-0215-36081) - 'the NAEVUS study' research grant and sponsored by the Manchester University NHS Foundation Trust. Consecutive patients attending the naevus clinics of MREH and MEH gave informed

consent and were included. Patients with pathologies other than choroidal naevi, such as erroneous referrals, including congenital hypertrophy of the retinal pigment epithelium, were excluded from the agreement analysis. Accuracy in recognising alternate pathologies between the virtual and face-to-face pathways was an additional outcome measure.

#### **4.2.2. Patient pathway, clinical and imaging assessments, management decisions**

Study subjects were assessed by an ophthalmologist with ophthalmic examination, including fundoscopy. Imaging tests were performed by a technician and stored in the relevant databases in MREH or MEH, including widefield colour imaging optos (Optos, Dumfermline, UK), fundus autofluorescence imaging AF (Optos, Dumfermline, UK), optical coherence tomography OCT (Spectralis, Heidelberg Engineering GmbH, Heidelberg, Germany) and B-scan ultrasound. Both centres used the same imaging modalities.

Management decisions (Table 8) were made by the ophthalmologist (the gold standard) and allowed one of three options:

1. Discharge to the care of referring community optometrist, following a single confirmatory follow-up visit at six months;
2. Follow up in hospital-based naevus clinic at a set interval; or
3. Referral for specialist opinion to ocular oncology on the basis of a specific decision-making algorithm.

All patients were offered a second appointment at six months, including in cases deemed of negligible risk, suitable for discharge to the care of community optometrists, as per existing protocols in relevant clinics. This fail-safe process was meant to verify the appropriateness of original decision-making and also in order to fulfil the guideline of the Royal College of Ophthalmologists for lesion growth to be examined amongst the criteria for patient referral to specialist ocular oncology services.

Study recruitment commenced in June 2016 and ended in July 2017. Interim safety analysis of prospectively collected data was carried out after ten months of commencement of the study.

The role of the present author in this study was to extract the data, analyse the results, discuss its meaning, and write the manuscript.

Management decisions		
<b>Refer to Ocular Oncology subspecialist clinic if</b>	<b>A: Any one of the following:</b> <ul style="list-style-type: none"> <li>▶ Thickness &gt;2.0 mm</li> <li>▶ Collar-stud configuration</li> <li>▶ Documented growth</li> </ul>	<b>OR B: Any two of the following:</b> <ul style="list-style-type: none"> <li>▶ Thickness &gt;1.5 mm</li> <li>▶ Orange pigment</li> <li>▶ Serous retinal detachment</li> <li>▶ Symptoms</li> </ul>
<b>Follow up in naevus clinic at set interval if anyone of the following is present</b>	<ul style="list-style-type: none"> <li>▶ Naevus detectable on ultrasound</li> <li>▶ Orange pigment</li> <li>▶ Subretinal fluid</li> <li>▶ Location in extreme periphery</li> <li>▶ Base diameter &gt;3 DD</li> <li>▶ More than one naevus in one eye</li> <li>▶ Within 1 DD of the optic disc</li> </ul>	
<b>Discharge back to the care of community optometrist</b>	If none of the criteria set out for follow up or refer are present	
Reading Centre graders and masked ophthalmologists assessing imaging test results in isolation had the option of the above management decisions. DD, disc diameter		

**Table 8:** Management algorithm

### 4.2.3. Masked grading and definition of gold standard

Imaging data, including widefield fundus images, AF and OCT, were transferred to the Reading Centre, UCL Institute of Ophthalmology, in a pseudo-anonymised coded form. These were assessed by both experienced non-medical graders (trained optometrists) and by medical graders (ophthalmologists) within the Reading Centre based on strict guidelines, with the same possible management outcomes as the gold standard. (Table 8)

The images were reviewed by two individual optometrists (non-medical graders in Reading Centre) and two ophthalmologists. Each case was assessed by a single grader after project-specific training. The gold standard management decision for validating the virtual service model was defined as the decision reached following combined clinical examination and assessment by imaging tests, confirmed at a follow-up visit at six months. If a different management decision was reached at the clinical follow-up visit than baseline, this was the one considered the gold standard.

### 4.2.4. Outcomes analysis

Three pathways for reaching management decisions for patients with choroidal naevi were evaluated: decisions made in clinic on the basis of imaging tests and direct clinical assessment as confirmed at six months (face-to-face pathway, gold standard); decisions made by two expert ophthalmologists in a masked fashion on the basis of imaging tests alone and decisions made by Reading Centre non-medical graders (specialist optometrists) on the basis of imaging tests alone (virtual pathways).

The degree of agreement between the gold standard management decisions and those reached by the two alternative 'virtual' pathways was calculated. In cases of disagreement in management decisions that questioned the gold standard, adjudication was made by an experienced ocular oncologist. These criteria were applied to cases where patient safety could be affected by a failure in the gold standard ('discharge' or 'follow up' recommended by the gold standard as opposed to 'referral' by grader). The primary outcome was the agreement in clinical management decisions

between the face-to-face clinical pathway (gold standard) and each of the two virtual clinical pathways (medical and non-medical).

Secondary outcomes included the following:

- Rate of incorrect and unsafe decisions in the virtual pathways (refer to oncology by gold standard and otherwise by masked non-medical grader/masked ophthalmologist in the virtual pathway).
- Rate of incorrect yet safe decisions (discharge by gold standard and otherwise by masked non-medical grader/ masked ophthalmologist).
- Agreement in correct diagnosis (choroidal naevi or other) between gold standard and virtual pathways. Other lesions included congenital hypertrophy of the RPE, scar tissue, RPE changes and any other lesions referred as suspicious choroidal naevi that were deemed to be an alternative pathology.
- Agreement on feature-based measurements for known risk factors for growth (orange pigment, SRF, increased AF and its origin) between gold standard and virtual pathways

Additionally, to the absolute agreement presented in absolute and percentual calculations, the kappa agreement characterised by the kappa score was determined. Cohen's kappa coefficient ( $\kappa$ ) is a statistic that is used to measure inter-rater reliability for categorical items.<sup>452</sup> It is generally thought to be a more robust measure than simple percent agreement calculation, as  $\kappa$  takes into account the possibility of the agreement occurring by chance.

Cohen's kappa measures the level of agreement between two raters who each classify items into mutually exclusive categories. The formula for Cohen's kappa is calculated as  $\kappa = (p_o - p_e) / (1 - p_e)$  where  $p_o$  = relative observed agreement among raters, and  $p_e$  = hypothetical probability of chance agreement.<sup>453</sup> If the raters are in complete agreement, then  $\kappa = 1$ .

In dependency of the type of the outcome, the agreement was determined for dichotomous (e.g., diagnosis naevus/other) or ordinal ratings (e.g., management decision discharge/follow-up/refer).

Cohen's kappa that has been used for dichotomous ratings takes into account disagreement between the two raters, but not the degree of disagreement. This is especially relevant when the ratings are ordered. To address this issue, there is a modification to Cohen's kappa called weighted Cohen's kappa ( $\kappa(w)$ ). The weighted kappa is calculated as  $\kappa(w) = 1 - (\sum w(ij) \times p_{o}(ij)) / (\sum w(ij) \times p_{e}(ij))$ , using a predefined table of weights that measure the degree of disagreement between the two raters. The higher the disagreement the higher the weight.<sup>454</sup>

For ordinal ratings, the agreement was measured by weighted kappa score using quadratic weights in which the weight assigned to each cell is  $1 - ((i-j)/(k-1))^2$ , where  $i$  and  $j$  index are the rows and columns of the ratings by the two graders, respectively, and  $k$  is the maximum number of possible ratings (herein 3). Therefore, the further apart the two ratings are, the smaller weight is assigned to the relevant cell.

Finally, bootstrapping was used to estimate a bias-corrected 95% Confidence Interval (CI) for the kappa agreement ( $\kappa$ ). It is a resampling method with replacement to mimic the sampling variability found by collecting data from a population. A so-called bootstrap sample is taken of the original sample and allows to produce an interval estimate for kappa, concluding to be 95% confident that the population kappa falls within this range.<sup>455</sup>

All analyses were performed with Stata software version IC 13.1 (StataCorp, College Station, TX, USA).

### 4.3. Results

During the study period from June 2016 to July 2017, 400 cases were collected and analysed in three pathways of gold standard assessment in naevus face-to-face clinic, virtual image analysis by a masked ophthalmologist and virtual image analysis by a masked trained non-medical grader. A total of 200 patients from MREH and 200 patients from MEH were recruited, of which 4 (1%) did not have a complete set of images and were excluded from the analysis.

Image grading at the Moorfields Reading Centre was based on the presence or absence of known clinical imaging features in line with established risk stratification algorithms for choroidal naevi (e.g., Royal College of Ophthalmologists Guidelines).<sup>456</sup> Features include orange pigment (n=256), SRF on OCT scan (n=218), increased AF (n=220) and presence of drusen (n=198).

#### 4.3.1. Agreement of clinical management decision between gold standard versus masked ophthalmologist and masked non-medical reader

As a primary outcome of this study, the absolute agreement for the total of all clinical management decisions between gold standard and masked non-medical grader was 83.1% (329/396, 95% CI 79.0% to 86.6%, kappa 0.77), while the absolute agreement between gold standard and masked ophthalmologist was 82.6% (327/396, 95% CI 78.5% to 86.2%, kappa 0.76). (Table 9)

The agreement of clinical management decisions was less for Discharge and higher for Follow up and Refer, with 75.7% (159/210), 91.6% (153/167), 89.5% (17/19) between gold standard and masked non-medical grader, and 76.7% (161/210), 89.2% (149/167), 89.5% (17/19) between gold standard and masked ophthalmologist, respectively.



		Masked non-medical grader			Masked ophthalmologist			
		Clinical decision						
		Discharge	Follow up	Refer	Discharge	Follow up	Refer	
Gold standard	Clinical decision	Discharge	159	51	0	161	49	0
		Follow up	2	153	12	6	149	12
		Refer	0	2	17	0	2	17
		Absolute agreement, n (%) (95% CI)	329/396 (83.1%) (79.0% to 86.6%)			327/396 (82.6%) (78.5% to 86.2%)		
		Kappa agreement, (95% CI)	0.77 (0.72 to 0.82)			0.76 (0.71 to 0.82)		
		Sensitivity in decision to refer, (95% CI)*	89.5% (66.9%, 98.7%)			89.5% (66.9% to 98.7%)		
		Rate of under-referral, n (%) (95% CI)	2/19 (10.5%) (1.3% to 33.1%)			2/19 (10.5%) (1.3% to 33.1%)		
		Specificity in decision to discharge, (95% CI)†	75.7% (69.3% to 81.4%)			76.7% (70.4% to 82.2%)		
	Rate of over-referral, n (%) (95% CI)	51/210 (24.3%) (18.6% to 31.0%)			49/210 (23.3%) (17.8% to 29.7%)			

\*Sensitivity or true-positive rate where positive is 'Refer to oncology'.  
 †Specificity or true-negative rate where negative is 'Discharge'.

**Table 9:** Summary of comparisons of clinical management decisions between face-to-face (gold standard) and virtual pathways (masked non-medical graders)

Images A–C in Figure 16 show an example of a case where all graders and the gold standard agreed to discharge back to the care of a community optometrist. More patients were sent for a follow-up or were referred by masked non-medical grader or masked ophthalmologist while more patients were discharged by gold standard.

The agreement for the management decision between masked ophthalmologist and masked non-medical grader was high at 98.5% (390/396, 95% CI 96.7% to 99.4%, kappa 0.98) (Table 10)

		Masked non-medical grader		
		Discharge	Follow up	Refer
Masked ophthalmologist	Discharge	161	6	0
	Follow up	0	200	0
	Refer	0	0	29
	Absolute agreement, n (%) (95% CI)	390/396 (98.5%) (96.7% to 99.4%)		
	Kappa agreement, (95% CI)	0.98 (0.96 to 0.99)		

**Table 10:** Comparison of clinical management decisions between two versions of virtual pathway (masked ophthalmologist vs masked non-medical grader)

‘Under-referral’ and ‘incorrect and potentially unsafe’ were cases that were referred to an ocular oncologist by gold standard but decided otherwise (follow up or discharge) by masked non-medical grader or masked ophthalmologist. The sensitivity of the masked non-medical grader or masked ophthalmologist in deciding to refer was calculated at 89.5% (95% CI 66.9% to 98.7%). The rate of under-referral was 10.5% (2/19, 95% CI 1.3% to 33.1%) by both, masked grader and masked ophthalmologist. No cases of lesion growth were identified at the 6-month safety-net appointment for the group with a decision to discharge to community optometry.

Two cases were referred to ocular oncology by gold standard, but both masked non-medical grader and masked ophthalmologist decided not to refer. A review of these cases showed that both were borderline, and the masked non-medical grader and masked ophthalmologist recommended close monitoring within two months. In one case, both masked non-medical grader and masked ophthalmologist decided to follow up because the lesion was within 1 DD of the optic disc, while the gold standard

advised referral to oncology. (Figure 16, D–F)

In that case, both masked assessors did not grade for the presence of subtle peripapillary SRF. Adjudication by the expert ocular oncologist confirmed that the management of these cases was safe. Therefore, the overall rate of potentially unsafe decisions was 2/186 (1.1%, 95% CI 0.1% to 3.8%) in both virtual pathways and the sensitivity in the decision to refer or follow up was 98.9% (95% CI 96.2% to 99.9%). (Table 11) (Table 12)

		Gold standard	
		Referred/F-up	Discharge
Masked non-medical grader	Referred/ F-up	184	51
	Discharge	2	159
Masked ophthalmologist	Referred/ F-up	180	49
	Discharge	6	161

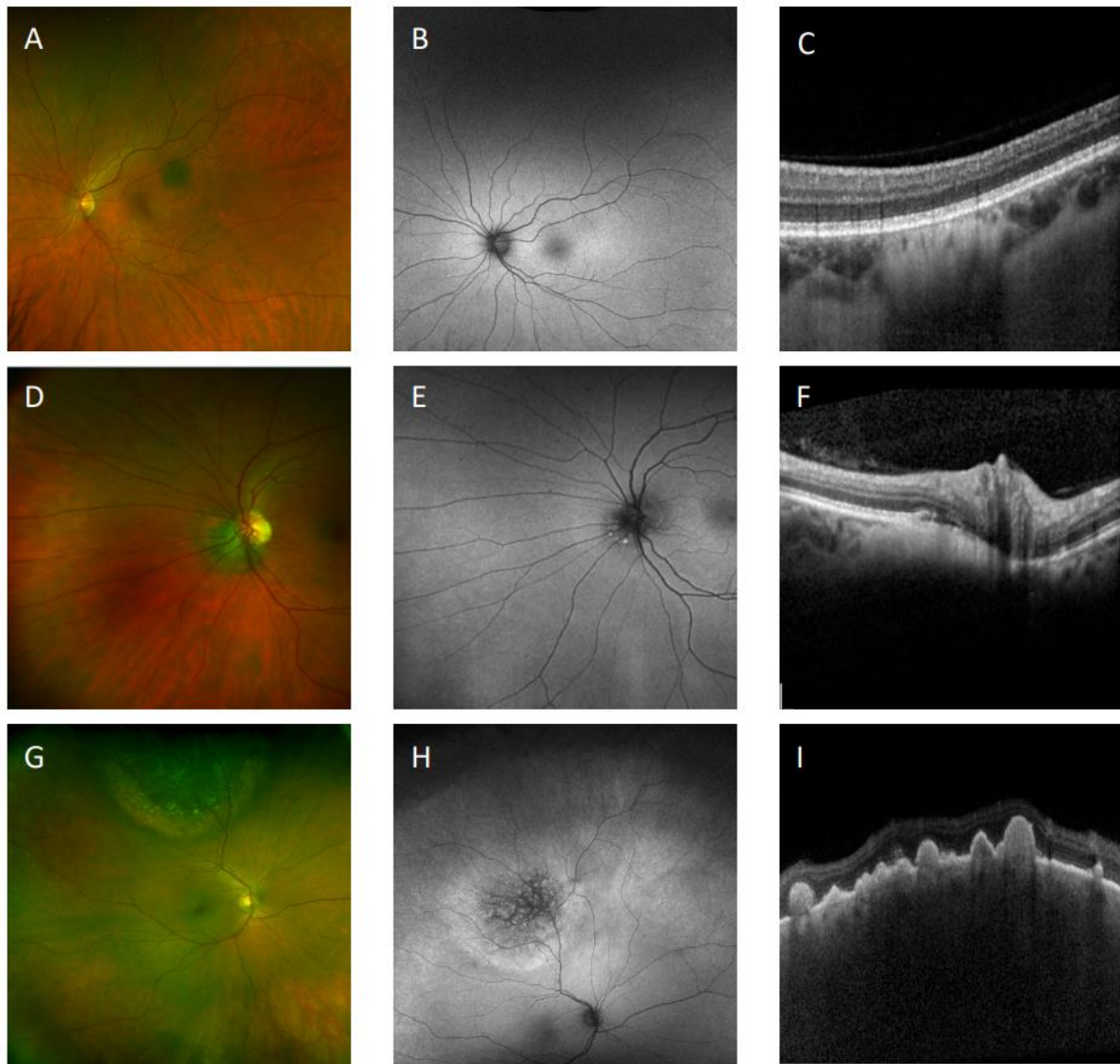
**Table 11:** Comparison of clinical management decisions between face-to-face (gold standard) and virtual pathways (masked non-medical grader and masked ophthalmologist) when refer and follow up decisions are pooled

		Masked non-medical grader	Masked ophthalmologist
Gold standard	Sensitivity in decision to refer or F-up, (95% CI)*	98.9% (96.2% to 99.9%)	96.8% (93.1% to 98.8%)
	Rate of under-referral, n (%) (95% CI)	2/186 (1.1%) (0.1% to 3.8%)	6/186 (3.2%) (1.2% to 6.9%)

**Table 12:** Comparison of clinical management decisions between face-to-face (gold standard) and virtual pathways (masked non-medical grader and masked ophthalmologist) when refer and follow up decisions are pooled (sensitivity analysis)

Similarly, ‘over-referral’ and ‘incorrect yet safe’ were cases that were discharged by gold standard but managed otherwise (follow up or refer) by masked non-medical grader or masked ophthalmologist. The rate of over-referral was 24.3% (51/210, 95% CI 18.6% to 31.0%) by masked non-medical grader and 23.3% (49/210, 95% CI 17.8%

to 29.7%) by masked ophthalmologist. Images G–I in Figure 16 show an over-referred case where masked non-medical grader decided to refer to oncology because visual acuity (VA) was reduced in the affected eye associated with thickness >1.5 mm on ultrasound. The gold standard instead advised to follow up because reduced VA was not considered a related symptom in this case.



**Figure 16:** Colour photographs, OCTs and fundus autofluorescence images of 3 cases: **(A–C)** Total agreement case between gold standard versus masked reader and masked ophthalmologist, with basal diameter <3 DD, no SRF and US no thickness detected. **(D–F)** Under-referral case, where masked graders decided to follow up because of lesion within 1 DD of optic disc and no presence of subtle peripapillary SRF graded, while the gold standard advised referral to oncology. **(G–I)** Over-referral case, where masked graders referred to ocular oncology due to physical findings and symptoms, but the gold standard advised to follow up in a naevus monitoring clinic. DD, disc diameter; OCT, optical coherence tomography; SRF, subretinal fluid; US, ultrasound.

### 4.3.2. Agreement of diagnosis of choroidal naevi or other lesions between gold standard versus masked non-medical grader

Nine cases were excluded from this part of the analysis because no diagnosis was recorded. In distinguishing between choroidal naevi and ‘other’ lesions, the masked non-medical grader demonstrated absolute agreement in 85.5% cases (331/387, 95% CI 81.6% to 88.9%). The kappa agreement was 0.67 (95% CI 0.59 to 0.75). (Table 13)

		Diagnosis by masked non-medical grader	
		Naevus	Other
Diagnosis by gold standard	Naevus	234	21
	Other	35	97
	Absolute agreement, n (%) (95% CI)	331/387 (85.5%) (81.6% to 88.9%)	
	Kappa agreement, (95% CI)	0.67 (0.59 to 0.75)	
	Sensitivity in detecting erroneous referrals, (95% CI)	73.5% (65.1% to 80.8%)	

**Table 13:** Comparison of choroidal naevi or ‘other’ diagnosis between face-to-face (gold standard) and virtual pathway (masked non-medical grader)

### 4.3.3. Agreement between gold standard and masked non-medical grader for risk factors of growth

The agreement rate for the presence of orange pigment detected on clinical photography by a masked non-medical grader in comparison with gold standard was 97.3% (249/256, 95% CI 94.2% to 98.8%, kappa 0.71), for SRF on OCT 96.3% (210/218, 95% CI 92.6% to 98.3%, kappa 0.82) and for presence of increased AF in widefield AF imaging 82.3% (181/220, 95% CI 76.4% to 86.9%, kappa 0.27). Increased AF attributable to drusen only had agreement of 84.8% (168/198, 95% CI 79.9% to 89.4%, kappa 0.48). (Table 14)

			Masked non-medical grader			
			No	Yes	Kappa (95% CI)	Absolute agreement
Gold standard	Orange pigment (n=256)	No	240	2	0.71 (0.45 to 0.89)	97.3% (249/256)
		Yes	5	9		
	Subretinal fluid on OCT scan (n=218)	No	189	3	0.82 (0.69 to 0.92)	96.3% (210/218)
		Yes	5	21		
	Increased autofluorescence (n=220)	No	170	31	0.27 (0.11 to 0.43)	82.3% (181/220)
		Yes	8	11		
	Presence of drusen (n=198)	No	149	25	0.48 (0.32 to 0.63)	84.8% (168/198)
		Yes	5	19		

**Table 14:** Agreement between gold standard and masked non-medical grader for risk factors of growth

## 4.4. Discussion

### 4.4.1. Discussion of results

Choroidal naevi are a frequent incidental finding,<sup>77</sup> but distinguishing between a choroidal naevus and a small choroidal melanoma is not universally straightforward.<sup>52</sup> Choroidal naevi are generally stable, and growth of a choroidal naevus is usually a sign of malignant transformation,<sup>56, 60</sup> especially in a relatively short time period. With an increasing number of such lesions referred from the community, there is a burden on ophthalmologists and ocular oncologists for their timely management and the reassurance to the referrer and the patient that the lesion has no suspicious features. This prospective study aimed to answer the question of whether those low-risk, incidental findings might be safely managed using clinical imaging and an algorithm to make an appropriate management decision in a virtual clinical pathway by masked non-medical graders and/or masked ophthalmologist graders, using a prospective protocol rather than a retrospective chart review.<sup>53</sup>

400 participants have been studied and assessed over a 13-month period in two major centres in a dedicated naevus clinic, comparing masked decisions made by a trained non-medical grader and an ophthalmologist against the gold standard of a full clinical evaluation performed by an expert ophthalmologist, that was confirmed at a 6-month follow-up visit.

The primary outcome of the decision agreement between the gold standard ophthalmologist and masked grader or masked ophthalmologist was 83.1% and 82.6%, respectively. Within these figures, more patients would be followed up in the naevus clinic by the masked grader and ophthalmologist alike, while more patients were discharged back to the community from the face-to-face clinic. This indicates that the discrepancies in performance between the face-to-face and the virtual pathways were driven by a tendency of virtual clinic graders to be conservative. The suggestion that the virtual pathway is robust enough to be used by a masked ophthalmologist or trained non-medical grader is further supported by their agreement in decision-making, which was 98.5%, carrying a kappa value of 0.98. Hence, a virtual naevus

clinic model could be staffed by trained non-medical graders rather than being reliant on ophthalmologists to carry out standardised decision-making.

The major aim of this study was to test the safety of the virtual naevus clinic pathway rather than diagnostic or clinical factors' agreement. As long as a decision by the masked ophthalmologist or masked non-medical grader resulted in a safe outcome, the pathway and associated algorithm can be deemed unlikely to cause harm. An incorrect decision can be safe or unsafe, and it is the latter, an under-referral to an ocular oncologist, that is potentially most serious. The overall sensitivity of all graders was 89.5%, but 98.9% of management decisions were considered safe. The decision defined as potentially unsafe for the purposes of this analysis was not a complete discharge from the review, but to follow up in the naevus clinic or discharge back to a community optometrist for a follow-up. It is likely that even with such an outcome, a lesion suspicious for a small melanoma would have been picked up during that follow-up. Agreement on growth at follow-up is possible to include in a separate study.

#### 4.4.2. Limitations of this study

A potential limitation of this study is that the non-medical graders, although trained optometrists, were also expert Reading Centre graders, experienced in reviewing imaging data for research purposes. This may not fully represent optometrists in purely clinical roles or in community practice. However, the non-medical graders achieved a slightly better agreement with the gold standard than medical graders in several features. A potential explanation is that non-medical graders had limited previous clinical exposure to choroidal naevi, received task-specific training for assessing images of choroidal naevi and are generally more likely to adhere closely to the image grading protocol. This is a pattern observed in other use cases where optometrists are upskilled to deliver shared care for diabetic retinopathy and age-related macular degeneration clinics, where consistent adherence to grading and decision-making algorithms has led to high levels of performance.<sup>457</sup>

In the 6-month follow-up period, there were no cases of documented growth or malignant transformation. This is a short interval, and melanomas are slow-growing



tumours. Although this is a limitation, the design of the study was to test the virtual versus face-to-face decision at first presentation, with the follow-up being a safety net. There is scope for further studies to document follow-up protocols for malignant transformation, either virtual or with a clinician. In the COVID-19 pandemic, where progress in tele-ophthalmology has accelerated, it is possible that many naevi can be followed on virtual pathways to avoid patient travel and exposure.

In planning a virtual naevus clinic service, the reported 23–24% rate of over-referrals must be factored in. In this scenario, patient safety is not compromised, but the service model of a combination of virtual and face-to-face encounters becomes less efficient. A cost-effectiveness analysis could be undertaken to help inform policy decision-makers on commissioning such innovative virtual pathways.

The non-medical grader was tested in two other ways against the gold standard: the distinction between choroidal naevi and ‘other lesion’ and for the risk factors for growth. In 85.5% of the cases, the masked non-medical grader made the same diagnosis as the gold standard. The agreement for the individual risk factors of naevus growth ranges from 82.3% to 97.3%. These agreement rates are already high, but to optimise the decisions performed by non-medical professionals, a regular audit of grading outcomes should be undertaken in combination with continued training and education among graders to improve their skills.

Finally, despite the large number of patients, no formal sample size calculation has been conducted, so further robust studies are required to confirm the validity of the research findings.

#### **4.4.3. Benefits and outlook**

The idea of a virtual naevus clinic is attractive for patients and healthcare systems. A fast, one-stop, streamlined and comprehensive service seeks to optimise patient experience. It is anticipated to reduce delays and inconvenience from repeated visits. A safe, standardised model ensures homogeneous management of cases, appropriate and prompt return of care closer to home to community-based

optometrists and minimises unnecessary referrals to ophthalmologists and ocular oncology centres.

For healthcare systems, there is an efficient use of resources in terms of staff and clinical investigations. A virtual naevus clinic with graders maximises expanded skills for allied health professionals. This research work, as well as strategies such as the MOLES scoring system for triage,<sup>79, 430</sup> could empower community-based providers to deliver management of benign choroidal naevi without referral to specialist units.

Following validation for safety and patient satisfaction, the model will be able to replicate and achieve widespread use within the NHS, especially in the context of large tertiary referral centres receiving a constant flow of referrals with relevant pathology, providing the clear potential to benefit both patients and the public.

Ocular oncology clinics are currently funded centrally by NHS England. Many naevi are seen in these clinics, which could be better managed by the alternative model of healthcare tested in this study and would be a practical, cost-effective alternative to the established tertiary and quaternary care services. A Health economics analysis is expected to demonstrate the cost-effectiveness of the proposed service model as well as efficiency savings for the NHS compared to current models of service delivery.

This research work could ignite further spin-off projects to generate evidence to inform the optimal management strategy for choroidal naevomelanocytic lesions both on a community base and in the context of hospital eye units. Another exciting aspect of introducing a virtual service could be a follow-up study that analyses the potential use of artificial intelligence by developing an AI algorithm that can support or even autonomously perform image grading and subsequent management decisions.

## 5. CHAPTER FIVE: Model of a Virtual Naevus Clinic in Practice at Moorfields Eye Hospital

### 5.1. Purpose and scope

Choroidal naevomelanocytic lesions (CNL) are a frequent incidental finding<sup>39</sup> but distinguishing between a choroidal naevus and a small choroidal melanoma is not universally a straightforward task.<sup>59, 78</sup> Choroidal naevi are generally considered to be stable lesions, and growth of a choroidal naevus is usually believed to be a sign of malignant transformation, especially if it occurs in a relatively short period of time.<sup>78</sup> With the number of these lesions referred from the community, there is a burden on ophthalmologists and ocular oncologists for timely management and to reassure the referrer and the patient that the lesion has the features of a naevus rather than a melanoma.<sup>65</sup>

Those low-risk, incidental findings might be safely managed using clinical imaging and an algorithm to make an appropriate management decision in a virtual clinical pathway by non-medical and ophthalmologist graders.<sup>95</sup> Transforming the traditional Naevus Service into a dedicated, 'one-stop' virtual clinic model for the safe management of patients with choroidal naevomelanocytic lesions will allow efficient use of resources with a dedicated service maximising shared care with allied health professionals and could also result in additional cost savings, while ensuring an optimal experience of care.

A virtual naevus clinic offering a fast, one-stop, streamlined and comprehensive service is beneficial for patients and healthcare systems alike.<sup>53</sup> It can optimise patient experience and reduce delays and inconvenience from repeated visits. A safe, standardised model ensures consistent management of cases, appropriate and timely return of care closer to home to community-based optometrists in order to minimise unnecessary referrals to ophthalmologists and ocular oncology centres. For healthcare systems, efficient use of resources in terms of staff and clinical

investigations can be realised. A virtual naevus clinic with graders maximises expanded skills for allied health professionals.

Based on this publication<sup>95</sup> and the positive evaluation of the MOLES scoring system,<sup>79</sup> the author has designed this model of a 'Virtual Naevus Clinic' at Moorfields Eye Hospital to prove its feasibility. The virtual naevus clinics were also developed in response to the COVID-19 pandemic and the long-term need to maintain social distancing.<sup>238, 458, 459</sup> The requirement of a rapid flow of patients enabled by high-quality digital imaging is essential. The purpose of these clinics is to reduce in-hospital patient journey times and increase capacity in the naevus clinics. This is also in response to the need to avoid crowding in the waiting area and ensure patients are safe.

In June 2020, the author of the PhD thesis developed a standard operating procedure (SOP) which comprises the design, pathways, and operating procedures for the digitally enabled naevus clinics in Moorfields Eye Hospital. It details what this service provides and how it will be delivered and supported.

The objectives of the digital clinics are; to provide safe and efficient clinical care for patients via a digitally enabled model, increase capacity in the Naevus Service, maintain social distancing between patients in the Naevus Service, and efficiently use resources, as well as maximise shared care with allied health professionals and additional cost savings.

The scope of this guideline sets out the duties and targets for:

- Design of the digital clinics
- Conditions managed and eligibility of patients
- Referral guidelines to other services
- Operating procedures for technicians and nurses
- Guidelines for optometrist/doctor assessors
- Administrative guidelines
- Training

## 5.2. The MOLES Scoring System and its rationale

MOLES is a scoring system for diagnosing melanocytic choroidal tumours based on the presence of Mushroom shape, Orange pigment, Large tumour size, Enlarging tumour, and Subretinal fluid. (Table 15)

Several studies have proved that the MOLES scoring system compares well with expert diagnosis in differentiating choroidal melanomas from choroidal naevi and that MOLES is a safe tool to optimise referral of melanocytic choroidal tumours for specialist care.<sup>79, 86, 430</sup>

Therefore, the decision was made to apply the MOLES scoring system to be used for management in the new Naevus Virtual Service.

MOLES scoring system				
Risk Factor	Severity			MOLES Score
Mushroom shape	0 Absent			0
	1 Incipient			1
	2 Present			2
Orange pigment	0 Absent			0
	1 Trace			1
	2 Confluent			2
Large Size		<b>Thickness</b>	<b>Base Diameter</b>	
	0 Small	<1 mm	& <3 DD	0
	1 Borderline	1 – 2 mm	or 3-4 DD	1
	2 Large	>2 mm	or >4 DD	2
Enlargement	0 None			0
	1 Uncertain			1
	2 Definite			2
Subretinal fluid	0 Absent			0
	1 Trace			1
	2 Significant			2
			Total Score	

Total MOLES scores
0 = Common Naevus
1 = Low-risk Naevus
2 = High-risk Naevus
>2 = Probable Melanoma




Table 15: MOLES scoring system (simplified)

### 5.3. Design

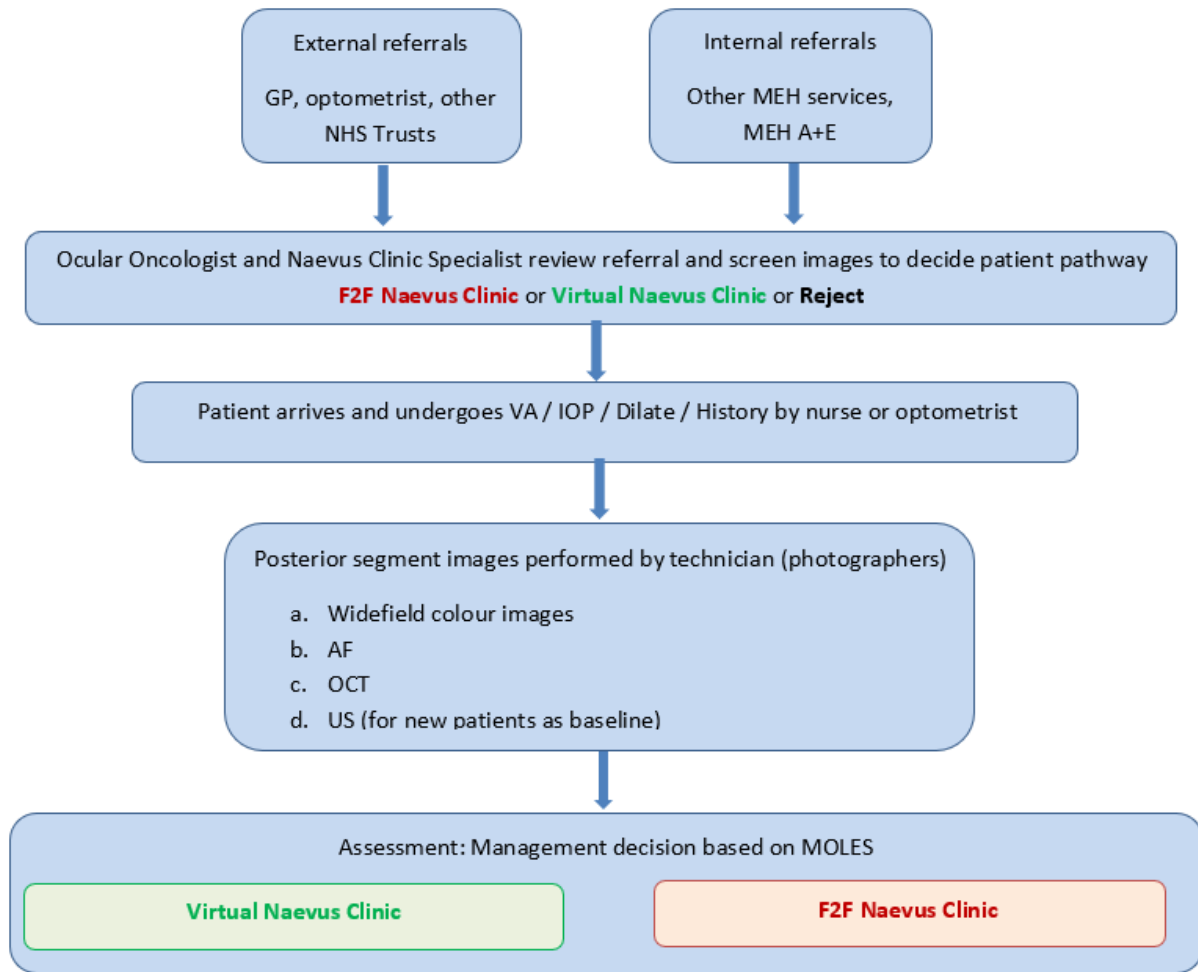
The clinic pathways within the Naevus Service consist of the 'Virtual Naevus Clinic' and the 'Face to Face (F2F) Naevus Clinic'.

The virtual naevus clinic comprises a diagnostic hub followed by a virtual assessment. It is a standalone, technician-only clinic that performs diagnostic imaging clinic appointments with a virtual asynchronous review of images. Imaging will take place in a diagnostic hub which is delivered by technicians. The virtual clinic pathway is used for low-risk cases with a low probability of requiring treatment.

The face-to-face (F2F) naevus clinic is a traditional naevus clinic with a diagnostic bundle before the face-to-face assessment. It is taking place within the naevus outpatient department in the main facility and is performed by qualified ophthalmologists. The face-to-face pathway is used for high-risk cases with a high probability of requiring treatment.

All imaging of both pathways will be pre-determined at triage and performed at the diagnostic hub.

Figure 17 shows a diagram depicting the flow of patients via diagnostic hub through the two different clinic models within the Naevus Service.



**Figure 17:** Diagram depicting the flow of patients via diagnostic hub through the two different clinic models within the Naevus Service

The individual eligibility criteria for each clinic pathway are listed in Table 16.

	Virtual Naevus Clinic	F2F Naevus Clinic
<b>General Eligibility</b>	<ul style="list-style-type: none"> <li>• Able to obtain good quality images – WF, OCT and US-B scan, and in some cases VF (e.g., optic disc melanocytoma)</li> </ul>	
<b>General exclusion</b>	<ul style="list-style-type: none"> <li>• Patients with cognitive impairment/dementia</li> <li>• Dense cataract</li> <li>• Unmanaged narrow angle patients/risk of angle closure</li> </ul>	
<b>Conditions</b>	<ul style="list-style-type: none"> <li>• Choroidal Naevus (Follow-up)</li> <li>• Uveal Melanocytoma (Follow-up)</li> <li>• Congenital Hypertrophy of the RPE (CHRPE)</li> <li>• Combined Hamartoma of the retina and RPE (Follow-up)</li> <li>• Simple Hamartoma of the RPE</li> <li>• Epithelioma (Adenoma) of the RPE</li> <li>• Choroidal Osteoma (Follow-up)</li> <li>• Choroidal Haemangioma (Follow-up)</li> </ul>	<ul style="list-style-type: none"> <li>• Benign Conjunctival tumours (New + Follow-up)</li> <li>• Iris Naevi (New + Follow-up)</li> <li>• Choroidal Naevus (New + Follow-up)</li> <li>• Congenital Ocular Melanocytosis</li> <li>• Combined Hamartoma of the retina and RPE (New)</li> <li>• Choroidal Osteoma (New)</li> <li>• Choroidal Haemangioma (New)</li> <li>• Uveal Melanocytoma</li> </ul>

**Table 16:** Eligibility criteria for the two specific Naevus clinics in Moorfields Eye Hospital



## 5.4. Virtual Naevus Clinic: Diagnostic Hub and Virtual Assessment

### 5.4.1. Diagnostic Hub

As a first step, the clinic staff confirms the patient's identity, and the technician obtains the patient's history (Appendix 1 – Guide for diagnostic hub technicians to collect patients history for virtual naevus clinics), which will be incorporated into the Moorfields electronic patient record 'OpenEyes'.

Second, the visual acuity (VA) is measured using Snellen or LogMAR and documented in 'OpenEyes'. If the IT system is down, the information will be recorded in a paper document and signed with patient details. The completed paper will be stored and later transferred into 'OpenEyes' once the system resumes before the end of the clinic. If 'OpenEyes' does not resume, these are scanned and emailed to the Naevus Virtual failsafe officer. The document is then disposed of in the confidential waste.

After visual acuity, intraocular pressure (IOP) is measured using i-care with the following outcomes:

- If IOP <24 mmHg, continue as normal
- If IOP >24 mmHg, <30 mmHg, do not dilate and continue with imaging undilated
- If IOP >30 mmHg, give iopidine 1.0% (provided no allergy) and inform Hub Supervisor. Obtain imaging undilated and recheck IOP in 60mins

If there is no contraindication, both eyes will be dilated with tropicamide 1.0%, provided no allergy. If the patient is driving, the clinic staff advise the patient to be accompanied when leaving the hospital. If this is not possible, the patient should wait until the drop's effect wears off. However, if the patient refuses, imaging will be continued in the undilated eye, and the patient is made aware that another appointment may be needed if the image quality is poor. The medical photographer is conducting retinal imaging as per pre-determined diagnostic bundle.

Finally, the patient is informed they will receive written correspondence on their outcome with a new follow-up appointment if needed. If urgent pathology is detected or further information is required, a phone call will be made in addition.

If urgent cases emerge in the diagnostic hub, immediate advice and support for technicians are available and can be contacted in the following order:

1. Diagnostic hub supervisor
2. Senior technician/nurse in the centre
3. Adjacent naevus clinic in City Road
4. Naevus consultant in charge
5. Doctor in Accident and Emergency at City Road  
(patients should not be sent directly to MEH, without prior agreement from the naevus service staff)

Red flags, such as being unable to obtain images, an IOP result >30 mmHg or the presence of suspicious and significant macula pathology, should be identified by the diagnostic hub team (technicians/imaging team). As per protocol, the Hub ophthalmologist in charge should be informed. If the patient is a F2F Naevus patient, no further action is needed, and the patient pathway can continue. If it is a virtual patient, the diagnostic hub supervisor will decide to see the patient in the F2F naevus clinic.

The diagnostic hub supervisor should be an experienced clinician, nurse, or technician to supervise the diagnostic hub. This is ideally a doctor initially and training should be provided for an appropriate nurse/technician to be a team leader subsequently. The responsibility includes to ensure good patient flow, support technicians, and address red flags.

Figure 18 presents an overall patient flow diagram for the diagnostic hub and virtual assessment clinic model described in the subsequent chapter 5.4.2.

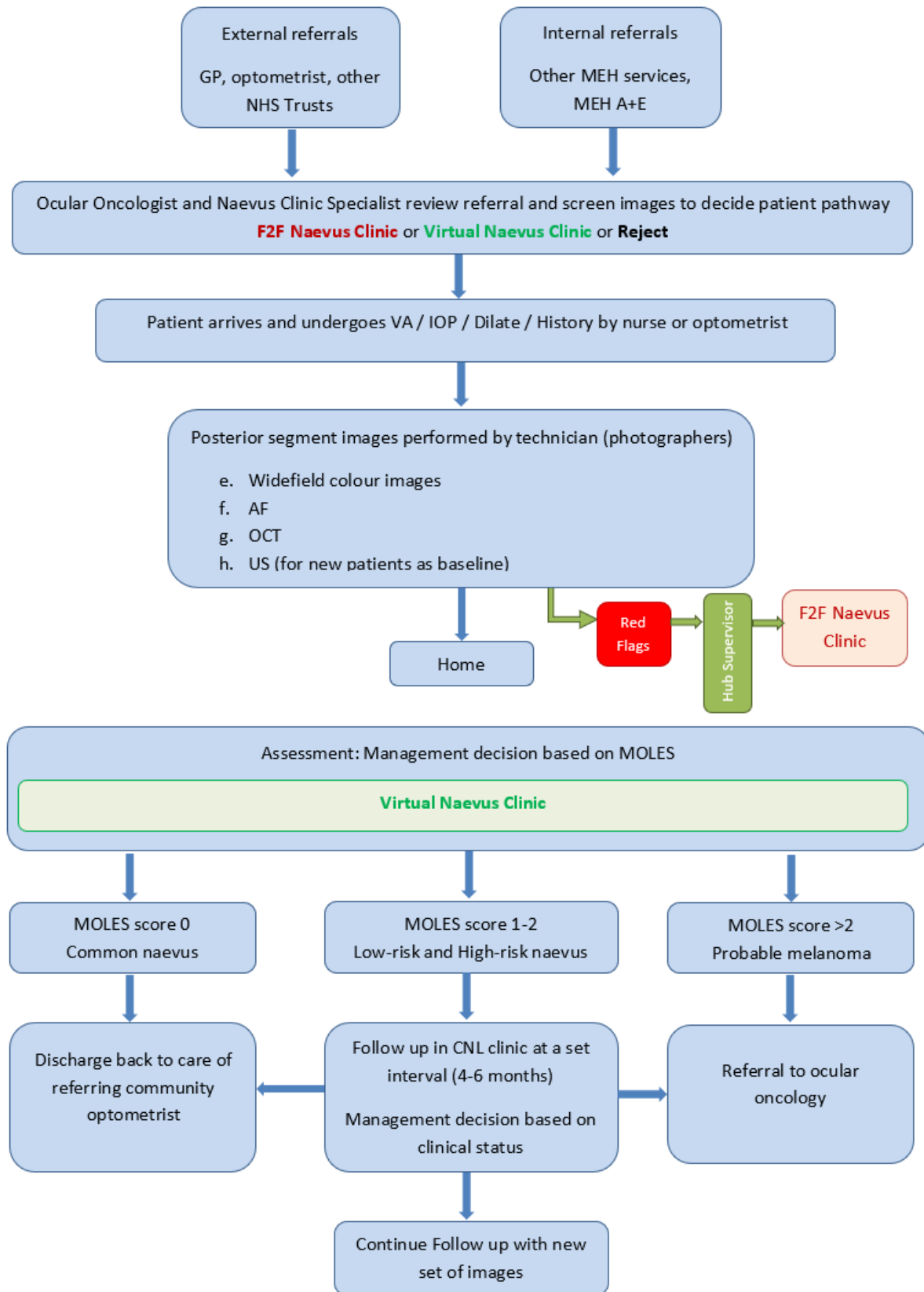


Figure 18: Patient flow diagram for the diagnostic hub and virtual assessment clinic model

### 5.4.2. Virtual Assessment Centre

The capacity for the virtual assessment centre starts with eight patients per assessor per session. After one month of pilot activity, the patient number will be reviewed and adapted accordingly to increase up to 15 patients.

The virtual assessments are consultant delivered and supported by a team of technicians, nurses and optometrists. All assessments must be completed within two working days. A dedicated virtual naevus clinic failsafe officer/administrator allocates patients into assessment clinics within the time frame mentioned which is shared on an excel spreadsheet sorted by date.

All assessments are performed remotely, and a written correspondence is completed on OpenEyes. For routine follow-ups, a written correspondence is sufficient. For patients requiring treatment, a phone consultation is made to discuss possible treatment and a booking is made for appropriate therapy after multidisciplinary team meeting input. If further information is required, a phone consultation is made. For selective cases requiring phone consultation, the patient's ID will be confirmed by name, hospital number and date of birth. Discussions conducted are documented on 'OpenEyes' examination page, and a brief letter is completed on OpenEyes. Patients who are not contactable will receive a written detailed letter.

Assessors must update a shared Microsoft Excel file (Washington, USA) with the appropriate outcomes capturing clinic type, diagnostic bundle, duration, patient information leaflet (PIL), and that a phone consultation has been performed. If any urgent cases require high priority attention, the administrative team is informed to trigger urgent action, and the patient will be contacted to return for a face-to-face clinic.

Management decisions are made based on possible outcomes from the virtual assessment and according to the MOLES score algorithm. (Table 15) If the MOLES score is 0 (Common naevus), the patient will be discharged back to the care of referring community optometrist. With a MOLES score of 1-2 (low-risk and high-risk naevus), a follow-up in the CNL clinic at a set interval (4-6 months) will be arranged, and a management decision will be made based on the clinical status. The case will then be followed up with a new set of images. If the MOLES score is >2 (probable melanoma), the patient will be referred to the ocular oncology service. (Figure 18)

The administrative team acts based on the outcomes and sends correspondence within two working days from the assessment clinic.

### 5.4.3. Failsafe

A dedicated virtual naevus failsafe officer will be identified to work closely with the naevus administrative team. The responsibilities of this role entail: ensuring all virtual patients seen in the diagnostic hub are reviewed, updating the shared Microsoft Excel file of patients in virtual clinics, allocating patients to the assessment teams, ensuring all patients are reviewed, and confirming that all 'did not attends' (DNAs) are listed in the shared excel and are reviewed by the virtual assessment team with appropriate outcomes.

All virtual patients that attend diagnostic hub appointments are booked into a clinic on the patient administration system (PAS). Attendance to this clinic will be recorded. Patients attending diagnostic hub appointments will be booked into an assessment clinic which will be reviewed remotely by the virtual team. All outcomes will be actioned, and patients with missing outcomes in the virtual PAS clinic will be identified and flagged.

### 5.4.4. Roles and responsibilities

This subchapter outlines an overview of the various individual roles that play an essential part within the virtual pathway, including a list of their responsibilities for the virtual naevus clinic.

#### **Diagnostic hub supervisor**

The diagnostic hub supervisor should be an experienced clinician, nurse, or technician to supervise the diagnostic hub. This is ideally a doctor initially, and training should be provided for an appropriate nurse or technician to be a team leader subsequently. The responsibility includes ensuring good patient flow, supporting technicians, and addressing red flags.

### **Administrative team – virtual**

The administrative support for the virtual naevus clinics is provided by the Medical Retina (MR) administrative team. The team's responsibilities include that patients are booked into the appropriate clinics, that diagnostic hub outcomes are actioned within the same day, and to ensure that patients are booked into assessment clinics within two working days. Furthermore, the virtual administrative team informs the naevus failsafe officer regarding all patients who did not attend (DNAs) and that assessment clinics will be templated at 15 patients per ophthalmologist. The team will work from the shared excel file used for the assessment clinics and document this information in this file once actioned. After the clinic is completed, the file is saved and closed from any further edits to avoid data corruption. Lastly, the team ensures outcomes from assessment clinics are actioned within one working day with appropriate letters and PIL sent out.

### **Virtual naevus failsafe officer**

A dedicated virtual naevus failsafe officer will be identified to work closely with the naevus administrative team. The responsibilities of this role entail: ensuring all virtual patients seen in the diagnostic hub are reviewed, updating the shared excel file of patients in virtual clinics, allocating patients to the assessment teams, ensuring all patients are reviewed, and confirming that all 'did not attends' (DNAs) are listed in the shared excel and are reviewed by the virtual assessment team with appropriate outcomes.

### **Patient support**

All patients assessed in the virtual clinics whereby a phone consultation was not performed should be provided with contact details for the virtual naevus failsafe officer. It ensures that patients with queries regarding their written correspondence can discuss them should they wish to. This is not a dedicated hotline for emergencies or for naevus/ ocular oncology pathology.

As per protocol for clinical queries, patient details and the name of the consultant in the virtual assessment clinic will be captured, and the relevance related to the virtual naevus clinic outcome will be ascertained. If relevant, the patient support team should

book the patient a phone consultation at the next working day virtual assessment clinic. The booking is made preferably with the same named consultant but not compulsory to avoid delay. If not relevant, the patient's case can be discussed with the virtual assessment team and directed to the appropriate department.

### **Training graders / optometrists**

Virtual assessments will be done by consultants but also in parallel with autonomous support of optometrists. To ensure high diagnostic accuracy, optometrists need to undergo appropriate training. The regular training schedule incorporates shadowing sessions with consultants in Virtual and F2F clinics and attending continued medical education (CME) sessions. In order to improve and optimise decisions, a regular audit of grading outcomes should be undertaken with continuous training and education among graders to improve their skills.

## **5.5. Face-to-face (F2F) naevus clinic**

The capacity for the F2F naevus clinic is set at 14 patients per assessor per session. Patients are booked in and undertake VA, dilation, and imaging as per the diagnostic bundle. (Figure 17) Patients are then located in the waiting room for a face-to-face assessment in the clinic.

This reduced number accounts for high-risk patients with a high probability of requiring treatment, minimises waiting time for patients, and allows additional urgent patients triaged from the diagnostic hub.

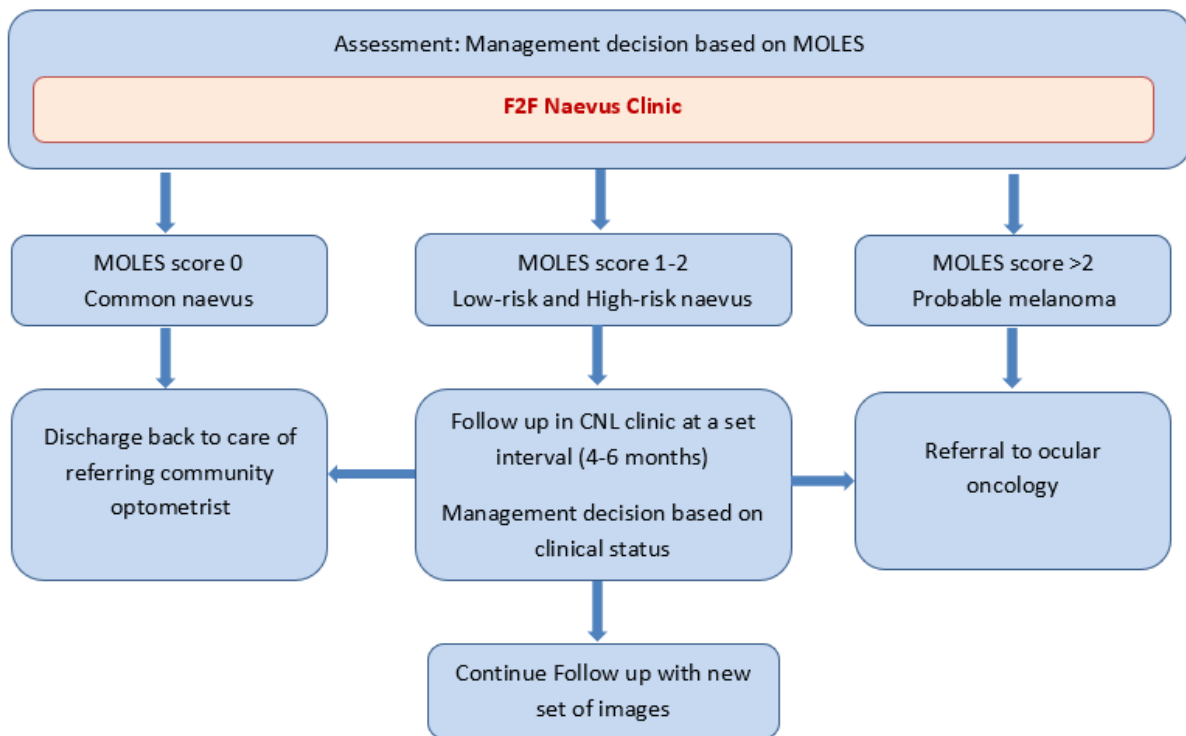
Referrals to the F2F clinic will be done via the booking centre and oncology team. All assessments are performed in the F2F clinic, and a written correspondence is completed on OpenEyes.

Management decisions are made based on possible outcomes from the virtual assessment and according to the MOLES score algorithm. (Table 15) If the MOLES score is 0 (Common naevus), the patient will be discharged back to the care of referring community optometrist. With a MOLES score of 1-2 (low-risk and high-risk

naevus), a follow-up in the naevus clinic at a set interval (4-6 months) will be arranged, and a management decision will be made based on the clinical status. The case will then be followed up with a new set of images. If the MOLES score is  $>2$  (probable melanoma), the patient will be referred to the ocular oncology service. (Figure 19)

The administrative team will action outcomes and send correspondence.

Despite the MOLES scoring system is primarily designed for guiding optometrist in triaging melanocytic lesions, ophthalmologists in the F2F clinic also use MOLES for an optimal collaboration and consistent documentation.



**Figure 19:** Patient flow diagram for the F2F assessment clinic model



## 5.6. Experience and future plans

The overall experience of implementing and running a virtual model of the naevus clinic at Moorfields Eye Hospital was positive and processes went smooth, so that after a one-month pilot with an initial capacity for the virtual assessment centre with 8 patients per assessor per session, the number of patients could be increased to 15 patients.

As of today, a further increase of the capacity of the virtual naevus clinic to 25-30 patients per assessor per session could be achieved, with the result that, essentially, the patient capacity has been doubled to what the face-to-face clinic can manage. However, it must be noted that triage will place lower risk naevus cases into the virtual pathway and the more complex cases into the F2F pathway.

Initial individual patient feedback was positive in terms of shorter waiting times and having offered correspondence by post. Other patients would have been happier to wait longer to see a doctor on the day in addition to receiving remote results.

Some patients may have difficulties reading letters due to visual impairment, disability or language barriers, and a letter alone may not be suitable for communicating clinic outcomes for all patients. With the increased use of telephone and video consultations during COVID-19,<sup>460</sup> further research into which methods patients preferred for communicating virtual clinical outcomes would be useful.

To support factual evidence of reduced waiting times in the virtual naevus clinic, as well as to prove financial savings for patients and the institution, additional studies and audits are needed to evaluate these factors. An economic evaluation and patient and healthcare practitioner acceptability analysis can be undertaken to inform further implementation plans for virtual pathways in terms of their safety, cost-effectiveness and acceptability.

Clinical audits form the system for improving standards of clinical practice. Aspects of patient care should be evaluated against expected standards of care and, where necessary, changes made at an individual, service or team level. A re-audit can then be executed to confirm that improvements have been effective.

It is essential to have robust risk management in place to efficiently monitor the virtual clinic service and address any potential patient safety risks. Creating an IT-supported real-time capacity and risk dashboard would be helpful, displaying patient volume per pathway, staffing (technicians, nurses, consultants), cases with red flags, calls planned, patients with urgent referrals, and DNAs and cancellations to trigger patient attendance.

Patient satisfaction can be assessed by a well-validated 'Patient Satisfaction Questionnaire' (PSQ), providing a scale that can be a practical tool for evaluating patient satisfaction with service provision to support general practices in establishing how well they are meeting the needs of their patients.

There is limited research on clinician experiences and perceptions of these clinics, and conducting a staff satisfaction survey, in addition to the patient satisfaction PSQ, would be crucial to ensure the future success of the virtual naevus clinic.

Virtual assessments will be performed by trained ophthalmologists but also in parallel with autonomous support of optometrists. Any staff members involved in grading, such as optometrists, should undergo appropriate training to ensure high diagnostic accuracy. The COVID-19 pandemic imposed unprecedented challenges in the educational field of ophthalmology, and Moorfields Education has launched a Virtual Observership Programme by leveraging existing expertise to not only maintain the standard of education but also create alternative learning environments that are collaborative, inclusive and productive.<sup>461</sup>

The regular training schedule incorporates shadowing sessions with consultants in Virtual and F2F clinics and attending continued medical education (CME) sessions to improve and optimise medical decisions and grading skills.

Virtual clinics can have the capacity to deliver on their expectations of reducing patient waiting times and improving patient care, service capacity and efficiency. However, it requires meticulous integration into the existing system to convince patients of the

advantages that it may offer.<sup>462,463</sup> Additional studies with longer follow-ups are needed to determine the safety and long-term outcomes of the virtual naevus clinic. Virtual clinics seem to be the way forward for managing and diagnosing naevomelanocytic lesions, as they can act as first-line rapid access clinics for low-risk referrals. Together with optimising existing resources, virtual clinics reduce the burden on hospital eye services. Existing healthcare team members can be trained without compromising the quality of clinical standards. Artificial intelligence and deep learning algorithms applied to medical imaging can be integrated in the future to promote upskilling of the workforce and provision of resources.

The Royal College of Ophthalmologists also recently highlighted the role of telemedicine and remote consultation in increasing capacity. Royal College of Ophthalmologists.<sup>460</sup>

Tele-oncology platforms for monitoring choroidal and iris naevi have been previously reported.<sup>232</sup> Alternative healthcare delivery platforms continue to be developed, and there may be a bigger scope for virtual consultation and remote triaging of patients.<sup>95</sup> Previous studies evaluating optometric referrals found that triage via tele-ophthalmology reduced office visits to retina specialists by 48%, saving patients time and cost associated with travel and improving efficiency of clinical examination and testing for those requiring treatment.<sup>440</sup> Expanding the virtual naevus service, including utilising the MOLES scoring system, may similarly avoid referrals for benign lesions.

For over a year, it could be demonstrated that a virtual naevus clinic model in practice at Moorfields Eye Hospital is feasible and safe. Patient capacity could be increased while maintaining social distancing between patients is maintained. However, a variety of analyses, surveys and audits will be required to back the model's benefits and to monitor the continued success of the clinic by applying lessons learned to improve the naevus service overall – virtual and F2F.

## 6. CHAPTER SIX: Artificial Intelligence in Ocular Oncology: Differentiating Benign Choroidal Naevus from Choroidal Melanoma

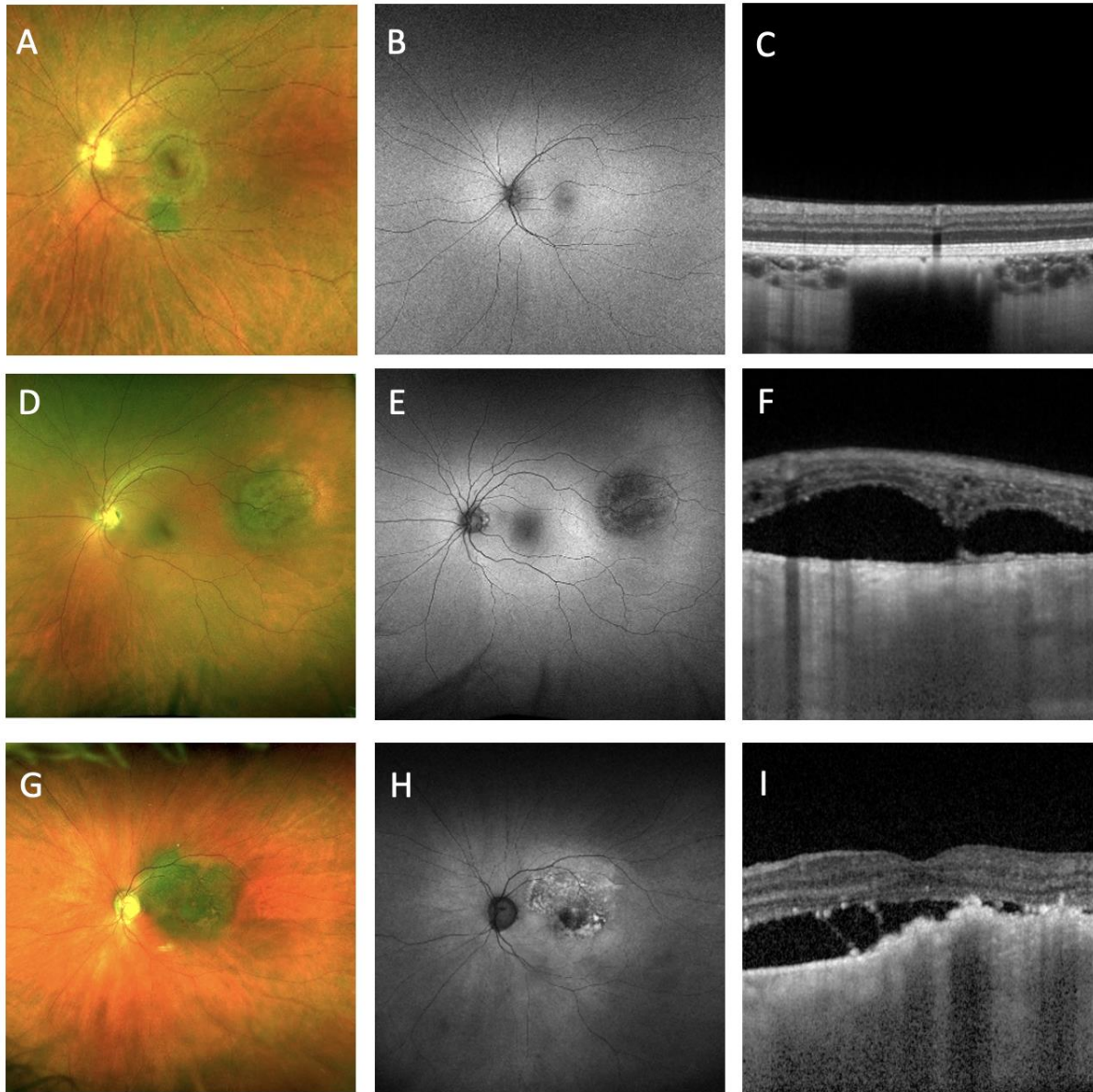
### 6.1. Background

Choroidal naevus is the most commonly encountered intraocular tumour and is benign with low malignant potential.<sup>63</sup> Choroidal melanoma is rare, and phenotypically comprises a wide spectrum - from large tumours which require enucleation, to small lesions with well-characterised high risk clinical features. There also exists a 'grey area' of lesions which can be labelled suspicious naevus, nevoma, indeterminate lesion, or small melanoma, depending on their clinical characteristics. There has been a drive to use imaging to document these lesions, growth being a surrogate marker for malignant transformation.<sup>65</sup>

Although pigmented fundus tumours are common, and the large majority are not harmful, distinguishing small melanomas from benign naevi remains a challenge.<sup>77, 146</sup> A major unmet need is an easy method to differentiate suspicious choroidal naevi from small choroidal melanoma, especially in the community or for triage. Choroidal naevus and small choroidal melanoma can show several overlapping features, and the challenge is to identify the single small malignant melanoma among the thousands of benign choroidal naevi.<sup>75, 406</sup> Biopsy to secure the diagnosis is often not possible or undesirable, so traditionally, observation for growth has been the paradigm for managing such indeterminate lesions. However, to improve survival, many ocular oncology centres have taken the approach of offering treatment earlier, diagnosing choroidal melanoma when small, based mainly on well-described clinical and imaging features,<sup>409</sup> despite the risk to vision in some cases.

The mnemonic 'To Find Small Ocular Melanoma Doing Imaging' (TFSOM-DIM) represents (T) for thickness over two millimetres on ultrasonography (USG), (F) for subretinal fluid on optical coherence tomography (OCT), (S) for symptoms of reduced

Snellen visual acuity <20/50, (O) for orange pigment on autofluorescence, (M) for melanoma hollow on USG, and (DIM) for diameter greater than five millimetres on colour photography. The more risk factors, the higher is the risk of growth into a melanoma.<sup>41, 55, 59, 65, 406</sup> The recently described MOLES clinical scoring system represents Mushroom shape, Orange pigment (i.e., lipofuscin), Large tumour size, Enlarging tumour, and Subretinal fluid (SRF). Each of these features is scored between 0 and 2, and tumours are diagnosed according to their sum total as 'common naevus', 'low-risk naevus', 'high-risk naevus' or 'probable melanoma'.<sup>79, 86, 430, 464</sup> (Figure 20)



**Figure 20:** Colour fundus photographs, fundus autofluorescence images, and OCTs of three cases: **(A–C)** with basal diameter 2mm, no subretinal fluid (SRF) and flat on ultrasonography (USG), representing choroidal naevus. **(D–F)** with basal diameter 5 mm, presence of SRF, and 1.1mm thickness on USG, representing indeterminate choroidal lesion. **(G–I)** with basal diameter >5 mm, confluent orange pigment, presence of SRF, and 1.6mm thickness on USG, representing choroidal melanoma.

Driven by the strong interest for early, objective, and repeatable diagnosis of choroidal melanoma, algorithmic image analysis techniques have garnered interest for differentiating between these lesions. Artificial intelligence (AI) describes the creation of computerised systems which perform tasks requiring synthesising knowledge and intelligence, and ophthalmic screening is well-suited for the application of AI due to well-understood relationships between clinical features and disease severity and the ready availability of imaging to effectively capture these features.

Healthcare imaging generates large amounts of data, and more than 97% of it is unanalysed or unused.<sup>465</sup> AI will be a critical factor in managing and analysing these datasets with the potential of doing this time-intensive work in as little as a few seconds.<sup>412-415, 466-468</sup>

Deep learning (DL), a new branch of AI, has shown robust results that have surpassed human performance in many areas of healthcare.<sup>411, 414, 415</sup> As a subset of machine learning (ML), DL is a highly specialised artificial neural network that consists of layers of 'neurons' with activation functions forming complex neural networks inspired by the ones constituting the human brain. Similar to human learning from experience, DL algorithms are trained on a task and fine-tune based on specific examples allowing for generalisation and inference on previously unseen input. These attributes make them powerful tools for segmentation, classification, and predictive modeling.<sup>414,416</sup>

This chapter will also discuss the potential role of AI in differentiating benign choroidal naevus from choroidal melanoma. The published clinical and imaging risk factors for malignant transformation of choroidal naevus will be reviewed in the context of how AI applied to existing ophthalmic imaging systems might be able to determine features on medical images in an automated way.

In February 2021, a '*White Paper on Ophthalmic Imaging for Choroidal Nevus Identification and Transformation into Melanoma*' was published by Shields et al. to discuss the evolution of non-invasive diagnostic methods for identification of choroidal naevus and determination of risk factors for malignant transformation, as well as introduce the novel role that AI can play in the diagnostic process.<sup>94</sup>

In June 2022, a further paper ‘*Artificial Intelligence in ocular oncology: Differentiating benign choroidal nevus from choroidal melanoma*’ was submitted for publication by Al Harby et al. to explore in detail the role of AI in differentiating benign choroidal naevus from small choroidal melanoma, and how AI applied to existing ophthalmic imaging systems may be able to determine features on medical images, in an automated way.<sup>469</sup>

### 6.1.1. Imaging in ocular melanocytic lesions

Uveal melanoma most often arises in the choroid and often from a pre-existing choroidal naevus. The naevus may be clinically apparent at an earlier stage prior to malignant transformation, allowing for the possibility of early detection and intervention based upon risk factors associated with the naevus.<sup>63, 77</sup>

In the past, diagnostic risk factors were based on subjective clinical observations alone, before multimodality ophthalmic imaging was available.<sup>74, 113, 406</sup> These factors have been improved over decades of research to more accurately identify melanoma at an earlier stage in transformation, with the goal to diagnose and treat melanoma at the smallest possible size.<sup>406</sup> More recently, high-resolution multimodality ophthalmic imaging has become available for identification of objective and reproducible risk factors for naevus transformation into melanoma.<sup>65, 72, 107</sup>

Several imaging modalities, including US, AF, and OCT, were recently combined to evaluate a series of 3806 choroid naevi.<sup>65, 406</sup> Using multimodal ophthalmic imaging, objective risk factors for naevus transformation into melanoma have been identified including Thickness >2 mm (USG), Fluid (OCT), Symptoms (Snellen visual acuity loss to 20/50 or worse), Orange pigment (AF), Melanoma acoustic hollowness (USG), and tumour Diameter >5 mm (fundus photography).<sup>65, 406</sup> Based on these recent findings, the mnemonic for choroidal naevus transformation to melanoma was updated to ‘*To Find Small Ocular Melanoma Doing Imaging*’ (TFSOM-DIM) to reflect



the importance of integrating objective imaging modalities into the clinical assessment of these tumours. As with clinical risk factors, the mean 5-year rate for naevus growth to melanoma increases as more multimodal imaging features are positive, as any two factors promote a mean 22% risk, three factors show 34% risk, and four factors promote >50% risk for transformation.<sup>65, 406</sup>

### 6.1.2. AI in other medical conditions

Recently, the Food & Drug Administration (FDA) has cleared or approved several digital health technologies. In April 2018, the FDA authorised the first stand-alone diagnostic system, the Diabetic Retinopathy Detection Device (IDx-DR), designed to automatically detect the presence of more-than-mild diabetic retinopathy.<sup>470, 471</sup> In August 2020 it has also been announced that EyeArt, an autonomous AI system for diabetic retinopathy screening has received FDA clearance for its AI technology to detect both, more-than-mild and vision-threatening diabetic retinopathy.<sup>472</sup>

There are also FDA-cleared systems for use in breast cancer detection including QuantX,<sup>473</sup> for computer-aided imaging diagnosis detection granted in July 2017 and MammoScreen<sup>473</sup> a radiologic computer-assisted software for lesions suspicious for cancer, cleared by the FDA in March 2020. Recently, the FDA granted the 'breakthrough' designation to 3Derm Spot for evaluating skin images to autonomously detect cutaneous melanoma, squamous cell carcinoma, and basal cell carcinoma.<sup>474</sup> A full list of devices authorised for marketing including 510(k) 'premarket notification' and 'de novo' are available in the FDA searchable medical device database.<sup>475</sup> The FDA's Center for Devices and Radiological Health (CDRH) embraces development of digital health technologies which include AI, ML, DL, and other types of software systems known as Software as a Medical Device (SaMD).<sup>476, 477</sup> Implementing CDRH's latest policies for digital health technologies will facilitate innovation in SaMD for diagnosis of choroidal naevus and prediction of risk for malignant transformation.

### 6.1.3. Lessons from cutaneous melanoma

Approximately 90%-95% of all melanomas are found in the skin. Cutaneous melanoma can be fatal and is increasing in frequency, mostly due to overexposure to solar radiation.<sup>478-481</sup> The uveal tract is the second most frequent location of malignant melanoma, representing about 5% of all melanomas. Although cutaneous and uveal melanoma are two distinct diseases biologically, both occur most often in patients with fair-skin complexion and blue or green eyes. Uveal melanoma has not clearly been found to be related to sunlight exposure, but similar to cutaneous melanoma, it can arise from a pre-existing naevus or de novo.<sup>481</sup> For both diseases, early detection is key for survival.

In 2004, Lindholm et al. documented that early cutaneous melanoma (<1 mm in thickness) had a 5-year survival rate of 94%, and this decreased to 49% in patients with thickness greater than 4 mm.<sup>480</sup> Major advances in the dermatology literature have helped in early detection of cutaneous melanoma. The mnemonic ABCDE (Asymmetry, Border irregularity, Colour, Diameter >6 mm, Evolving size, shape, or colour) simplified the key features of early cutaneous melanoma and helped physicians and non-physicians diagnose 'suspicious' lesions before they grew.<sup>479</sup> Skin self-examination has helped improve early detection of cutaneous melanoma.<sup>478</sup> Further advances with the use of instruments like dermoscopy, a handheld device that allows magnified, high resolution visualisation of the skin, has also improved detection.<sup>482</sup> Automated computer-assisted differentiation performed by an expert system has provided 95% sensitivity and 70% specificity.<sup>482</sup>

### 6.1.4. AI applications in differentiating choroidal naevi from melanoma

The long-standing use of clinically identified risk factors in differentiating choroidal naevus from melanoma<sup>74, 406, 417</sup> and the more recent extensive use of ophthalmic diagnostic imaging to both identify and monitor choroidal naevus and melanoma<sup>65, 72, 406, 417</sup> provide substantial data to explore applications of AI.

Machine learning (ML) approaches may be supervised, where the algorithm is trained on human-labelled data, or unsupervised, where the algorithm is trained on unlabelled data and will identify patterns by itself<sup>470, 483</sup> as well as numerous other methods of learning and model creation. Supervised learning and models tend to be excellent classifiers of disease type (e.g. naevus vs. no naevus) and disease stage (e.g. low risk vs. high risk naevus).<sup>470, 483</sup> For instance, a supervised ML model can be trained with a dataset consisting of labelled fundus photographs of choroidal naevi and photographs of the normal fundus. The trained model, through supervised learning, may identify a naevus in a fundus photograph, with a sufficiently high sensitivity and specificity. For the model to achieve a high performance and high levels of accuracy, a large dataset of fundus photographs of choroidal naevi is required so that the model can identify any choroidal naevus by learning varied representations of shape, size (small vs. large), location (macular vs. extramacular), degree of pigmentation (pigmented vs. non-pigmented), or associated clinical features (subretinal fluid, orange pigment, overlying drusen, overlying RPE atrophy, RPE hyperplasia, or RPE fibrosis). Another potential use case may be differentiation of choroidal naevi labelled as low risk or high risk based on high-risk clinical features identified on fundus examination (presence of overlying subretinal fluid, presence of overlying orange pigment, diameter > 5 mm).

DL systems allow models to not only be excellent ‘classifiers’ of disease but also ‘feature extractors’.<sup>470, 483</sup> An unsupervised DL model may be trained with unlabelled photographs of the normal fundus as well as photographs of various choroidal naevi with a range of risk factors for malignant transformation. A DL algorithm’s process of progressive, layered data extraction allows the model to infer qualities from the input fundus photographs and cluster them based on computational features and then further identify patterns within those features. It may then learn not only to identify a naevus, but also to classify it based on risk of malignant transformation. In this regard, DL algorithms hold the potential to find novel or unexpected computational features which may predict naevus at risk for malignant transformation. In other words, DL may uncover risk factors for uveal melanoma that are currently not known from clinical studies.

### 6.1.5. Summary of the Collaborative Community on Ophthalmic Imaging (CCOI)

As part of the Collaborative Community on Ophthalmic Imaging (CCOI) conference 2020, the ocular oncology working group collaboratively presented and explored the role of AI in the diagnosis and management of intraocular tumours. The group discussed basic clinical features of choroidal naevus and melanoma, as well as imaging, and how it can be improved by using advanced techniques like swept-source (SS-OCT), which recently became available. It has an increased signal penetration with a greater potential to detect specific vascular patterns and can also perform a better tumour depth assessment. Machine learning using SS-OCT could predict new features on images discovering malignancy or malignant transformation.

With the focus on the importance of distinguishing choroidal naevus from choroidal melanoma, the group highlighted important considerations when examining patients with choroidal naevus, comprising (1) multimodal imaging risk factors which can predict risk for choroidal naevus transformation to melanoma, (2) features of chronicity (drusen, RPE changes, fibrous metaplasia) providing reassurance, and (3) change over time parameters (expansion of basal diameter, increased thickness, new risk factors) that can indicate benign naevus growth or transformation to melanoma.

To bring ocular oncology to the next technological level, AI could be utilised to read images and identify patients at high risk. The six known multimodal imaging risk factors for transformation to melanoma can be identified by machines for computer interpretation. If all naevi can be successfully identified, and if the ML model can discriminate those at risk for malignant transformation, it might be possible to treat melanoma very early or even eradicate melanoma by treating those naevi at highest risk.

Would it be possible for AI to detect a choroidal naevus? Reports demonstrated that similar approaches in ophthalmology and oncology specialities successfully applied AI for diagnostic imaging and lesion classification. A 2016 publication on AI for skin lesion classification utilising the dermatoscope was cited, showing that AI could successfully

reproduce the decision-making process of dermatologists.<sup>484</sup> Other reports described the application of AI for image analysis for diabetic retinopathy, glaucoma, and age-related macular degeneration with similar successful outcomes.<sup>470</sup>

A major interest lies in the exciting opportunities of deep learning methodology. The continuous refinement of the model and the ability to derive independent criteria for classification, segmentation, and prediction based on the images has even greater potential. In dermatology, a DL model allowed it to grow from a classifier to an identifier. By learning from a large number of dermatoscope images, AI was able to generate its own diagnostic criteria for detecting melanoma, achieving a higher sensitivity in correctly identifying the melanoma and higher specificity correctly identifying the naevus.<sup>485</sup>

It seems reasonable that applying a similar methodology to choroidal naevus holds the potential to provide beneficial results with AI, specifically with DL methodology.

Focus points for ocular oncology are to improve the detection of choroidal naevus and to find a way to obliterate a suspicious choroidal naevus or early melanoma without harming a patient's vision. Next to multimodal imaging features, AI has the potential to help with the improved detection of suspicious features. Installing such technologies in community care would provide convenient and early access to care for patients.

Despite general ophthalmologists being well-trained and capable of recognising abnormal lesions, there are two barriers that impede accurate diagnosis. First is the concern of a misdiagnosis, so there can be a push to upgrade a lesion. Second, not all of the specialised imaging that is common in a tertiary level ocular oncology clinic is available in a general community clinic. Reliance on only a few modalities rather than multimodal imaging may miss important imaging features. Both factors generate over-referrals into tertiary care. Using AI with or without remote advice from a specialist would support those in primary and secondary eye care.

To manage ocular melanoma in an ideal setting, important factors include finding the tumour at the earliest possible time and treating it directly with preservation of vision. In cases with metastatic potential, an adjuvant treatment would improve prognosis,

and in established metastasis, an efficacious treatment is needed. In this multifaceted approach, the potential of AI for early diagnosis is keenly anticipated. An added advantage is the cost efficiency for healthcare systems and providing patients with a remote, AI-based diagnosis. If the AI system can differentiate melanocytic lesions from other pseudotumours, its utility would be even greater.

AI can allow national or international standardisation of protocols for diagnosis, monitoring and treatment. Pooled data can be used to increase the sensitivity and specificity of the system, especially with greater quantity, quality, and diversity of collected data settings. Analysing large datasets can be computationally heavy and time-consuming, a challenge that can be overcome with the advent of novel computers with increased computing power. In addition, a robust ML model requires strong datasets that consist of data that meet certain predetermined standards, for example, the colour photographs needing to be a particular area of the fundus or using standardised camera settings.

In other fields, AI detection of cancers has been attempted. Published studies from 2020 demonstrate that AI detection of prostate cancer shows more than 98% sensitivity and 97% specificity. Using mammography imaging for detection of breast cancer looking at mammography, the AI was 95% sensitive, whereas radiologists were about 81% sensitive.<sup>486, 487</sup> In ocular oncology, the initial aim of AI in melanoma detection is to achieve  $\geq 99\%$  sensitivity, even if AI is less specific. To reach the highest possible sensitivity and specificity, many image combinations with a DL model might be necessary.

It will be challenging to develop an AI model on a limited number of photographs, especially if these have been captured by potentially six different modalities on the same patients. Multi-centre efforts to use images not only for choroidal naevus and melanoma but also for indeterminate cases would be a critical factor for a DL model to be accurate. The barrier to this is the varying camera and imaging systems used in different clinics.

Using the multimodal approach could optimise the advancement of DL models to uncover features that practitioners cannot see with their own viewing of images or

clinically. There might be inconspicuous information on OCT, fundus photography, autofluorescence, and the other modality imaging that help to detect melanoma earlier.

## 6.2. Introducing automated deep learning design for differentiating benign choroidal naevus from choroidal melanoma (A proof of concept)

### 6.2.1. Introduction

In a previous study,<sup>95</sup> a model of managing melanocytic lesions in a virtual pathway was described. The results show that images of choroidal naevi evaluated remotely using a decision-making algorithm by masked non-medical graders or masked ophthalmologists is safe. This work prospectively validates a virtual naevus clinic model focusing on patient safety as the primary consideration.

Further development of virtual pathways could embed artificial intelligence decision support systems for image grading and classification to make processes even more effective, and differentiation between choroidal naevi and choroidal melanomas may be enhanced by the application of image analysis using deep learning techniques.

In artificial intelligence (AI), the method of deep learning uses artificial neural networks as a computational model to discover intricate structures and patterns in large, high-dimensional datasets such as medical images. A central characteristic of these networks is their ability to fine-tune based on experience, allowing them to adapt to their inputs and become capable of evolving. This feature makes them powerful tools for classification, pattern recognition, and prediction.<sup>416</sup>

There have been previous reports on the ability of physicians to create automated machine learning (AutoML) models for medical image analysis.<sup>488</sup> Since that proof of concept, AutoML platforms have advanced significantly, with multiple employing code-free deep learning (CFDL). It has been demonstrated that AutoML can serve as a tool

for automated discovery of novel insights, for example, by performing sex classification from retinal fundus photos using automated deep learning.<sup>489, 490</sup>

Deep learning, a subset of ML and AI, has the potential to transform health care,<sup>416, 416, 491, 492</sup> and deep learning techniques are evolving rapidly and will become more integrated into ophthalmic care.<sup>409, 413</sup> The author explored the feasibility of developed automated deep learning models and investigated the performance of these models in diagnosing choroidal naevomelanocytic lesions (CNL) based on medical imaging, including colour fundus and autofluorescence fundus photographs. The aim of this project was to determine the sensitivity and specificity of an automated deep learning algorithm used for binary classification to differentiate choroidal melanomas from choroidal naevi and prove that a differentiation concept utilising an ML algorithm is feasible.

## 6.2.2. Methods

### 6.2.2.1. Datasets and study design

Two de-identified ophthalmic imaging datasets for training and validating two deep learning models were utilised, one for autofluorescence fundus and one for colour fundus images, using Google's Cloud AutoML platform.

The two selected datasets, consisting of Moorfields Eye Hospital set 1 with  $n = 402$  for model training and development, and Moorfields Eye Hospital set 2 with  $n = 208$  for internal validation, included autofluorescence fundus (AF) and colour fundus (CL) photography images, representing diagnoses of choroidal naevus and choroidal melanoma.

For the deep learning model development and model training, the first dataset comprised 402 images from 201 patients from Moorfields Eye Hospital (MEH) utilised



in the MOLES study '*Distinguishing Choroidal Nevi from Melanomas Using the MOLES Algorithm: Evaluation in an Ocular Nevus Clinic*'.<sup>79</sup>

For the internal validation to test the models, a second dataset was extracted consisting of 208 images from 104 patients from Moorfields Eye Hospital (MEH) utilised in the follow-up studies '*The MOLES system for planning management of melanocytic choroidal tumours: is it safe?*'<sup>493</sup> and '*Prospective Validation of a Virtual Clinic Pathway in the Management of Choroidal Naevi*'<sup>95</sup>

Both MOLES studies, where the datasets have been extracted from, were approved by the Moorfields Eye Hospital clinical audit department (No; 452) and were conducted in accordance with the declaration of Helsinki.

#### **6.2.2.2. Dataset details**

The imaging dataset 1 used for model training and machine learning algorithm development has been extracted from the Moorfields Eye Hospital (MEH) patient cohort used in study '*Distinguishing Choroidal Nevi from Melanomas Using the MOLES Algorithm: Evaluation in an Ocular Nevus Clinic*'. As part of the methods of this study, colour photographs, fundus autofluorescence images, and optical coherence tomography of 222 melanocytic choroidal tumours were reviewed. MOLES features/ risk factors were scored between 0 and 2, and tumours were categorised as 'common naevus', 'low-risk naevus', 'high-risk naevus', and 'probable melanoma', according to the sum total of 0, 1, 2 and >2, respectively.

The results have shown the MOLES scoring system indicated 81 melanomas (MOLES score >2) and 135 naevi (MOLES score 0 or 1). Six tumours had discordant diagnoses (MOLES score 2). These 6 cases classified as indeterminate lesions have been excluded from this AutoML study, as well as further 15 cases where image quality was insufficient. The final dataset included images from 201 patients.

From these 201 patients, 402 images, of which 201 autofluorescence fundus photographs (AF) with 82 melanomas and 119 naevi and 201 colour fundus photographs (CL) (Optos California [Optos plc, Dunfermline, Scotland]) with equally 82 melanomas and 119 naevi have been collected and prepared for data processing and labelling. The AutoML platform excluded further 3 images so that the final dataset used for training comprised 199 AF images and 200 CL images.

Dataset 2 used for internal validation that is used to test the developed machine learning model has been extracted to some parts from the Moorfields Eye Hospital (MEH) patient cohort used in study *'The MOLES system for planning management of melanocytic choroidal tumours: is it safe?'* As part of the methods of this study, records of 615 patients treated for choroidal melanoma between January 2017 and December 2019 were reviewed. Patients were excluded if iris and/or ciliary body involvement, inadequate fundus photography, no images available for review and/or treatment was not primary. Dataset 2 has also used data from study *'Prospective Validation of a Virtual Clinic Pathway in the Management of Choroidal Naevi'*, which included prospective analysis of the clinical details and imaging of 400 patients attending the naevus clinics at the Manchester Royal Eye Hospital (MREH) and Moorfields Eye Hospital (MEH). Patients with pathologies other than choroidal naevi, such as erroneous referrals, including congenital hypertrophy of the retinal pigment epithelium, were excluded from the study.

Colour fundus and autofluorescence photographs (AF), optical coherence tomography (OCT) and B-scan ultrasounds were prospectively reviewed, and MOLES scores were assigned accordingly. 104 have been selected, representing equal parts of melanocytic lesions graded with MOLES score >2 and MOLES 0, 1 or 2.

From these 104 patients, 208 images of which 104 autofluorescence fundus photographs (AF) with 54 melanomas and 50 naevi and 104 colour fundus photographs (CL) (Optos California [Optos plc, Dunfermline, Scotland]) with equally 54 melanomas and 50 naevi have been collected.

### 6.2.2.3. Data processing and labelling

A retrospective collection of the images used for all datasets has been performed as part of the MOLES studies.<sup>79, 430</sup> The images have been downloaded from OptosAdvance™ - OptosCloud platform with its original standardised format, including default image settings, size and resolution. To further prepare the image dataset, the downloaded images have been cropped to exact equal size, as required by AutoML.

The 402 images from the first dataset have been split into two subsets, 201 AF and 201 CL images, in preparation to be used to train an AF model and a CL model, respectively.

The previously determined classification of the images of each subset as categories 'common naevus' and 'probable melanoma' have been given binary diagnostic labels of 'nevus' and 'melanoma', resulting in 82 melanoma and 119 naevi labelled images for each model, AF and CL.

Training supervised deep learning models involves splitting datasets into training, validation, and test sets. The labelled 201 AF and 201 CL images have subsequently been further split randomly into sub-datasets for training (80%), validating (10%), and testing (10%) of the respective AF and CL deep learning models, (Table 17) whereby the percentage levels have been suggested by the AutoML platform. Proportions of both diagnostic labels were preserved in each split to ensure the datasets were not class imbalanced between splits.

During the image data import, there is the possibility that the AutoML platform flags specific images automatically for exclusion based on the threshold for the classification. This can occur if images are considered not representative enough for one of the classes (melanoma or naevus) because the prediction probability score was too close to the threshold (e.g. either > or < than 0.5).

AutoML excluded 3 images, so that the final dataset for training comprised 199 AF images and 200 CL images with data splits presented in Table 17.

Dataset initially imported						
Model	AF deep learning model			CL deep learning model		
Dataset	AF image dataset (n=201)			CL image dataset (n=201)		
	n (%)	naevus (n=119)	melanoma (n=82)	n (%)	naevus (n=119)	melanoma (n=82)
Train	159 (80%)	95	64	159 (80%)	95	64
Validate	21 (10%)	12	9	21 (10%)	12	9
Test	21 (10%)	12	9	21 (10%)	12	9

Dataset used by the platform						
Model	AF deep learning model			CL deep learning model		
Dataset	AF image dataset (n=199)			CL image dataset (n=200)		
	n (%)	naevus (n=118)	melanoma (n=81)	n (%)	naevus (n=119)	melanoma (n=81)
Train	158 (80%)	95	63	158 (80%)	95	63
Validate	20 (10%)	11	9	21 (10%)	12	9
Test	21 (10%)	12	9	21 (10%)	12	9

**Table 17:** Dataset splits for AF and CL deep learning models (imported and used)

The 208 images from the internal validation dataset have been divided into 104 AF and 104 CL images and subsequently categorised as naevus and melanoma based on their MOLES score results. Suspicious cases with a MOLES score of 2, representing indeterminate lesions (5 cases), were considered to belong to the naevus group. Since the model in this study has only been trained to distinguish naevus from melanoma, these cases have been considered and labelled as naevus as not proven malignant and, therefore, not melanoma. Each subset of AF and CL images included 54 melanomas and 50 naevi.

#### 6.2.2.4. AutoML platform selection

Various AutoML platforms are available on the market, such as Apple Create ML (Apple), Google Cloud AutoML Vision (Google), Amazon Rekognition Custom Labels (Amazon), Clarifai Train (Clarifai), Microsoft Azure Custom Vision (Microsoft), and MedicMind Deep Learning Training Platform (MedicMind). In April 2021, a study<sup>494</sup> evaluated thirteen candidate platforms for characteristics including the need for coding requirements, English language, availability of usage within the region (UK), and the inclusion of a free trial period.

The study's evaluation did not show notable performance differences among the leading platforms (Google, Amazon and Microsoft). However, these platforms varied significantly regarding the availability of the critically important evaluation features, such as providing threshold adjustments, precision-recall curves and confusion matrices through their respective graphical user interfaces (GUIs). Google provided all of these, Amazon provided none of these, and Microsoft provided only threshold adjustment. Of these three platforms, only Google has batch prediction capability, which allows external validation at scale.<sup>494</sup>

Cloud AutoML services allow to build highly accurate machine learning systems with minimal knowledge or experience. Google AutoML Vision enables easily build custom image classification systems according to own defined labels that take advantage of deep learning algorithms that would normally require significant experience to configure and use.

A high-level process overview of AutoML vision for medical image classification starts with the option to import the images either via upload from the computer or from a CSV file into cloud storage which specifies file location and labels, including label statistics. There is an option to filter labelled and unlabelled images, and labels can be assigned ad hoc or be changed if needed. Once the dataset and labels are satisfactory, the model can be trained. The time to train can be selected; however, the model automatically stops training when it stops improving, and it will be notified when training is completed. After the model is trained, detailed statistics, including precision-recall curves, can be viewed. A score threshold can be set, and the confusion matrix

can be reviewed where true positives and false negatives are visualised. The data can be exported into a CSV file showing which image was included in the training, validation, or test set for further model interrogation. Once the model has been deemed satisfactory, it can be used to make predictions on new images.

#### **6.2.2.5. Model training**

Our AF and CL deep learning models were trained using code-free deep learning (CFDL) with the Google Cloud AutoML platform. The platform provides a graphical user interface for data upload, labelling, and model training. The author utilised the alternative option to upload and import the training, validation and testing images via a CSV spreadsheet containing labels with associated cloud storage locations for the efficient management of the datasets.

Automated machine learning was then deployed, which entails neural architecture search and hyperparameter tuning. In detail, this means that the training data built up the machine learning algorithm by feeding the algorithm input data, which corresponds to the expected output. The model evaluated the data repeatedly to learn more about the data's behaviour and then adjusted itself to serve its intended purpose. During training, the validation dataset infused new data into the model that it had not evaluated before. The validation data provided the first test against unseen data, allowing evaluation of how good the ML model makes predictions based on the new data and, if needed, optimises hyperparameters, which influence how the model assesses data. After the model is complete, testing data once again validated that the model could make accurate predictions. Test data offers a final, real-world check of an unseen dataset to confirm that the ML algorithm was trained effectively.<sup>495</sup>

The training of the AF and CI models was performed with maximum allowable cloud graphics processing unit (GPU) hours, and early stopping was enabled, which automatically terminated training when no further model improvement was noted after 8 node-hours. Each node-hour represents eight cloud nodes used in parallel, and each node is equivalent to an NVIDIA® Tesla® V100 GPU.<sup>496</sup>

#### 6.2.2.6. Model output & evaluation

After successful training of an ML model, the AutoML platform will provide a summary of the custom model's performance based on the model's output on test data and a range of common machine learning metrics. This section will give an overview of what each of these concepts means.<sup>497</sup>

The score threshold refers to the level of confidence the model must have to assign a category to a test item. The score threshold is a number that ranges from 0 to 1. It provides a way to specify the minimum confidence level where a given prediction value should be taken as true.<sup>497, 498</sup>

If the score threshold is low, the model will classify more images, but runs the risk of misclassifying a few images in the process. If the score threshold is high, the model will classify fewer images, but it will have a lower risk of misclassifying images. After applying the score threshold, the predictions made by the model will fall into one of the following four categories: true positives, true negatives, false positives, and false negatives.<sup>497</sup>

The prediction results on a classification problem can be summarised in a confusion matrix where true positives, true negatives, false positives, and false negatives are visualised in cross-tabulated sections ground truth labels versus model prediction labels. (Table 18) The correct and incorrect predictions are summarised with count values and broken down by each class. As opposed to the model prediction, the ground truth refers to the actual nature of the problem, which is the target of a machine learning model, reflected by the relevant datasets associated with the use case in question.

Confusion Matrix			
		Ground Truth	
		Actual positive	Actual negative
Model Prediction	Predicted positive	True positive	False positive
	Predicted negative	False negative	True negative

**Table 18:** Confusion matrix for deep learning model validation

These four categories can be used to calculate precision and recall, which are metrics that help gauge the effectiveness of the model. Precision and recall help understand how well the model captures information and how much it leaves out.

Precision shows, from all the test examples that were assigned a label, how many actually were supposed to be categorised with that label. Precision also refers to positive predictive value (PPV).

Recall shows, from all the test examples that should have had the label assigned, how many were actually assigned the label. Recall also refers to true positive rate (TPR) and sensitivity.

The trade-off between precision and recall is displayed in the precision-recall curve (PR curve). This curve combines precision (PPV) and recall (TPR) in a single visualisation. Knowing that the score threshold affects precision and recall, the curve changes in dependency where the score threshold is set.

It is desired that the algorithm has both, high precision, and high recall. However, most machine learning algorithms often involve a trade-off between the two. A good PR curve has a greater area under the curve. In different words, a great area under the curve represents both, high precision and high recall, where high precision relates to a low false positive rate, and high recall to a low false negative rate.<sup>499, 500</sup>

This so-called ‘Area Under the Precision-Recall Curve’ (AUPRC or PR AUC) can also be referred to as ‘Average precision’ and is stated as a score. The closer to 1.0 this score is, the better the model performs on the test set.



The true-positive rate, the proportion of positives that are correctly identified, is also known as sensitivity or probability of detection. The false-positive rate is also known as the probability of false alarm.<sup>501</sup>

For evaluating the performance of the deep learning models, including internal validation, the aim is to provide meaningful statistical parameters. Next to sensitivity, measuring the proportion of positives (melanoma) that are correctly identified (TPR), and specificity, measuring the proportion of negatives (naevus) that are correctly identified (TNR), two other useful parameters are the positive predictive value (PPV) and the negative predictive value (NPV). The PPV indicates that if a test prediction is positive (melanoma), what is the probability that the image shows a melanoma indeed. The NPV indicates that if the test prediction is negative (naevus), what is the probability that the image shows indeed a naevus, and not a melanoma.

Another essential metric is the accuracy (ACC) of the model, which represents how well the test predicts both TPR and TNR by measuring how many classified observations, both positive and negative, were correctly classified. Accuracy should only be used if the dataset is sufficiently balanced.<sup>502</sup>

Finally, the F1-score is another evaluation metric in machine learning. It sums up the predictive performance of a model by combining two otherwise competing metrics - precision and recall. It combines precision and recall into one metric by calculating the harmonic mean between those two.<sup>503</sup> An F1 score is considered perfect when it is 1, or 100% respectively, but it is usually lower because all models will generate some false negatives, some false positives, and possibly both.

#### **6.2.2.7. Model test & use**

After successful evaluation of the ML model with satisfactory performance, it can be deployed and is available for prediction requests. Via AutoML function 'Test & Use', the model can be further tested, validated, and verified with a new separate dataset. For this step, the author utilised the prepared dataset for internal validation and imported the images to test the completed trained AF and CL models.

### 6.2.2.8. Statistical analysis

The AutoML Cloud Vision platform provides various model metrics, including confusion matrices, precision and recall percentage values, and the area under the precision-recall curve (AUPRC) or average precision for the default confidence threshold of 0.5 that has been set for the two models.

Contingency tables have been constructed, and statistical analysis was performed with Microsoft Excel to calculate clinical metrics, including sensitivity, specificity, positive and negative predictive value (PPV and NPV), F1 score, and accuracy (ACC) using the values in the confusion matrices provided by the AutoML platform. (Table 19)

Model Evaluation & Internal Validation			
		Ground Truth	
		Actual positive	Actual negative
Model Prediction	Predicted positive	True positive (TP)	False positive (FP)
	Predicted negative	False negative (FN)	True negative (TN)
		<b>Formula</b>	
Statistical Metrics	Sensitivity	$TP / (TP + FN)$	
	Specificity	$TN / (TN + FP)$	
	PPV	$TP / (TP + FP)$	
	NPV	$TN / (TN + FN)$	
	F1	$2 * PPV * Sensitivity / (PPV + Sensitivity)$	
	ACC	$TP + TN / (TP + TN + FP + FN)$	

**Table 19:** Confusion matrix and statistical parameters with formulae

### 6.2.3. Results

#### 6.2.3.1. Evaluation of the trained models

The AF and CL deep learning models were effectively trained on 199 AF images and 200 CL images, respectively, (Table 17) and the models have been evaluated based on the binary classification task results to differentiate choroidal naevus from choroidal melanoma.

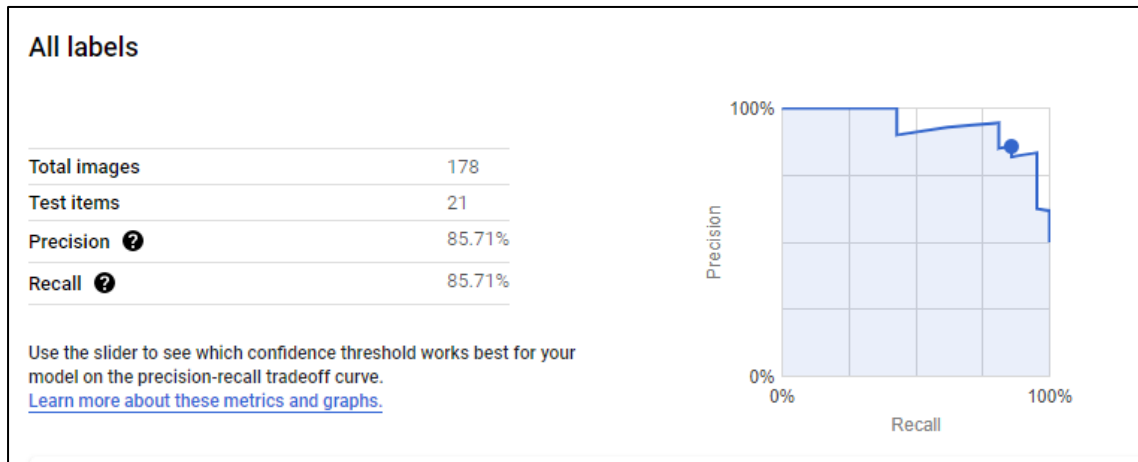
For each of the two models, AF and CL, four individual models have been trained (Appendix 2 – AutoML screenshots of AF and CL model evaluation) using the identical pre-defined training datasets and platform settings, except for one model where 16 node hours have been set instead of 8, which, however, did not lead to improved performance and will not be part of this analysis.

The best model for each imaging type has been chosen based on established model performance parameters, high precision and high recall values, as well as a high AUPRC value, to be further used for detailed model evaluation and continued testing/verification of the model using the separate internal validation dataset.

##### 6.2.3.1.1. AF model evaluation

The evaluation of the AF model demonstrates a precision of 85.71% and recall of 85.71% with an AUPRC/average precision value of 0.933 at a confidence threshold of 0.5, which indicates an excellent performance of this model. (Figure 21)

It is to mention that precision and recall values reported by the AutoML dashboard are calculated using micro-average for binary and multiclass classification models, and the calculations include the sum of the TP, TN, FN, FP for each individual class, melanoma and naevus.<sup>498, 504</sup>



**Figure 21:** Precision and Recall and PR curve of the AF model

Table 20 shows the confusion matrix of how the 21 test images have been classified by the model, with 7 correctly classified melanomas (true positives) and 2 melanomas incorrectly classified as naevus (false negatives), 11 correctly classified naevi (true negatives), and 1 naevus incorrectly identified as melanoma (false positives).

AF Model Evaluation			
		Ground Truth	
		melanoma	naevus
Model Prediction	melanoma	7	1
	naevus	2	11
Statistical Metrics	Sensitivity	77.78%	
	Specificity	91.67%	
	PPV	87.50%	
	NPV	84.62%	
	F1	82.35%	
	ACC	85.71%	

**Table 20:** Confusion matrix and statistical parameters of the AF model evaluation

The sensitivity of the AF model, how well melanoma is detected, is 77.78% and the specificity, how well naevus is detected, is very high at 91.67%.

The PPV shows that there is an 87.50% probability, if the prediction is positive (melanoma), that the patient does have a melanoma.

Based on the NPV, there is an 84.62% probability, if the prediction is negative (naevus), that the patient does have a naevus. However, there is still a 15.38% chance that the patient does have a melanoma.

In general, the AF model presents a good F1 score of 82.35% and a good overall accuracy of 85.71%, showing that over 85% of the classified observations, both positive (melanoma) and negative (naevus), were correctly classified.

One feature that AutoML Vision contains is the possibility for the end-user to fine check the performance of the trained model for each different class. The manual calculations of sensitivity, specificity, PPV and NPV can be confirmed by comparing them with the model performance metrics of the individual diagnostic class. For melanoma representing the positive label in the models, the precision (PPV) is 87.50%, and recall (sensitivity) is 77.78%. For naevus representing the negative label, precision (NPV) and recall (specificity) are 84.62% and 91.67%, respectively. (Figure 22)

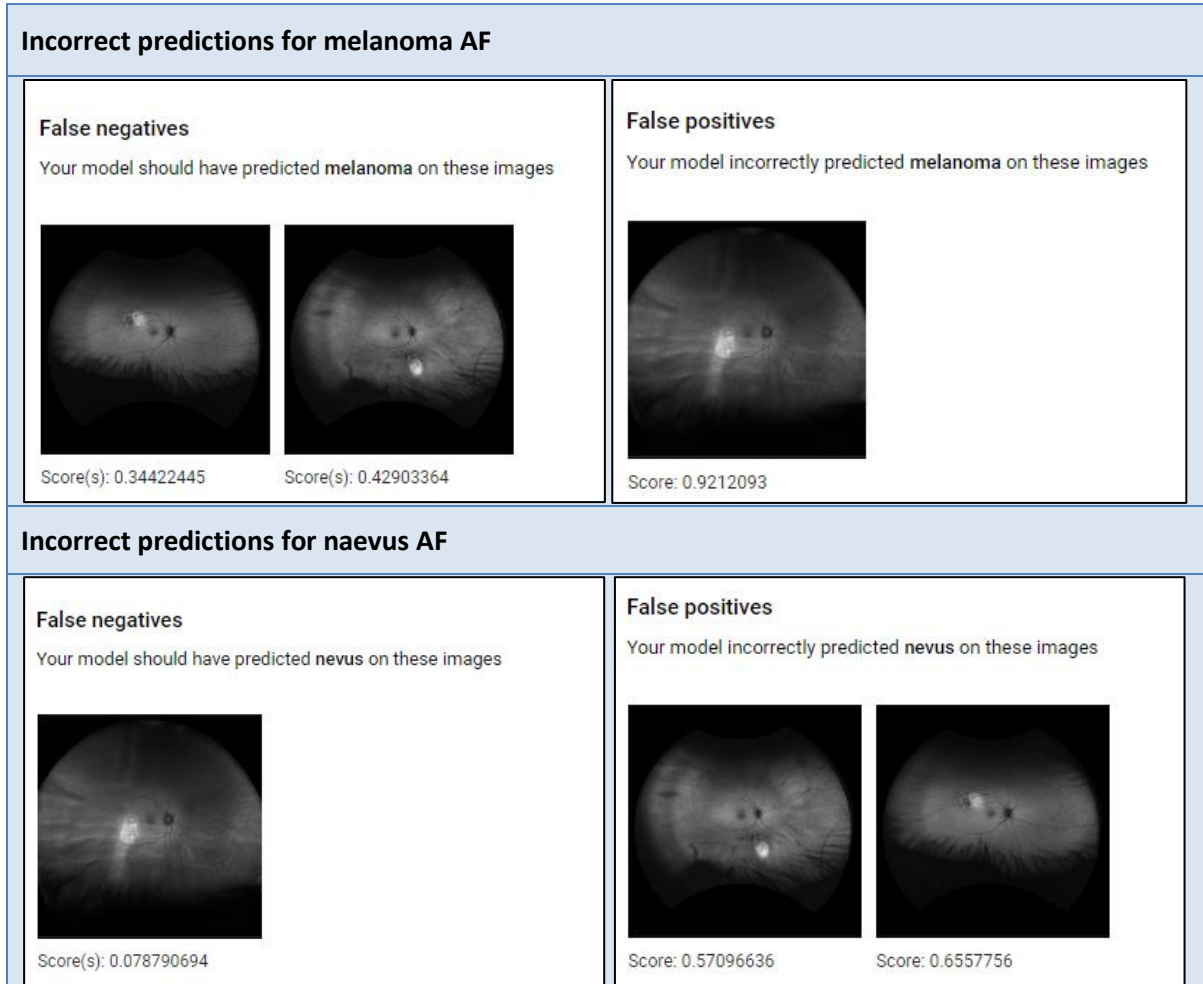
melanoma	
Total images	178
Test items	0
Precision ?	87.5%
Recall ?	77.78%

nevus	
Total images	178
Test items	0
Precision ?	84.62%
Recall ?	91.67%

Figure 22: Precision and Recall of the AF model for individual diagnostic classes

As part of the individual model performance check per class, it can also be verified how the model classified each image in the test set, separated by true positives, false negatives and false positives. This is useful to better understand the model's ability to distinguish naevi from melanoma.<sup>504</sup>

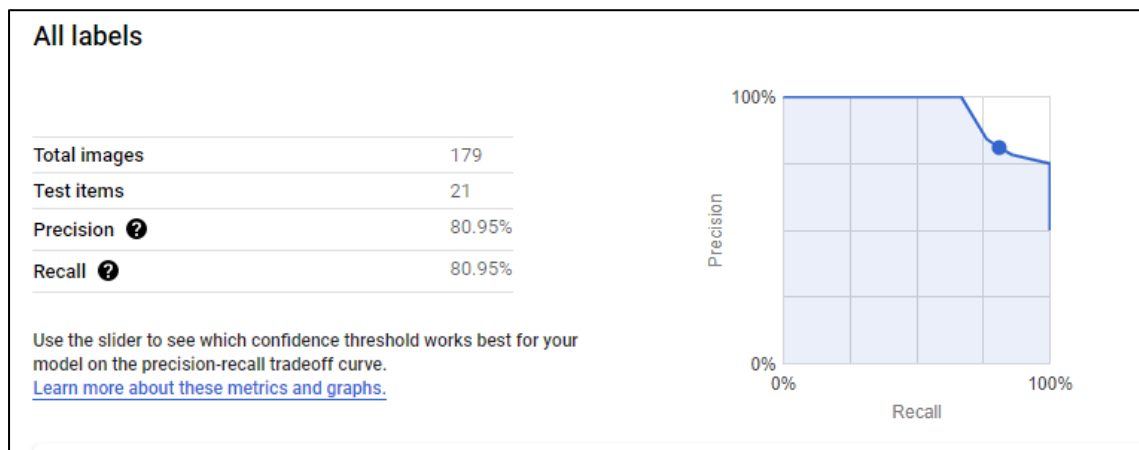
Figure 23 displays images, the AutoML platform returned with false negative and false positive predictions, along with a score between 0-1, letting the end-user know the confidence the decision has been taken.



**Figure 23:** Examples of incorrect predictions for melanoma and naevus in AF images

### 6.2.3.1.2. CL model evaluation

The evaluation of the CL model demonstrates a precision of 80.95% and recall of 80.95% with an AUPRC/average precision value of 0.928 at a confidence threshold of 0.5, which indicates an excellent performance of this model. (Figure 24)



**Figure 24:** Precision and Recall and PR curve of the CL model

Table 21 shows the confusion matrix of how the 21 test images have been classified by the model, with 8 correctly classified melanomas (true positives) and 1 melanoma incorrectly classified as naevus (false negatives), 9 correctly classified naevi (true negatives), and 3 naevi incorrectly identified as melanoma (false positives).

CL Model Evaluation			
		Ground Truth	
		melanoma	naevus
Model Prediction	melanoma	8	3
	naevus	1	9
Statistical Metrics	Sensitivity	88.89%	
	Specificity	75.00%	
	PPV	72.73%	
	NPV	90.00%	
	F1	80.00%	
	ACC	80.95%	

**Table 21:** Confusion matrix and statistical parameters of the CL model evaluation



The sensitivity of the CL model, how well melanoma is detected, is high at 88.89% and the specificity, how well naevus is detected, is lower at 75.00%.



The PPV shows that there is a 72.73% probability, if the prediction is positive (melanoma), that the patient does have a melanoma.

Based on the NPV, there is a 90.00% probability, if the prediction is negative (naevus), that the patient does have a naevus. However, there is still a 10.00% chance that the patient does have a melanoma.

In general, the CL model presents a good F1 score of 80.00% and a good overall accuracy of 80.95%, showing that over 80% of the classified observations, both positive (melanoma) and negative (naevus), were correctly classified.

The individual check of the performance per diagnostic class confirmed the manual calculations of sensitivity, specificity, PPV and NPV of the CL model, with precision (PPV) of 72.73% and recall (sensitivity) of 88.89% for melanoma class, and precision (NPV) of 90.00% and recall (specificity) of 75.00% for the naevus class. (Figure 25)

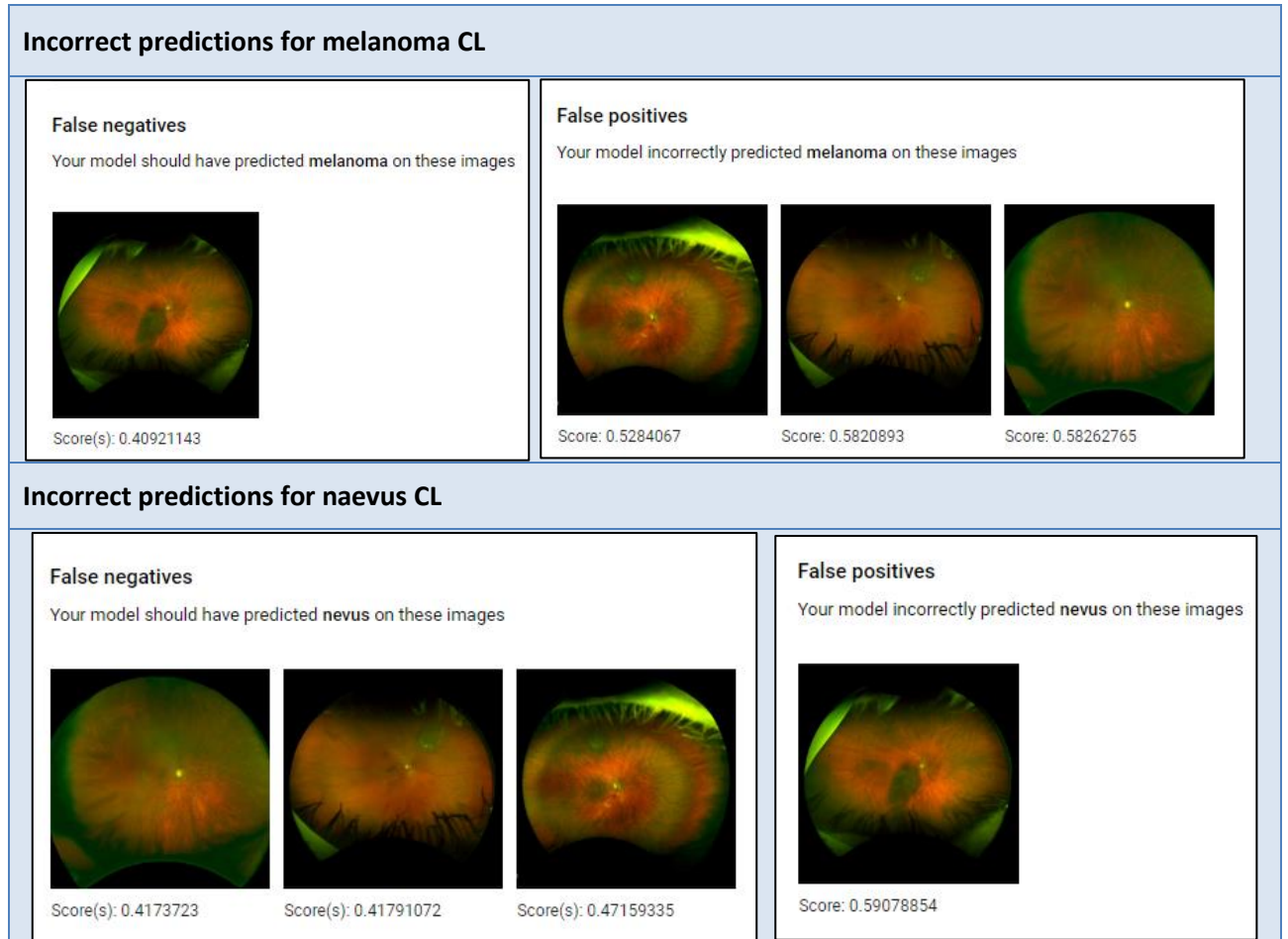
melanoma	
Total images	179
Test items	0
Precision 	72.73%
Recall 	88.89%

nevus	
Total images	179
Test items	0
Precision 	90%
Recall 	75%

**Figure 25:** Precision and Recall of the CL model for individual diagnostic classes



As for the AF model, as part of the detailed model evaluation per class, the AutoML platform returned images with false negative and false positive predictions, individually for melanomas and naevi, for the CL model. (Figure 26)



**Figure 26:** Examples of incorrect predictions for melanoma and naevus in CL images

### 6.2.3.2. Internal validation

The evaluation of the two developed models showed for the AF model a precision and recall value of each 85.71% with an AUPRC value of 0.933, and for the CL model, a precision and recall value of each 80.95% with an AUPRC value of 0.928.

The AUPRC values above 0.9 demonstrate that both models are performing well, and individual evaluation proved their readiness to be further tested and used with new unknown datasets.

Internal validation was performed on a second Moorfields (MEH) imaging dataset comprising 104 AF and 104 CL images with 54 melanomas and 50 naevi in each subset.

#### 6.2.3.2.1. AF internal validation

The results of sensitivity, specificity, positive predictive value (PPV), negative predictive value (NPV), F1 score, and accuracy (ACC) for autofluorescence images were 77.78%, 96.00%, 95.45%, 80.00%, 85.71%, and 86.54%, respectively. (Table 22)

From the 104 AF images, 2 naevus labels have been predicted as melanoma (false positives), and 12 melanoma labels have been predicted as naevus (false negatives), with a total of 14 wrong predictions out of 104 images.

AF Internal Validation			
		Ground Truth	
		melanoma	naevus
Model Prediction	melanoma	42	2
	naevus	12	48
Statistical Metrics	Sensitivity	77.78%	
	Specificity	96.00%	
	PPV	95.45%	
	NPV	80.00%	
	F1	85.71%	
	ACC	86.54%	

**Table 22:** Internal validation MEH confusion matrix and statistical parameters for the AF model

### 6.2.3.2.2. CL internal validation

The results of sensitivity, specificity, PPV, NPV, F1 score, and ACC for colour Images were 87.04%, 92.00%, 92.16%, 86.79%, 89.52%, and 89.42%, respectively. (Table 23)

From the 104 CL images, 4 naevus labels have been predicted as melanoma (false positives), whereas 7 melanoma labels have been predicted as naevus (false negatives), with a total of 11 wrong predictions out of 104 images.

CL Internal Validation			
		Ground Truth	
		melanoma	naevus
Model Prediction	melanoma	47	4
	naevus	7	46
Statistical Metrics	Sensitivity	87.04%	
	Specificity	92.00%	
	PPV	92.16%	
	NPV	86.79%	
	F1	89.52%	
	ACC	89.42%	

**Table 23:** Internal validation MEH confusion matrix and statistical parameters for the CL model

## 6.2.4. Discussion

### 6.2.4.1. Summary and discussion of results

The evaluation of the developed AF model showed a precision and recall value of 85.71% each, with an AUPRC/ average precision value of 0.933.

The results for sensitivity, specificity, PPV, NPV, F1 score, and ACC of the AF model imaging test set, were 77.78%, 91.67%, 87.50%, 84.62%, 82.35% and 85.71%, respectively.

The results for sensitivity, specificity, PPV, NPV, F1 score, and ACC of the internal validation where the AF model has been further tested with new unknown autofluorescence images, were 77.78%, 96.00%, 95.45%, 80.00%, 85.71% and 86.54%, respectively. (Table 24)

The evaluation of the developed CL model showed a precision and recall value of 80.95% each, with an AUPRC/ average precision value of 0.928.

The results for sensitivity, specificity, PPV, NPV, F1 score, and ACC of the CL model imaging test set, were 88.89%, 75.00%, 72.73%, 90.00%, 80.00% and 80.95%, respectively.

The results for sensitivity, specificity, PPV, NPV, F1 score, and ACC of the internal validation where the CL model has been further tested with new unknown colour fundus images, were 87.04%, 92.00%, 92.16%, 86.79%, 89.52% and 89.42%, respectively. (Table 24)

Summary of results for model evaluation and internal validation for AF and CL models									
		Ground Truth							
		AF model eval.		AF internal val.		CL model eval.		CL internal val.	
		mel*	naevus	mel*	naevus	mel*	naevus	mel*	naevus
Model Prediction	melanoma	7	1	42	2	8	3	47	4
	naevus	2	11	12	48	1	9	7	46
Statistical Metrics	Sensitivity	77.78%		77.78%		88.89%		87.04%	
	Specificity	91.67%		96.00%		75.00%		92.00%	
	PPV	87.50%		95.45%		72.73%		92.16%	
	NPV	84.62%		80.00%		90.00%		86.79%	
	F1	82.35%		85.71%		80.00%		89.52%	
	ACC	85.71%		86.54%		80.95%		89.42%	
*melanoma									

**Table 24:** Summary of results for model evaluation and internal validation for AF and CL models

The AUPRC values of above 0.9, the results of the individual model evaluation of both models, and the results of the internal validation, proved that both AF and CL models are capable of distinguishing naevi from melanoma based on autofluorescence and colour fundus imaging.

Precision and recall are slightly higher when using AF images (85.71%) compared to CL images (80.95%), leading to the conclusion that the AF model supposedly performs better overall; however, there is still the need to include other model performance and statistical parameters into evaluation.

The high specificity (91.67%) and lower sensitivity (77.78%) of the AF model indicate that the AF model is better at identifying naevi than melanomas in autofluorescence images, and that the CL model with lower specificity (75%) and higher sensitivity (88.89%), is better at identifying melanomas than naevi in colour fundus images. However, the sample size of only 21 images in the test set is very small and therefore, differences are expected.

Both models continued to perform well when presented with unknown images and confirmed the initial good performance and ability to differentiate naevi from melanoma based on the small test set.

The results of the internal validation of the AF model using a bigger sample size of 104 AF images verified the clinical metrics presenting similar values for sensitivity, specificity, F1 score and accuracy, and the model's excellent ability to detect naevi rather than melanoma.

For the CL model, the results of the internal validation using 104 CL images verified the high sensitivity and underlined the model's good performance in detecting melanoma better than the AF model. However, it is interesting to see that the specificity of the internal validation dataset is significantly higher than that of the small test dataset used for model development (92% vs 75%), which also leads to supposedly higher accuracy (89.42% vs 80.95%) and better ability to detect naevus.

Facing this kind of discrepancy could have a variety of causes, such as the small sample size of the initial test dataset, the quality and characteristics of the images used for testing, and also flaws in the model training itself. Further testing and investigations are required, and potentially the need to retrain the model if generalisability cannot be achieved.

Another area of focus is the machine learning algorithm's interpretability and how easy it is for humans to understand the processes the model uses to predict its outcomes. It is important to know which features the model did and did not take into account to decide on a diagnosis. If the model lacks interpretability, it might not be legally permitted to use, particularly in heavily regulated industries such as healthcare.<sup>505</sup>

#### 6.2.4.2. Discussion of methods

Imbalanced data with images not equally distributed across both classes can be a problem when developing a model that is supposed to perform well in detecting both melanoma and naevus. The model will be biased towards the majority class only and won't be successful in the prediction of the minority class, e.g., melanoma. Therefore, it is important to not just rely on a single model performance parameter, such as accuracy, which can be impacted and falsely high. Table 17 displays that there is a slight imbalance between the number of naevus (119) versus melanoma (82) images for both AF and CL models. However, the model's test results and consistently good internal validation performance in detecting melanoma and naevus, represented by various performance parameters, show that our models do not have misleading high model performance values.<sup>506</sup>

Good prediction results can also be impacted by a data sample size that is too small and does not represent a variance that is broad enough. If melanoma prediction of the AF model is considered too low, it could be improved by increasing the number of melanoma images in the training dataset to ensure precise predictions and minimise overfitting. The sample size for our models is relatively small, specifically when evaluating the results of the initial test data consisting of only 21 images. Nevertheless, as a proof of concept and confirmation via internal validation, the models show satisfactory results despite the small data size.<sup>507</sup>

The AF and CL models were trained with a default score threshold of 0.5. This score provides a way to specify the minimum confidence level where a given prediction value should be taken as true. The lower the score threshold, the more images the model will classify, but runs the risk of misclassifying a few images in the process. If the score threshold is high, the model will classify fewer images, but it will have a lower risk of misclassifying images. With a different threshold choice, it is possible to control the number of false positives (FP) versus false negatives (FN), so that either specificity or sensitivity of the test can be improved.<sup>497, 508</sup>

A specific use case of changing the threshold to a higher value could be applied to the developed AF model with an NPV value that shows an 84.62% probability, if the

prediction is negative (naevus), that the patient does have a naevus. However, there is still a 15.38% chance that the patient does have a melanoma. If the NPV is not high enough, there is still a significant risk that the prediction is false negative (naevus) and the patient actually has a melanoma. To reduce the risk of false negatives, the score threshold could be set to a higher value of  $>0.5$  and, therefore, towards a higher confidence level. The result can lead to a higher NPV value and a higher probability of correctly classifying a naevus, resulting in a lower risk of misclassifying melanoma as naevus.

While AutoML provides a user-friendly platform to allow building machine learning systems with minimal knowledge or experience, it is costly, and it would be insightful to explore further binary classification models, developed either bespoke or on other platforms, and subsequently compare their performances to the AutoML models.

It is noteworthy that true colour fundus photographs are often chosen as initial training data for the ML models. With the advent of widefield digital true colour fundus cameras, a single photograph is enough in most cases to capture a choroidal naevus with its associated clinical features in contrast to the other ophthalmic imaging modalities such as OCT and OCTA where often a series of cuts are needed to capture the entire lesion. This allows for easier labelling of the data as well as faster training of the ML model. In addition, training of future ML models can be expanded to include pseudocolour fundus photographs as this carries the potential of providing AI assistance where clinical expertise might be needed the most, such as in optometry offices where pseudocolour fundus photograph cameras are often used for patient screening.<sup>94</sup>

#### **6.2.4.3. Future outlook and how to overcome limitations**

Despite the potential of AI models to diagnose choroidal naevus and predict risk for malignant transformation, challenges remain, including the homogeneity of the training dataset, the potential of DL models to be 'black boxes,' and the use of two-dimensional images that lack stereoscopic qualities.<sup>489</sup> Using fundus photographs



taken with a specific digital fundus camera with a pre-set width of field, image magnification and resolution, and from patients of similar race may induce bias to the results precluding their generalisability and the use of the model in different clinical settings.<sup>470</sup> A technical challenge of reliance solely on fundus photographs arises from their two-dimensional nature. Without stereo fundus photographs or focus differential data, the aspect of ‘thickness’, an important imaging feature found to be a significant predictor for malignant transformation,<sup>65, 68, 72, 406, 489</sup> is greatly diminished. However, AI might detect other features that could serve as a surrogate for thickness.<sup>94</sup>

Guided by the understanding that, based on melanoma size at the time of treatment, smaller melanoma (earlier detection) portends a better life prognosis, this early detection has the potential to save lives.<sup>170, 409, 509</sup>

Furthermore, it needs to be considered that all images in the datasets used for model development and internal validation, have been collected from the same institution where images have been graded with the same grading system and rules (e.g., MOLES), and where also the same imaging modalities (e.g., Optos California [Optos plc, Dunfermline, Scotland]) with consistent settings have been used.

In order to prove the model’s generalisability as a prerequisite that it can be used outside of Moorfields Eye Hospital, there is the need to externally validate the model algorithm and its performance by using multivariable imaging dataset collected from another external institution.

To proactively prevent performance issues of the model and prevent limitations in its application, there are several factors to consider when developing the ML model to be used at large scale, and across institutions and geographies.

When choosing the ideal dataset for the model development, it has to be assured that the ground truth and, therefore, the images grading criteria are comparable. This is most important for correct labelling when creating the training dataset.

Essential questions have to be identified and clarified, such as: what grading system is used, how granular is it, what is the threshold between naevus, suspicious naevi

and melanoma (e.g., what thickness and/or basal diameter), is a specific unit of measure used (e.g., disc diameter), and how are adjudication and arbitration addressed (e.g., two independent graders, approval by a senior grader).

Another area where discrepancies can significantly impact the success of the model development is the difference in either image acquisition or imaging modality. Varying cameras and imaging systems used in individual clinical settings could be a barrier, and a standardised way of capturing images needs to be explored, including the exact imaging modality, the device settings, image resolution, image size parameters and any other imaging features.

Images used for training should be sufficient and balanced with an equal number of images from each class. The dataset should not just be balanced regarding the labels given, but also in the representation of a variety of demographics, so that differences between age, gender, ethnicity, etc., are represented in the training dataset. Organising sufficient data can also be a challenge, considering that ocular tumours are rare compared to conditions such as age-related macular degeneration, diabetic macular oedema or glaucoma.

In general, a pool of data used for model training from individual sources and institutions is desirable and would increase the sensitivity and specificity of the system but also the generalisability of the model. With greater quantity, quality, and diversity of collected data, potential discrepancies in the characteristics of the dataset could be avoided and would prevent that the model overfits on one specific feature of the training data.

One of the future goals is to expand the binary classification model's capability to differentiate indeterminate lesions, and by incorporating mitigations of the outlined challenges, such as ensuring generalisability through external validation, [Figure 27](#) shows an enhanced flow of how to develop, train, validate, test and deploy a potential future AI model.

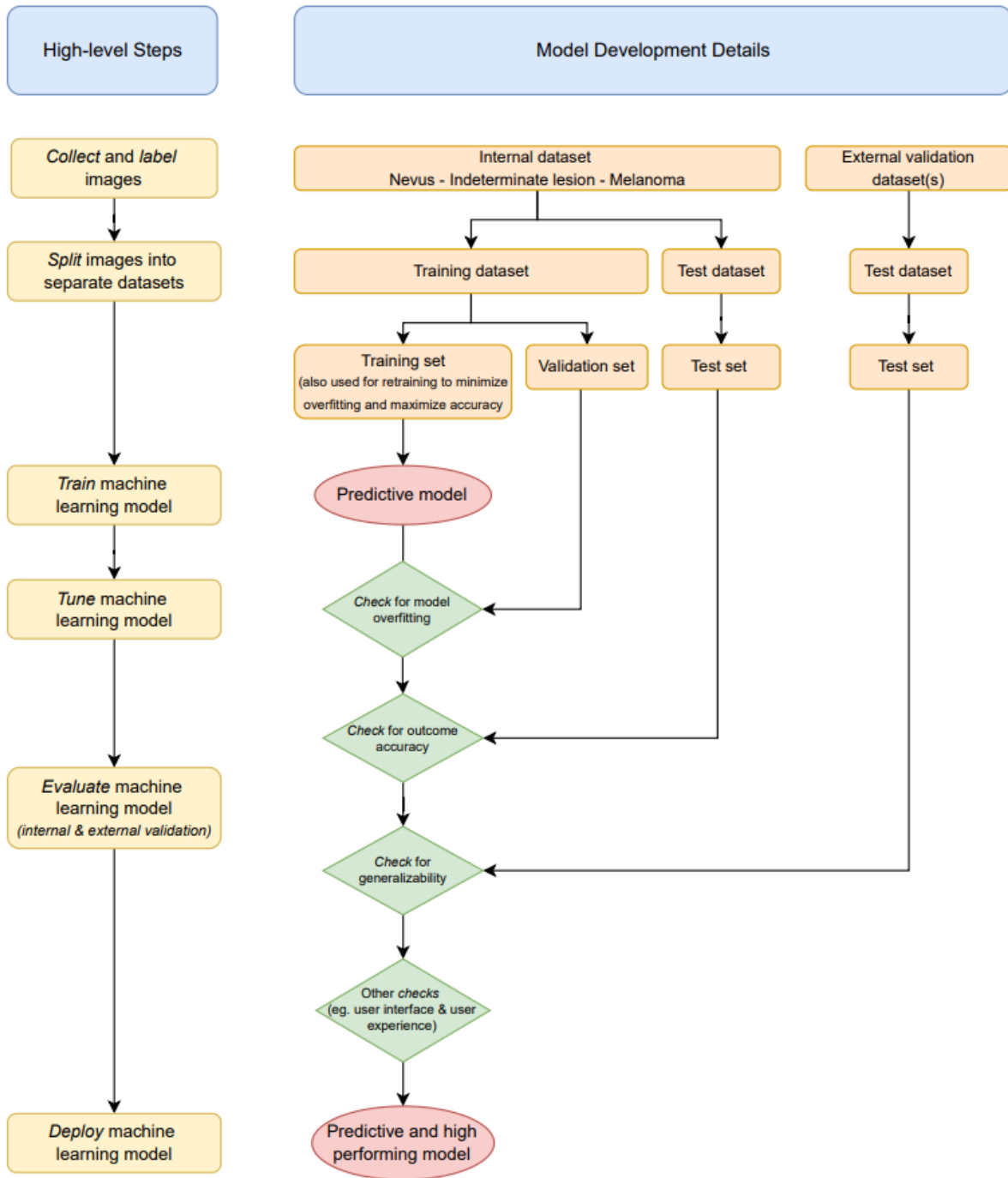


Figure 27: Flowchart depicting the Development of AI models for distinguishing choroidal lesions

### 6.3. General discussion of AI in ocular oncology

#### 6.3.1. Potential benefits of AI

Undoubtedly, AI is a tool with enormous potential. Algorithms can integrate complex information faster and more reproducibly than humans.<sup>510</sup> A big focus of the implementation of AI in the healthcare sector lies in medical imaging, automated clinical decision-making, diagnosis and prognosis.

AI has the potential to improve the current landscape of imaging systems in at least three ways. First, it can help in terms of time efficiency and speed up processes. AI systems can effectively recognise subtleties in visual images that might suggest various disease scenarios in near real-time.<sup>511</sup> Also, applying AI in the hospital and clinical setting will allow physicians more time to focus on doing the tasks that computers cannot do. The healthcare system will become more efficient, and doctors will have more time to take care of patients. Where AI is used for imaging systems, AI-driven image analysis software will allow specialists such as ophthalmologists, who commonly analyse images, to spend less time screening and instead concentrate on diagnosis and decision-making. The same technology will provide non-specialised physicians with digital assistance to interpret medical images, making them less reliant on specialised hospital departments.<sup>512</sup>

Second, AI may help in terms of cost. It is expensive to hire professionals to read medical images, and when having limited resources, it is important to employ them as efficiently as possible. AI can accomplish accurate image analysis in a cost-efficient manner.

The third benefit of AI is diagnostic performance. Numerous studies have revealed evidence that AI can grade images as accurately or potentially even more accurately than professional graders. For example, one criterion for intermediate-stage or moderate non-proliferative diabetic retinopathy can involve counting the number of haemorrhages or other features in the image indicating different stages of the disease.

If a human is conducting this task, it can be very time-consuming and not necessarily more accurate than if a machine does the analysis.<sup>104, 411-415, 468</sup>

Studies have also shown successful results in detecting and differentiating malignancy with high accuracy by using AI for image analysis.<sup>513-515</sup>

Furthermore, by deploying DL methodologies to advance AI-based ophthalmic image analysis, AI may possibly uncover associations between disease and detectable characteristics in the eye that doctors are currently unaware of. By scanning patterns among millions of pixels per image, comprised in datasets of millions of patients, that will never be matched by ophthalmologists, DL will perhaps detect new features outside the well-known risk factors. It might also be capable of correlating to other ophthalmic clinical characteristics and predict the patient's individual risk for certain diseases.<sup>490, 516</sup> AI may not only provide information about the patient's existing disease state but furthermore might present insights into the pathophysiology of diseases through discovering novel features.<sup>410, 510</sup>

### 6.3.2. Key challenges of AI

Like other powerful technologies, AI and ML offer significant benefits and opportunities. To reap their full potential, organisations must mitigate the considerable risks these innovations introduce.<sup>474</sup> Legal issues, data privacy and security concerns are some of the biggest challenges, with a specific caveat when evaluating AI use in healthcare. AI applications with an incorrect algorithm and an ill-defined data governance strategy can cause significant legal challenges for an organisation and its services.

Computing power will also be a challenge. Powerful algorithms utilised for ML and DL methods require an ever-increasing computational power to execute these algorithms successfully. Cloud computing and parallel processing systems allow developers to work with AI systems more efficiently; however, the increase of extraordinary amounts of data, and the development of increasingly complex algorithms, poses a real burden.

Besides, there is limited knowledge and scarcity of field specialists in AI.<sup>517</sup> The development of AI technologies requires specialists who need to undergo a complex and demanding education to acquire the relevant knowledge, represent it, and utilise it appropriately to create models and explain the findings. AI specialists are expensive and desired in many sectors and industries.<sup>416, 494</sup>

Ethical concerns will become apparent as AI can be applied to almost any field in medicine, and its potential contribution to healthcare seems limitless.<sup>518</sup> Scientific and academic institutions play a key role in promoting and supporting ethical AI. Increasing accuracy, minimising bias, maximising generalisability, broadening utility, assuring safety, enhancing transparency, and ensuring accountability are all ethical obligations and are complementary to strive for autonomy, beneficence, and justice.

The culture of medical institutions is often slow to accept change in working practices. Physicians may show concern regarding the loss of jobs as AI becomes more integrated; in one study, 14% were worried about loss of their job and 30% regarding loss of professional skills.<sup>518</sup> Image intensive specialities such as radiology could even be threatened by AI, though the human interpersonal interaction in ophthalmology makes it less vulnerable.<sup>410, 510</sup> The concern that AI could cause ophthalmologists' skills to deteriorate is counterbalanced by the argument that AI is a new way to address the global shortage of healthcare professionals.<sup>510, 519, 520</sup>

Explainability and trust deficit are emerging issues in AI. Over time, humans entrust more decisions to ever more complex computer systems, and there is a tendency to overtrust automated decision-making systems.<sup>521-523</sup>

Some scientists caution that there is a threat in relying on AI systems for explainability and consistency, and unpredictability and variance of outcomes ought to be acknowledged. On the other hand, AI systems are often provided as being 'black boxes' that are difficult to explain. This black box problem presents concerns for users that lack insight into what the AI is in fact doing, and they are worried about basing decisions on information they cannot see. Given how mathematical modelling works

in these AI systems, it is difficult to detect what the decision tree looks like. When a user, such as an ophthalmologist, does not understand that a new feature in the image leads to a clinical diagnosis of choroidal melanoma, they may be sceptical. In an ideal scenario, the ophthalmologist could interrogate the black box and see how AI came to its response, and that access might also provide physicians with information from which they can learn. Due to the inability to interrogate a DL model, some caution should be exercised when making assumptions about a model's generalisability. For example, an algorithm could incorrectly form associations with confounding non-pathological features in an image (such as imaging device, acquisition protocol, or hospital label) simply due to differences in disease prevalence concerning those parameters.<sup>524</sup>

In clinical models, there are some significant risks to be aware of, the foremost being patient safety. An ML algorithm can be likened to a blood laboratory test that predicts a disease, replacing cellular or biochemical data with software. A laboratory investigation has to be tested, validated, and calibrated. The same would be true for a software algorithm.<sup>525</sup>

Explainability is an intensely debated topic, specifically when it comes to the application of AI in healthcare.<sup>526</sup> There are alternative approaches of so-called 'Intelligible Machine Learning', which eliminate some of the downsides of the 'black box'. This refers to systems that are able to describe what they have learned, which would be very significant for AI use in healthcare. If an AI system produces an error, it may be problematic to identify the precise place where the fault occurred within the 'black box' like system. Scientists succeeded in developing methods for 'white box' testing for DL systems.<sup>468</sup> This tests neural networks with a large number of inputs and detects where their responses are incorrect so they can be rectified. Other methods include the generation of saliency maps that help pinpoint which areas in an image the AI focused on in its decision-making process.

Data scarcity and quality are important considerations, as having a sufficient quantity of data is a critical element of AI. Usually, a high number of labelled data, e.g., labelled images, is used to train machines to learn effectively and make accurate predictions.

Several studies have proven that more data leads to better model performance.<sup>104, 527</sup> In the publication by Shields et al., image labelling techniques and various types of AI learning approaches, such as supervised learning and deep learning, are described in detail, with special consideration for choroidal lesions.<sup>94</sup> Different hospitals and services handle tumour samples with various instruments and protocols. Teaching one algorithm to navigate all that variability will be a steep task, and training the AI model with more data from more varied sources is essential for achieving near-perfect reliability.<sup>527</sup> There are further considerations on how the data should be labelled for the AI model to learn and on how to feed acquired knowledge back into the system. To improve the effectiveness and accuracy of the AI model, generating a feedback loop to continuously enhance the model on the basis of people's actions and decisions is an important step.<sup>528</sup>

The need for suitable training data and external verification is a technical challenge that needs to be addressed to facilitate generalisability and translation of AI solutions.<sup>529</sup> A recommendation would consist of categorising the datasets associated with the development of an algorithm into three sets: a training set (for training the algorithm), a validation set (for tuning hyperparameters which are set before the learning process and used to optimise model training), and a test set (for estimating the performance of a final tuned model when comparing it to other final models). It is crucial that the test set contains data independent to training or validation data and is used only for assessing the final model. To define the different types of test sets, the guidance by Altman and Royston can be followed to perform internal validation, temporal validation, and external validation.<sup>530</sup>

AI bias is an irregularity in the output of ML algorithms and may occur due to prejudiced assumptions made during the formation and development of the algorithm or bias in the training data. Literature shows that AI-based systems applied in healthcare have flaws that adversely impact their capability to perform at an expected level. Three parameters can be recognised that result in a bias in the knowledge base of an AI system:<sup>531</sup> (a) Bias due to inaccurate data analysis, (b) Bias due to incorrect information derived from a credible resource and (c) Bias due to experimental design and implementation. AI systems may also contain biases due to cognitive biases and



lack of complete data.<sup>532</sup>

A difficulty with ML models is that there are always imperfections in the dataset used to train the model. Datasets may include or omit certain specifications, with the consequence that the ML model learns based on flawed data, and the output may impact patient safety. Performance on artificial datasets may be different from the real world due to different testing conditions such as lighting, software and imaging variables, as well as patient variables. AI image analysis can be confused by parts of an image that would not influence a human, an unintentional bias. DL systems may draw false conclusions based on information we would not want them to include. The consequence could be a risk to patient safety.

AI is sometimes unintentionally used on a diverse population from the one on which it was trained, and it would be unsuitable for a model to be applied to a population that differs in crucial ways from the learning dataset. The same would be valid for patient demographics. Because AI decisions are a direct reflection of its input data, the data it acquires must have an accurate representation of patient demographics; for example, white males are overly represented in medical datasets.<sup>487</sup> Training on minimal minority data may cause the AI to generate more accurate predictions for majority populations, resulting in unintended poor medical outcomes for minorities.<sup>533-535</sup>

To make an appropriate diagnostic decision for choroidal naevus, indeterminate lesion or a choroidal melanoma based on the pigmentation of the eye, considering the differences in demographics will be significant. Therefore, an AI algorithm trained on images collected from only a specific part of the population may introduce bias, and potentially limit its use for other parts of the population.

Another bias could be introduced by taking images with a particular imaging device using a unique setting, limiting the algorithm's ability to be applied to a broad range of different imaging devices.

There could also be a fear that AI might miss a sign such as a risk factor of malignancy

if it is not looking for it, giving ophthalmologists and patients a false sense of security. Findings from studies comparing performance on internal versus external validation revealed that, as expected, internal validation overestimates diagnostic accuracy in both healthcare professionals and DL algorithms. This finding highlights the need for out-of-sample external validation in all predictive models.<sup>536</sup>

### **6.3.3. Regulatory concerns in US, Europe, and Globally**

In many countries, regulatory approval is required before AI and ML algorithms are allowed to be used for clinical care. This is to limit the potential for harm, ensuring confidentiality and mitigating risks.<sup>486</sup>

#### **6.3.3.1. The U.S. approach**

At the end of 2016, the 21st Century Cures Act<sup>476</sup> defined the scope of FDA regulatory jurisdiction over software use in healthcare, specifying that a medical device is an instrument or other tool intended for use in the diagnosis of disease or other conditions, or in the cure, mitigation, treatment, or prevention of disease, in man or other animals, or intended to affect the structure or any function of the body of man or other animals.<sup>537</sup> Every AI system falling within this definition will be regulated by the FDA, as provided by the Federal Food, Drug and Cosmetic Act.<sup>538</sup> The FDA categorises the medical devices into three classes, according to their uses and risks, and regulates them accordingly where Class III is the category that includes the devices involving the most significant risk. In recent years companies using AI-based clinical support software applications and medical devices, e.g., for analysing computed tomography (CT) angiogram images or diabetic retinopathy screening, requested de novo classification from the FDA. This alternate pathway of FDA regulatory approval applies to novel medical devices whose type the FDA has not previously classified and which allows a more streamlined risk-based classification based on reasonable assurances of safety and efficacy.

The FDA also initiated the Expedited Access Pathway (EAP) and established another category of so-called ‘breakthrough devices’ for medical devices that demonstrate the potential to address unmet medical needs for life-threatening or irreversibly debilitating diseases or conditions. Under the EAP, the FDA works with device sponsors to reduce the time and cost from development to marketing decision.<sup>539</sup>

The black box nature and the rapid growth of AI/ML applications, including the volume and complex nature of testing and verification, are challenging factors for the FDA to approve the numerous new medical devices and algorithms that are continuously being developed. As of September 2021, there are >120 AI/ML-based FDA approved medical devices and algorithms, with the number of approvals constantly increasing and spanning across various medical specialties such as Radiology, Cardiology, and Internal Medicine.<sup>540, 541</sup>

The FDA’s 2021 paper, ‘Artificial Intelligence and Machine Learning (AI/ML) Software as a Medical Device Action Plan’ acknowledged the unique challenges in regulating AI systems and proposed a new regulatory framework in which adaptive algorithms may not need to be reapproved.<sup>476</sup> An initial consultation described the FDA’s foundation for a potential approach to premarket review for AI and ML-driven software modifications. In this approach, the FDA expressed an expectation for transparency and real-world performance monitoring by manufacturers that could enable the FDA and manufacturers to evaluate and monitor a software product from its premarket development through postmarket performance. This framework would enable the FDA to provide a reasonable assurance of safety and effectiveness while embracing the iterative improvement power of AI and ML-based software as a medical device (SaMD). The Action Plan highlights five intended actions and goals including Tailored Regulatory Framework for AI/ML-based SaMD, Good Machine Learning Practice (GMLP), Patient-Centered Approach Incorporating Transparency to Users, Regulatory Science Methods Related to Algorithm Bias & Robustness and Real-World Performance (RWP). The FDA’s vision is that, with appropriately tailored total product lifecycle-based regulatory oversight, AI/ML-based SaMD will deliver safe and effective software functionality that improves the quality of care that patients receive.<sup>476</sup>

The Health Insurance Portability and Accountability Act of 1996 (HIPAA) is another central compliance focus,<sup>542</sup> which defines the use of personally identifiable health information for AI development with the purpose to prevent harms related to privacy and security.<sup>543</sup> The majority of AI systems require extensive datasets for training and validation, and in clinical settings, these usually originate from aggregated personal health information. Re-purposing personal health information for use in establishing an AI system is a secondary use. Many patients are not aware of common secondary uses of their health data and biological material. Consent for data collection does not ensure continuing consent for other purposes.<sup>544</sup> In medicine, healthcare datasets usually are de-identified before being used by developers. Under HIPAA, a dataset where all identifiers have been removed is no longer subject to HIPAA privacy restrictions.<sup>545</sup>

However, this does not universally satisfy the ethical requirement for patient autonomy. Expectations may vary around transparency concerning the uses of de-identified data, along with the ability to agree or disagree on whether or not patient data is included in certain uses. De-identification is not the same as permanent anonymisation. Even when de-identified information within a dataset is not identifiable by a human reader, it might be possible for software to re-identify the underlying individual by cross-referencing against other accessible datasets.<sup>472, 546, 547</sup> Protecting strict patient autonomy for individuals who do not consent to have their personal information used for algorithm development, then, raises considerable technical and practical challenges.<sup>548</sup> The conditions for situations in which the need for patient consent can be waived, require a clear policy at the institutional level and within the healthcare industry. As AI becomes more prevalent in healthcare, questions might arise about when a patient may need to be informed about, and essentially consent to, the use of an AI application in their care.<sup>547</sup> Even though courts have traditionally regarded it as impossible for machines to have legal responsibility, the practicing physician remains liable irrespective of how medical decisions are made. Ultimately, it is the physician who must maintain the ability to choose between a range of competing options, as possibly presented by AI algorithms.<sup>549</sup>

Breaches of privacy typically emerge from unauthorised access to personally

identifiable information (PII), while security describes controls that prevent access by unauthorised individuals. If additionally, protected health information (PHI) is accessed against a person's wish, this can be considered harm in itself. Regarding AI development and utilisation, the most apparent way privacy can be compromised is a breach of a database storing personally identifiable health information. Unfortunately, these are more regular and severe than expected.<sup>550</sup> Privacy can also be compromised because of inadequate de-identification of medical records. That includes fragments of electronic reports and digitised images. Frequently, these datasets are stripped of identifiers before developers can use them, particularly when they are employed in a separate organisation or company.<sup>551</sup>

In 2018, the American Medical Association (AMA) released a policy report on clinical AI. It included the principles that clinical AI should demonstrate best clinical practices, be reproducible and transparent, avoid disparities and bias, and protect patients' privacy.<sup>552</sup>

### **6.3.3.2. The EU and UK approach**

The European Union (EU) is reforming AI regulation in the context of medical device development with new legislation such as the General Data Protection Regulation [GDPR],<sup>542</sup> Cybersecurity Directive, and Medical Devices Regulation/In Vitro Diagnostic Medical Device Regulation. This reform will be realised gradually with the GDPR and the Cybersecurity Directive having taken effect in May 2018.

The General Data Protection Regulation (GDPR) includes a right to an explanation of automated decisions.<sup>553</sup> Article 22(3) GDPR holds that, in certain cases of automated processing, the data controller ought to implement acceptable measures to safeguard the individual's data rights and freedoms and legitimate interests. If AI is used in an organisation, the organisation needs to consider how the GDPR impacts the way data is used by the AI. The implications of understanding this regulation incorrectly can be substantial and result in significant fines.

In July 2016, the EU adopted the 'Cyber Security' Directive on security of network and

information systems (2016/1148) ('NIS Directive'). Digital service providers and companies that operate essential services must protect their information technology systems and inform security incidents to the appropriate regulatory body. It was introduced to provide a coordinated EU-wide response to the increasing threat of cyber-attacks. The NIS Directive requires member States to establish a framework to respond and prevent these attacks.<sup>554</sup>

In the EU and UK, the definition of medical device is provided by Article 1(2) of Directive 93/42/EEC.<sup>542, 555</sup> The European Commission has also published guidelines to interpret requirements set out in the Directive (the MEDDEVs).<sup>556</sup> The MEDDEVs are non-legally binding guidelines to guide stakeholders in complying with legislation related to medical devices.<sup>557</sup>

Depending on its functionality, the term medical device is applied to any instrument or tool, including any kind of software, intended by the manufacturer to be used for human beings for the purpose, among others, of diagnosis, prevention, monitoring, treatment, or alleviation of disease. This definition requires manufacturers to ensure that the devices they produce are fit for their intended purpose.<sup>557-559</sup> This regulatory framework has been reformed by the new Medical Devices Regulation (MDR)<sup>559</sup> and the new In Vitro Diagnostic Medical Device Regulation (IVDR) which both came into force on 25 May 2017.<sup>557</sup>

In the UK, the United Kingdom National Health Service (NHS) has issued a 'Code of Conduct for Data-Driven Health and Care Technologies', of which the principles consist of comprehending persons' needs, distinctly specifying the expected outcomes and benefits, lawful data processing, transparency, and evidence of effectiveness and safety.<sup>556</sup> NHS England's Long Term Plan sets the direction towards widespread digitally enabled care. The Secretary of State's Technology Vision goes on to articulate a clear ambition for the generation of more digital services designed around user need and adhering to key principles of privacy, security, interoperability, and inclusion.<sup>556</sup> The NHS AI Lab aims to bring together policies, partners, and programs to develop and deploy safe, effective artificial intelligence applications.<sup>557</sup>

### 6.3.3.3. WHO guidelines for digital health (A global approach)

In 2019, the World Health Organization (WHO) started developing a framework for the adoption of digital innovations and technology in healthcare. The WHO recommendations on digital interventions in healthcare promotes assessment on the basis of 'benefits, harms, acceptability, feasibility, resource use and equity considerations'.<sup>560</sup> Digital technologies in the healthcare sector are increasingly adopted by the WHO member States, investing in the use of data for decision-making and considering modern solutions to empower their health systems.<sup>561</sup>

The WHO has made a commitment to address ethics, governance and regulation of artificial intelligence for health and in 2019 established an expert group to help develop a global framework for ethics and governance in artificial intelligence. The goal of this initiative is to ensure that these technologies are aligned with the overarching aims of promoting fair and equitable global health, meeting human rights standards and supporting member States' commitments to achieve universal health coverage.<sup>562</sup>

### 6.3.4. Society and patient perspective

AI could potentially play a significant role in supporting the diagnosis and treatment of ocular melanoma, but how do patients perceive the use of AI as part of their healthcare?

A study for skin cancer screening in March 2020,<sup>563</sup> showed that 75% of the patients stated that they would recommend AI to friends and family members, indicating the increased diagnostic speed associated with early skin cancer detection and lifesaving potential. In general, many perceived AI benefits, including the prospect of increased healthcare access also supported by remote diagnosis, reduced healthcare cost, increased triage efficiency, and even unburdening of the healthcare system.

However, 94% of patients in that study expressed the importance of symbiosis between physicians and AI. Some patients pointed out the potential risk of human loss of social interaction, patient loss of privacy, patient loss to follow-up, and nefarious use

of AI and human deskilling. Others also anticipate a lack of verbal and non-verbal communication and emotion. There were concerns about the inability of AI to answer follow-up questions, discuss treatment options, educate and reassure the patient and reduce anxiety.

Another key finding of that study was the split perception concerning the accuracy of diagnosis. While 69% perceived more accurate diagnosis as the greatest strength of AI compared with humans due to the ability of AI to draw on more data or experience than humans, learn, evolve, and share data; 85% perceived less accurate diagnosis as the greatest weakness of AI, based on the potential for false positives and false negatives. Outside the clinical scope, where credibility is crucial to trust the AI, the study also revealed that AI could have the strength to drive patient activation to seek health information and patient education.<sup>563</sup>

Another study from June 2019 examining patients' views of wearable devices and AI in healthcare supports the notion that most patients were ready to accept the use of AI but only under human control and if the integrity of the human physician-patient relationship is preserved.<sup>564</sup>

Though there is some room for extrapolation, additional research specific for AI acceptance by ophthalmic patients is required. At the COOI conference 2020, the impact of ocular melanoma on patients and their families was discussed, realising that there are just a few centres around the world that offer expertise in this rare disease and that there is the need to put more effort into building accessible resources for the greater patient community. The use of AI could be a vital aspect to back the mission of newly established initiatives, to support research and accelerate the development of effective treatments, and ultimately a cure for ocular melanoma through innovative strategies, including international and interdisciplinary collaborations to improve the lives of people affected by ocular melanoma, by creating systems and programs to provide education and support and to advocate for the ocular melanoma community.



### 6.3.5. How to implement AI in ocular oncology

The implementation of AI needs a clear strategy. Initial framing should include intimately understanding the use case, considering potential solutions, and specifying how AI could help develop a real-world solution to the defined problem. It is also essential to gather appropriate knowledge and manage expectations regarding what AI can and cannot yet do for the organisation and their services.

As a fundamental integration challenge, data infrastructure requirements and data storage will need to be considered, along with how the data should be labelled and fed into the system. To develop the effectiveness of the AI model, a strategy needs to be determined on how the model will be trained and tested in the best way.<sup>528</sup> Dataset curation should proceed in a use-case first approach, which aims to match the training data to that encountered in a real-world implementation.

The final model would then need to be integrated into the existing IT infrastructure of the clinic or into the community services to serve as decision support for diagnostic and subsequent referral action.

Workflow integration and user experience are important factors for acceptance. If the AI system is unwieldy to access and not a natural part of the work the ophthalmologist is doing, it will be difficult to adopt and utilise. In addition, workflow integration helps to minimise the cognitive load. For example, if the AI system is presented in the workflow concurrent with the patients' visit, it reduces the additional effort for the ophthalmologist, such as accessing another tool to review the AI's decision and then going back and updating the documentation in the electronic patient record.<sup>525</sup>

The field of 'computer-human interaction' is concerned with how to design interfaces and realise interactions between computers and humans. The computer-human interface can be described as the point of communication between the computer and the human user. The flow of information between the computer and the human is defined as the loop of interaction. Unexpected problems can occur if these interfaces are poorly designed. One of the best practices in many successful AI deployments is

termed 'human-in-the-loop' computing. The AI model takes a first pass on analysing the data, an image or document that needs labelling, and assigns a confidence score on how sure the algorithm is making the appropriate judgment. If the confidence score is lower than an accepted certain value, it circulates the data to a human expert to make a final decision. That new human judgment is used for both the clinical process as well as fed back into the AI algorithm to improve its clinical accuracy. This hybrid approach combines the best of human intelligence and artificial intelligence to create a collective super-intelligence that could enhance applications to work most reliably.<sup>565-567</sup>

Another major question is: how can AI be responsibly applied to ensure that physicians can trust the information presented? One principle is content transparency. To reduce the black box phenomenon and to focus on building trust, the AI algorithm should be as interpretable as possible, so ophthalmologists fundamentally understand how it arrived at a specific diagnostic decision of a choroidal naevus, an indeterminate lesion or a choroidal melanoma. In practice, text displaying the rationale for each decision may be helpful, so the ophthalmologist understands at the time when they are making the final decisions what feature and clinical evidence was found.

Proving value is another step to support trust in the AI system by giving the end-user the opportunity to run a test drive of the product in a sandbox environment before making the decision to use it in the real clinic setting.<sup>525</sup>

The trust deficit can further be managed with thorough education, demonstration, extensive validation, and general communication of the many benefits of AI investment. Applying ML systems to guide users toward clinical decisions could improve quality measures but not automatically reflect improved care. The installation of ML in complex care practices will require ongoing audits of diagnoses to complete cycles of learning to improve diagnostic accuracy. Integrating a unique diagnosis or method of practice into an algorithm too early might indicate authenticity that is not supported by the data.<sup>568</sup>

Clinical validation is hence a key aspect of managing trust in this area. It ensures that

the appropriate clinical evidence is found for every documented diagnosis and also ensures that it was present and treated if it has been documented. When starting to implement the AI system in ophthalmic practice, it would be an option to let the ophthalmologist always make the final medical decision by providing actions to either accept or dismiss an AI decision and give an opportunity to even select a different diagnosis. 'Human-in-the-loop' computing would allow leveraging the advantages of the AI model with an ophthalmology expert at certain checkpoints to fill gaps where the algorithm is not yet confident or where it may fall short due to potential underlying biases.

A cautious approach to applying AI in a real-world clinical setting may prevent a model from being deployed without a full understanding of the risks involved. A bad outcome could significantly set back the entire field. When deploying an AI learning system to distinguish choroidal naevus from choroidal melanoma, it will be important to have substantial monitoring and quality control in place. In this way, potential mistakes or wrong decisions, such as a missed detection of a risk factor of growth, could be recognised quickly and appropriate actions completed to mitigate patient safety risk. Once AI is deployed on a broader scale, there will still be a period where we learn and refine. Updated knowledge in clinical and diagnostic areas could mean that the accuracy of the model can drift, so the algorithm is no longer accurate, which can potentially lead to over- or under-prediction. A reasonable algorithm change control would be required, which ensures validation of its reliability, credibility, and applicability.

## 7. CHAPTER SEVEN: Summary of the Research Conclusions and Recommendations

Pigmented lesion of the fundus is a common condition which can be benign and malignant. The research subjects performed in this PhD thesis should help accomplish an organised approach and an optimal way to differentiate these lesions by using advanced imaging technology and new innovative techniques to diagnose and manage pigmented fundus tumours in different clinical settings in ocular oncology.

A part of this research work seeks to equip community optometrists and general ophthalmologists with a new system to evaluate pigmented fundus lesions. The study '*Distinguishing Choroidal Nevi from Melanomas using the MOLES Algorithm: Evaluation in an Ocular Naevus Clinic*' aimed to determine the sensitivity and specificity of the MOLES scoring system in differentiating choroidal melanomas from naevi according to the five risk factors Mushroom shape, Orange pigment, Large tumour size, Enlarging tumour, and Subretinal fluid (SRF). The results (chapter 3.3) show that when melanocytic choroidal tumours are assessed with the aid of multimodal imaging, such as colour photography, fundus autofluorescence imaging, optical coherence tomography and ultrasonography, the MOLES scores correlate well with the diagnosis made by ocular oncologists at a specialist clinic. Further studies are needed to deploy this system in general ophthalmic clinics and community optometric practices, and evaluate its application by general ophthalmologists and community optometrists as an aid to individualise the management of patients with melanocytic choroidal tumours.

After evaluating the MOLES system for identifying malignancy in melanocytic choroidal tumours in patients treated for choroidal melanoma, overall, the results (chapter 3.5.3) of the related study '*The MOLES system for planning management of melanocytic choroidal tumours: is it safe?*' support the use of the MOLES scoring system as a tool to optimise referral of patients with melanocytic choroidal tumours to ocular oncology centres. The MOLES scoring system is amenable to being used via tele-oncology platforms, where it may have the potential to increase access to sub-

speciality care and early treatment while minimising unnecessary travel to an ocular oncology centre for low-risk lesions. Further study is required to determine the importance of ancillary imaging, such as OCT and AF on the overall MOLES score and recommended management. Finally, the application of the MOLES scoring system by the targeted end-users, such as general ophthalmologists, optometrists and other primary eye care providers, is currently underway to evaluate its external validity.

Furthermore, the related study '*Detecting progression of melanocytic choroidal tumours by sequential imaging: Is ultrasonography necessary?*' determined if ultrasonography is necessary to detect progression of choroidal melanocytic tumours undergoing sequential multimodal imaging with colour photography, autofluorescence (AF) and optical coherence tomography (OCT). In summary, the results (chapter 3.6.3) demonstrate that the majority of melanocytic choroidal tumours can be safely monitored without the need for routine ultrasonography. This insight appears to be particularly true for naevi, categorised as MOLES 1 or 2, of which progression could be detected using colour photography alone in 100% of cases. The sensitivity for detecting subtle progression is further enhanced by incorporating AF and OCT. The findings are particularly relevant in the current climate, where virtual care models are being adopted rapidly because of the COVID-19 pandemic.

Choroidal naevi are a common incidental finding prompting specialist referrals to ocular oncology. Rarely do such lesions have sufficient suspicious features to diagnose a small melanoma. The study '*Prospective Validation of a Virtual Clinic Pathway in the Management of Choroidal Naevi*' aimed to show that 'virtual' imaging-based pathways are a safe and efficient option for managing such referrals.

The clinical evaluation of this research project has led to the validation of a dedicated, 'one-stop' virtual clinic model for the safe management of patients with choroidal naevomelanocytic lesions (CNL) while ensuring an optimal experience of care.

In conclusion, the results (chapter 4.3) show that images of choroidal naevi evaluated remotely using a decision-making process by masked non-medical graders or masked ophthalmologists are feasible and safe. The rate of under-referral was not associated with safety concerns for relevant cases. There was, however, an increased chance of

more frequent follow-up in the context of the 'virtual' service as opposed to the face-to-face service.

This work prospectively validates a virtual naevus clinic model focusing on patient safety as the primary consideration while also highlighting a potential for inefficiency associated with a high rate of over-referrals. Additional review is needed in conjunction with the economic evaluation of this model and any further iteration of the virtual pathways that could improve efficiencies, such as enhanced adjudication and quality review of performance by ocular oncologist specialists.

Following validation for safety and patient satisfaction, the model will be possible to replicate and achieve widespread use within the NHS, especially in the context of large tertiary referral centres receiving a constant flow of referrals with relevant pathology, providing the clear potential to benefit both patients and the public.

Further development of the proposed virtual pathway could embed artificial intelligence decision support systems for image grading and classification to make the process even more effective.

Based on the positive outcome of the prospective validation of a virtual clinic pathway and validation of the MOLES scoring system, the author has designed and adapted this model of a 'Virtual Naevus Clinic' at Moorfields Eye Hospital and proved its feasibility as a response to the COVID-19 pandemic, and with the purpose of reducing in-hospital patient journey times and increasing the capacity of the naevus clinics, while providing safe and efficient clinical care for patients.

The overall experience of implementing and running a virtual model of the naevus clinic at Moorfields Eye Hospital was positive. The capacity of the virtual naevus clinic could be increased from initial 8 patients to 25-30 patients per assessor per session, which is double compared to what the face-to-face clinic can manage.

Initial individual patient feedback was positive, but additional studies, audits, and an economic evaluation are needed to support factual evidence of reduced waiting times in the virtual naevus clinic, and to prove financial savings for patients and the institution.

Patient and staff satisfaction questionnaires to analyse patient and staff acceptability should be undertaken, as well as clinical audits to improve standards in clinical practice. Having robust risk management to efficiently monitor the virtual clinic service and address any potential patient safety risks is essential, as well as ensuring that regular training and continued medical education (CME) sessions are conducted for staff members involved in the diagnostic and management of patients and their conditions.

Finally, the PhD thesis covered a deep discussion of the potential role of artificial intelligence in ocular oncology and its possible use for differentiating benign choroidal naevus from choroidal malignant melanoma.

To overcome the variety of challenges outlined in this thesis, the principal approach of using AI for this purpose should include the utilisation of multimodal imaging, identification of a unique standard that everyone can use, and, most importantly, international collaboration to collect a pool of relevant images from a variety of populations. This may lead to robust algorithms, which could be used in various clinical settings and diverse populations. Consequently, the AI model may then successfully differentiate not only choroidal naevus from choroidal melanoma but also distinguish indeterminate choroidal lesions. Successful implementation could lead to AI being extended to other tumour diagnoses as well as to histopathological evaluations of the specimens generated by ocular oncologists.

The PhD also explored the feasibility of developed automated deep learning models by investigating the performance of these models in diagnosing choroidal naevomelanocytic lesions based on medical imaging, including colour fundus and autofluorescence fundus photographs. This research proved that an, with AutoML developed, automated deep learning algorithm used for binary classification to differentiate choroidal melanomas from choroidal naevi as a differentiation concept is feasible (chapter 6.2.3).

Translating and fine-tuning the use of this model from the differentiation between melanoma and naevi to a refer vs non-refer model, would be most useful to be applied in the community supporting referral decisions.

To further develop this binary classification model, the goal is to expand the model's capability to differentiate indeterminate lesions, which would be most beneficial for supporting the oncologists in their diagnostic decisions.

Finally, automated machine learning with AutoML can be utilised by healthcare professionals with limited coding experience, and in the future, may enable clinician-driven automated discovery of novel insights from image artefacts specific for melanoma or naevi.

Considering the longstanding clinical diagnostic process, the potential that AI and DL can base risk of malignant transformation on non-interpretable computational features<sup>417</sup> might raise trust questions among clinicians that will necessitate resolution before full acceptance of the models. While challenges will need to be addressed, the potential benefits of AI and ML are substantial, especially with continued development of more refined models that ensure a higher confidence in the results.<sup>409</sup>

In ophthalmology and ocular oncology, AI may make fundamental contributions toward the provision of high-quality and sustainable eye care. Nevertheless, challenges also associated with implementing these technologies remain, including validation, trust and patient acceptance, as well as education and training of end-users on these technologies. Ophthalmologists must continue to adapt to the changing models of care delivery and collaborate with broader teams, including technology experts and data scientists, to achieve universal quality and sustainable ophthalmic services.



---

## REFERENCES

1. Gass JD. Focal congenital anomalies of the retinal pigment epithelium. *Eye (Lond)*. 1989;3 ( Pt 1):1-18.
2. Materin M, Singh AD. Benign melanocytic tumors of the uvea. *Clinical Ophthalmic Oncology*: Springer, 2019.
3. Harbour J, Brantley M, Hollingsworth H, Gordon M. Association between posterior uveal melanoma and iris freckles, iris naevi, and choroidal naevi. *British journal of ophthalmology*. 2004;88(1):36-8.
4. Shields CL, Kaliki S, Hutchinson A, et al. Iris nevus growth into melanoma: analysis of 1611 consecutive eyes: the ABCDEF guide. *Ophthalmology*. 2013;120(4):766-72.
5. Rodriguez-Sains RS. Ocular findings in patients with dysplastic nevus syndrome: an update. *Dermatologic clinics*. 1991;9(4):723-8.
6. Toth-Molnar E, Olah J, Dobozy A, Hammer H. Ocular pigmented findings in patients with dysplastic naevus syndrome. *Melanoma Research*. 2004;14(1):43-7.
7. Territo C, Shields CL, Shields JA, et al. Natural course of melanocytic tumors of the iris. *Ophthalmology*. 1988;95(9):1251-5.
8. HALE PN, ALLEN RA, STRAATSMA BR. Benign melanomas (nevi) of the choroid and ciliary body. *Archives of Ophthalmology*. 1965;74(4):532-8.
9. Li B, Sun X, Zheng B, et al. The histogenesis, clinical features and histopathological analysis on 52 cases of ciliary body neoplasms. [*Zhonghua yan ke za Zhi*] *Chinese Journal of Ophthalmology*. 2000;36(4):250-4.
10. Gordon E. Nevus of the choroid and pars plana. Enucleation for suspected malignant melanoma. *Survey of ophthalmology*. 1963;8:507-11.
11. Taban M, Sears JE, Singh AD. Ciliary body naevus. *Eye (Lond)*. 2007;21(12):1528-30.
12. Bajaj MS, Khuraijam N, Sen S, Pushker N. Congenital melanocytoma manifesting as proptosis with multiple cutaneous melanocytic nevi and oculodermal melanosis. *Archives of Ophthalmology*. 2009;127(7):936-45.
13. Bhattacharya S, Girgla H, Singh G. Nevus of Ota. *International Journal of Dermatology*. 1973;12(6):344-7.
14. Kaliki S, Shields C. Uveal melanoma: relatively rare but deadly cancer. *Eye*. 2017;31(2):241-57.
15. Marous CL, Marous MR, Welch RJ, et al. Choroidal melanoma, sector melanocytosis, and retinal pigment epithelial microdetachments in Birt-Hogg-Dube Syndrome. *Retin Cases Brief Rep*. 2019;13(3):202-6.
16. Plateroti AM, Plateroti R, Mollo R, et al. Sturge-Weber Syndrome Associated with Monolateral Ocular Melanocytosis, Iris Mammillations, and Diffuse Choroidal Haemangioma. *Case Rep Ophthalmol*. 2017;8(2):375-84.
17. El Sanharawi M, Sandali O, Naudet F. Ultrasound biomicroscopy of the ciliary body in ocular/oculodermal melanocytosis. *Am J Ophthalmol*. 2013;156(3):627-8.
18. Qian Y, Zakov ZN, Schoenfield L, Singh AD. Iris melanoma arising in iris nevus in oculo (dermal) melanocytosis. *Survey of ophthalmology*. 2008;53(4):411-5.
19. Velazquez-Martin JP, Crema H, Fulda E, et al. Ultrasound biomicroscopy of the ciliary body in ocular/oculodermal melanocytosis. *Am J Ophthalmol*. 2013;155(4):681-7, 7.e1-2.

20. Odashiro M, Odashiro A, Leite L, et al. Melanocytoma of ciliary body and choroids simulating melanoma. *Pathol Res Pract*. 2010;206(2):130-3.
21. Howard GM, Forrest AW. Incidence and location of melanocytomas. *Arch Ophthalmol*. 1967;77(1):61-6.
22. Lee JS, Smith RE, Minckler DS. Scleral melanocytoma. *Ophthalmology*. 1982;89(2):178-82.
23. Verdaguer J, Valenzuela H, Strozzi L. Melanocytoma of the conjunctiva. *Arch Ophthalmol*. 1974;91(5):363-6.
24. Zimmerman LE. MELANOCYTES, MELANOCYTIC NEVI, AND MELANOCYTOMAS. *Invest Ophthalmol*. 1965;4:11-41.
25. LoRusso FJ, Boniuk M, Font RL. Melanocytoma (magnocellular nevus) of the ciliary body: report of 10 cases and review of the literature. *Ophthalmology*. 2000;107(4):795-800.
26. Mohmad Z, Aik Kah T, Chui Yong K, et al. Melanocytoma of the optic nerve head-a diagnostic dilemma. *Clinics and Practice*. 2011;1(3):e60.
27. Reidy JJ, Apple DJ, Steinmetz RL, et al. Melanocytoma: nomenclature, pathogenesis, natural history and treatment. *Surv Ophthalmol*. 1985;29(5):319-27.
28. Shields JA, Demirci H, Mashayekhi A, et al. Melanocytoma of the optic disk: A review. *Indian Journal of Ophthalmology*. 2019;67(12):1949.
29. Roth AM. Malignant change in melanocytomas of the uveal tract. *Surv Ophthalmol*. 1978;22(6):404-12.
30. Brownstein S, Dorey MW, Mathew B, et al. Melanocytoma of the choroid: atypical presentation and review of the literature. *Can J Ophthalmol*. 2002;37(4):247-52.
31. Frangieh GT, el Baba F, Traboulsi EI, Green WR. Melanocytoma of the ciliary body: presentation of four cases and review of nineteen reports. *Surv Ophthalmol*. 1985;29(5):328-34.
32. Lehman LJ, Hohberger GG, Buettner H, Campbell RJ. Necrotic melanocytoma of the choroid in a 2-year-old child. *J Pediatr Ophthalmol Strabismus*. 1997;34(1):40-3.
33. Haas BD, Jakobiec FA, Iwamoto T, et al. Diffuse choroidal melanocytoma in a child. A lesion extending the spectrum of melanocytic hamartomas. *Ophthalmology*. 1986;93(12):1632-8.
34. Shields JA, Font RL. Melanocytoma of the choroid clinically simulating a malignant melanoma. *Arch Ophthalmol*. 1972;87(4):396-400.
35. Kikuchi I, Kase S, Hashimoto Y, et al. Involvement of circulatory disturbance in optic disk melanocytoma with visual dysfunction. *Graefe's Archive for Clinical and Experimental Ophthalmology*. 2019;257(4):835-41.
36. Shields JA, Demirci H, Mashayekhi A, Shields CL. Melanocytoma of optic disc in 115 cases: the 2004 Samuel Johnson Memorial Lecture, part 1. *Ophthalmology*. 2004;111(9):1739-46.
37. Costa J, Vargas E, Mendonça AP, Barbosa MS. Growing optic disc melanocytoma: what to do? *Neuro-Ophthalmology*. 2002;27(1-3):39-43.
38. Shukla SY, Shields JA, Eagle RC, Shields CL. Transformation of optic disc melanocytoma into melanoma over 33 years. *Archives of Ophthalmology*. 2012;130(10):1344-7.
39. Desjardins L. Choroidal nevi. *Journal Francais d'Ophtalmologie*. 2010;33(2):136-41.
40. Johnston MC. A radioautographic study of the migration and fate of cranial neural crest cells in the chick embryo. *Anat Rec*. 1966;156(2):143-55.

41. Factors predictive of growth and treatment of small choroidal melanoma: COMS Report No. 5. The Collaborative Ocular Melanoma Study Group. *Arch Ophthalmol.* 1997;115(12):1537-44.
42. Weiss SJ, Stathopoulos C, Shields CL. Choroidal Nevus with Retinal Invasion in 8 Cases. *Ocul Oncol Pathol.* 2019;5(5):369-78.
43. Jones IS, Reese AB. Benign melanomas of the retinal pigment epithelium. *Am J Ophthalmol.* 1956;42(2):207-12.
44. Jovanovic P, Mihajlovic M, Djordjevic-Jocic J, et al. Ocular melanoma: an overview of the current status. *Int J Clin Exp Pathol.* 2013;6(7):1230-44.
45. Kaiserman I, Kaiserman N, Pe'er J. Long term ultrasonic follow up of choroidal naevi and their transformation to melanomas. *Br J Ophthalmol.* 2006;90(8):994-8.
46. Khan J, Damato BE. Accuracy of choroidal melanoma diagnosis by general ophthalmologists: a prospective study. *Eye (Lond).* 2007;21(5):595-7.
47. Kivela T. Diagnosis of uveal melanoma. *Dev Ophthalmol.* 2012;49:1-15.
48. Kivela T, Eskelin S. Transformation of nevus to melanoma. *Ophthalmology.* 2006;113(5):887-8.e1.
49. Li HK, Shields CL, Mashayekhi A, et al. Giant choroidal nevus clinical features and natural course in 322 cases. *Ophthalmology.* 2010;117(2):324-33.
50. Albertus DL, Schachar IH, Zahid S, et al. Autofluorescence quantification of benign and malignant choroidal nevi/melanocytic tumors. *JAMA Ophthalmol.* 2013;131(8):1004-8.
51. Aleksidze N, Medina CA, Singh AD. De novo Evolution of a Small Choroidal Melanoma. *Ocul Oncol Pathol.* 2015;1(2):83-7.
52. Augsburger JJ, Correa ZM, Trichopoulos N, Shaikh A. Size overlap between benign melanocytic choroidal nevi and choroidal malignant melanomas. *Invest Ophthalmol Vis Sci.* 2008;49(7):2823-8.
53. Balaskas K, Gray J, Blows P, et al. Management of choroidal naevomelanocytic lesions: feasibility and safety of a virtual clinic model. *Br J Ophthalmol.* 2016;100(5):665-70.
54. Butler P, Char DH, Zarbin M, Kroll S. Natural history of indeterminate pigmented choroidal tumors. *Ophthalmology.* 1994;101(4):710-6; discussion 7.
55. Chien JL, Sioufi K, Surakiatchanukul T, et al. Choroidal nevus: a review of prevalence, features, genetics, risks, and outcomes. *Curr Opin Ophthalmol.* 2017;28(3):228-37.
56. Doro D, Kotsafti O, Cimatti P. Long-term echographic surveillance of elevated choroidal nevi. *Am J Ophthalmol.* 2013;156(3):438-43.e1.
57. Ghassemi F, Mirshahi R, Fadakar K, Sabour S. Optical coherence tomography angiography in choroidal melanoma and nevus. *Clin Ophthalmol.* 2018;12:207-14.
58. Gonder JR, Augsburger JJ, McCarthy EF, Shields JA. Visual loss associated with choroidal nevi. *Ophthalmology.* 1982;89(8):961-5.
59. Harbour JW, Paez-Escamilla M, Cai L, et al. Are Risk Factors for Growth of Choroidal Nevi Associated With Malignant Transformation? Assessment With a Validated Genomic Biomarker. *Am J Ophthalmol.* 2019;197:168-79.
60. Mashayekhi A, Siu S, Shields CL, Shields JA. Slow enlargement of choroidal nevi: a long-term follow-up study. *Ophthalmology.* 2011;118(2):382-8.
61. Mims JL, 3rd, Shields JA. Follow-up studies of suspicious choroidal nevi. *Ophthalmology.* 1978;85(9):929-43.
62. Parikh R, Gal-Or O, Sakurada Y, et al. Documentation of a new choroidal nevus. *Retin Cases Brief Rep.* 2018.

63. Qiu M, Shields CL. Choroidal Nevus in the United States Adult Population: Racial Disparities and Associated Factors in the National Health and Nutrition Examination Survey. *Ophthalmology*. 2015;122(10):2071-83.
64. Say EA, Shah SU, Ferenczy S, Shields CL. Optical coherence tomography of retinal and choroidal tumors. *J Ophthalmol*. 2012;2012:385058.
65. Shields CL, Dalvin LA, Ancona-Lezama D, et al. Choroidal nevus imaging features in 3,806 cases and risk factors for transformation into melanoma in 2,355 cases: The 2020 Taylor R. Smith and Victor T. Curtin Lecture. *Retina*. 2019;39(10):1840-51.
66. Shields CL, Dalvin LA, Ancona-Lezama D, et al. CHOROIDAL NEVUS IMAGING FEATURES IN 3,806 CASES AND RISK FACTORS FOR TRANSFORMATION INTO MELANOMA IN 2,355 CASES: The 2020 Taylor R. Smith and Victor T. Curtin Lecture. *Retina*. 2019;39(10):1840-51.
67. Shields CL, Dalvin LA, Ancona-Lezama D, et al. CHOROIDAL NEVUS IMAGING FEATURES IN 3,806 CASES AND RISK FACTORS FOR TRANSFORMATION INTO MELANOMA IN 2,355 CASES: The 2020 Taylor R. Smith and Victor T. Curtin Lecture. *Retina*. 2018.
68. Shields CL, Furuta M, Berman EL, et al. Choroidal nevus transformation into melanoma: analysis of 2514 consecutive cases. *Arch Ophthalmol*. 2009;127(8):981-7.
69. Shields CL, Furuta M, Mashayekhi A, et al. Clinical spectrum of choroidal nevi based on age at presentation in 3422 consecutive eyes. *Ophthalmology*. 2008;115(3):546-52.e2.
70. Shields CL, Furuta M, Mashayekhi A, et al. Visual acuity in 3422 consecutive eyes with choroidal nevus. *Arch Ophthalmol*. 2007;125(11):1501-7.
71. Shields CL, Kaliki S, Rojanaporn D, et al. Enhanced depth imaging optical coherence tomography of small choroidal melanoma: comparison with choroidal nevus. *Arch Ophthalmol*. 2012;130(7):850-6.
72. Shields CL, Lim LS, Dalvin LA, Shields JA. Small choroidal melanoma: detection with multimodal imaging and management with plaque radiotherapy or AU-011 nanoparticle therapy. *Curr Opin Ophthalmol*. 2019;30(3):206-14.
73. Shields CL, Pirondini C, Bianciotto C, et al. Autofluorescence of choroidal nevus in 64 cases. *Retina*. 2008;28(8):1035-43.
74. Shields CL, Shields JA, Kiratli H, et al. Risk factors for growth and metastasis of small choroidal melanocytic lesions. *Ophthalmology*. 1995;102(9):1351-61.
75. Singh AD, Kalyani P, Topham A. Estimating the risk of malignant transformation of a choroidal nevus. *Ophthalmology*. 2005;112(10):1784-9.
76. Singh AD, Mokashi AA, Bena JF, et al. Small choroidal melanocytic lesions: features predictive of growth. *Ophthalmology*. 2006;113(6):1032-9.
77. Sumich P, Mitchell P, Wang JJ. Choroidal nevi in a white population: the Blue Mountains Eye Study. *Arch Ophthalmol*. 1998;116(5):645-50.
78. Thiagalingam S, Wang JJ, Mitchell P. Absence of change in choroidal nevi across 5 years in an older population. *Arch Ophthalmol*. 2004;122(1):89-93.
79. Al Harby L, Sagoo MS, O'Day R, et al. Distinguishing Choroidal Nevi from Melanomas using the MOLES Algorithm: Evaluation in an Ocular Nevus Clinic. *Ocular Oncology and Pathology*. 2021.
80. Chiang A, Bianciotto C, Maguire JL, et al. Intravitreal bevacizumab for choroidal neovascularization associated with choroidal nevus. *Retina*. 2012;32(1):60-7.

81. Kernt M, Schaller UC, Stumpf C, et al. Choroidal pigmented lesions imaged by ultra-wide-field scanning laser ophthalmoscopy with two laser wavelengths (Optomap). *Clin Ophthalmol*. 2010;4:829-36.
82. Jonna G, Daniels AB. Enhanced Depth Imaging OCT of Ultrasonographically Flat Choroidal Nevi Demonstrates 5 Distinct Patterns. *Ophthalmol Retina*. 2019;3(3):270-7.
83. Ramírez-Neria P. Congenital choroidal nevus in a two-month-old infant. *EC Ophthalmology*. 2019;10:511-4.
84. Ganley JP, Comstock GW. Benign nevi and malignant melanomas of the choroid. *Am J Ophthalmol*. 1973;76(1):19-25.
85. Raval V, Bellerive C, Singh AD, et al. Choroidal nevi in children: prevalence, age of onset, and progression. *Journal of American Association for Pediatric Ophthalmology and Strabismus*. 2021;25(4):225. e1- e6.
86. Roelofs KA, O'Day R, Al Harby L, et al. Detecting Progression of Melanocytic Choroidal Tumors by Sequential Imaging: Is Ultrasonography Necessary? *Cancers (Basel)*. 2020;12(7).
87. Shah SU, Kaliki S, Shields CL, et al. Enhanced depth imaging optical coherence tomography of choroidal nevus in 104 cases. *Ophthalmology*. 2012;119(5):1066-72.
88. Parodi MB. Transpupillary thermotherapy for subfoveal choroidal neovascularization associated with choroidal nevus. *Am J Ophthalmol*. 2004;138(6):1074-5.
89. Shields CL, Maktabi AM, Jahnle E, et al. Halo nevus of the choroid in 150 patients: the 2010 Henry van Dyke Lecture. *Arch Ophthalmol*. 2010;128(7):859-64.
90. Smith JH, Padnick-Silver L, Newlin A, et al. Genetic study of familial uveal melanoma: association of uveal and cutaneous melanoma with cutaneous and ocular nevi. *Ophthalmology*. 2007;114(4):774-9.
91. Fournier GA, Albert DM, Wagoner MD. Choroidal halo nevus occurring in a patient with vitiligo. *Survey of ophthalmology*. 1984;28(6):671-2.
92. Ng SR, Zhao W, Mitchell P, et al. Choroidal nevi in the Singapore epidemiology of eye disease study. *Ophthalmology*. 2018;125(5):784-6.
93. Levecq L, De Potter P, Guagnini A. Epidemiology of ocular and orbital lesions referred to an ocular oncology center. *Journal Francais D'ophtalmologie*. 2005;28(8):840-4.
94. Shields CL, Lally SE, Dalvin LA, et al. White Paper on Ophthalmic Imaging for Choroidal Nevus Identification and Transformation into Melanoma. *Translational Vision Science & Technology*. 2021;10(2):24-.
95. Al Harby L, Ali Z, Rajai A, et al. Prospective validation of a virtual clinic pathway in the management of choroidal naevi: the NAEVUS study Report no. 1: safety assessment. *Br J Ophthalmol*. 2020.
96. Nagiel A, Lalane RA, Sadda SR, Schwartz SD. Ultra-widefield fundus imaging: a review of clinical applications and future trends. *Retina*. 2016;36(4):660-78.
97. <https://www.optomap.com/optomap-screening/>. Why optomap ultra-widefield retinal imaging?
98. Almeida A, Kaliki S, Shields CL. Autofluorescence of intraocular tumours. *Current opinion in ophthalmology*. 2013;24(3):222-32.
99. Reznicek L, Stumpf C, Seidensticker F, et al. Role of wide-field autofluorescence imaging and scanning laser ophthalmoscopy in differentiation of choroidal pigmented lesions. *International journal of ophthalmology*. 2014;7(4):697.
100. Foster FS, Pavlin CJ, Harasiewicz KA, et al. Advances in ultrasound biomicroscopy. *Ultrasound in medicine & biology*. 2000;26(1):1-27.

101. Pavlin CJ, Harasiewicz K, Sherar MD, Foster FS. Clinical use of ultrasound biomicroscopy. *Ophthalmology*. 1991;98(3):287-95.
102. Wang ZY, Yang WL, Li DJ, et al. [Ultrasound diagnosis and differential diagnosis of medium and small choroidal melanomas]. *Zhonghua Yan Ke Za Zhi*. 2018;54(11):843-8.
103. Daftari I, Barash D, Lin S, O'Brien J. Use of high-frequency ultrasound imaging to improve delineation of anterior uveal melanoma for proton irradiation. *Phys Med Biol*. 2001;46(2):579-90.
104. Mursch-Edlmayr AS, Ng WS, Diniz-Filho A, et al. Artificial Intelligence Algorithms to Diagnose Glaucoma and Detect Glaucoma Progression: Translation to Clinical Practice. *Transl Vis Sci Technol*. 2020;9(2):55.
105. Shields CL, Mashayekhi A, Materin MA, et al. Optical coherence tomography of choroidal nevus in 120 patients. *Retina*. 2005;25(3):243-52.
106. Dolz-Marco R, Hasanreisoglu M, Shields JA, Shields CL. Posterior scleral bowing with choroidal nevus on enhanced-depth imaging optical coherence tomography. *JAMA Ophthalmol*. 2015;133(10):1165-70.
107. Welch RJ, Newman JH, Honig SE, et al. Choroidal amelanotic tumours: clinical differentiation of benign from malignant lesions in 5586 cases. *Br J Ophthalmol*. 2020;104(2):194-201.
108. Dalvin LA, Lim LS, Chang M, et al. Circumscribed choroidal hemangioma: Clinical features and outcomes by age category in 458 cases. *Saudi J Ophthalmol*. 2019;33(3):219-28.
109. Di Nicola M, Williams BK, Jr., Hua J, et al. Photodynamic Therapy (PDT) for Retinal Hemangioblastoma: Treatment Outcomes in 17 Consecutive Patients. *Ophthalmol Retina*. 2021.
110. Garcia-Arumi J, Amselem L, Gunduz K, et al. Photodynamic therapy for symptomatic subretinal fluid related to choroidal nevus. *Retina*. 2012;32(5):936-41.
111. Fabian ID, Stacey AW, Harby LA, et al. Primary photodynamic therapy with verteporfin for pigmented posterior pole cT1a choroidal melanoma: a 3-year retrospective analysis. *Br J Ophthalmol*. 2018;102(12):1705-10.
112. Fabian ID, Stacey AW, Papastefanou V, et al. Primary photodynamic therapy with verteporfin for small pigmented posterior pole choroidal melanoma. *Eye (Lond)*. 2017;31(4):519-28.
113. Shields CL, Cater J, Shields JA, et al. Combination of clinical factors predictive of growth of small choroidal melanocytic tumors. *Arch Ophthalmol*. 2000;118(3):360-4.
114. Shields JA, Shields CL, Shah PG, et al. Lack of association among typical congenital hypertrophy of the retinal pigment epithelium, adenomatous polyposis, and Gardner syndrome. *Ophthalmology*. 1992;99(11):1709-13.
115. Chen CS, Phillips KD, Grist S, et al. Congenital hypertrophy of the retinal pigment epithelium (CHRPE) in familial colorectal cancer. *Familial cancer*. 2006;5(4):397-404.
116. Buettner H. Congenital hypertrophy of the retinal pigment epithelium. *American journal of ophthalmology*. 1975;79(2):177-89.
117. Gass JD. An unusual hamartoma of the pigment epithelium and retina simulating choroidal melanoma and retinoblastoma. *Trans Am Ophthalmol Soc*. 1973;71:171-83; discussions 84-5.
118. Firestone BK, Arias JD, Shields CL, Shields JA. Bilateral Combined Hamartomas of the Retina and Retinal Pigment Epithelium as the Presenting Feature of Neurofibromatosis Type 2 (Wishart Type). *J Pediatr Ophthalmol Strabismus*. 2014;51 Online:e33-6.

119. Kang HM, Koh HJ, Chung EJ. Spectral-domain optical coherence tomography of combined hamartoma of the retina and retinal pigment epithelium in neurofibromatosis. *Korean J Ophthalmol*. 2013;27(1):68-71.
120. Sivalingam A, Augsburger J, Perilongo G, et al. Combined hamartoma of the retina and retinal pigment epithelium in a patient with neurofibromatosis type 2. *J Pediatr Ophthalmol Strabismus*. 1991;28(6):320-2.
121. Rishi P, Hirawat RS, Verma A. Association of bilateral, multiple presumed retinal astrocytic proliferations with combined hamartoma of retina and retinal pigment epithelium in a 9-year-old male child with neurofibromatosis type 2. *Indian J Ophthalmol*. 2016;64(11):850-2.
122. Laqua H. Tumors and tumor-like lesions of the retinal pigment epithelium. *Ophthalmologica*. 1981;183(1):34-8.
123. Shields CL, Shields JA, Marr BP, et al. Congenital simple hamartoma of the retinal pigment epithelium: a study of five cases. *Ophthalmology*. 2003;110(5):1005-11.
124. Shields JA, Shields CL, Gunduz K, Eagle RC, Jr. Adenoma of the ciliary body pigment epithelium: the 1998 Albert Ruedemann, Sr, memorial lecture, Part 1. *Arch Ophthalmol*. 1999;117(5):592-7.
125. Shields CL, Shields JA, Shields MB, Augsburger JJ. Prevalence and mechanisms of secondary intraocular pressure elevation in eyes with intraocular tumors. *Ophthalmology*. 1987;94(7):839-46.
126. Bellerive C, Biscotti CV, Singh N, Singh AD. Fine-needle aspiration biopsy for suspected uveal metastases. *Can J Ophthalmol*. 2019;54(6):694-8.
127. Shields JA, Shields CL. Surgical approach to lamellar sclerouvectomy for posterior uveal melanomas: the 1986 Schoenberg lecture. *Ophthalmic Surg*. 1988;19(11):774-80.
128. Chang AE, Karnell LH, Menck HR. The National Cancer Data Base report on cutaneous and noncutaneous melanoma: a summary of 84,836 cases from the past decade. The American College of Surgeons Commission on Cancer and the American Cancer Society. *Cancer*. 1998;83(8):1664-78.
129. Gündüz K, Pulido JS, Pulido JE, Link T. Correlation of fundus autofluorescence with fluorescein and indocyanine green angiography in choroidal melanocytic lesions. *Retina*. 2008;28(9):1257-64.
130. Singh N, Bergman L, Seregard S, Singh AD. Uveal melanoma: epidemiologic aspects. *Clinical Ophthalmic Oncology*. 2014:75-87.
131. Margo CE, McLean IW. Malignant melanoma of the choroid and ciliary body in black patients. *Arch Ophthalmol*. 1984;102(1):77-9.
132. Salvi SM, Singh AD. Diagnostic and Management Challenges of Ciliary Body Tumor in an African-American Patient. *Ocul Oncol Pathol*. 2015;2(1):16-9.
133. Singh AD, Bergman L, Seregard S. Uveal melanoma: epidemiologic aspects. *Ophthalmol Clin North Am*. 2005;18(1):75-84, viii.
134. Singh AD, Bergman L, Seregard S. Uveal malignant melanoma: epidemiologic aspects. *Essentials of ophthalmic oncology*. 2009:78.
135. Damato B, Lecuona K. Conservation of eyes with choroidal melanoma by a multimodality approach to treatment: an audit of 1632 patients. *Ophthalmology*. 2004;111(5):977-83.
136. Singh AD, Topham A. Survival rates with uveal melanoma in the United States: 1973-1997. *Ophthalmology*. 2003;110(5):962-5.
137. Strickland D, Lee JA. Melanomas of eye: stability of rates. *Am J Epidemiol*. 1981;113(6):700-2.

138. Singh AD, Shields CL, Shields JA, De Potter P. Bilateral primary uveal melanoma. Bad luck or bad genes? *Ophthalmology*. 1996;103(2):256-62.
139. Canning C, Hungerford J. Familial uveal melanoma. *British journal of ophthalmology*. 1988;72(4):241-3.
140. Singh AD, Shields CL, Shields JA, Sato T. Uveal melanoma in young patients. *Arch Ophthalmol*. 2000;118(7):918-23.
141. Greer CH. Congenital melanoma of the anterior uvea. *Arch Ophthalmol*. 1966;76(1):77-8.
142. Harbour JW, Onken MD, Roberson ED, et al. Frequent mutation of BAP1 in metastasizing uveal melanomas. *Science*. 2010;330(6009):1410-3.
143. Matatall KA, Agapova OA, Onken MD, et al. BAP1 deficiency causes loss of melanocytic cell identity in uveal melanoma. *BMC Cancer*. 2013;13:371.
144. Chau C, van Doorn R, van Poppel NM, et al. Families with BAP1-Tumor Predisposition Syndrome in The Netherlands: Path to Identification and a Proposal for Genetic Screening Guidelines. *Cancers (Basel)*. 2019;11(8).
145. Yanoff M, Zimmerman LE. Histogenesis of malignant melanomas of the uvea. 3. The relationship of congenital ocular melanocytosis and neurofibromatosis in uveal melanomas. *Arch Ophthalmol*. 1967;77(3):331-6.
146. Brihaye-Van G. Contribution to the study of melanotic tumors of the uvea and their origin. *Doc Ophthalmol*. 1963;17:163-248.
147. Jensen OA. Malignant melanomas of the human uvea. Recent follow-up of cases in Denmark, 1943-1952. *Acta Ophthalmol (Copenh)*. 1970;48(6):1113-28.
148. Honavar SG, Singh AD, Shields CL, et al. Iris melanoma in a patient with neurofibromatosis. *Surv Ophthalmol*. 2000;45(3):231-6.
149. Rootman J, Gallagher RP. Color as a risk factor in iris melanoma. *American journal of ophthalmology*. 1984;98(5):558-61.
150. Holly EA, Aston DA, Char DH, et al. Uveal melanoma in relation to ultraviolet light exposure and host factors. *Cancer research*. 1990;50(18):5773-7.
151. Regan S, Judge HE, Gragoudas ES, Egan KM. Iris color as a prognostic factor in ocular melanoma. *Archives of ophthalmology*. 1999;117(6):811-4.
152. Demirci H, Shields CL, Shields JA, et al. Diffuse iris melanoma: a report of 25 cases. *Ophthalmology*. 2002;109(8):1553-60.
153. Khan S, Finger PT, Yu GP, et al. Clinical and pathologic characteristics of biopsy-proven iris melanoma: a multicenter international study. *Arch Ophthalmol*. 2012;130(1):57-64.
154. Shields CL, Di Nicola M, Bekerman VP, et al. Iris Melanoma Outcomes Based on the American Joint Committee on Cancer Classification (Eighth Edition) in 432 Patients. *Ophthalmology*. 2018;125(6):913-23.
155. Hu D-N, Yu G-P, McCormick SA, et al. Population-based incidence of uveal melanoma in various races and ethnic groups. *American journal of ophthalmology*. 2005;140(4):612. e1- e8.
156. Hawkins BS. The Collaborative Ocular Melanoma Study (COMS) randomized trial of pre-enucleation radiation of large choroidal melanoma: IV. Ten-year mortality findings and prognostic factors. COMS report number 24. *American journal of ophthalmology*. 2004;138(6):936-51.
157. Maheshwari A, Finger PT. Cancers of the eye. *Cancer Metastasis Rev*. 2018;37(4):677-90.
158. Jager MJ, Shields CL, Cebulla CM, et al. Uveal melanoma. *Nat Rev Dis Primers*. 2020;6(1):24.



159. Kivelä T, Simpson E, Grossniklaus H. Uveal melanoma, 8th ed. New York, NY: Springer, 2017.
160. Sagoo MS, Filipovic A, Al Harby L, Stebbing J. Rare tumors: an eye on the future. *Future Oncol*. 2015.
161. Holly EA, Aston DA, Ahn DK, et al. Uveal melanoma, hormonal and reproductive factors in women. *Cancer research*. 1991;51(5):1370-2.
162. Singh AD, Rennie IG, Seregard S, et al. Sunlight exposure and pathogenesis of uveal melanoma. *Survey of ophthalmology*. 2004;49(4):419-28.
163. Mallet JD, Gendron SP, Drigeard Desgarnier MC, Rochette PJ. Implication of ultraviolet light in the etiology of uveal melanoma: A review. *Photochem Photobiol*. 2014;90(1):15-21.
164. Shields CL, Shields JA, Milite J, et al. Uveal melanoma in teenagers and children: a report of 40 cases. *Ophthalmology*. 1991;98(11):1662-6.
165. Averbook BJ, Lee SJ, Delman KA, et al. Pediatric melanoma: analysis of an international registry. *Cancer*. 2013;119(22):4012-9.
166. Al-Jamal RT, Cassoux N, Desjardins L, et al. The Pediatric Choroidal and Ciliary Body Melanoma Study: A Survey by the European Ophthalmic Oncology Group. *Ophthalmology*. 2016;123(4):898-907.
167. Palazzi MA, Ober MD, Abreu HF, et al. Congenital uveal malignant melanoma: a case report. *Canadian journal of ophthalmology*. 2005;40(5):611-5.
168. Posnick JC, Chen P, Zuker R, et al. Extensive malignant melanoma of the uvea in childhood: resection and immediate reconstruction with microsurgical and craniofacial techniques. *Annals of plastic surgery*. 1993;31(3):265-70.
169. Grabowska A, Abelairas J, Peralta J, et al. Uveal melanoma in a 19-month-old child. *Journal of American Association for Pediatric Ophthalmology and Strabismus*. 2011;15(6):606-8.
170. Shields CL, Furuta M, Thangappan A, et al. Metastasis of uveal melanoma millimeter-by-millimeter in 8033 consecutive eyes. *Arch Ophthalmol*. 2009;127(8):989-98.
171. Shields CL, Kaliki S, Furuta M, et al. Clinical spectrum and prognosis of uveal melanoma based on age at presentation in 8,033 cases. *Retina*. 2012;32(7):1363-72.
172. Shields CL, Kaliki S, Shah SU, et al. Iris melanoma: features and prognosis in 317 children and adults. *Journal of American Association for Pediatric Ophthalmology and Strabismus*. 2012;16(1):10-6.
173. Shields CL, Markowitz JS, Belinsky I, et al. Conjunctival melanoma: outcomes based on tumor origin in 382 consecutive cases. *Ophthalmology*. 2011;118(2):389-95. e2.
174. Shields CL, Shields JA, Materin M, et al. Iris melanoma: risk factors for metastasis in 169 consecutive patients. *Ophthalmology*. 2001;108(1):172-8.
175. Marigo FA, Finger PT, McCormick SA, et al. Iris and ciliary body melanomas: ultrasound biomicroscopy with histopathologic correlation. *Archives of Ophthalmology*. 2000;118(11):1515-21.
176. Relimpio-López MI, Garrido-Hermosilla AM. Intravitreal air bubble during exoresection of an iris-ciliary body melanoma. *Surg Oncol*. 2019;29:157-8.
177. Shamma HF, Blodi FC. Prognostic factors in choroidal and ciliary body melanomas. *Archives of ophthalmology*. 1977;95(1):63-9.
178. Demirci H, Shields CL, Shields JA, et al. CME ring melanoma of the ciliary body: report on twenty-three patients. *Retina*. 2002;22(6):698-706.

179. Xu TT, Pulido JS, Deufel CL, et al. Clinical outcomes of Modified Collaborative Ocular Melanoma Study IRIS plaques for treatment of iris, iridociliary, and ciliary body melanoma. *Eye (Lond)*. 2021;35(10):2754-62.
180. Accuracy of diagnosis of choroidal melanomas in the Collaborative Ocular Melanoma Study. COMS report no. 1. *Arch Ophthalmol*. 1990;108(9):1268-73.
181. Shields CL, Lim L-AS, Dalvin LA, Shields JA. Small choroidal melanoma: detection with multimodal imaging and management with plaque radiotherapy or AU-011 nanoparticle therapy. *Current opinion in ophthalmology*. 2019;30(3):206-14.
182. Raja MS, Goldsmith C, Burton BJ. Management of small choroidal melanocytic tumour. *Br J Ophthalmol*. 2013;97(2):241.
183. Gass JD. Problems in the differential diagnosis of choroidal nevi and malignant melanomas. The XXXIII Edward Jackson Memorial Lecture. *Am J Ophthalmol*. 1977;83(3):299-323.
184. Eskelin S, Pyrhönen S, Summanen P, et al. Screening for metastatic malignant melanoma of the uvea revisited. *Cancer*. 1999;85(5):1151-9.
185. Diener-West M, Reynolds SM, Agugliaro DJ, et al. Development of metastatic disease after enrollment in the COMS trials for treatment of choroidal melanoma: Collaborative Ocular Melanoma Study Group Report No. 26. *Arch Ophthalmol*. 2005;123(12):1639-43.
186. Shields CL, Sioufi K, Srinivasan A, et al. Visual Outcome and Millimeter Incremental Risk of Metastasis in 1780 Patients With Small Choroidal Melanoma Managed by Plaque Radiotherapy. *JAMA Ophthalmol*. 2018.
187. Papastefanou VP, Al-Jamal RaT, Ali ZC, et al. Ultra-wide-field imaging assessment of small choroidal pigmented lesions using red and green colour channels. *Eye*. 2021;35(1):282-8.
188. Callaway NF, Mruthyunjaya P. Widefield imaging of retinal and choroidal tumors. *International Journal of Retina and Vitreous*. 2019;5(1):1-10.
189. Folberg R. Tumor progression in ocular melanomas. *J Invest Dermatol*. 1993;100(3):326s-31s.
190. Shields CL, Manalac J, Das C, et al. Choroidal melanoma: clinical features, classification, and top 10 pseudomelanomas. *Curr Opin Ophthalmol*. 2014;25(3):177-85.
191. Lee DS, Anderson SF, Perez EM, Townsend JC. Amelanotic choroidal nevus and melanoma: cytology, tumor size, and pigmentation as prognostic indicators. *Optometry and vision science*. 2001;78(7):483-91.
192. Shields CL, Kaliki S, Furuta M, Shields JA. Diffuse versus nondiffuse small ( $\leq 3$  MM thickness) choroidal melanoma: comparative analysis in 1,751 cases. The 2012 F. Phinzy Calhoun lecture. *Retina*. 2013;33(9):1763-76.
193. Kivelä T, Summanen P. Retinoinvasive malignant melanoma of the uvea. *British journal of ophthalmology*. 1997;81(8):691-7.
194. Al-Haddab S, Hidayat A, Tabbara KF. Ciliary body melanoma with optic nerve invasion. *British journal of ophthalmology*. 1990;74(2):123-4.
195. Margo CE, Pautler SE. Granulomatous uveitis after treatment of a choroidal melanoma with proton-beam irradiation. *Retina (Philadelphia, Pa)*. 1990;10(2):140-3.
196. Feng L, Zhu J, Gao T, et al. Uveal melanoma in the peripheral choroid masquerading as chronic uveitis. *Optometry and Vision Science*. 2014;91(9):e222.
197. Fraser DJ, Font RL. Ocular inflammation and hemorrhage as initial manifestations of uveal malignant melanoma: incidence and prognosis. *Archives of Ophthalmology*. 1979;97(7):1311-4.

198. Shields JA, Eagle Jr RC, Shields CL, De Potter P. Pigmented adenoma of the optic nerve head simulating a melanocytoma. *Ophthalmology*. 1992;99(11):1705-8.
199. Lee J, Logani S, Lakosha H, et al. Preretinal neovascularisation associated with choroidal melanoma. *British journal of ophthalmology*. 2001;85(11):1309-12.
200. Guerin E, Hiscott P, Damato B. Choroidal neovascular membrane in a series of cases of malignant melanoma of the choroid. *Acta Ophthalmologica Scandinavica*. 2006;84(3):323-7.
201. Doescher J, Veit JA, Hoffmann TK. The 8th edition of the AJCC Cancer Staging Manual: Updates in otorhinolaryngology, head and neck surgery. *Hno*. 2017;65(12):956-61.
202. Huang SH, O'Sullivan B. Overview of the 8th Edition TNM Classification for Head and Neck Cancer. *Curr Treat Options Oncol*. 2017;18(7):40.
203. Kaneko A. TNM classification of ophthalmic malignant tumors. *Gan to Kagaku ryoho Cancer & Chemotherapy*. 1998;25(8):1231-40.
204. Brierley JD, Gospodarowicz MK, Wittekind C. TNM classification of malignant tumours: John Wiley & Sons, 2017.
205. Kivela T, Simpson ER, Grossniklaus HE, et al. Uveal melanoma In: *AJCC Cancer Staging Manual*. 8th ed. AJCC cancer staging manual. 2017;8:805-17.
206. Gospodarowicz MK, Miller D, Groome PA, et al. The process for continuous improvement of the TNM classification. *Cancer: Interdisciplinary International Journal of the American Cancer Society*. 2004;100(1):1-5.
207. Kujala E, Kivelä T. Tumor, node, metastasis classification of malignant ciliary body and choroidal melanoma: evaluation of the 6th edition and future directions. *Ophthalmology*. 2005;112(6):1135-44.
208. Kivelä T, Kujala E. Prognostication in eye cancer: the latest tumor, node, metastasis classification and beyond. *Eye*. 2013;27(2):243-52.
209. Damato B, Coupland SE. Classification of uveal tumors. *Clinical Ophthalmic Oncology*: Springer, 2014.
210. Rospond - Kubiak I, Wroblewska - Zierhoffer M, Twardosz - Pawlik H, Kociecki J. The liverpool uveal melanoma prognosticator online (lumpo) for prognosing metastasis free survival in the absence of cytogenetic data after ruthenium brachytherapy for uveal melanoma. *Acta Ophthalmologica*. 2015;93.
211. Cunha Rola A, Taktak A, Eleuteri A, et al. Multicenter external validation of the liverpool uveal melanoma prognosticator online: an OOG collaborative study. *Cancers*. 2020;12(2):477.
212. Nathan P, Cohen V, Coupland S, et al. Uveal melanoma UK national guidelines. *European journal of cancer*. 2015;51(16):2404-12.
213. <https://mpcetoolsforhealth.liverpool.ac.uk/LUMPONet/LUMPONet.html>. Liverpool Uveal Melanoma Prognosticator Online (LUMPO).
214. Damato B, Eleuteri A, Taktak AF, Coupland SE. Estimating prognosis for survival after treatment of choroidal melanoma. *Progress in retinal and eye research*. 2011;30(5):285-95.
215. Finger PT. The 7th edition AJCC staging system for eye cancer: an international language for ophthalmic oncology. *Arch Pathol Lab Med*. 2009;133(8):1197-8.
216. Baron ED, Nicola M, Shields CL. Updated AJCC Classification for Posterior Uveal Melanoma. *Retina Today*. 2018:30-4.
217. Ardjomand N, Komericki P, Langmann G, et al. Lymph node metastases arising from uveal melanoma. *Wien Klin Wochenschr*. 2005;117(11-12):433-5.

218. Spaide RF, Koizumi H, Pozonni MC. Enhanced depth imaging spectral-domain optical coherence tomography. *American journal of ophthalmology*. 2008;146(4):496-500.
219. Heimann H, Jmor F, Damato B. Imaging of retinal and choroidal vascular tumours. *Eye*. 2013;27(2):208-16.
220. Soliman AZ, Silva PS, Aiello LP, Sun JK. Ultra-wide field retinal imaging in detection, classification, and management of diabetic retinopathy. *Seminars in ophthalmology: Taylor & Francis*, 2012; v. 27.
221. Paul Brett J, Lake A, Downes S. Colour imaging in the monitoring and documentation of choroidal naevi. Are Optomap colour images adequate for this purpose? *Journal of Visual Communication in Medicine*. 2016;39(1-2):10-7.
222. Kumar V, Surve A, Kumawat D, et al. Ultra-wide field retinal imaging: A wider clinical perspective. *Indian Journal of Ophthalmology*. 2021;69(4):824.
223. Witmer MT, Parlitsis G, Patel S, Kiss S. Comparison of ultra-widefield fluorescein angiography with the Heidelberg Spectralis® noncontact ultra-widefield module versus the Optos® Optomap®. *Clinical ophthalmology (Auckland, NZ)*. 2013;7:389.
224. Onishi SM, Crabtree GS, Marks SJ, et al. Disappearing choroidal melanoma on optos: the nose artifact. *Retinal Cases and Brief Reports*. 2021;15(2):101-3.
225. Liegl R, Liegl K, Ceklic L, et al. Nonmydriatic ultra-wide-field scanning laser ophthalmoscopy (Optomap) versus two-field fundus photography in diabetic retinopathy. *Ophthalmologica*. 2014;231(1):31-6.
226. Matsui Y, Ichio A, Sugawara A, et al. Comparisons of effective fields of two ultra-widefield ophthalmoscopes, Optos 200Tx and Clarus 500. *BioMed research international*. 2019;2019.
227. Wu C, Petersen RA, VanderVeen DK. RetCam imaging for retinopathy of prematurity screening. *Journal of American Association for Pediatric Ophthalmology and Strabismus*. 2006;10(2):107-11.
228. Kim JW, Ngai LK, Sadda S, et al. Retcam fluorescein angiography findings in eyes with advanced retinoblastoma. *British Journal of Ophthalmology*. 2014;98(12):1666-71.
229. Murakami Y, Ngai L, Kim J. Retcam Fluorescein angiography findings in eyes with advanced retinoblastoma. *Investigative Ophthalmology & Visual Science*. 2013;54(15):3980-.
230. Shields CL, Manalac J, Das C, et al. Review of spectral domain-enhanced depth imaging optical coherence tomography of tumors of the retina and retinal pigment epithelium in children and adults. *Indian Journal of Ophthalmology*. 2015;63(2):128.
231. Lapere S, Weis E. Tele-ophthalmology for the monitoring of choroidal and iris nevi: a pilot study. *Can J Ophthalmol*. 2018;53(5):471-3.
232. Roelofs K, Weis E. Tele-Oncology: A Validation Study of Choroidal and Iris Nevi. *Ocul Oncol Pathol*. 2019;5(4):298-302.
233. Quinn GE, Ying GS, Daniel E, et al. Validity of a telemedicine system for the evaluation of acute-phase retinopathy of prematurity. *JAMA Ophthalmol*. 2014;132(10):1178-84.
234. Au A, Gupta O. The economics of telemedicine for vitreoretinal diseases. *Curr Opin Ophthalmol*. 2011;22(3):194-8.
235. Thomas SM, Jeyaraman MM, Hodge WG, et al. The effectiveness of teleglaucoma versus in-patient examination for glaucoma screening: a systematic review and meta-analysis. *PLoS One*. 2014;9(12):e113779.

236. Kirkizlar E, Serban N, Sisson JA, et al. Evaluation of telemedicine for screening of diabetic retinopathy in the Veterans Health Administration. *Ophthalmology*. 2013;120(12):2604-10.
237. Choudhry N, Duker JS, Freund KB, et al. Classification and Guidelines for Widefield Imaging: Recommendations from the International Widefield Imaging Study Group. *Ophthalmol Retina*. 2019;3(10):843-9.
238. Damato B. Managing patients with choroidal melanoma in the COVID-19 era: a personal perspective. *Br J Ophthalmol*. 2020.
239. Ayres B, Stacey A, Grant J, et al. Comparative study of clinical, ultrasonographic, conventional imaging, and ultra-wide-field fundus for measurements of the longest basal diameter of choroidal tumors. *Ophthalmic Surgery, Lasers and Imaging Retina*. 2017;48(6):459-64.
240. Shoughy SS, Arevalo JF, Kozak I. Update on wide-and ultra-widefield retinal imaging. *Indian Journal of Ophthalmology*. 2015;63(7):575.
241. Ye P-P, Xu J, Su Z-T, et al. The application of ultra-wide-field fundus autofluorescence in early metastatic choroidal tumor screening. *International Journal of Ophthalmology*. 2019;12(12):1978.
242. Balasubramanya R, Selvarajan SK, Cox M, et al. Imaging of ocular melanoma metastasis. *The British journal of radiology*. 2016;89(1065):20160092.
243. Lu JE, Welch RJ, Mishra KK, et al. Ultrasonography and transillumination for uveal melanoma localisation in proton beam treatment planning. *Eye*. 2019;33(12):1904-10.
244. Conway RM, Chew T, Golchet P, et al. Ultrasound biomicroscopy: role in diagnosis and management in 130 consecutive patients evaluated for anterior segment tumours. *Br J Ophthalmol*. 2005;89(8):950-5.
245. Bian A, Min H, Dai R, et al. Ring lymphoma: highly indicative ultrasound biomicroscopy findings of ciliary body lymphoma. *Graefes Arch Clin Exp Ophthalmol*. 2021;259(7):2005-8.
246. Sherar M, Foster F. The design and fabrication of high frequency poly (vinylidene fluoride) transducers. *Ultrasonic imaging*. 1989;11(2):75-94.
247. Coleman DJ, Abramson DH, Jack RL, Franzen LA. Ultrasonic diagnosis of tumors of the choroid. *Archives of Ophthalmology*. 1974;91(5):344-54.
248. Scott IU, Murray TG, Hughes JR. Evaluation of imaging techniques for detection of extraocular extension of choroidal melanoma. *Archives of ophthalmology*. 1998;116(7):897-9.
249. Fuller DG, Snyder WB, Hutton WL, Vaiser A. Ultrasonographic features of choroidal malignant melanomas. *Archives of Ophthalmology*. 1979;97(8):1465-72.
250. Fries PD, Char DH. Fluorescein angiography in ciliary body melanomas. *Ophthalmologica*. 1990;201(2):57-65.
251. Bakri S, Sculley L, Singh AD. Diagnostic techniques. *Essentials of Ophthalmic Oncology*. 2009;46:69.
252. Skalet AH, Li Y, Lu CD, et al. Optical coherence tomography angiography characteristics of iris melanocytic tumors. *Ophthalmology*. 2017;124(2):197-204.
253. Dart J, Marsh R, Garner A, Cooling R. Fluorescein angiography of anterior uveal melanocytic tumours. *British journal of ophthalmology*. 1988;72(5):326-37.
254. Davila JR, Mruthyunjaya P. Updates in imaging in ocular oncology. *F1000Research*. 2019;8.
255. Pavlin CJ, McWhae JA, McGowan HD, Foster FS. Ultrasound biomicroscopy of anterior segment tumors. *Ophthalmology*. 1992;99(8):1220-8.

- 
256. Ramasubramanian A, Shields CL, Harmon SA, Shields JA. Autofluorescence of choroidal hemangioma in 34 consecutive eyes. *Retina*. 2010;30(1):16-22.
257. Augsburger JJ, Golden MI, Shields JA. Fluorescein angiography of choroidal malignant melanomas with retinal invasion. *Retina (Philadelphia, Pa)*. 1984;4(4):232-41.
258. Shields CL, Shields JA, De Potter P. Patterns of indocyanine green videoangiography of choroidal tumours. *British journal of ophthalmology*. 1995;79(3):237-45.
259. Flower RW. Infrared absorption angiography of the choroid and some observations on the effects of high intraocular pressures. *American Journal of Ophthalmology*. 1972;74(4):600-14.
260. Amoaku W, Archer D. Fluorescein angiographic features, natural course and treatment of radiation retinopathy. *Eye*. 1990;4(5):657-67.
261. Brown GC, Shields JA, Sanborn G, et al. Radiation retinopathy. *Ophthalmology*. 1982;89(12):1494-501.
262. Sallet G, Amoaku WM, Lafaut BA, et al. Indocyanine green angiography of choroidal tumors. *Graefe's archive for clinical and experimental ophthalmology*. 1995;233(11):677-89.
263. Mueller A, Freeman W, Folberg R, et al. Evaluation of microvascularization pattern visibility in human choroidal melanomas: comparison of confocal fluorescein with indocyanine green angiography. *Graefe's archive for clinical and experimental ophthalmology*. 1999;237(6):448-56.
264. Shields CL, Shields JA, Cater J, et al. Transpupillary thermotherapy for choroidal melanoma: tumor control and visual results in 100 consecutive cases. *Ophthalmology*. 1998;105(4):581-90.
265. Hochheimer BF. Angiography of the retina with indocyanine green. *Archives of ophthalmology*. 1971;86(5):564-5.
266. Geeraets WJ, Berry ER. Ocular spectral characteristics as related to hazards from lasers and other light sources. *Amer J Ophthalmol*, 66: 15-20 (July 1968). 1968.
267. Baker KJ, Bradley SE. Binding of sulfobromophthalein (BSP) sodium by plasma albumin. Its role in hepatic BSP extraction. *The Journal of clinical investigation*. 1966;45(2):281-7.
268. Chang AA, Morse LS, Handa JT, et al. Histologic localization of indocyanine green dye in aging primate and human ocular tissues with clinical angiographic correlation. *Ophthalmology*. 1998;105(6):1060-8.
269. Hee MR, Izatt JA, Swanson EA, et al. Optical coherence tomography of the human retina. *Archives of ophthalmology*. 1995;113(3):325-32.
270. Olsen T. The accuracy of ultrasonic determination of axial length in pseudophakic eyes. *Acta ophthalmologica*. 1989;67(2):141-4.
271. Huang D, Swanson EA, Lin CP, et al. Optical coherence tomography. *science*. 1991;254(5035):1178-81.
272. Shields CL, Materin MA, Shields JA. Review of optical coherence tomography for intraocular tumors. *Current opinion in ophthalmology*. 2005;16(3):141-54.
273. Schaudig U, Hassenstein A, Bernd A, et al. Limitations of imaging choroidal tumors in vivo by optical coherence tomography. *Graefe's archive for clinical and experimental ophthalmology*. 1998;236(8):588-92.
274. Hee MR. Optical coherence tomography of the eye. Massachusetts Institute of Technology, 1997.

275. Hau SC, Papastefanou V, Shah S, et al. Evaluation of iris and iridociliary body lesions with anterior segment optical coherence tomography versus ultrasound B-scan. *British Journal of Ophthalmology*. 2015;99(1):81-6.
276. Papakostas TD, Lane AM, Morrison M, et al. Long-term outcomes after proton beam irradiation in patients with large choroidal melanomas. *JAMA ophthalmology*. 2017;135(11):1191-6.
277. Finger PT. Radiation therapy for choroidal melanoma. *Survey of ophthalmology*. 1997;42(3):215-32.
278. Gragoudas ES, Lane AM, Regan S, et al. A randomized controlled trial of varying radiation doses in the treatment of choroidal melanoma. *Archives of ophthalmology*. 2000;118(6):773-8.
279. Levitz LM. The use of optical coherence tomography to determine the severity of radiation retinopathy. Slack Incorporated Thorofare, NJ, 2005; v. 36.
280. Finger PT, Iezzi R, Esteveo ML, et al. Diode-light transillumination for ophthalmic plaque localization around juxtapapillary choroidal melanomas. *Int J Radiat Oncol Biol Phys*. 1999;44(4):887-90.
281. Umlas J, Diener-West M, Robinson NL, et al. Comparison of transillumination and histologic slide measurements of choroidal melanoma. *Arch Ophthalmol*. 1997;115(4):474-7.
282. Kaliki S, Shields CL, Shields JA. Uveal melanoma: estimating prognosis. *Indian J Ophthalmol*. 2015;63(2):93-102.
283. Naumann G, Yanoff M, Zimmerman LE. Histogenesis of malignant melanomas of the uvea. I. Histopathologic characteristics of nevi of the choroid and ciliary body. *Arch Ophthalmol*. 1966;76(6):784-96.
284. Burris CKH, Papastefanou VP, Thaug C, et al. Detection of extrascleral extension in uveal melanoma with histopathological correlation. *Orbit*. 2018;37(4):287-92.
285. Shields JA, Shields CL, De Potter P, Singh AD. Diagnosis and treatment of uveal melanoma. *Seminars in oncology*1996; v. 23.
286. Folberg R, Rummelt V, Parys-Van Ginderdeuren R, et al. The prognostic value of tumor blood vessel morphology in primary uveal melanoma. *Ophthalmology*. 1993;100(9):1389-98.
287. Corrêa ZM, Augsburger JJ. Indications for Fine Needle Aspiration Biopsy of Posterior Segment Intraocular Tumors. *Am J Ophthalmol*. 2019;207:45-61.
288. Damato B. Time to treatment of uveal melanoma in the United Kingdom. *Eye*. 2001;15(2):155-8.
289. Bechrakis NE, Foerster MH, Bornfeld N. Biopsy in indeterminate intraocular tumors. *Ophthalmology*. 2002;109(2):235-42.
290. Kujala E, Damato B, Coupland SE, et al. Staging of ciliary body and choroidal melanomas based on anatomic extent. *Journal of clinical oncology*. 2013;31(22):2825-31.
291. Char DH, Kroll S, Phillips TL. Uveal melanoma: growth rate and prognosis. *Archives of ophthalmology*. 1997;115(8):1014-8.
292. Seddon JM, Albert DM, Lavin PT, Robinson N. A prognostic factor study of disease-free interval and survival following enucleation for uveal melanoma. *Archives of ophthalmology*. 1983;101(12):1894-9.
293. Folberg R, Pe'er J, Gruman LM, et al. The morphologic characteristics of tumor blood vessels as a marker of tumor progression in primary human uveal melanoma: a matched case-control study. *Hum Pathol*. 1992;23(11):1298-305.

294. Koopmans AE, Verdijk RM, Brouwer RW, et al. Clinical significance of immunohistochemistry for detection of BAP1 mutations in uveal melanoma. *Mod Pathol*. 2014;27(10):1321-30.
295. Woodman SE. Metastatic uveal melanoma: biology and emerging treatments. *Cancer journal (Sudbury, Mass)*. 2012;18(2):148.
296. Njauw C-NJ, Kim I, Piris A, et al. Germline BAP1 inactivation is preferentially associated with metastatic ocular melanoma and cutaneous-ocular melanoma families. *PloS one*. 2012;7(4):e35295.
297. Sisley K, Rennie IG, Parsons MA, et al. Abnormalities of chromosomes 3 and 8 in posterior uveal melanoma correlate with prognosis. *Genes, Chromosomes and Cancer*. 1997;19(1):22-8.
298. van den Bosch T, van Beek JG, Vaarwater J, et al. Higher percentage of FISH-determined monosomy 3 and 8q amplification in uveal melanoma cells relate to poor patient prognosis. *Investigative ophthalmology & visual science*. 2012;53(6):2668-74.
299. Dogrusöz M, Bagger M, van Duinen SG, et al. The Prognostic Value of AJCC Staging in Uveal Melanoma Is Enhanced by Adding Chromosome 3 and 8q Status. *Invest Ophthalmol Vis Sci*. 2017;58(2):833-42.
300. Shields CL, Say EAT, Hasanreisoglu M, et al. Cytogenetic Abnormalities in Uveal Melanoma Based on Tumor Features and Size in 1059 Patients: The 2016 W. Richard Green Lecture. *Ophthalmology*. 2017;124(5):609-18.
301. Horsman DE, White VA. Cytogenetic analysis of uveal melanoma consistent occurrence of monosomy 3 and trisomy 8q. *Cancer*. 1993;71(3):811-9.
302. Sisley K, Rennie IG, Cottam DW, et al. Cytogenetic findings in six posterior uveal melanomas: involvement of chromosomes 3, 6, and 8. *Genes, Chromosomes and Cancer*. 1990;2(3):205-9.
303. Bornfeld N, Prescher G, Becher R, et al. Prognostic implications of monosomy 3 in uveal melanoma. *The Lancet*. 1996;347(9010):1222-5.
304. Singh AD, Tubbs R, Biscotti C, et al. Chromosomal 3 and 8 status within hepatic metastasis of uveal melanoma. *Arch Pathol Lab Med*. 2009;133(8):1223-7.
305. Martorell-Calatayud A, Nagore E, Botella-Estrada R, et al. Defining fast-growing melanomas: reappraisal of epidemiological, clinical, and histological features. *Melanoma research*. 2011;21(2):131-8.
306. Raivio I. Uveal melanoma in Finland. An epidemiological, clinical, histological and prognostic study. *Acta ophthalmologica Supplementum*. 1977(133):1-64.
307. Damato BE. An approach to the management of patients with uveal melanoma. *Eye*. 1993;7(3):388-97.
308. <https://www.england.nhs.uk/wp-content/uploads/2013/06/d12-ocular-oncology-ad.pdf>. NHS standard contract for ocular oncology service( adults and adolescence)
- .
309. Summa P, Immonen I, Kivelä T, et al. Visual outcome of eyes with malignant melanoma of the uvea after ruthenium plaque radiotherapy. SLACK Incorporated Thorofare, NJ, 1995; v. 26.
310. Shields CL, Shields JA, Cater J, et al. Plaque radiotherapy for uveal melanoma: long-term visual outcome in 1106 consecutive patients. *Archives of Ophthalmology*. 2000;118(9):1219-28.
311. Summanen P, Immonen I, Kivelä T, et al. Radiation related complications after ruthenium plaque radiotherapy of uveal melanoma. *British journal of ophthalmology*. 1996;80(8):732-9.



312. O'Day RFJ, Roelofs KA, Negretti GS, et al. Long-term visual outcomes after ruthenium plaque brachytherapy for posterior choroidal melanoma. *Eye (Lond)*. 2022.
313. <https://dokumen.pub/clinical-ophthalmic-oncology-uveal-tumors-3nbsped-9783030178796-303017879x-i-1841815.html>. *Clinical Ophthalmic Oncology : Uveal Tumors*.
314. Harbour JW, Char DH, Kroll S, et al. Metastatic risk for distinct patterns of postirradiation local recurrence of posterior uveal melanoma. *Ophthalmology*. 1997;104(11):1785-93.
315. Egan KM, Ryan LM, Gragoudas ES. Survival implications of enucleation after definitive radiotherapy for choroidal melanoma: an example of regression on time-dependent covariates. *Archives of Ophthalmology*. 1998;116(3):366-70.
316. Melia M, Moy CS, Reynolds SM, et al. Quality of life after iodine 125 brachytherapy vs enucleation for choroidal melanoma: 5-year results from the Collaborative Ocular Melanoma Study: COMS QOLS Report No. 3. *Archives of ophthalmology (Chicago, Ill: 1960)*. 2006;124(2):226-38.
317. Stallard H. Radiotherapy for malignant melanoma of the choroid. *The British journal of ophthalmology*. 1966;50(3):147.
318. Jampol LM, Moy CS, Murray TG, et al. The COMS randomized trial of iodine 125 brachytherapy for choroidal melanoma: IV. Local treatment failure and enucleation in the first 5 years after brachytherapy. COMS report no. 19. *Ophthalmology*. 2002;109(12):2197-206.
319. Tarmann L, Wackernagel W, Avian A, et al. Ruthenium-106 plaque brachytherapy for uveal melanoma. *British Journal of Ophthalmology*. 2015;99(12):1644-9.
320. Caminal JM, Mejia K, Masuet-Aumatell C, et al. Endoresection versus iodine-125 plaque brachytherapy for the treatment of choroidal melanoma. *Am J Ophthalmol*. 2013;156(2):334-42.e1.
321. Sagoo MS, Shields CL, Mashayekhi A, et al. Plaque radiotherapy for juxtapapillary choroidal melanoma: tumor control in 650 consecutive cases. *Ophthalmology*. 2011;118(2):402-7.
322. Reichstein D, Karan K. Plaque brachytherapy for posterior uveal melanoma in 2018: improved techniques and expanded indications. *Current opinion in ophthalmology*. 2018;29(3):191-8.
323. Gragoudas ES, Goitein M, Verhey L, et al. Proton beam irradiation: an alternative to enucleation for intraocular melanomas. *Ophthalmology*. 1980;87(6):571-81.
324. Zografos L, Gailloud C, Perret C, et al. Rapport sur le traitement conservateur des mélanomes de l'uvée a la clinique ophtalmologique universitaire de Lausanne. *Klinische Monatsblätter für Augenheilkunde*. 1988;192(05):572-8.
325. Dendale R, Lumbroso-Le Rouic L, Noel G, et al. Proton beam radiotherapy for uveal melanoma: results of Curie Institut-Orsay proton therapy center (ICPO). *International Journal of Radiation Oncology\* Biology\* Physics*. 2006;65(3):780-7.
326. Damato B, Kacperek A, Chopra M, et al. Proton beam radiotherapy of choroidal melanoma: the Liverpool-Clatterbridge experience. *International Journal of Radiation Oncology\* Biology\* Physics*. 2005;62(5):1405-11.
327. Egger E, Zografos L, Schalenbourg A, et al. Eye retention after proton beam radiotherapy for uveal melanoma. *International Journal of Radiation Oncology\* Biology\* Physics*. 2003;55(4):867-80.

328. Konstantinidis L, Roberts D, Errington RD, et al. Transpalpebral proton beam radiotherapy of choroidal melanoma. *British Journal of Ophthalmology*. 2015;99(2):232-5.
329. Afshar AR, Damato BE. Choroidal melanoma overlying scleral buckle evading detection treated with proton beam radiotherapy. *American Journal of Ophthalmology Case Reports*. 2020;18:100688.
330. Riechardt AI, Cordini D, Willerding GD, et al. Proton beam therapy of parapapillary choroidal melanoma. *American Journal of Ophthalmology*. 2014;157(6):1258-65.
331. Verma V, Mehta M. Clinical outcomes of proton radiotherapy for uveal melanoma. *Clinical Oncology*. 2016;28(8):e17-e27.
332. Papastefanou VP, Pefkianaki M, Al Harby L, et al. Intravitreal bevacizumab monotherapy for choroidal neovascularisation secondary to choroidal osteoma. *Eye (Lond)*. 2016;30(6):843-9.
333. Russo A, Reibaldi M, Avitabile T, et al. Dexamethasone intravitreal implant VS Ranibizumab in the treatment of macular edema secondary to brachytherapy for choroidal melanoma. *Retina*. 2018;38(4):788-94.
334. Kim IK, Lane AM, Jain P, et al. Ranibizumab for the Prevention of Radiation Complications in Patients Treated With Proton Beam Irradiation for Choroidal Melanoma. *Trans Am Ophthalmol Soc*. 2016;114:T2.
335. Lima BR, Schoenfield LR, Singh AD. The impact of intravitreal bevacizumab therapy on choroidal melanoma. *Am J Ophthalmol*. 2011;151(2):323-8.e2.
336. Giuliari GP, Sadaka A, Hinkle DM, Simpson ER. Current treatments for radiation retinopathy. *Acta Oncol*. 2011;50(1):6-13.
337. Marchini G, Gerosa M, Piovan E, et al. Gamma Knife stereotactic radiosurgery for uveal melanoma: clinical results after 2 years. *Stereotactic and Functional Neurosurgery*. 1996;66(Suppl. 1):208-13.
338. van Beek JGM, Buitendijk GHS, Timman R, et al. Quality of life: fractionated stereotactic radiotherapy versus enucleation treatment in uveal melanoma patients. *Acta Ophthalmol*. 2018;96(8):841-8.
339. Xu TT, Pulido JS, Parney IF, et al. Carbon Fiducial Markers for Tumor Localization in Stereotactic Irradiation of Uveal Melanoma. *Ocul Oncol Pathol*. 2021;7(5):368-75.
340. Mueller AJ, Talies S, Schaller UC, et al. Stereotactic radiosurgery of large uveal melanomas with the gamma-knife. *Ophthalmology*. 2000;107(7):1381-7.
341. Muller K, Nowak PJ, de Pan C, et al. Effectiveness of fractionated stereotactic radiotherapy for uveal melanoma. *International Journal of Radiation Oncology\* Biology\* Physics*. 2005;63(1):116-22.
342. Furdova A, Sramka M, Chorvath M, et al. Stereotactic radiosurgery in intraocular malignant melanoma--retrospective study. *Neuro Endocrinol Lett*. 2014;35(1):28-36.
343. Furdova A, Strmen P, Waczulikova I, et al. One-day session LINAC-based stereotactic radiosurgery of posterior uveal melanoma. *Eur J Ophthalmol*. 2012;22(2):226-35.
344. Kang DW, Lee SC, Park YG, Chang JH. Long-term results of Gamma Knife surgery for uveal melanomas. *J Neurosurg*. 2012;117 Suppl:108-14.
345. Furdova A, Sramka M, Chorvath M, et al. Clinical experience of stereotactic radiosurgery at a linear accelerator for intraocular melanoma. *Melanoma Res*. 2017;27(5):463-8.

- 
346. van Beek JGM, van Rij CM, Baart SJ, et al. Fractionated stereotactic radiotherapy for uveal melanoma: Long-term outcome and control rates. *Acta Ophthalmol.* 2022;100(5):511-9.
347. Bornfeld N, Talies S, Anastassiou G, et al. [Endoscopic resection of malignant melanomas of the uvea after preoperative stereotactic single dose convergence irradiation with the Leksell gamma knife]. *Ophthalmologe.* 2002;99(5):338-44.
348. Shields JA, Glazer LC, Mieler WF, et al. Comparison of xenon arc and argon laser photocoagulation in the treatment of choroidal melanomas. *American journal of ophthalmology.* 1990;109(6):647-55.
349. Meyer-Schwickerath G, Vogel M. Treatment of malignant melanomas of the choroid by photocoagulation. *Transactions of the ophthalmological societies of the United Kingdom.* 1977;97(3):416-20.
350. Oosterhuis JA, Journée-de Korver HG, Kakebeeke-Kemme HM, Bleeker JC. Transpupillary thermotherapy in choroidal melanomas. *Archives of ophthalmology.* 1995;113(3):315-21.
351. Singh AD, Kivelä T, Seregard S, et al. Primary transpupillary thermotherapy of "small" choroidal melanoma: is it safe? *British Journal of Ophthalmology.* 2008;92(6):727-8.
352. Shields CL, Cater J, Shields JA, et al. Combined plaque radiotherapy and transpupillary thermotherapy for choroidal melanoma: tumor control and treatment complications in 270 consecutive patients. *Archives of Ophthalmology.* 2002;120(7):933-40.
353. Robertson DM. Small choroidal melanomas treated with transpupillary thermotherapy and cryotherapy. *Arch Ophthalmol.* 2008;126(8):1156-7.
354. Parrozzani R, Boccassini B, De Belvis V, et al. Long-term outcome of transpupillary thermotherapy as primary treatment of selected choroidal melanoma. *Acta Ophthalmol.* 2009;87(7):789-92.
355. Mashayekhi A, Shields CL, Rishi P, et al. Primary transpupillary thermotherapy for choroidal melanoma in 391 cases: importance of risk factors in tumor control. *Ophthalmology.* 2015;122(3):600-9.
356. Shields CL, Shields JA, Perez N, et al. Primary transpupillary thermotherapy for small choroidal melanoma in 256 consecutive cases: outcomes and limitations. *Ophthalmology.* 2002;109(2):225-34.
357. Yarovoy AA, Magaramov DA, Bulgakova ES. Which choroidal melanoma should be treated with primary transpupillary thermotherapy? Our experience from 78 patients. *Eur J Ophthalmol.* 2010;20(1):186-93.
358. Damato BE. Local resection of uveal melanoma. *Dev Ophthalmol.* 2012;49:66-80.
359. Damato B, Groenewald C, McGalliard J, Wong D. Endoresection of choroidal melanoma. *British Journal of Ophthalmology.* 1998;82(3):213-8.
360. Shields JA, Shields CL, Donoso LA. Management of posterior uveal melanoma. *Survey of ophthalmology.* 1991;36(3):161-95.
361. Vidoris AAC, Maia A, Lowen M, et al. Outcomes of primary endoresection for choroidal melanoma. *Int J Retina Vitreous.* 2017;3:42.
362. Konstantinidis L, Groenewald C, Coupland SE, Damato B. Long-term outcome of primary endoresection of choroidal melanoma. *Br J Ophthalmol.* 2014;98(1):82-5.
363. Rice JC, Stannard C, Cook C, et al. Brachytherapy and endoresection for choroidal melanoma: a cohort study. *Br J Ophthalmol.* 2014;98(1):86-91.

364. Bechrakis NE, Bornfeld N, Zöller I, Foerster MH. Iodine 125 plaque brachytherapy versus transscleral tumor resection in the treatment of large uveal melanomas. *Ophthalmology*. 2002;109(10):1855-61.
365. Gündüz K, Bechrakis NE. Exoresection and endoresection for uveal melanoma. *Middle East Afr J Ophthalmol*. 2010;17(3):210-6.
366. Garcia-Arumi J, Distefano LN, Quijano C. Endoresection of a high equatorial choroidal melanoma. *Retin Cases Brief Rep*. 2015;9(1):30-2.
367. Damato B. Choroidal melanoma endoresection, dandelions and allegory-based medicine. *British Journal of Ophthalmology*. 2008;92(8):1013-4.
368. Damato B, Foulds W. Indications for trans-scleral local resection of uveal melanoma. *The British Journal of Ophthalmology*. 1996;80(11):1029.
369. Damato B. Progress in the management of patients with uveal melanoma. The 2012 Ashton Lecture. *Eye (Lond)*. 2012;26(9):1157-72.
370. Kurt RA, Gündüz K. Exoresection via partial lamellar sclerouvectomy approach for uveal tumors: A successful performance by a novice surgeon. *Clin Ophthalmol*. 2010;4:59-65.
371. Rennie I. Local resection of choroidal melanoma. *Br J Ophthalmol*. 1993;77(10):613.
372. <https://columbusvp.com/aura-biosciences-presents-updated-clinical-data-for-au-011/#:~:text=AU-011%20is%20a%20first-in-class%20targeted%20therapy%20in%20development>. Light-Activated AU-011 Holds Significant Potential as a First Line Treatment for Choroidal Melanoma.
373. Wilson DJ, Klein ML. Cryotherapy as a primary treatment for choroidal melanoma. *Arch Ophthalmol*. 2002;120(3):400-3.
374. Wilson DJ, Klein ML. Choroidal melanoma treated with cryotherapy. *Arch Ophthalmol*. 2002;120(3):393-5.
375. Damato BE, Paul J, Foulds WS. Predictive factors of visual outcome after local resection of choroidal melanoma. *British journal of ophthalmology*. 1993;77(10):616-23.
376. Singh A, Rennie I, Kivela T, et al. The Zimmerman-McLean-Foster hypothesis: 25 years later. *British Journal of Ophthalmology*. 2004;88(7):962-7.
377. Rennie IG. Uveal melanoma: the past, the present and the future. *Eye*. 1997;11(2):255-64.
378. Zimmerman LE, McLean I, Foster WD. Does enucleation of the eye containing a malignant melanoma prevent or accelerate the dissemination of tumour cells. *British Journal of Ophthalmology*. 1978;62(6):420-5.
379. Damato B. Does ocular treatment of uveal melanoma influence survival? *British journal of cancer*. 2010;103(3):285-90.
380. Group COMS. The Collaborative Ocular Melanoma Study (COMS) randomized trial of pre-enucleation radiation of large choroidal melanoma III: local complications and observations following enucleation COMS report no. 11. *American Journal of Ophthalmology*. 1998;126(3):362-72.
381. Gamel JW, McLean IW, McCurdy JB. Biologic distinctions between cure and time to death in 2892 patients with intraocular melanoma. *Cancer*. 1993;71(7):2299-305.
382. Damato BE, Heimann H, Kalirai H, Coupland SE. Age, survival predictors, and metastatic death in patients with choroidal melanoma: tentative evidence of a therapeutic effect on survival. *JAMA Ophthalmol*. 2014;132(5):605-13.
383. Radivoyevitch T, Zabor EC, Singh AD. Uveal melanoma: Long-term survival. *PLoS One*. 2021;16(5):e0250939.

- 
384. Kujala E, Mäkitie T, Kivelä T. Very long-term prognosis of patients with malignant uveal melanoma. *Invest Ophthalmol Vis Sci.* 2003;44(11):4651-9.
385. Mäkitie T, Kivelä T. Cardiac metastasis from uveal melanoma. *Archives of Ophthalmology.* 2001;119(1):139-40.
386. Eskelin S, Pyrhonen S, Summanen P, et al. Tumor doubling times in metastatic malignant melanoma of the uvea: tumor progression before and after treatment. *Ophthalmology.* 2000;107(8):1443-9.
387. Einhorn LH, Burgess MA, Gottlieb JA. Metastatic patterns of choroidal melanoma. *Cancer.* 1974;34(4):1001-4.
388. Chandran SS, Somerville RPT, Yang JC, et al. Treatment of metastatic uveal melanoma with adoptive transfer of tumour-infiltrating lymphocytes: a single-centre, two-stage, single-arm, phase 2 study. *Lancet Oncol.* 2017;18(6):792-802.
389. Albert DM, Niffenegger AS, Willson JK. Treatment of metastatic uveal melanoma: review and recommendations. *Survey of ophthalmology.* 1992;36(6):429-38.
390. Kaštelan S, Mrazovac Zimak D, Ivanković M, et al. Liver metastasis in uveal melanoma - treatment options and clinical outcome. *Front Biosci (Landmark Ed).* 2022;27(2):72.
391. Rowcroft A, Loveday BPT, Thomson BNJ, et al. Systematic review of liver directed therapy for uveal melanoma hepatic metastases. *HPB (Oxford).* 2020;22(4):497-505.
392. Gragoudas ES, Egan KM, Seddon JM, et al. Survival of patients with metastases from uveal melanoma. *Ophthalmology.* 1991;98(3):383-90.
393. Carvajal RD, Schwartz GK, Tezel T, et al. Metastatic disease from uveal melanoma: treatment options and future prospects. *Br J Ophthalmol.* 2017;101(1):38-44.
394. Komatsubara KM, Manson DK, Carvajal RD. Selumetinib for the treatment of metastatic uveal melanoma: past and future perspectives. *Future Oncol.* 2016;12(11):1331-44.
395. Mallone F, Sacchetti M, Lambiase A, Moramarco A. Molecular Insights and Emerging Strategies for Treatment of Metastatic Uveal Melanoma. *Cancers (Basel).* 2020;12(10).
396. Pelster MS, Gruschkus SK, Bassett R, et al. Nivolumab and Ipilimumab in Metastatic Uveal Melanoma: Results From a Single-Arm Phase II Study. *J Clin Oncol.* 2021;39(6):599-607.
397. Augsburger JJ, Corrêa ZM, Trichopoulos N. An alternative hypothesis for observed mortality rates due to metastasis after treatment of choroidal melanomas of different sizes. *Transactions of the American Ophthalmological Society.* 2007;105:54.
398. Fournier GA, Albert DM, Arrigg CA, et al. Resection of solitary metastasis: approach to palliative treatment of hepatic involvement with choroidal melanoma. *Archives of ophthalmology.* 1984;102(1):80-2.
399. Salmon R, Levy C, Plancher C, et al. Treatment of liver metastases from uveal melanoma by combined surgery—chemotherapy. *European Journal of Surgical Oncology (EJSO).* 1998;24(2):127-30.
400. Aoyama T, Mastrangelo MJ, Berd D, et al. Protracted survival after resection of metastatic uveal melanoma. *Cancer: Interdisciplinary International Journal of the American Cancer Society.* 2000;89(7):1561-8.
401. Dogrusöz M, Jager MJ, Damato B. Uveal melanoma treatment and prognostication. *The Asia-Pacific Journal of Ophthalmology.* 2017;6(2):186-96.

- 
402. Singh AD, Grossniklaus HE. What's in a Name? Large Choroidal Nevus, Small Choroidal Melanoma, or Indeterminate Melanocytic Tumor. *Ocular Oncology and Pathology*. 2021;7(4):235-8.
403. Finger PT. Eye: choroidal melanoma, retinoblastoma, ocular adnexal lymphoma and eyelid cancers. *UICC manual of clinical oncology*. 2015:726-44.
404. <https://eyecancer.com/dr-fingers-desk/to-diagnose-choroidal-melanoma-just-remember-most/>. To diagnose choroidal melanoma, just remember MOST.
405. Damato BE, Rospond-Kubiak I. Uveal Tumors: Examination Techniques. *Clinical Ophthalmic Oncology*: Springer, 2019.
406. Shields CL, Dalvin LA, Michael DY, et al. Choroidal nevus transformation into melanoma per millimeter increment in thickness using multimodal imaging in 2355 cases: the 2019 Wendell L. Hughes Lecture. *Retina*. 2019;39(10):1852-60.
407. Dalvin LA, Shields CL, Ancona-Lezama DA, et al. Combination of multimodal imaging features predictive of choroidal nevus transformation into melanoma. *British Journal of Ophthalmology*. 2019;103(10):1441-7.
408. McCarthy J, Minsky ML, Rochester N, Shannon CE. A proposal for the dartmouth summer research project on artificial intelligence, august 31, 1955. *AI magazine*. 2006;27(4):12-.
409. Ting DSW, Pasquale LR, Peng L, et al. Artificial intelligence and deep learning in ophthalmology. *Br J Ophthalmol*. 2019;103(2):167-75.
410. Korot E, Wagner SK, Faes L, et al. Will AI Replace Ophthalmologists? *Transl Vis Sci Technol*. 2020;9(2):2.
411. Schlegl T, Waldstein SM, Bogunovic H, et al. Fully Automated Detection and Quantification of Macular Fluid in OCT Using Deep Learning. *Ophthalmology*. 2018;125(4):549-58.
412. Bojikian KD, Lee CS, Lee AY. Finding Glaucoma in Color Fundus Photographs Using Deep Learning. *JAMA Ophthalmol*. 2019.
413. Grewal PS, Oloumi F, Rubin U, Tennant MTS. Deep learning in ophthalmology: a review. *Can J Ophthalmol*. 2018;53(4):309-13.
414. Arcadu F, Benmansour F, Maunz A, et al. Deep learning algorithm predicts diabetic retinopathy progression in individual patients. *NPJ Digit Med*. 2019;2:92.
415. De Fauw J, Ledsam JR, Romera-Paredes B, et al. Clinically applicable deep learning for diagnosis and referral in retinal disease. *Nat Med*. 2018;24(9):1342-50.
416. Livia Faes SKW, Dun Jack Fu, Xiaoxuan Liu, Edward Korot, Joseph R Ledsam, Trevor Back, Reena Chopra, Nikolas Pontikos, Christoph Kern, Gabriella Moraes, Martin K Schmid, Dawn Sim, Konstantinos Balaskas, Lucas M Bachmann, Alastair K Denniston, Pearse A Keane. Automated deep learning design for medical image classification by health-care professionals with no coding experience: a feasibility study. *The Lancet Digital Health*. 2019;1(5):e232-e42.
417. Augsburger J, Schroeder R, Territo C, et al. Clinical parameters predictive of enlargement of melanocytic choroidal lesions. *British journal of ophthalmology*. 1989;73(11):911-7.
418. Snyder H. Literature review as a research methodology: An overview and guidelines. *Journal of business research*. 2019;104:333-9.
419. Damato B. Ocular treatment of choroidal melanoma in relation to the prevention of metastatic death - A personal view. *Prog Retin Eye Res*. 2018.
420. Damato EM, Damato BE. Detection and Time to Treatment of Uveal Melanoma in the United Kingdom: An Evaluation of 2384 Patients. *Ophthalmology*. 2012.

- 
421. Damato EM, Damato BE. Detection and time to treatment of uveal melanoma in the United Kingdom: an evaluation of 2,384 patients. *Ophthalmology*. 2012;119(8):1582-9.
422. Damato BE. Can the MOLES acronym and scoring system improve the management of patients with melanocytic choroidal tumours? *Eye (Lond)*. 2022;1-7.
423. Group COMS. Comparison of clinical, echographic, and histopathological measurements from eyes with medium-sized choroidal melanoma in the collaborative ocular melanoma study: COMS report no. 21. *Archives of ophthalmology (Chicago, Ill: 1960)*. 2003;121(8):1163-71.
424. Augsburger JJ, Schroeder RP, Territo C, et al. Clinical parameters predictive of enlargement of melanocytic choroidal lesions. *Br J Ophthalmol*. 1989;73(11):911-7.
425. Dalvin LA, Shields CL, Ancona-Lezama DA, et al. Combination of multimodal imaging features predictive of choroidal nevus transformation into melanoma. *Br J Ophthalmol*. 2019;103(10):1441-7.
426. Almeida A, Kaliki S, Shields CL. Autofluorescence of intraocular tumours. *Curr Opin Ophthalmol*. 2013;24(3):222-32.
427. Riechardt AI, Gundlach E, Jousseaume AM, Willerding GD. The Development of Orange Pigment Overlying Choroidal Metastasis. *Ocul Oncol Pathol*. 2015;1(2):93-7.
428. Fry MV, Augsburger JJ, Hall J, Corrêa ZM. Posterior uveal melanoma in adolescents and children: current perspectives. *Clinical Ophthalmology (Auckland, NZ)*. 2018;12:2205.
429. Damato BE, Foulds WS. Tumour-associated retinal pigment epitheliopathy. *Eye (Lond)*. 1990;4 ( Pt 2):382-7.
430. Roelofs KA, O'Day R, Harby LA, et al. The MOLES System for Planning Management of Melanocytic Choroidal Tumors: Is It Safe? *Cancers (Basel)*. 2020;12(5).
431. Flanagan JP, O'Day RF, Roelofs KA, et al. The MOLES system to guide the management of melanocytic choroidal tumours: can optometrists apply it? *Clin Exp Optom*. 2022;1-5.
432. Hemmerdinger C, Beech M, Groenewald C, Damato B. Validation of an online referral guide for melanocytic fundus lesions. *Ophthalmic Physiol Opt*. 2011;31(6):574-9.
433. Torres R, Lang UE, Hejna M, et al. MicroRNA ratios distinguish melanomas from nevi. *J Invest Dermatol*. 2019.
434. Roelofs KA, O'Day R, Harby LA, et al. Reply to Comment on Roelofs, KA; et al. "Detecting Progression of Melanocytic Choroidal Tumours by Sequential Imaging: Is Ultrasonography Necessary?" *Cancers* 2020, 12, 1856. *Cancers*. 2021;13(6):1320.
435. Shields JA, Mashayekhi A, Ra S, Shields CL. Pseudomelanomas of the posterior uveal tract: the 2006 Taylor R. Smith Lecture. *Retina*. 2005;25(6):767-71.
436. Kivelä T, Eskelin S. Transformation of nevus to melanoma. *Ophthalmology*. 2006;113(5):887-8 e1.
437. Char DH. *Tumors of the eye and ocular adnexa*: BC Decker, 2001.
438. Damato BE, Singh AD. *Clinical Ophthalmic Oncology*, 3 ed. Switzerland Springer International Publishing, 2019.
439. Damato B. Ocular treatment of choroidal melanoma in relation to the prevention of metastatic death - A personal view. *Prog Retin Eye Res*. 2018;66:187-99.
440. Hanson C, Tennant MT, Rudnisky CJ. Optometric referrals to retina specialists: evaluation and triage via teleophthalmology. *Telemed J E Health*. 2008;14(5):441-5.

441. Resnikoff S, Felch W, Gauthier TM, Spivey B. The number of ophthalmologists in practice and training worldwide: a growing gap despite more than 200,000 practitioners. *Br J Ophthalmol*. 2012;96(6):783-7.
442. Bellan L, Buske L, Wang S, Buys YM. The landscape of ophthalmologists in Canada: present and future. *Can J Ophthalmol*. 2013;48(3):160-6.
443. Jones S, Edwards RT. Diabetic retinopathy screening: a systematic review of the economic evidence. *Diabet Med*. 2010;27(3):249-56.
444. Jonas JB, You QS, Xu L, Wang YX. Choroidal nevi in adult chinese. *Ophthalmology*. 2008;115(6):1102- e1.
445. Greenstein MB, Myers CE, Meuer SM, et al. Prevalence and characteristics of choroidal nevi: the multi-ethnic study of atherosclerosis. *Ophthalmology*. 2011;118(12):2468-73.
446. Ng CH, Wang JJ, Mitchell P, et al. Prevalence and characteristics of choroidal nevi in an Asian vs white population. *Arch Ophthalmol*. 2009;127(3):314-9.
447. Nangia V, Jonas JB, Agarwal S, et al. Choroidal nevi in adult Indians: The Central India Eye and Medical Study. *Br J Ophthalmol*. 2012;96(11):1443-4.
448. Al-Harby L, Sagoo M, O'Day R, et al. External validation of the MOLES scoring system for estimating risk of malignancy in melanocytic choroidal tumors. *In Press*. 2020.
449. Gass JD. Observation of suspected choroidal and ciliary body melanomas for evidence of growth prior to enucleation. *Ophthalmology*. 1980;87(6):523-8.
450. Doro D, Kotsafti O, Cimatti P. Long-term echographic surveillance of elevated choroidal nevi. *Am J Ophthalmol*. 2013;156(3):438-43 e1.
451. Barsam AS, Gibbons A, McClellan AJ, et al. Follow the nevus: the cost-utility of monitoring for growth of choroidal nevi. *Int J Ophthalmol*. 2019;12(9):1456-64.
452. McHugh ML. Interrater reliability: the kappa statistic. *Biochem Med (Zagreb)*. 2012;22(3):276-82.
453. [https://www.statology.org/cohens-kappa-calculator/#:~:text=Cohen's%20kappa%20measures%20the%20level%20of%20agreement%20between%20wApoAR](https://www.statology.org/cohens-kappa-calculator/#:~:text=Cohen's%20kappa%20measures%20the%20level%20of%20agreement%20between%20wApoAR,Cohen's Kappa Calculator). Cohen's Kappa Calculator.
454. <https://www.real-statistics.com/reliability/interrater-reliability/weighted-cohens-kappa/>. Weighted Cohen's Kappa.
455. <https://openintro-ims.netlify.app/foundations-bootstrapping.html#:~:text=We%20can%20summarize%20the%20bootstrap%20process%20as%20follows%3A> ti. Confidence intervals with bootstrapping.
456. Ophthalmologists 'TRCo. Referral pathways for adult ocular tumours. 2020.
457. Kern C, Kortuem K, Hamilton R, et al. Clinical Outcomes of a Hospital-Based Teleophthalmology Service: What Happens to Patients in a Virtual Clinic? *Ophthalmol Retina*. 2019;3(5):422-8.
458. Scott DAR, Hadden PW, Wilson GA. Impact of the COVID-19 pandemic lockdown on public sector ophthalmic work by New Zealand's ophthalmologists. *N Z Med J*. 2021;134(1538):120-7.
459. Gallenga CE, Agnifili L, D'Aloisio R, et al. Virtual learning solutions in COVID-19 era: University Italian Ophthalmology department perspective. *Eur J Ophthalmol*. 2021;32(2):11206721211015576.
460. Safadi K, Kruger JM, Chowes I, et al. Ophthalmology practice during the COVID-19 pandemic. *BMJ open ophthalmology*. 2020;5(1):e000487.
461. <https://checkout.moorfields.nhs.uk/catalog?pagename=Virtual-Observership>. Virtual Observership Programme.



462. Rutherford E, Noray R, HEarráin CÓ, et al. Potential benefits and drawbacks of virtual clinics in general surgery: pilot cross-sectional questionnaire study. *JMIR perioperative medicine*. 2020;3(1):e12491.
463. El-Khayat AR, Anzidei R, Konidaris V. Ophthalmic photographer virtual clinics in medical retina. *International Journal of Ophthalmology*. 2020;13(4):677.
464. Roelofs KA, O'Day R, Harby LA, et al. Reply to Comment on Roelofs, K.A.; et al. "Detecting Progression of Melanocytic Choroidal Tumours by Sequential Imaging: Is Ultrasonography Necessary?" *Cancers* 2020, 12, 1856. *Cancers (Basel)*. 2021;13(6).
465. <https://www.gehealthcare.com/article/beyond-imagingthe-paradox-of-ai-and-medical-imaging-innovation>. Beyond Imaging:the paradox of AI and medical imaging innovation.
466. LeCun Y, Bengio Y, Hinton G. Deep learning. *Nature*. 2015;521(7553):436-44.
467. Hestness J, Ardalani N, Diamos G. Beyond human-level accuracy: Computational challenges in deep learning. *Proceedings of the 24th Symposium on Principles and Practice of Parallel Programming*2019.
468. Pei K, Cao Y, Yang J, Jana S. Deepxplore: Automated whitebox testing of deep learning systems. *proceedings of the 26th Symposium on Operating Systems Principles*2017.
469. Lamis Al Harby EK, Sara E. Lally, Sandor Ferenczy, Lauren A. Dalvin, Marco Pellegrini, Jay Duker, Adrian Fung, Swathi Kaliki, Kaan Gunduz, Minoru Furuta, Antonio Yaghy, Carol Shields, Prithvi Mruthyunjaya, Mandeep S. Sagoo. White paper on Artificial Intelligence in ocular oncology: Differentiating benign choroidal nevus from choroidal melanoma. *Ophthalmology*. 2022:In press.
470. Schmidt-Erfurth U, Sadeghipour A, Gerendas BS, et al. Artificial intelligence in retina. *Progress in retinal and eye research*. 2018;67:1-29.
471. Food, Administration D. Device classification under Section 513 (f)(2)(de novo). 2018.
472. Adnan M, Kalra S, Cresswell JC, et al. Federated learning and differential privacy for medical image analysis. *Scientific Reports*. 2022;12(1):1-10.
473. <https://fda.report/PMN/K192854>. [MammoScreen].
474. <https://www.massdevice.com/3derm-lands-fda-breakthrough-device-designations-for-autonomous-skin-cancer-ai/>. 3Derm lands FDA breakthrough device designations for autonomous skin cancer AI.
475. <https://www.fda.gov/medical-devices/device-advice-comprehensive-regulatory-assistance/medical-device-databases>. Medical Device Databases [FDA].
476. <https://www.fda.gov/medical-devices/software-medical-device-samd/artificial-intelligence-and-machine-learning-software-medical-device>. Artificial Intelligence and Machine Learning (AI/ML) Software as a Medical Device Action Plan.
477. <https://www.fda.gov/media/100714/download>. Software as a Medical Device (SAMD): Clinical Evaluation.
478. Weinstock MA. Progress and prospects on melanoma: the way forward for early detection and reduced mortality. *Clinical cancer research*. 2006;12(7):2297s-300s.
479. Rigel DS, Friedman RJ, Kopf AW, Polsky D. ABCDE—an evolving concept in the early detection of melanoma. *Archives of dermatology*. 2005;141(8):1032-4.
480. Lindholm C, Andersson R, Dufmats M, et al. Invasive cutaneous malignant melanoma in Sweden, 1990-1999: A prospective, population - based study of survival and prognostic factors. *Cancer*. 2004;101(9):2067-78.

- 
481. Pampena R, Kyrgidis A, Lallas A, et al. A meta-analysis of nevus-associated melanoma: Prevalence and practical implications. *Journal of the American Academy of Dermatology*. 2017;77(5):938-45. e4.
482. Elbaum M, Kopf AW, Rabinovitz HS, et al. Automatic differentiation of melanoma from melanocytic nevi with multispectral digital dermoscopy: a feasibility study. *Journal of the American Academy of Dermatology*. 2001;44(2):207-18.
483. Food U, Administration D. Artificial intelligence and machine learning in software as a medical device. Silver Spring: US Food and Drug Administration. 2019.
484. Jaworek-Korjakowska J, Kłeczek P. Automatic Classification of Specific Melanocytic Lesions Using Artificial Intelligence. *Biomed Res Int*. 2016;2016:8934242.
485. Brinker TJ, Hekler A, Enk AH, et al. Deep learning outperformed 136 of 157 dermatologists in a head-to-head dermoscopic melanoma image classification task. *Eur J Cancer*. 2019;113:47-54.
486. Bærøe K, Miyata-Sturm A, Henden E. How to achieve trustworthy artificial intelligence for health. *Bulletin of the World Health Organization*. 2020;98(4):257.
487. Nordling L. A fairer way forward for AI in health care. *Nature*. 2019;573(7775):S103-s5.
488. Faes L, Wagner SK, Fu DJ, et al. Automated deep learning design for medical image classification by health-care professionals with no coding experience: a feasibility study. *The Lancet Digital Health*. 2019;1(5):e232-e42.
489. Poplin R, Varadarajan AV, Blumer K, et al. Prediction of cardiovascular risk factors from retinal fundus photographs via deep learning. *Nature Biomedical Engineering*. 2018;2(3):158-64.
490. Korot E, Pontikos N, Liu X, et al. Predicting sex from retinal fundus photographs using automated deep learning. *Scientific reports*. 2021;11(1):1-8.
491. Barret Zoph VV, Jonathon Shlens and Quoc Le, Research Scientists, Google Brain Team AutoML for large scale image classification and object detection. *Google AI Blog* 2017.
492. Barret Zoph QVL. Neural architecture search with reinforcement learning. 2017.
493. Roelofs KA, O'Day R, Al Harby L, et al. The MOLES system for planning management of melanocytic choroidal tumors: is it safe? *Cancers*. 2020; In Press.
494. Korot E, Guan Z, Ferraz D, et al. Code-free deep learning for multi-modality medical image classification. *Nature Machine Intelligence*. 2021:1-11.
495. <https://www.applause.com/blog/training-data-validation-data-vs-test-data>. Training Data vs. Validation Data vs. Test Data for ML Algorithms.
496. <https://www.nvidia.com/en-gb/data-center/tesla-v100/>. Welcome to the era of AI.
497. <https://cloud.google.com/vision/automl/docs/beginners-guide>. AutoML Vision Beginner's guide.
498. <https://cloud.google.com/automl-tables/docs/evaluate#score-threshold>. Evaluating models in Google AutoML.
499. <https://www.geeksforgeeks.org/precision-recall-curve-ml/>. Precision-Recall Curve | ML.
500. [https://docs.w3cub.com/scikit\\_learn/auto\\_examples/model\\_selection/plot\\_precision\\_recall.html](https://docs.w3cub.com/scikit_learn/auto_examples/model_selection/plot_precision_recall.html). Precision-Recall.
501. [https://bookdown.org/jkylearmstrong/jeff\\_data\\_wrangling/two-factor-classification-with-a-single-continuous-feature.html](https://bookdown.org/jkylearmstrong/jeff_data_wrangling/two-factor-classification-with-a-single-continuous-feature.html). 6 Two Factor Classification with a Single Continuous Feature.
-

- 
502. <https://www.geeksforgeeks.org/calculate-efficiency-binary-classifier/>. Calculate Efficiency Of Binary Classifier.
503. <https://neptune.ai/blog/f1-score-accuracy-roc-auc-pr-auc>. F1 Score vs ROC AUC vs Accuracy vs PR AUC: Which Evaluation Metric Should You Choose?
504. <https://medium.com/@lucasov/solving-the-mystery-of-google-cloud-automl-metrics-3251131b8ee6>. Solving the Mystery of Google Cloud AutoML Metrics.
505. <https://www.datarobot.com/wiki/interpretability/>. Model Interpretability in Machine Learning
- .
506. <https://www.r-bloggers.com/2020/06/why-balancing-your-data-set-is-important/>, <https://towardsdatascience.com/dealing-with-imbalanced-dataset-642a5f6ee297>. Why balancing your data set is important?
507. Beleites C, Neugebauer U, Bocklitz T, et al. Sample size planning for classification models. *Analytica chimica acta*. 2013;760:25-33.
508. <https://towardsdatascience.com/classification-metrics-thresholds-explained-caff18ad2747>. Classification Metrics & Thresholds Explained.
509. Shields CL, Pefkianaki M, Mashayekhi A, et al. Cytogenetic results of choroidal nevus growth into melanoma in 55 consecutive cases. *Saudi Journal of Ophthalmology*. 2018;32(1):28-32.
510. <https://www.reviewofophthalmology.com/article/ai-and-ophthalmology-the-pros-and-cons>. AI & Ophthalmology: The Pros and Cons.
511. Pisarchik AN, Maksimenko VA, Hramov AE. From Novel Technology to Novel Applications: Comment on "An Integrated Brain-Machine Interface Platform With Thousands of Channels" by Elon Musk and Neuralink. *J Med Internet Res*. 2019;21(10):e16356.
512. <https://www.thebalancecareers.com/artificial-intelligence-is-changing-your-career-in-medicine-4586781>. How Artificial Intelligence is Changing Your Career in Medicine.
513. <https://www.theguardian.com/society/2018/may/29/skin-cancer-computer-learns-to-detect-skin-cancer-more-accurately-than-a-doctor>. Computer learns to detect skin cancer more accurately than doctors.
514. Hosny A, Parmar C, Quackenbush J, et al. Artificial intelligence in radiology. *Nat Rev Cancer*. 2018;18(8):500-10.
515. Pantanowitz L, Quiroga-Garza GM, Bien L, et al. An artificial intelligence algorithm for prostate cancer diagnosis in whole slide images of core needle biopsies: a blinded clinical validation and deployment study. *Lancet Digit Health*. 2020;2(8):e407-e16.
516. Varadarajan AV, Bavishi P, Ruamviboonsuk P, et al. Predicting optical coherence tomography-derived diabetic macular edema grades from fundus photographs using deep learning. *Nat Commun*. 2020;11(1):130.
517. Inozemtsev V, Ivleva M, Ivlev V. Artificial intelligence and the problem of computer representation of knowledge. 2nd International Conference on Contemporary Education, Social Sciences and Humanities (ICCESSH 2017): Atlantis Press, 2017.
518. <https://www.aain.healthcare/topics/emerging-technologies/computer-vision-icu-concerns-privacy-lawsuits>. Computer vision holds promise for the ICU but may face opposition from clinicians, patients, families.
519. [https://www.nhsx.nhs.uk/media/documents/NHSX\\_AI\\_report.pdf](https://www.nhsx.nhs.uk/media/documents/NHSX_AI_report.pdf). Artificial Intelligence: How to get it right.
-

- 
520. <https://www.modernhealthcare.com/indepth/artificial-intelligence-in-healthcare-makes-slow-impact/>. The slow upgrade to artificial intelligence.
521. <https://www.ft.com/content/0e086832-5c5c-11ea-8033-fa40a0d65a98>. Trusting AI too much can turn out to be fata.
522. <https://m-cacm.acm.org/magazines/2018/9/230593-overtrust-in-the-robotic-age/fulltext?mobile=true>. Overtrust in the Robotic Age.
523. <https://core.ac.uk/download/pdf/7306882.pdf>. Human performance, awareness situation and automation.
524. Zech JR, Badgeley MA, Liu M, et al. Variable generalization performance of a deep learning model to detect pneumonia in chest radiographs: A cross-sectional study. *PLoS Med*. 2018;15(11):e1002683.
525. <https://www.cerner.com/cernerhealthforum>. Leverage data, information and intelligence to improve clinical decision-making.
526. Amann J, Blasimme A, Vayena E, et al. Explainability for artificial intelligence in healthcare: a multidisciplinary perspective. *BMC Med Inform Decis Mak*. 2020;20(1):310.
527. <https://www.wired.com/story/google-ai-tool-identifies-a-tumors-mutations-from-an-image/>. Google AI Tool Identifies a Tumor's Mutations From an Image.
528. Mosavi A, Varkonyi-Koczy AR. Integration of machine learning and optimization for robot learning. *Recent Global Research and Education: Technological Challenges*: Springer, 2017.
529. Goh JHL, Lim ZW, Fang X, et al. Artificial Intelligence for Cataract Detection and Management. *Asia Pac J Ophthalmol (Phila)*. 2020;9(2):88-95.
530. Altman DG, Royston P. What do we mean by validating a prognostic model? *Stat Med*. 2000;19(4):453-73.
531. Nelson GS. Bias in artificial intelligence. *North Carolina medical journal*. 2019;80(4):220-2.
532. Challen R, Denny J, Pitt M, et al. Artificial intelligence, bias and clinical safety. *BMJ Quality & Safety*. 2019;28(3):231-7.
533. Reddy S, Allan S, Coghlan S, Cooper P. A governance model for the application of AI in health care. *J Am Med Inform Assoc*. 2020;27(3):491-7.
534. Buolamwini J, Gebru T. Gender shades: Intersectional accuracy disparities in commercial gender classification. *Conference on fairness, accountability and transparency*: PMLR, 2018.
535. Parikh RB, Teeple S, Navathe AS. Addressing Bias in Artificial Intelligence in Health Care. *Jama*. 2019.
536. Liu X, Faes L, Kale AU, et al. A comparison of deep learning performance against health-care professionals in detecting diseases from medical imaging: a systematic review and meta-analysis. *Lancet Digit Health*. 2019;1(6):e271-e97.
537. <https://www.fda.gov/medical-devices/classify-your-medical-device/how-determine-if-your-product-medical-device>. U.S. Food & Drug Administration (2018) Is The Product A Medical Device? U.S. Department of Health and Human Services.
538. Tsang L, Kracov DA, Mulryne J, et al. The impact of artificial intelligence on medical innovation in the European Union and United States. *Intellect Prop Technol Law J*. 2017;29(8):3-12.
539. <https://news.bloomberglaw.com/tech-and-telecom-law/fda-signals-fast-track-approval-for-ai-based-medical-devices-1>. FDA Signals Fast-Track Approval for AI-Based Medical Devices.

- 
540. <https://www.nature.com/articles/s41746-020-00324-0/tables/2>. Database of the 29 FDA-approved, AI/ML-based medical technologies.
541. <https://aicentral.acrdsi.org>. ACR Data Science Institute AI Central.
542. Giovanni Sartor FL. The impact of the General Data Protection Regulation (GDPR) on artificial intelligence. In: EPRS, ed. Brussels © European Union: Panel for the Future of Science and Technology (STOA), 2020.
543. Jackson BR, Ye Y, Crawford JM, et al. The Ethics of Artificial Intelligence in Pathology and Laboratory Medicine: Principles and Practice. *Academic Pathology*. 2021;8:2374289521990784.
544. Botkin JR, Rothwell E, Anderson R, et al. Public attitudes regarding the use of electronic health information and residual clinical tissues for research. *J Community Genet*. 2014;5(3):205-13.
545. Portability I, Act A. Guidance Regarding Methods for De-identification of Protected Health Information in Accordance with the Health Insurance Portability and Accountability Act (HIPAA) Privacy Rule. 2012.
546. Rocher L, Hendrickx JM, de Montjoye YA. Estimating the success of re-identifications in incomplete datasets using generative models. *Nat Commun*. 2019;10(1):3069.
547. Schiff D, Borenstein J. How Should Clinicians Communicate With Patients About the Roles of Artificially Intelligent Team Members? *AMA J Ethics*. 2019;21(2):E138-45.
548. Demuro PR, Petersen C. Managing Privacy and Data Sharing Through the Use of Health Care Information Fiduciaries. *Stud Health Technol Inform*. 2019;265:157-62.
549. Chung J, Zink A. Hey Watson-Can I Sue You for Malpractice-Examining the Liability of Artificial Intelligence in Medicine. *Asia Pacific J Health L & Ethics*. 2017;11:51.
550. Jiang JX, Bai G. Types of Information Compromised in Breaches of Protected Health Information. *Ann Intern Med*. 2020;172(2):159-60.
551. Thomas SM, Mamlin B, Schadow G, McDonald C. A successful technique for removing names in pathology reports using an augmented search and replace method. *Proc AMIA Symp*. 2002:777-81.
552. <https://www.ama-assn.org/system/files/2019-01/augmented-intelligence-policy-report.pdf>. Augmented intelligence in health care.
553. Hacker P, Krestel R, Grundmann S, Naumann F. Explainable AI under contract and tort law: legal incentives and technical challenges. *Artificial Intelligence and Law*. 2020:1-25.
554. <https://www.linklaters.com/en/insights/blogs/digilinks/eu--the-implementation-of-the-cyber-security-directive>. EU – The implementation of the “Cyber Security” Directive.
555. Pesapane F, Volonté C, Codari M, Sardanelli F. Artificial intelligence as a medical device in radiology: ethical and regulatory issues in Europe and the United States. *Insights into imaging*. 2018;9(5):745-53.
556. Guidelines on the Qualification and Classification of Stand Alone Software used in Healthcare within the Regulatory Framework of Medical Devices. 2016; v. MEDDEV 2.1/6.
557. <https://ec.europa.eu/docsroom/documents/28668>. European Commission (2018) MDCG 2018–2 Future EU medical device nomenclature – Description of requirements. Available via.
558. [https://ec.europa.eu/growth/single-market/european-standards/harmonised-standards/iv-diagnostic-medical-devices\\_en](https://ec.europa.eu/growth/single-market/european-standards/harmonised-standards/iv-diagnostic-medical-devices_en). European Commission (1998) Directive
-

- 98/79/EC of the European Parliament and of the Council on in vitro diagnostic medical devices. Official Journal of the European Communities.
559. <https://eur-lex.europa.eu/legal-content/EN/TXT/?uri=CELEX%3A32017R0745>. The European Parliament and the Council of The European Union (2017) Regulation (EU) 2017/745 of the European Parliament and of the Council on medical devices, amending Directive 2001/83/EC, Regulation (EC) No 178/2002 and Regulation (EC) No 1223/2009 and repealing Council Directives 90/385/EEC and 93/42/EEC. Official Journal of the European Communities.
560. Organization WH. WHO guideline: recommendations on digital interventions for health system strengthening: web supplement 2: summary of findings and GRADE tables. World Health Organization, 2019.
561. Zandi D, Reis A, Vayena E, Goodman K. New ethical challenges of digital technologies, machine learning and artificial intelligence in public health: a call for papers. Bulletin of the World Health Organization. 2019;97(1):2-.
562. Goodman K, Zandi D, Reis A, Vayena E. Balancing risks and benefits of artificial intelligence in the health sector. Bulletin of the World Health Organization. 2020;98(4):230.
563. Nelson CA, Pérez-Chada LM, Creadore A, et al. Patient Perspectives on the Use of Artificial Intelligence for Skin Cancer Screening: A Qualitative Study. JAMA Dermatology. 2020;156(5):501-12.
564. Tran VT, Riveros C, Ravaud P. Patients' views of wearable devices and AI in healthcare: findings from the ComPaRe e-cohort. NPJ Digit Med. 2019;2:53.
565. Patel BN, Rosenberg L, Willcox G, et al. Human-machine partnership with artificial intelligence for chest radiograph diagnosis. NPJ digital medicine. 2019;2(1):1-10.
566. <https://psu.pb.unizin.org/ist110/chapter/5-2-human-computer-interaction/>. Human-computer Interaction.
567. <https://www.computerworld.com/article/3004013/why-human-in-the-loop-computing-is-the-future-of-machine-learning.html>. Why human-in-the-loop computing is the future of machine learning.
568. Char DS, Shah NH, Magnus D. Implementing Machine Learning in Health Care - Addressing Ethical Challenges. N Engl J Med. 2018;378(11):981-3.

## APPENDICES

### Appendix 1 – Guide for diagnostic hub technicians to collect patients history for virtual naevus clinics

#### **Naevus New**

1. Confirm ID – name/Dob/1<sup>st</sup> line of address

#### 2. HISTORY & DURATION

- Reduced Vision: Yes/No
- Photopsia: Yes/No
- Pain: Yes/No
- Lump: Yes/No
- Other

#### 3. PAST OCULAR HISTORY

- Wearing glasses? Contact lenses?
- Any eye surgery in the past?
- Any previous issues with your eyes?
- Are you under any other eye clinics?

#### 4. PAST MEDICAL HISTORY

- Dysplastic Naevus Syndrome?
- Any history of Skin Moles?
- Any History of Cancer?
- Any History of Cardiac problems?
- Any other past medical history: Yes/No

#### 5. DRUG HISTORY

#### 6. ANTICUAGULANTS

#### 7. ALLERGIES

#### 8. SOCIAL HISTORY

- Smoking?
- Alcohol?
- Sunlight Exposure / Outdoor Hobbies?

## 9. FAMILY HISTORY

- Any of the family has Dysplastic Naevus Syndrome?
- Any history of Cancer in the family?

### **Naevus Follow-up**

1. ID confirmed: Yes / No
2. Any new symptoms: Yes / No
  - If Yes: What? / Duration?
3. Vision: Better / Stable / Worse
  - If worse: Gradual / Sudden/Duration
4. Pregnant: Yes / No / Not applicable
5. Any significant recent medical events?
6. Any recent changes to medications?
7. Preferred contact number:

### **Orientation screening questions**

Orientation screening questions to assess mental capacity

#### 1. TIME:

- Day=
- Month=
- Year=

#### 2. PLACE:

- Home=
- Where are we now?=  
• Do you know why you are here today?=

#### 3. PERSON

- Name=
- DOB=
- What job do I do? (after an earlier introduction)=



## Appendix 2 – AutoML screenshots of AF and CL model evaluation

### Overview - all Datasets (AF + CL)

Name	Type	Total images	Labelled images	Last updated	Status	Migrated
naevus2_melanoma_cl ICN7344327555706519552	Single-Label Classification	200	200	30 Sept 2020, 09:48:25	Success: Exporting data	No
naevus_melanoma_af ICN4403125155312697344	Single-Label Classification	199	199	28 Sept 2020, 10:16:02	Success: Exporting data	No
naevus_melanoma_af ICN3498746055141359616	Single-Label Classification	199	199	28 Sept 2020, 10:13:09	Warning: Importing images	No
naevus_melanoma_cl ICN6766081196519587840	Single-Label Classification	200	200	25 Sept 2020, 12:37:48	Success: Training model	No
naevus_melanoma_cl ICN6585937211424768000	Single-Label Classification	196	196	24 Sept 2020, 22:09:15	Warning: Importing images	No

### AF model

#### Labelled images of dataset 'naevus\_melanoma\_af' for training

naevus\_melanoma\_af | LABEL STATS | EXPORT DATA

IMPORT | IMAGES | TRAIN | EVALUATE | TEST & USE | Single-Label Classification

All images: 199 | Filter: Filter images

Labelled: 199 | Unlabelled: 0 | Select all

Filter: Filter label

- melanoma: 81
- nevus: 118

ADD NEW LABEL

nevus(1) | nevus(1) | melanoma(1) | nevus(1)

nevus(1) | nevus(1) | melanoma(1) | nevus(1)

nevus(1) | nevus(1) | melanoma(1) | nevus(1)

Developed models (4) for AF dataset

The screenshot shows the Google Cloud Platform Vision API interface. The main content area displays the details for a model named 'naevus\_melanoma\_af'. The model ID is 'naev\_mel\_af\_harby20220605114846'. The average precision is 0.933, with both precision and recall at 85.71%. The model was created on 5 Jun 2022 at 11:49:53. It is based on 'None' and trained on 199 images. The model type is 'Cloud', with a train cost of 8 node hours and a deployment state of 'Not deployed'. The interface includes a 'TRAIN NEW MODEL' button and links for 'SEE FULL EVALUATION' and 'RESUME TRAINING'.

Model ID	ICN3542293312671055872
Created	5 Jun 2022, 11:49:53
Base model	None
Data	199 images
Model type	Cloud
Train cost	8 node hours
Deployment state	Not deployed

Model ID: naevus3\_melanoma\_a20220604074411  
 Average precision: 0.884  
 Precision\*: 80.95%  
 Recall\*: 80.95%  
 \* Using a score threshold of 0.5

Model ID	ICN4619779523519447040
Created	4 Jun 2022, 19:44:33
Base model	ICN6837802339999416320
Data	199 images
Model type	Cloud
Train cost	0.308 node hours
Deployment state	Not deployed

Model ID: naevus2\_melanoma\_a20220604050706  
 Average precision: 0.951  
 Precision\*: 80.95%  
 Recall\*: 80.95%  
 \* Using a score threshold of 0.5

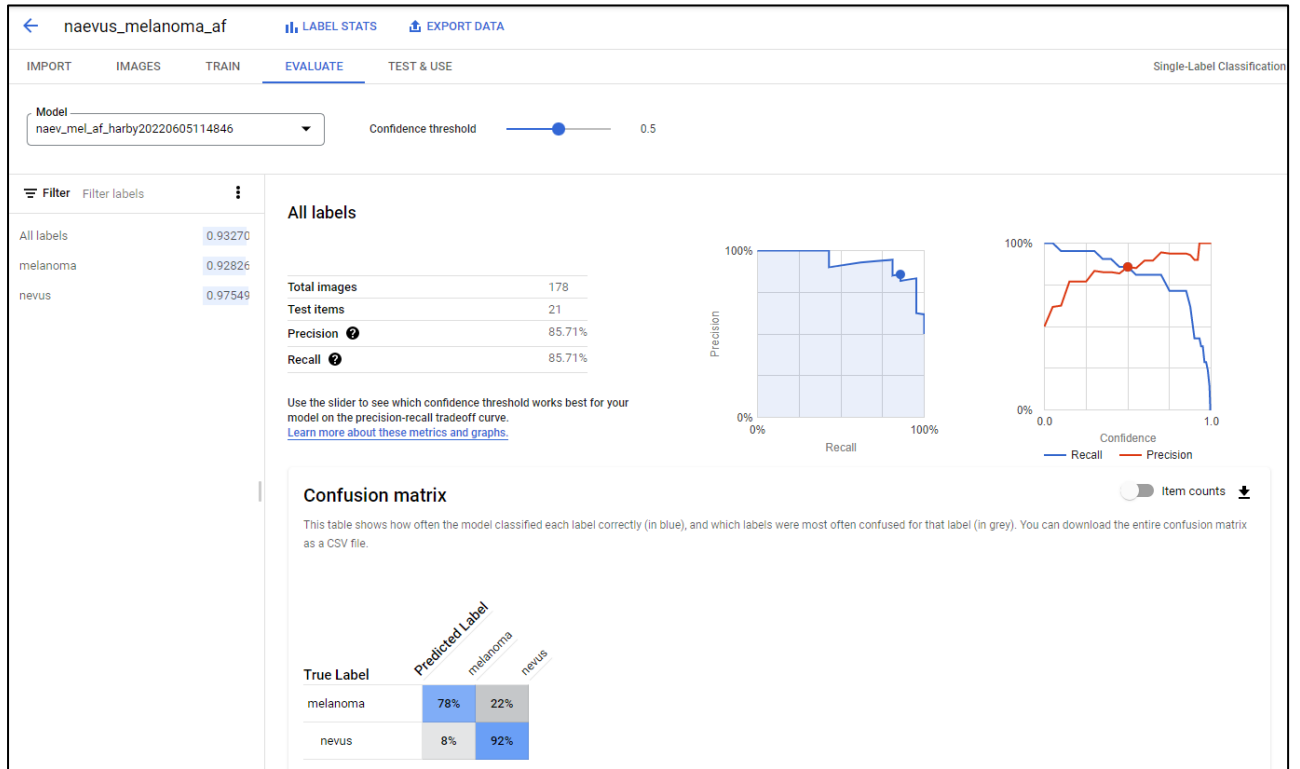
Model ID	ICN6837802339999416320
Created	4 Jun 2022, 17:12:16
Base model	None
Data	199 images
Model type	Cloud
Train cost	16 node hours
Deployment state	Not deployed

Model ID: naevus\_melanoma\_af20200928110354  
 Average precision: 0.915  
 Precision\*: 76.19%  
 Recall\*: 76.19%  
 \* Using a score threshold of 0.5

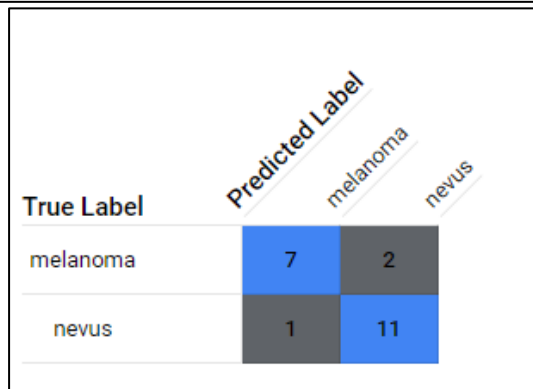
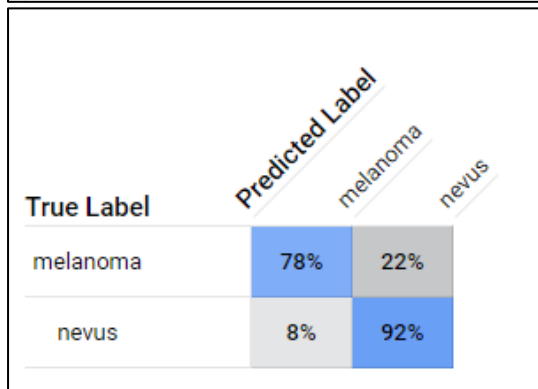
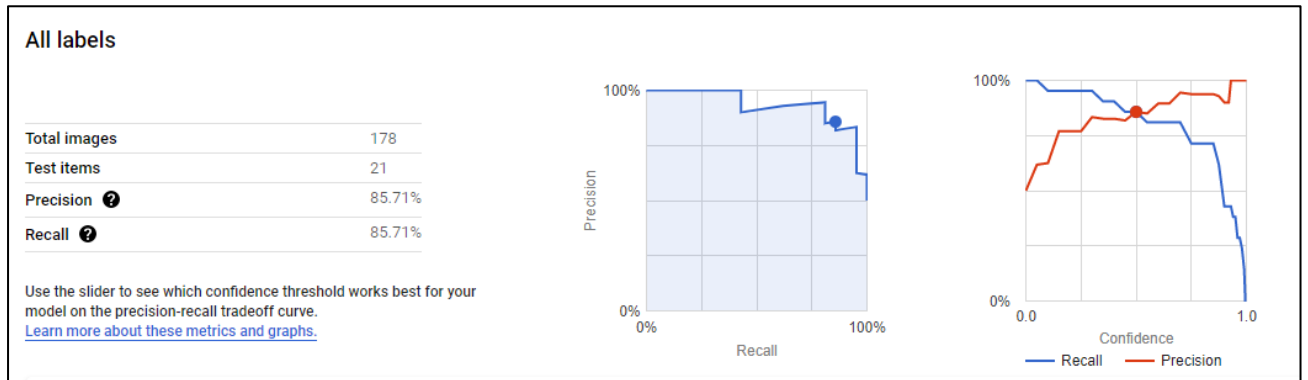
Model ID	ICN631157057738768384
Created	28 Sept 2020, 11:07:03
Base model	None
Data	199 images
Model type	Cloud
Train cost	8 node hours
Deployment state	Not deployed

Full evaluation of best performing AF model 'naev\_mel\_af\_harby20220605114846'

Overview



AF – all labels



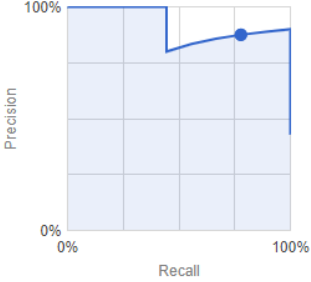
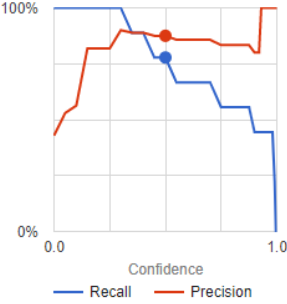
## AF - melanoma

**melanoma**

Total images	178
Test items	0
Precision	87.5%
Recall	77.78%

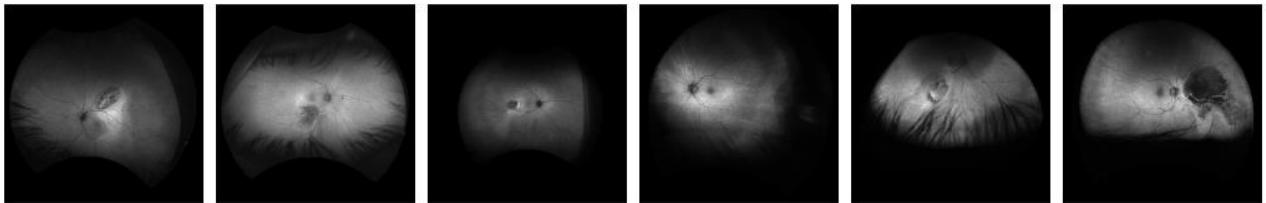
Use the slider to see which confidence threshold works best for your model on the precision-recall tradeoff curve.  
[Learn more about these metrics and graphs.](#)

All test images are evaluated at the time of training. If you modify your data set after training, these results will not be accurate.

### True positives

Your model correctly predicted **melanoma** on these images



Score: 0.5120067

Score: 0.73363274

Score: 0.87809765

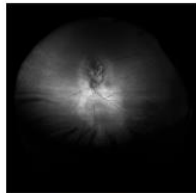
Score: 0.9808747

Score: 0.9880843

Score: 0.9923701

### True positives

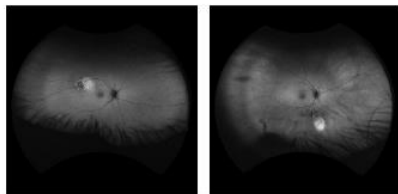
Your model correctly predicted **melanoma** on these images



Score: 0.9930582

### False negatives

Your model should have predicted **melanoma** on these images

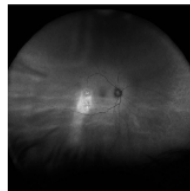


Score(s): 0.34422445

Score(s): 0.42903364

### False positives

Your model incorrectly predicted **melanoma** on these images



Score: 0.9212093

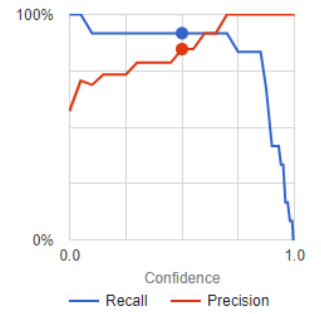
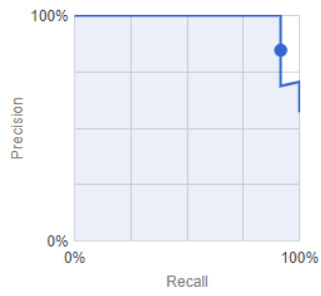
## AF – nevus

### nevus

Total images	178
Test items	0
Precision ?	84.62%
Recall ?	91.67%

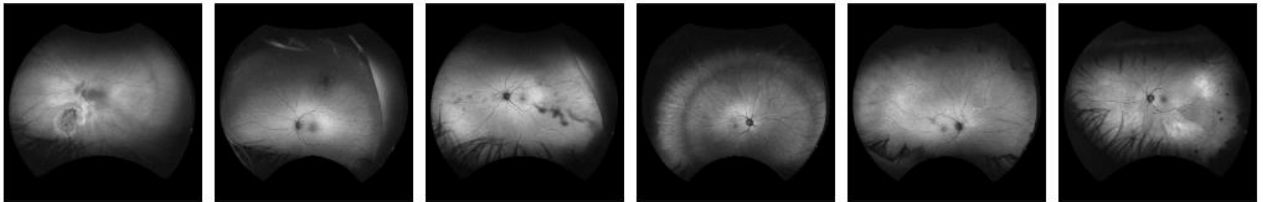
Use the slider to see which confidence threshold works best for your model on the precision-recall tradeoff curve.  
[Learn more about these metrics and graphs.](#)

All test images are evaluated at the time of training. If you modify your data set after training, these results will not be accurate.



### True positives

Your model correctly predicted nevus on these images



Score: 0.7374459

Score: 0.85228705

Score: 0.8529701

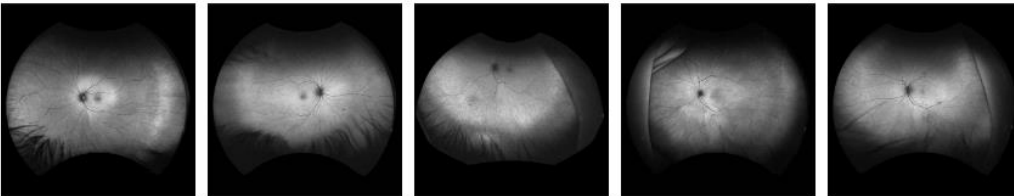
Score: 0.8786694

Score: 0.8883847

Score: 0.88946015

### True positives

Your model correctly predicted nevus on these images



Score: 0.93259954

Score: 0.9507676

Score: 0.95692474

Score: 0.97040814

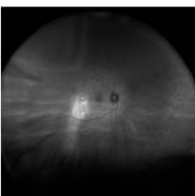
Score: 0.99273866

7 - 11 of 11 < >

Already on the last page.

### False negatives

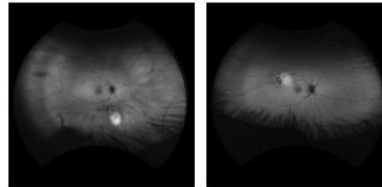
Your model should have predicted nevus on these images



Score(s): 0.078790694

### False positives

Your model incorrectly predicted nevus on these images



Score: 0.57096636

Score: 0.6557756

## CL model

Labelled images of dataset 'naevus2\_melanoma\_cl' for training

The screenshot displays the Google Cloud Vision API interface for a dataset named 'naevus2\_melanoma\_cl'. The interface includes a navigation sidebar on the left with options for 'Dashboard', 'Data sets', and 'Models'. The main content area shows the dataset's 'IMAGES' tab, with a summary table and a grid of image thumbnails.

Category	Count
All images	200
Labelled	200
Unlabelled	0
melanoma	81
nevus	119

The image grid shows 15 individual image thumbnails, each with a label below it: 'nevus(1)', 'nevus(1)', 'melanoma(1)', 'melanoma(1)', 'nevus(1)', 'melanoma(1)', 'melanoma(1)', 'nevus(1)', 'melanoma(1)', 'nevus(1)', 'melanoma(1)', 'nevus(1)', 'melanoma(1)', 'nevus(1)', and 'nevus(1)'. The images are skin lesions with a color overlay (green and red) indicating the model's classification confidence.

Developed models (4) for CL dataset

Google Cloud Platform My First Project Search Products, resources, docs (/)

Vision naevus2\_melanoma\_cl LABEL STATS EXPORT DATA

IMPORT IMAGES TRAIN EVALUATE TEST & USE Single-Label Classification

Models TRAIN NEW MODEL

naevus2\_melanoma\_c20200930095038

**Average precision** 0.928

Precision\* 80.95%

Recall\* 80.95%

\* Using a score threshold of 0.5

Model ID	ICN5566820774360121344
Created	30 Sept 2020, 09:52:15
Base model	None
Data	200 images
Model type	Cloud
Train cost	8 node hours
Deployment state	Not deployed

SEE FULL EVALUATION

RESUME TRAINING

naev\_mel\_harby\_20220605111940

**Average precision** 0.827

Precision\* 61.9%

Recall\* 61.9%

\* Using a score threshold of 0.5

Model ID	ICN152349430656270336
Created	5 Jun 2022, 11:20:38
Base model	None
Data	200 images
Model type	Cloud
Train cost	8 node hours
Deployment state	Not deployed

SEE FULL EVALUATION

RESUME TRAINING

naevus5\_melanoma\_20220605091538

**Average precision** 0.902

Precision\* 66.67%

Recall\* 66.67%

\* Using a score threshold of 0.5

Model ID	ICN7331650186638262272
Created	5 Jun 2022, 09:16:50
Base model	None
Data	200 images
Model type	Cloud
Train cost	16 node hours
Deployment state	Not deployed

SEE FULL EVALUATION

RESUME TRAINING

naevus3\_melanoma\_c20220604085031

**Average precision** 0.87

Precision\* 71.43%

Recall\* 71.43%

\* Using a score threshold of 0.5

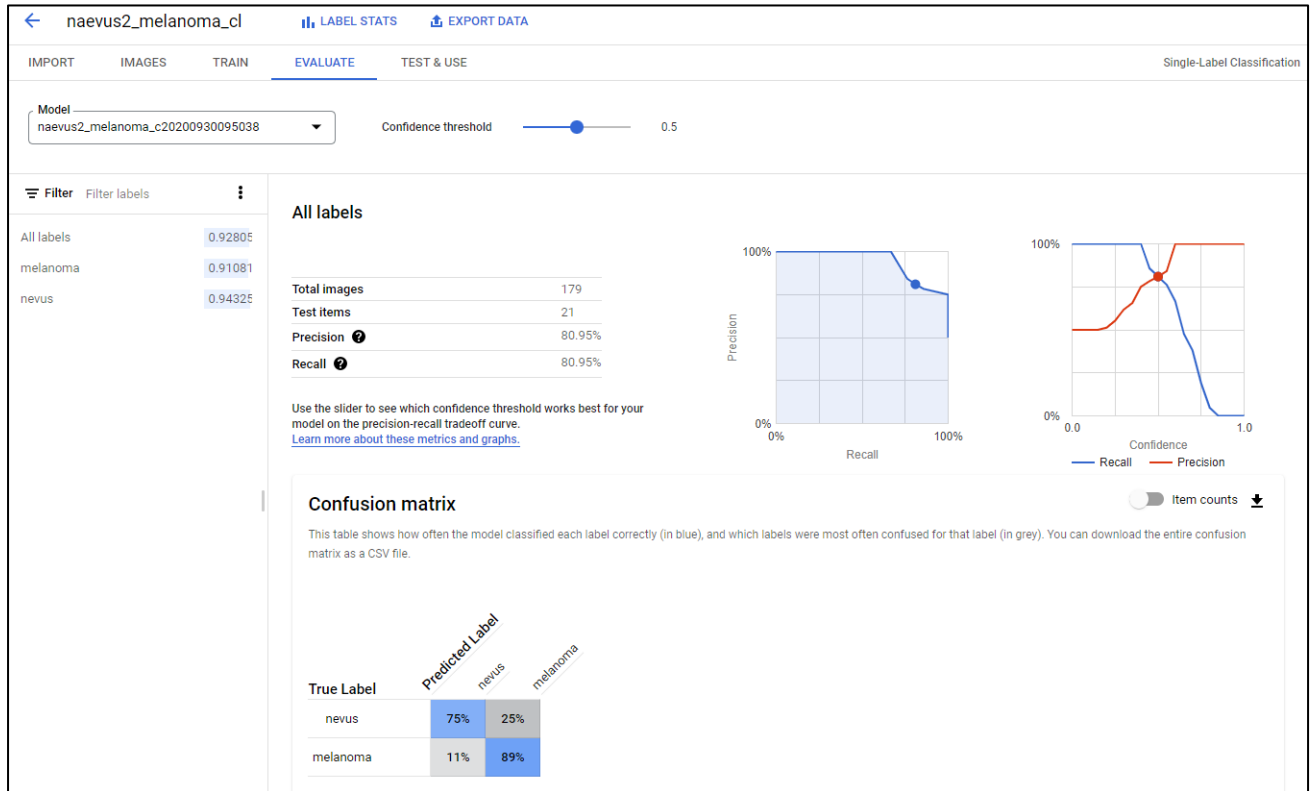
Model ID	ICN5986199797961326592
Created	4 Jun 2022, 20:51:47
Base model	None
Data	200 images
Model type	Cloud
Train cost	16 node hours
Deployment state	Not deployed

SEE FULL EVALUATION

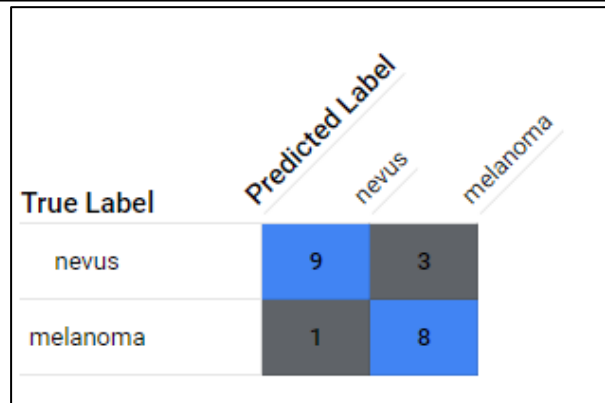
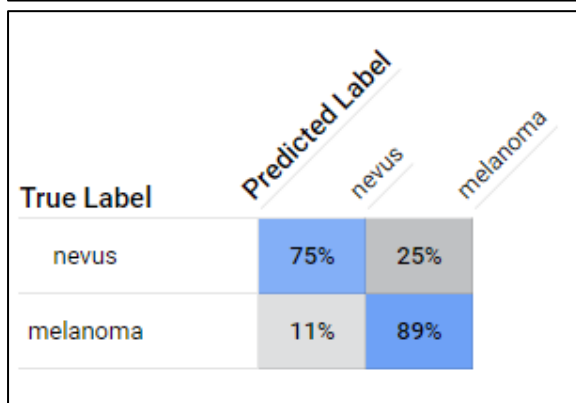
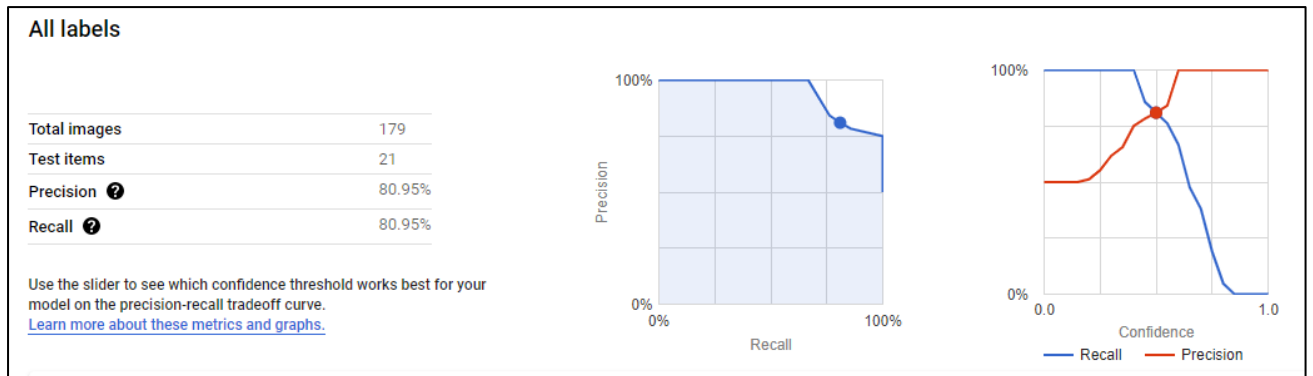
RESUME TRAINING

Full evaluation of best performing CL model 'naevus2\_melanoma\_c20200930095038'

Overview



CL – all labels





CL – melanoma

**melanoma**

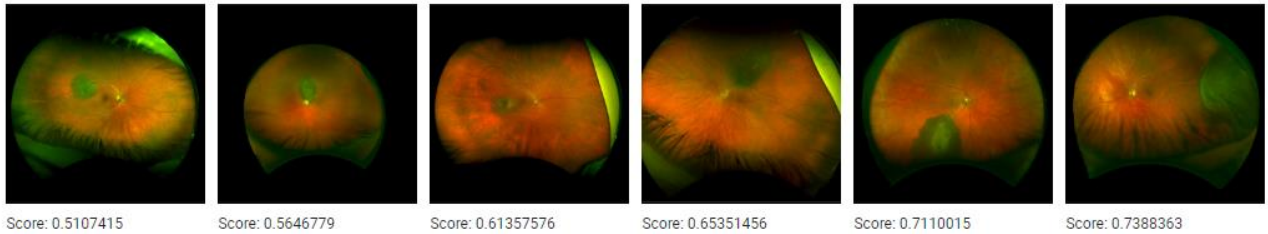
Total images	179
Test items	0
Precision	72.73%
Recall	88.89%

Use the slider to see which confidence threshold works best for your model on the precision-recall tradeoff curve.  
[Learn more about these metrics and graphs.](#)

All test images are evaluated at the time of training. If you modify your data set after training, these results will not be accurate.

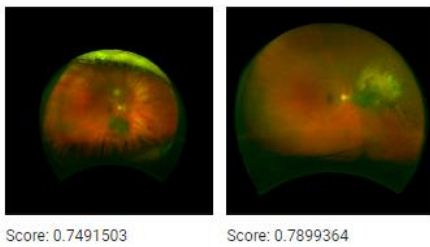
**True positives**

Your model correctly predicted melanoma on these images



**True positives**

Your model correctly predicted melanoma on these images



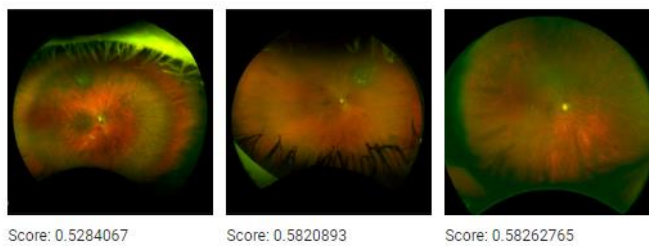
**False negatives**

Your model should have predicted melanoma on these images



**False positives**

Your model incorrectly predicted melanoma on these images



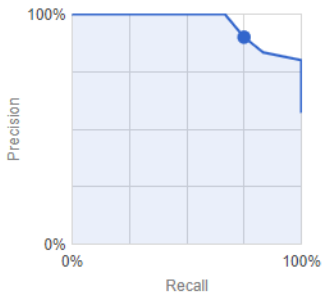

CL – nevus

**nevus**

Total images	179
Test items	0
Precision	90%
Recall	75%

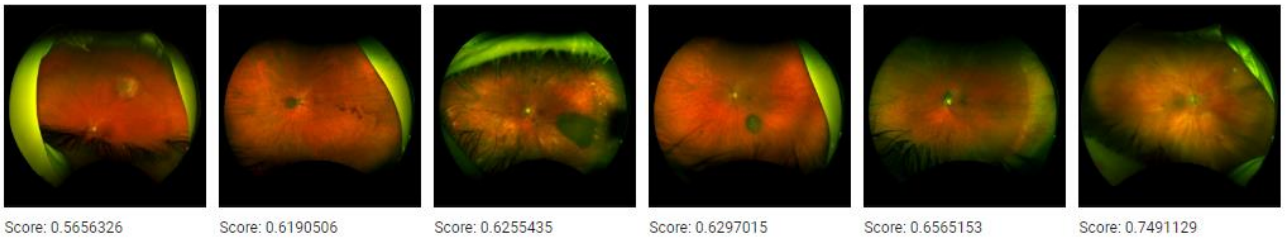
Use the slider to see which confidence threshold works best for your model on the precision-recall tradeoff curve. [Learn more about these metrics and graphs.](#)

All test images are evaluated at the time of training. If you modify your data set after training, these results will not be accurate.

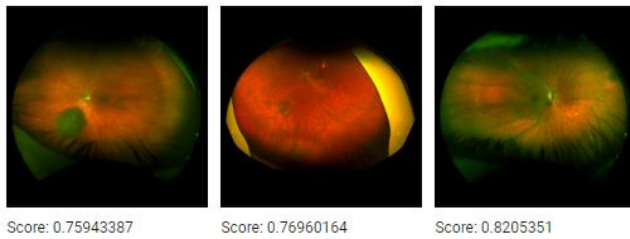
**True positives**

Your model correctly predicted **nevus** on these images



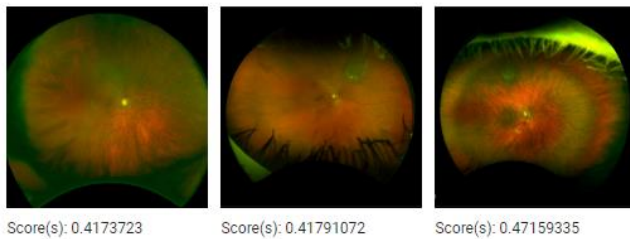
**True positives**

Your model correctly predicted **nevus** on these images



**False negatives**

Your model should have predicted **nevus** on these images



**False positives**

Your model incorrectly predicted **nevus** on these images

